The role of uterine natural killer cell-inhibition in pregnancy

Norman Edward Shreeve

King's College, University of Cambridge

This thesis is submitted for the degree of Doctor of Philosophy

January 2020

PREFACE

This thesis is the result of my own work and includes nothing which is the outcome of work done in collaboration except as declared in the preface and specified in the text.

It is not substantially the same as any work that has already been submitted before for any degree or other qualification except as declared in the preface and specified in the text.

It does not exceed the prescribed word limit for the Clinical Medicine and Clinical Veterinary Medicine Degree Committee

ABSTRACT

Education of natural killer (NK) cells is a genetically determined process that primes NK-cell activity upon the binding of their inhibitory receptors to self-ligands. Although NK-cell education is predictable and measurable in the laboratory, its biological significance is unknown. This thesis shows that the inhibitory NK cell receptor NKG2A protects against the hypertensive disorder of pregnancy pre-eclampsia in individuals genetically programmed to favour the engagement of NKG2A with its ligand HLA-E. Using NKG2A-deficient Klrc1$^{-/-}$ mice, this thesis demonstrates that NKG2A is required to educate uterine NK cells to regulate uterine vascular adaptation to pregnancy, placental function and transcriptome, as well as fetal growth. Immune checkpoint blockade of NKG2A during pregnancy in wild-type mice did not affect fetal growth, suggesting acute ablation of this pathway does not interfere with pregnancy outcome. In addition, generation of a humanised mouse model to test the notion that uterine NK cell inhibition driven by KIR: HLA interactions leads to poor pregnancy outcomes, was attempted.

DEDICATION

This is dedicated to my wonderful family, who support me in everything I do.

Without the selflessness of my wife, Becky, none of this would have been possible. Over countless cups of tea, she provided me with encouragement and confidence, when my own was in short supply. More importantly, in allowing me time to blow-off steam and run around muddy fields every day, she kept me sane.

Finally, to our beautiful son Joseph – never do a PhD.

CONTENTS

1.0   INTRODUCTION

Background

Pre-eclampsia is a hypertensive disorder that affects 3-5% of all pregnancies and is associated with fetal growth restriction (FGR) (Mol 2016). Characterised by new-onset hypertension and proteinuria, it is a leading cause of maternal and perinatal morbidity and mortality. The pathophysiology of pre-eclampsia is multi-factorial, however abnormal placental development is likely to underpin the majority of cases (Burton 2019) and the immune system is believed to participate in its pathogenesis (Redman & Sargent 2005). Specialised uterine natural killer (uNK) cells appear to contribute to maternal vascular remodelling and early placentation, and therefore contribute significantly to reproductive processes in humans and mice (Moffett & Shreeve 2015). Certain variants of fetal human leucocyte antigen (HLA) genes and maternal killer cell immunoglobulin-like receptor (KIR) genes alter the risk of pre-eclampsia and recurrent miscarriage, and regulate birthweight, suggesting uNK cells participate in placentation and fetal growth (Moffett & Colucci 2014).

1.1 Natural Killer cells

First discovered in 1975 (Kiessling 1975; Herberman 1975), natural killer (NK) cells are classified as a lymphocyte subset based on their morphology and expression of lymphoid markers. They play a pivotal role in the innate immune system in peripheral blood, the lymphatic system and within tissues. They are also important in connecting innate and adaptive immunity. They develop from a common lymphoid progenitor, which also gives raise to the other lymphocytes: B cells and T cells. Their lineage is distinct from cells that populate the myeloid division, e.g. macrophages, neutrophils and basophils. Cells characteristic of the innate immune system do not express antigen receptors and typically exert rapid effector function through an array of germline-encoded cell surface receptors, although recent research has suggested that NK cells may exhibit characteristics typical of acquired immunity through antigen-specific memory (Paust 2010). Additionally, cells of the adaptive immune system (T and B cells) interact with antigenic targets in specialized lymphoid organs where they clonally express a vast number of antigen-specific receptors, produced through somatic recombination (Vivier 2012).

NK cells comprise approximately 2–7% of lymphocytes in murine peripheral blood, and 5–15% of peripheral blood mononuclear cells (PBMCs) in humans (Paul & Lal 2017), but both their representation and absolute number vary (Pascal 2004). Their importance in normal immunological physiology is underlined by their overall representation, with NK cells outnumbering B cells in the circulation by 3-to-1 (Caligiuri 2008). The primary role of NK cells

is to act as a first line defence against pathogens and tumour cells (Shifrin 2014). Specifically, NK cells are capable of recognising and eliminating cells showing signs of stress, which usually occurs through viral infection or tumorigenesis (Paul & Lal 2017). Through a combination of increasing their activating ligands and down-regulating their major histocompatibility complex I (MHC-I), target cells shift the balance towards NK-cell activation which results in direct cytotoxicity and the secretion of pro-inflammatory cytokines (Lanier 2008).

For many years, it was only the role of NK cells in the periphery and lymphatic organs that was the focus of most investigation. However, the more recent discovery that NK cells exist as heterogeneous and diverse tissue-resident innate lymphoid cells (ILCs) in various organs has helped our understanding of their role in physiological and disease states (Spits & Di Santo 2011). NK cells (which belong to Group 1 ILCs) can be found in the gut, skin, kidney, lung, liver, joints (Carrega & Ferlazzo 2012) and importantly, the non-pregnant endometrium and decidua of the uterus during pregnancy (Moffett & Colucci 2014). NK cells in the uterus will be discussed at length later in this chapter, but it would be beyond the scope of this thesis to discuss all tissue-resident NK cells (a comprehensive review of tissue-resident NK cells can be found in Peng 2017). However, ILCs, their categories, and what differentiates them from each other functionally and phenotypically will be discussed below.

1.2 Innate lymphoid cells

Innate lymphoid cells comprise a number of cell types within the innate immune system, most of which are tissue-resident (Vivier 2018). Their discovery over recent years has hugely advanced our understanding of how the immune system not only functions to defend the host against pathogens, but also how it contributes to tissue homeostasis. Broadly speaking, ILCs can be classified into 3 groups, all of which closely mirror T-cell subsets Th1, Th2 and Th17. ILC1 cells mirror CD4+ T-helper cells and the Th1 response, which is characterised by an ability to respond to intracellular pathogens. ILC1 cells are in general poorly cytotoxic but act as important components in the defence against infectious agents such as *toxoplasma gondii, clostridium difficile* and mouse cytomegalovirus (MCMV) (Klose 2014; Abt 2015; Weizman 2017). NK cells are functionally distinct to ILC1s, however both are often grouped together and termed 'Group 1 ILCs'. All members of this family express the transcription factor T-bet (a T-box family member) which optimises interferon-gamma production (IFN-γ) (Lugo-ViLlarino 2003). Mature NK cells differ from most other Group 1 ILCs as they don't express CD127 (Lanier 2019) and in that they are effective mediators of cytotoxicity. In this way, they perform a similar function to their adaptive counterparts the CD8+ cytotoxic T-cells. In further functional contrast, ILC1s display reduced levels of perforin, a pore-forming proteolytic protein

important in degranulation and target cell elimination (Osińska 2014). In the uterus, the role of tissue-resident ILC1s is still emerging. It is believed that, amongst the other Group 1 ILCs in the pregnant mouse uterus (groups explained in depth later), they dominate before puberty, and specifically expand in second pregnancies. This has led to the suggestion that these cells could exhibit 'memory', as the expression of the memory cell marker CXCR6 is also upregulated in second pregnancies (Filipovic 2018).

Cells belonging to the ILC2 group express the transcription factor GATA-3 and have been shown to mimic the Th2 component of the adaptive immune system, producing cytokines such as IL-5 and IL-13. This component of the immune system is known to be pivotal to the response to large extracellular parasites, such as helminths (Monticelli 2011) and in allergic reactions. These cells have previously been known as nuocytes, innate helper 2 cells, or natural helper cells (Walker & McKenzie 2013). They are known to be enriched at barrier surface tissue and are helpful in the homeostasis and repair of damaged tissues following parasitic infection, especially in the lung, and are characterised by high expression of the transcription factor GATA-3 and their developmental dependency on interleukin-33 (IL-33) (Bernink 2013; Monticelli 2015). Far from understanding a role for ILC2 in human reproduction, their presence in human endometrium or pregnancy-associated decidua in such few numbers has yet to be clearly linked to any function. In contrast however, they are known to be regulated by oestrogen in the pregnant mouse uterus and may contribute to decidual homeostasis and the maintenance of successful murine pregnancy (Bartemes 2018).

ILC3s are commonly found at mucosal sites and are thought to be important in the host response to extracellular bacteria and the control of floral bacteria in the alimentary tract (Vivier 2018). They are thought to function in a similar way to T-helper 17 (Th17) cells in the adaptive immune system, a unique subset of CD4+ T cells which produce the inflammatory cytokine IL-17, and participate in tumorigenesis and several immune-mediated diseases such as rheumatoid arthritis and inflammatory bowel disease (Tesmer 2008). ILC3s also produce IL-22 and are key to gut homeostasis and the proliferation of intestinal stem cells, where they are capable of regulating Th17 responses from the adaptive immune system (Hepworth 2013). Both human and murine ILC3s produce granulocyte-macrophage colony-stimulating factor (GM-CSF), however, in mice, the characteristic transcription factor is RORγt, which is vital for development. In contrast, the IL-22-producing subset of ILC3s is preserved in humans lacking the *RORC* gene, which encodes the RORγt protein (Lim 2017). ILC3s have been detected in both human and mouse uteri, and have recently been shown to express programmed death-1

(PD-1) and TIM-3 during early human pregnancy, leading to the suggestion that they may play a role in pregnancy failure in altered states of PD-1 expression (Vacca 2019).

Finally, and perhaps confusingly, many leaders in the field have now suggested that ILCs should in fact be classified into five categories: NK cells, ILC1s, ILC2s, ILC3s and lymphoid tissue-inducer cells (LTis) (Vivier 2018). LTi cells are key during embryonic development where have long been known to be pivotal contributors to the development and formation of secondary lymph nodes and Peyer's patches (small lymphoid nodules found in close association with the small intestine) (Mebius 1997). They are perhaps the ILC group least understood with regard to their role in pregnancy, though this could be due to them historically often being regarded as ILC3s (Spits 2013), and are absent in the murine decidua, although they are found in the muscle layer of the uterus known as the myometrium (Doisne 2015). That said, uterine LTi-like cells are present in human uterine tissue during pregnancy and are more abundant in early pregnancy (Miller 2018), however their precise role is far from being fully understood.

Important work in establishing the roles of ILCs in uterine and other tissue was performed by Doisne et al in 2015. This paper helped better characterise and understand the composition and development of uterine ILCs (uILC) in both mouse and human pregnancy, and helped provide the foundation to gaining insight into ILC function in the specialized uterine mucosa. This initial work has recently been supported by using tissue samples from early human pregnancy, where mass cytometry was used to characterise and confirm the presence of three subsets of decidual ILCs, alongside proliferating NK cells and ILC3s, in the pregnant human uterus (Huhn 2020).

The significant contribution of NK cells to human and mouse reproduction is rapidly emerging. However, knowing how NK cells function in the periphery also helps one understand their potential roles in pregnancy, other physiological processes and in states of disease. Thus, some of their key biological mechanisms will now be explored.

1.3 NK cell biology
a. The missing-self phenomenon
Activated NK cells produce a wide range of pro-inflammatory cytokines including GM-CSF, tumour necrosis factor-α (TNF-α) and the potent IFN-γ (Fauriat 2010). The production of IFN-γ can be also be induced through the production of IL-12 by other immune cells such as

macrophages (Ortaldo 2006), whereas TGF-beta 1 (TGF-β) inhibits its production (Bellone 1995).

How NK cells are stimulated to produce cytokines and eliminate virally infected and tumour cells, without the specific need for prior antigen priming, has long been studied. As previously discussed, NK cells express inhibitory receptors specific for polymorphic self-MHC class I molecules. This receptor-ligand combination ensures that NK cells are constantly inhibited upon interaction with self-cells. To this end, cells not expressing complementary MHC or those whose MHC expression has been altered due to disease or cellular stress, become targets for NK cell-mediated cytotoxicity.

This overarching hypothesis for NK cell-controlled peripheral surveillance has become known as the 'missing-self' phenomenon, first postulated by a PhD student as far back as 1981 (Kärre 2008; Raulet 2006). Formal evidence supporting this hypothesis was provided using transgenic mouse models, in a landmark paper (Bieberich 1986). C57BL/6 mice express the *b* allelic variant of mouse MHC, known as H-2^b. As such, the two MHC class I proteins on most nucleated cells in C57BL/6 mice are H-2K^b and H-2D^b. In contrast, mice of the BALB/c strain express the *d* allelic variant of mouse MHC, known as H-2^d, so their cells express H-2K^d and H-2D^d. By microinjecting the *H2D^d* gene into C57BL/6 embryos, transgenic mice, normally called 'D8' were generated (Bieberich 1986), which display their endogenous H-2K^b and H-2D^b and, in addition, the transgenic H-2D^d. It had previously been shown that bone marrow grafts from C57BL/6 mice had been rejected by NK cells in the H2-D^d expressing strain B10.D2, presumably due to the absence of H2-D^d in the graft. In support of this theory, D8 mice also rejected bone marrow grafts from C57BL/6 mice. In addition, bone marrow grafts from H-2D^d-expressing D8 transgenic mice were not rejected by H2-D^d-expressing B10.D2 mice, but were rejected by MHC-disparate B10.BR mice, which lack H2-D^d, and instead express H-2^k. This process was shown to be dependent on NK-cells as D8 mice were unable to reject C57BL/6 grafts when NK cells were depleted using an anti-NK1.1 antibody (Ohlén 1989).

NK cells also express activating receptors, some of which are specific for non-MHC ligands. Given the breadth of evidence now available for such pathways, it seems likely that the absence of self-MHC molecules alone is not sufficient to initiate an NK cell response. Examples include the Ly49H receptor in mice and the NKp46 receptor (mouse and human). It was shown that in a large proportion of NK cells, NKp46 binds the haemaglutinin of influenza and parainfluenza viruses, and that this is key to the lysis of cells expressing certain viral glycoproteins (Mandelboim 2001). Similar findings in mice have also been reported. MCMV

encodes the m157 protein that displays a putative MHC-l structure. In mice resistant to MCMV, it was shown that this viral protein is capable of ligating the activating receptor Ly49-H and conferring protection to the host, through NK-cell cytotoxicity and interferon gamma (INF-γ) production (Arase 2002).

b. Major NK cell receptor systems

NK cells display an extremely polymorphic repertoire of cell-surface receptors, in both humans and mice. It is beyond the scope of this chapter to sufficiently discuss all of them, however MHC-binding receptors can be classified into two evolutionarily distinct major sub-types (Sato 2003). The two groups most relevant to this project are the polymorphic KIR (human) and Ly49 (mouse) receptors that recognise MHC-I, and the conserved killer cell C-type lectin receptors (KLR), which bind MHC-Ib in both species (Natarajan 2002).

KIRs are expressed on NK cells and a proportion of T-cells in humans. KIR genes evolved in primates to generate a diverse family of transmembrane glycoprotein receptors that regulate development, tolerance and activation of NK cells (Campbell & Purdy, 2011). The diversity of individual KIR structure enables them to recognize MHC-I molecules with locus and allele-specificity. This diversity is the result of three key variable components that classify KIR: number of extracellular Ig-like domains; cytoplasmic length, and sequence similarity (Vilches & Parham 2002). Moreover, it is the length of the cytoplasmic tail, which seems to govern overall polarity of the signal transmitted. KIR with long (L) tails (e.g. KIR2DL1) will transmit an inhibitory signal via immunoreceptor tyrosine-based inhibition motif (ITIM)-associated phosphatases Src homology region 2 domain-containing phosphatase-1 (SHP-1), whereas receptors with shorter (S) tails (e.g. KIR2DS1) couple with the adapter DAP12, which in turn signals through Src and SYK-family kinases (Lanier 1998).

C-type lectin is a carbohydrate-binding protein domain with functions including pathogen recognition, glycoprotein homeostasis and the initiation of immune responses in vertebrates (Mayer 2017). KLRs are type II transmembrane homo- or heterodimers. They differ from conventional C-type lectin receptors because they lack the characteristic calcium-binding site (Drickamer & Taylor 1993). Of particular relevance to NK cell function within this receptor class is the activating NKG2C (encoded by KLRC2) and the inhibitory NKG2A (encoded by KLRC1). Both are found on human chromosome 12 within the NK gene complex (NKC) and both form a heterodimer with CD94, whose expression is necessary for them to reach the cell surface (Lanier 1998).

Unlike the inhibitory NKG2A, NKG2C contains an immunoreceptor tyrosine-based activation motif (ITAM) in its cytoplasmic domain. As a result, when NKG2C is bound by either HLA-E in humans, or Qa-1 in mice, an activating signal is transmitted (Vance 1999, Braud 1998a). This signalling is orchestrated by the disulphide-bonded, ITAM-associated homodimer, DAP12 (also known as TYRO protein tyrosine kinase-binding protein), which triggers protein tyrosine kinase pathways. DAP12 associates directly with NKG2C in humans (Lanier 1998) and indirectly through CD94 in mice (Smith 2000). Cell surface expression of NKG2C on human NK cells is approximately 10% in the peripheral blood (Rölle 2014). In contrast, current evidence suggests that there are almost no NKG2C+ mouse NK cells under normal conditions (Kawamura 2009; Vance 2002). However, the expression of NKG2C by murine NK cells significantly increases in response to human cytomegalovirus (HCMV) infection (Gumá 2004) in experimental conditions, suggesting a clear role for the receptor in certain effector phase responses.

c. NKG2A structure and cellular pathways

The human CD94-NKG2x group of receptors can only recognise the MHC-Ib molecule HLA-E. This is at distinct odds with most other more promiscuous NK receptors (Braud 1998a; Lee 1998a; Borrego 1998). Determination of the crystal structure of NKG2A reveals two crucial components that facilitate interaction with HLA-E. The variable peptide C-terminal only interacts with the invariant CD94. Residues 167-70 of NKG2A/C do not come into direct contact with HLA-E, but allow for the approximately 6-fold higher affinity of HLA-E for NKG2A compared to NKG2C (Kaiser 2008). In mice, NKG2A recognises the MHC H2-D^b-derived leader peptide known as Qdm (AMAPRTLLL), which is presented by Qa-1^b (Vance 1998).

HLA-E is an MHC class Ib heterodimer composed of a variable heavy chain and a light chain of beta-2 microglobulin (genes referred to as B2M (human) /*B2m* (mouse) throughout this thesis, but also commonly known as beta2-M, beta2 microglobulin or β_2M), making it structurally similar to classical MHC molecules. It is a monomorphic receptor expressed on several cell types, including human extravillous trophoblast (EVT, an early placental cell type) alongside HLA-C and the non-classical HLA-G (King 2000a). HLA-E evolved to selectively bind peptides derived from the leader sequences of other MHC-I molecules (Braud 1997). Thus, HLA-E expression essentially acts as a barometer for the expression of other MHC-I molecules within a cell, as down-regulation of these proteins leads to a proportional down-regulation of HLA-E at the cell surface (Braud 1998a).

HLA-E relies on this supply of signal peptides from classical HLA-A, -B or -C for appropriate folding and transport to the cell surface. The signal peptides that bind HLA-E and Qa-l[b] depend on the transporter associated with antigen presentation (TAP) for their loading. TAP shuttles these leader peptides into the endoplasmic reticulum from the cell's cytoplasm to undergo appropriate cleavage (Lee 1998b; Braud 1998b). The liberated MHC class I signal peptide is next processed by signal peptide peptidase (SPP) (Lemberg 2001). This SPP cleavage step is vital for the release of the HLA-E epitope-containing fragment and its subsequent transport into the lumen of the endoplasmic reticulum in association with the TAP. These 9mer endogenous signal peptides which combine with HLA-E are predominantly cleavage products consisting of amino acid residues 3-11 of HLA-A, -B, -C and –G signal peptides (Braud 1997; Borrego 1998; Bland 2003). Only after this process is complete can HLA-E fully assemble with its leader peptide and translocate to the cell surface stably. There it can bind with NKG2A to inhibit NK-mediated cell-lysis or confer educating signals. Interestingly, it has also been shown that certain isoforms of the non-classical IgG (expressed on trophoblast) (King 2000a) can increase HLA-E expression (Teklemariam 2012; Sala 2004), whereas truncated IgG isoforms are retained in the endoplasmic reticulum and do not effect HLA-E expression (Ulbrecht 2004).

Like many inhibitory NK receptors, NKG2A operates through a well-described cellular pathway involving ITIMs. ITIM-containing receptors (ITIM-R) exert a local and transient inhibition, which abrogates activating signals, and does not commit the cell to a sustained period of non-responsiveness. Binding of ligands to ITIM-R results in the phosphorylation of two tyrosines within cytoplasmic ITIMs. This phosphorylation is usually mediated by Src-family kinase. The next step involves the recruitment and activation of the tyrosine phosphatase SHP-1 to the previously tyrosine-phosphorylated region of the ITIM, where dephosphorylation occurs. This results in dampening of the activation receptors and other signalling molecules (Long, 2008), and relative inhibition.

Key to the functioning of NK cells lies a process termed education, or licensing (discovered in 2005 and described below). It has become the focus of much research in recent years, and its significant contribution to NK cell activity is becoming ever more evident.

1.4 NK CELL EDUCATION
a. NK cell education pathways
It has long been established that NK cell functional development, at least in part, requires the interaction between inhibitory receptors and MHC-I molecules (Höglund & Brodin 2010). This

was first named *NK licensing*, which is now used interchangeably with the term *NK education*. Initial work described how mouse NK cells can fall into two distinct groups, both of which exhibit tolerance to self; a) NK cells expressing inhibitory receptors for self MHC molecules are educated and therefore functional, but also capable of being inhibited and b) NK cells lacking inhibitory receptors for self MHC molecules fail to reach functional potential and exhibit anergy that prevents auto immunity.

This was first evidenced through a target cell-free assay to test intrinsic NK cell functional ability. Antibody cross-linking of the activating mouse NK receptor NK1.1 (present on all $CD3^-$ NK cells) in $B2m^{-/-}$ mice and $K^{b-/-}D^{b-/-}$ mice lacking the dominant mouse class Ia MHC alleles resulted in fewer IFN-γ producing NK cells compared to C57BL/6 wild-type mice. This approach is useful as it depends on one specific activating receptor and therefore controls for the poorly defined potential for widely variable inhibitory/activating receptor engagement by any target cells. It was also shown that licensed NK cells could be found in mice lacking DAP12, an important adaptor protein in NK cell activation (but not required by the activating NK1.1 receptor), indicating that activating MHC receptors are not required and MHC-dependent inhibition is sufficient to result in NK-cell licensing (Kim 2005). Further studies confirmed that mouse NK cells lacking inhibitory receptors remain unlicensed (Joncker 2009; Bélanger 2012). The reported 10-13% of NK cells in C57BL/6 mice lacking the self-specific inhibitory receptors Ly49-C, Ly49-I, and NKG2A did not significantly respond to MHC-deficient $B2m^{-/-}$ or $K^{b-/-}D^{b-/-}$ lymphoblasts, or standard tumour target cells YAC-1 or RMA (Fernandez 2005).

The first paper to show that NK cell education may be a quantitative process was published in 2005 (Johansson 2005). This study used mouse models of single MHC-I allele expression e.g. H2-D^b, -K^b, -D^d and models where a combination of certain MHC-I alleles were expressed. They then measured each strain's ability to reject class-I negative grafts *in vivo*. They showed that the presence of certain MHC-I alleles (e.g. K^b and D^b) in the host conferred a greater response *in vivo*, whereas the weakly expressed allele-expressing mice performed poorly. These data suggested that, in mice, the education response for any given MHC-I allele was controlled by the number of NK cells expressing its cognate Ly49 receptor.

Evidence for NK education in humans followed shortly after. Early work suggested that NK cells lacking all known inhibitory receptors do exist in the periphery, and that they are functionally mature. This subset of $KIR^-/NKG2A^-$ cells was hyporesponsive when co-cultured with standard target K562 (MHC-I negative) cells, and produced almost half the amount of

IFN-γ and CD107a as 'educated' controls expressing inhibitory receptors. Other useful data reported in this study showed that the non-educated NK-cell subset displayed the same expression of various other cell-surface receptors, including many activating receptors such as NKp46 and NKG2D (Anfossi 2006).

This discovery in humans led to a number of theories as to how precisely NK education occurs. An obvious question is whether education occurs in –*cis* or –*trans,* i.e. are cells capable of educating themselves, or do they rely on local interactions with other cells expressing MHC molecules. A number of studies have demonstrated that certain educating receptors can recognise their MHC ligands in *cis* (Doucey 2004; Back 2009; Andersson 2007). Key early evidence of whether these interactions influenced education status was found by utilising the Ly49-A inhibitory receptor in mice. Ly49-A is constitutively expressed in association with H2-D^d in NK cell membranes. By replacing the Ly49-A stalk region with a longer stalk (CD72, a c-type lectin), the mutant Ly49-A was unable to bind with H2-D^d in *cis*, but was able to engage other MHC-I in *trans*. This resultant phenotype was of uneducated NK cells, which interestingly, could still undergo inhibition (Chalifour 2009). Another important study in addressing this question utilised patients undergoing HLA-mismatched haematopoietic cell transplantation (HCT) and mice transgenic for HLA-B* 27:05 allele. They showed that NK cells derived from human stem cells underwent education by HLA from both donor and host stromal cells, and that the silencing of HLA in primary NK cells (removing *cis* interaction, achieved through diminishing HLA class I expression by using short hairpin RNA against β2m) led to reduced NK reactivity. They also reported that HLA-Bw4 in *trans* was able to re-educate mature human NK cells expressing the cell surface cognate receptor KIR3DL1, by transferring these cells into transgenic mice either positive or negative for HLA-B27. After a period of 2 weeks post-transfer into the transgene positive mice, the human NK cells displayed increased responsiveness compared with their pre-transfer levels, or when compared with NK cells from the same donor which were incubated in mice lacking the educating HLA-B*27:05 transgene (Boudreau 2016).

Other models of NK cell education are based upon signalling arising from their surrounding and interacting cells. It is believed that this can possibly be occurring in two distinct ways; i) NK cells are naturally hyporesponsive and become 'armed' through the ligation of an inhibitory receptor which promotes functional maturity (Yokoyama, 2008), or ii) NK cells are constitutively responsive, but those deficient in inhibitory receptors specific for MHC-I are 'disarmed' or anergic and therefore incapable of autoimmunity (Raulet, 2006). A final theory

which encompasses both aspects of arming and disarming to essentially quantitatively 'tune' NK cell responsiveness termed the 'rheostat' model has also been mooted (Brodin 2009).

A marker for NK education has yet to be discovered, although surrogate markers such as lymphocyte function-associated antigen 1 (LFA-1) and DNAX accessory molecule-1 (DNAM-1), whose expression is elevated on educated NK cells, have been suggested (Enqvist 2015). Thus, we can define an educated cell from an uneducated cell by how it performs in specific functional assays of education. It could be argued that any test of NK function could be considered an indirect measure of education, however there are three established education assays used by researchers in the field to report functional outcomes (Figure 1). These include *in vivo* rejection studies in mice (described in more detail in 3.0 Chapter 1 - Methodology); cell-cell interaction assays where cytokine secretion can be measured following interaction of all NK receptor: target cell ligand combinations; the less physiological but specific antibody cross-linking assay (also discussed in more detail in 3.0 Chapter 1 - Methodology). Finally, education status can be inferred according to the presence of inhibitory receptors on the cell surface that bind self MHC class I molecules (Höglund & Brodin 2010).

The intracellular pathways and mechanisms contributing to NK education are as yet not understood. Recent work, however, has suggested the possibility that NK education is governed by calcium fluxes in secretory lysosomes. Granzyme B is a well-characterised NK cell protease, released into the cytoplasm of target cells with the help of perforin (Prager 2019). It was shown that granzyme B accumulates in dense-core secretory lysosomes in NK cells, where the genetic silencing of a lysosomal calcium channel, TRPML1, led to increased granzyme B and increased functional potential - similar to that seen in educated cells expressing self-specific inhibitory receptors (Goodridge 2019).

SHP-1 (encoded by *Ptpn6*) is a cytosolic protein key to NK cell inhibition, but it also acts as a negative regulator of T cells and other leucocytes and is strongly expressed by haematopoietic cells (Nakase 2009). Previous mouse models of global SHP-1-deficiency (*motheaten* and *motheaten-viable* strains) have displayed mixed effects on NK functionality, often clouded by pathological phenotypes too complex to discern the direct effects of SHP-1 signalling (Lorenz 2009). To address the controversy surrounding the role of SHP-1 in NK education, conditional knockout models have been utilised. Transgenic mice with an NK-specific SHP-1 knockout ($Ptpn^{+/+}NCRI^{cre/+}$) have been shown to display normal development of NK cells with no discernible inflammatory phenotype. It now appears clear that SHP-1 is important in NK education as these mice were unable to reject MHC-I deficient targets as expected, and were

incapable of controlling tumours *in vivo* (Viant 2014). To date, this model has not been used to study pregnancy – so provides a useful opportunity to test the hypothesis that NK cell-specific inhibitory signalling provides functional inhibition and education during early gestation in mice.
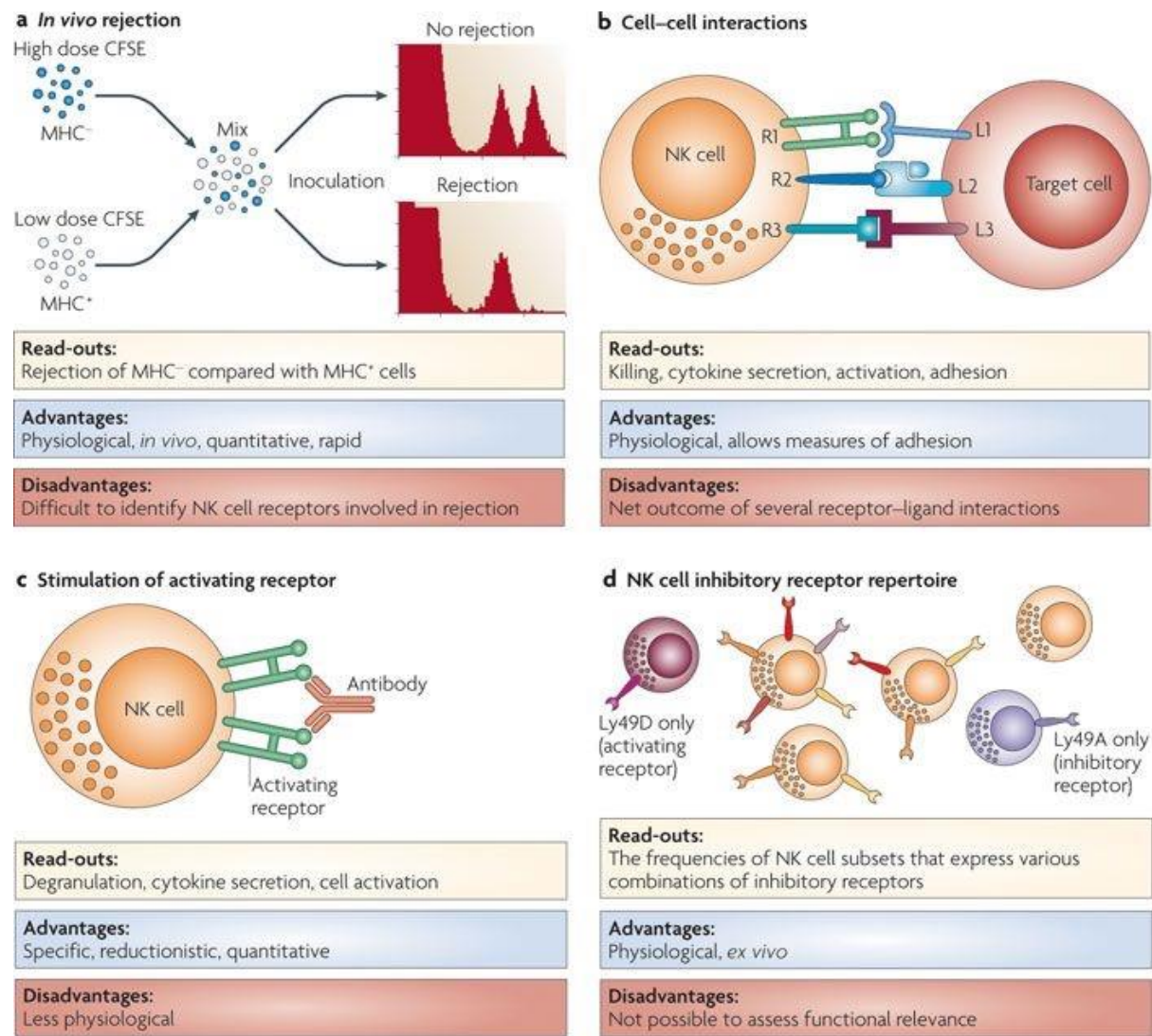
Figure 1. A schematic showing the advantages and disadvantages of common assays to measure NK cell education. *Figure taken from Höglund & Brodin, 2010.

It is also worth noting that some studies have suggested NK education is possible via MHC-independent pathways. Many pathways and receptor-ligand combinations have been postulated in recent years, however, below is perhaps the most notable and well-evidenced example. The signalling lymphocytic activation molecule (SLAM) family of receptors and SLAM-associated protein (SAP) family of intracellular adaptors are one such example. The murine receptor 2B4 recognises its cognate SLAM molecule CD48 with high specificity, and is believed to be an MHC-I-independent inhibitor of NK cells, especially in the absence of its

adapter SAP. It has been shown to inhibit NK cells from killing CD48-sufficient tumour cells (Lee 2004). Interestingly, inducing a knockout in either 2B4 (Lee 2004) or CD48 (Lee 2006) renders the NK cells in the host mice incapable of rejecting CD48-deficient tumour cells.

Taken together, these studies suggest that the engagement of 2B4-CD48 is needed for NK cell-mediated recognition of missing-self targets, and represents an MHC-I-independent education pathway in NK cell physiology (He 2017).

b. NKG2A and its role in education

Evidence for the importance of NKG2A in NK cell education is convincing. In mice, the triggering of activating receptors e.g. anti-NK1.1, as a stimulus to measure downstream functional capacity/education status has been previously discussed as a measure of NK education. NKG2A single positive NK cells (expressing none of the other known educating MHC receptors) display a functional capacity consistent with other educated subsets, however a significantly stronger response was seen upon the addition of a class I allele that contributes leader peptides for Qa-1^b presentation (e.g. H2-D^d) essential to NKG2A-dependent education (Brodin 2009).

Furthermore, a recent paper has also highlighted the contribution of both NKG2A and Ly49 systems to murine NK education by using genetic deletion. In *Klrc1*$^{-/-}$ mice (where CrispR-Cas9 was used to delete *Klrc1*), NKG2A+ NK cells were found to be more educated as they displayed an increase in response to a number of stimuli in terms of IFN-γ production, when compared to NKG2A- controls in wild-type mice. Furthermore, the *Klrc1*$^{-/-}$ mice also showed a decrease in the *in vivo* rejection of MHC-deficient donor cells, another marker of NK education. Interestingly, the effect of NKG2A on murine NK education was found to be synergistic with Ly49 receptors, where NKG2A appeared to compensate for a lack of Ly49 receptors by increasing responsiveness, but when both receptor systems were missing, there was an almost complete loss of education (Zhang 2019).

Education by self-KIRs or NKG2A also modulates cytotoxic responses in human NK cells (Bjorkstrom 2010). When co-cultured with target 721.221 cells (a B-lymphoblastoid cell line which lacks HLA-A, -B, and -C class I antigen surface expression), NKG2A single-positive subsets demonstrated enhanced responses when measured through the number of CD107a and IFN-γ expressing cells. In this study (Yawata 2008), all 58 donors exhibited constant and enhanced responses in NKG2A single-positive NK cells, whereas the effects on KIR single-positive cells varied with donor KIR genotype and HLA expression. Furthermore, enhanced degranulation was seen in all NKG2A expressing subsets, regardless of KIR expression.

Corroborating evidence for the role of NKG2A in human NK education soon followed. It was demonstrated that NKG2A expression was independent of KIR expression, and that NKG2A acted as a buffer for functional responses in NK populations expressing low levels of KIR. Individuals whose NK cell repertoires were dominated by KIR-deficient NK cells were reliant upon those KIR- cells that also expressed NKG2A in order to achieve appropriate functionality and CD107a release (Andersson 2009). Recently, it has also been shown that NKG2A educates fetal as well as adult NK cells. In response to various stimuli including 721.221 and K562 target cells lacking MHC-I expression, and rituximab-coated 721.221 cells. Rituximab is a monoclonal anti-CD20 antibody which, when coated on CD20-expressing 721.221 cells, triggers NK cell antibody-dependent cell-mediated cytotoxicity by binding Fc receptors. They showed that KIR⁻ NKG2A⁺ cells consistently responded better than their NKG2A⁻ counterparts in terms of degranulation in fetal lung and adult PBMC, when measured through CD107a expression (Ivarsson 2013).

The potential role of NK education in pregnancy is clearly pertinent. This is due to the body of evidence implicating uNK as being important for reproduction, and that these cells simultaneously express educating receptors and their ligands. That these ligands are also often expressed by the invading EVT that uNK interact with, adds further weight to this notion. Only one study has comprehensively aimed to address this specific issue in humans, and found interesting results. Sharkey et al. (2015) found that the KIR receptor repertoire capable of binding C1+HLA-C and C2+HLA-C2 of uNK was different to that found in peripheral NK cells and that maternal HLA-C expression modulated KIR expression in the decidua, but not in the periphery. This suggested a specialised microenvironment is at large during pregnancy, where uNK are educated for specific functions in human pregnancy. They also assessed functional responsiveness in different uNK subsets and found that uNK are educated by maternal HLA-C molecules, where the highest performing subset in terms of degranulation were those cells positive for NKG2A, KIR3DL1 and KIR2DL1. They also showed that NKG2A independently increased degranulation in a number of NK subsets educated by other receptors, including KIR3DL1.

c. HLA-B -21 dimorphism in NKG2A education

Histocompatibility complex genes, located on chromosome 6 in humans and chromosome 17 in mice display extremely high allelic diversity, and can vary between individuals widely. In humans, the MHC region spans around 3600 kilobases of DNA (Beck 2000), and is divided into three main regions. The Class I region contains genes which encode for the heavy chain (alpha chain) of HLA-A, -B and –C. The class II region encodes for the MHC class II genes

(products of which are important in the presentation of exogenous antigens by antigen presenting cells) – these include both DRA and DRB genes. Finally, the class III region which does not encode HLA genes, but instead codes for proteins involved in the complement cascade, among others (Choo 2007). The *Mhc* genomic region in the mouse is named *H2,* and the genes within it display striking similarities to those found in the human genome. Also classified into three regions, similar to humans, class I molecules in mice are able to elicit immune responses by presenting peptide antigens derived from intracellular proteins to T cells. The classical *Mhc* class Ia genes, such as *H2-K* and *-D* in the mouse, are also highly polymorphic and expressed widely (Ohtsuka 2008).

Whilst the three main classical MHC class I alpha chain genes (HLA -A, -B and -C) are stably expressed in humans, their polymorphism and huge allelic variation confers significant genetic diversity between humans. For example, there are more than 200 variations of some MHC alleles, resulting in most individuals being heterozygotes at both their MHC genetic loci. Despite this relatively large polymorphism seen in MHC genes, only two alleles can be expressed at an individuals' single locus. The result of this is a highly varied combination of inherited alleles that determines an individuals' overall MHC genetic haplotype (referred to later), where protein expression of these alleles is also co-dominant. This adds further complexity as it means two allele products per gene can be presented on the cell surface (Janeway 2001). In contrast, non-classical MHC class I genes, which remain peptide-dependent (HLA-E and HLA-G), display much lower heterogeneity than classical genes (Halenius 2015).

HLA-B derived signal peptides are supplied in two forms, depending on their position-2 anchor residue, which corresponds to residue -21 of the HLA leader sequence. Methionine at position -21 (VMAPKTVLL and VMAPRTLL) provides an effective and functional anchor for HLA-E folding, and is found in all HLA-A and HLA-C allotypes, but only in a small proportion of HLA-B allotypes (HLA-B -21M) (Braud 1997; Braud 1998a; Lee 1998a). It is worth noting though that HLA-C is expressed in very low levels in most adult cell types, around 13- to 18-fold less on the cell surface than HLA-A (Apps 2015), for example. It has been shown that where threonine, and not methionine, is in position -21 of HLA-B, aberrant protein folding results in unstable HLA-E expression (Merino 2013). Whilst all Bw4+HLA-A contain -21 methionine, nearly all Bw4+HLA-B have -21 threonine (HLA-B -21T), and C2+HLA-C individuals almost always encode HLA-B -21T too. This means that HLA-B -21T individuals can provide the Bw4, C2 and C1 ligands for KIR3DL1, KIR2DL1/S1 and KIR2DL2/3, respectively, but they are not able to supply peptides taken from the HLA-B leader sequence that promote the formation of HLA-E for the ligation of NKG2A. Ultimately, this single nucleotide

polymorphism (SNP) separates individuals into those who can provide functional peptides for HLA-E expression and NKG2A ligation/education (M/X), and those who cannot (T/T) (Figure 2).
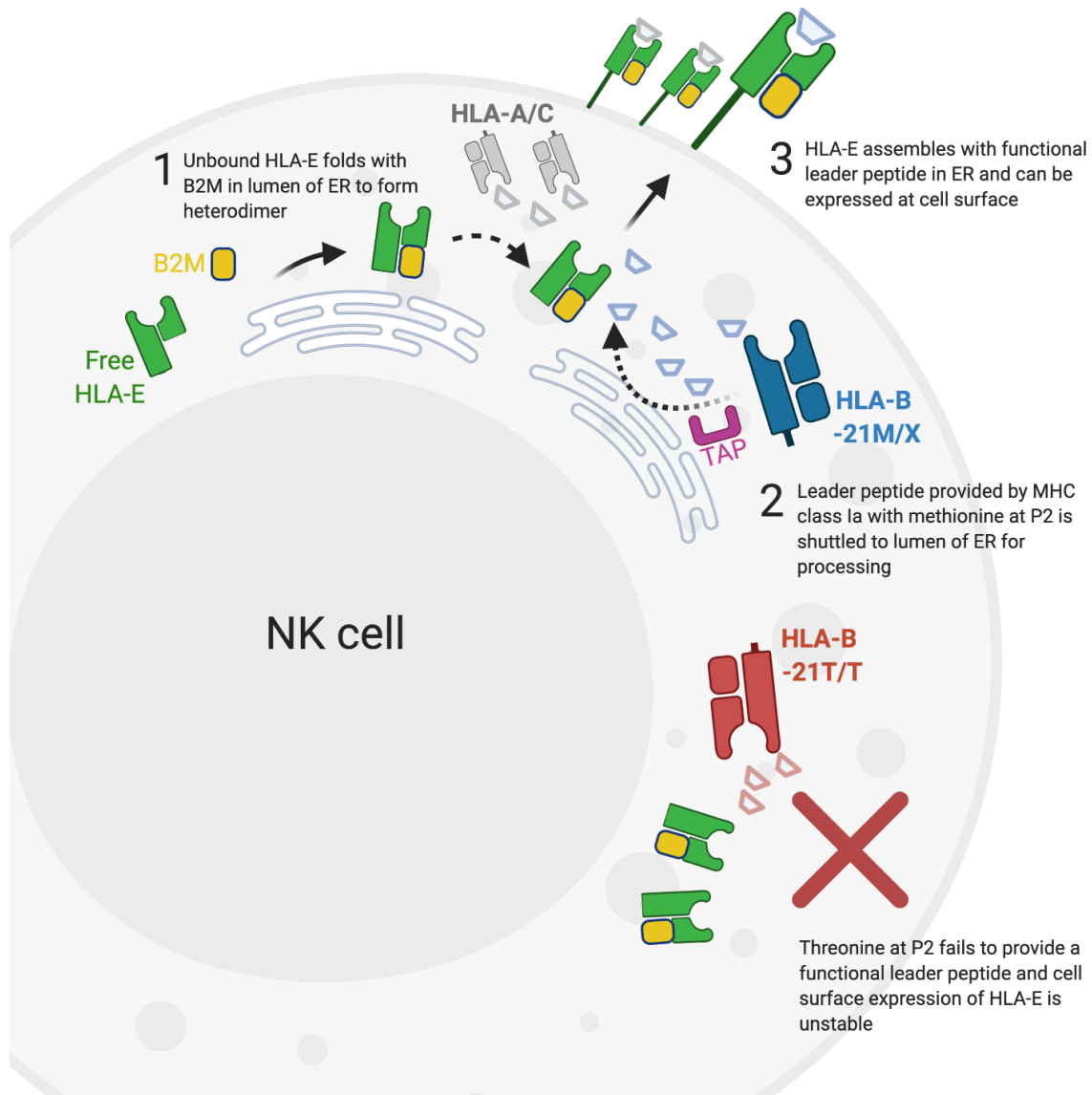
Figure 2. A schematic representing the pathways influencing HLA-E cell-surface expression. B2M (beta 2-microglobulin), P2 (position 2 anchor residue), TAP (transporter associated with antigen presentation), ER (endoplasmic reticulum).

An interesting discovery has recently highlighted how this dimorphism ultimately impacts on NK cell function (Horowitz 2016). In the initial analysis of approx. 16000 individuals' HLA haplotypes from around the world, it was reported that the clear majority of haplotypes encoding C2+HLA-C also encode -21T at HLA-B -21 residue. This indicates that C2+HLA-C, which is capable of strongly binding educating KIR, is usually found alongside HLA-B genotypes incapable of providing peptides to facilitate NKG2A-derived education. Linkage disequilibrium (LD) can be defined as '...*the non-random association of alleles at two loci or*

more...' (Slatkin 2008), and broadly, means neither a linkage nor a complete segregation between two genetic sites. Interestingly, it was also reported that linkage disequilibrium exists between HLA-C position 80 (the determinant of C1/C2 dimorphism) and HLA-B -21, where -21M is almost never found with C2+HLA-C in non-Africans. This is pertinent to the field of reproductive immunology, where C2+HLA-C drives many of the immunogenetic associations found in poor pregnancy outcomes. Furthermore, it was also found that Bw4+HLA-B, the ligand for the educating NK receptor KIR3DL1, was almost always found with -21 threonine (see Figure 3). This is also interesting, as Bw4+HLA-B serves as a ligand for the KIR3DL1 receptor (as does Bw4+HLA-A) (Hollenbach 2016), another important educating pathway for NK cells.
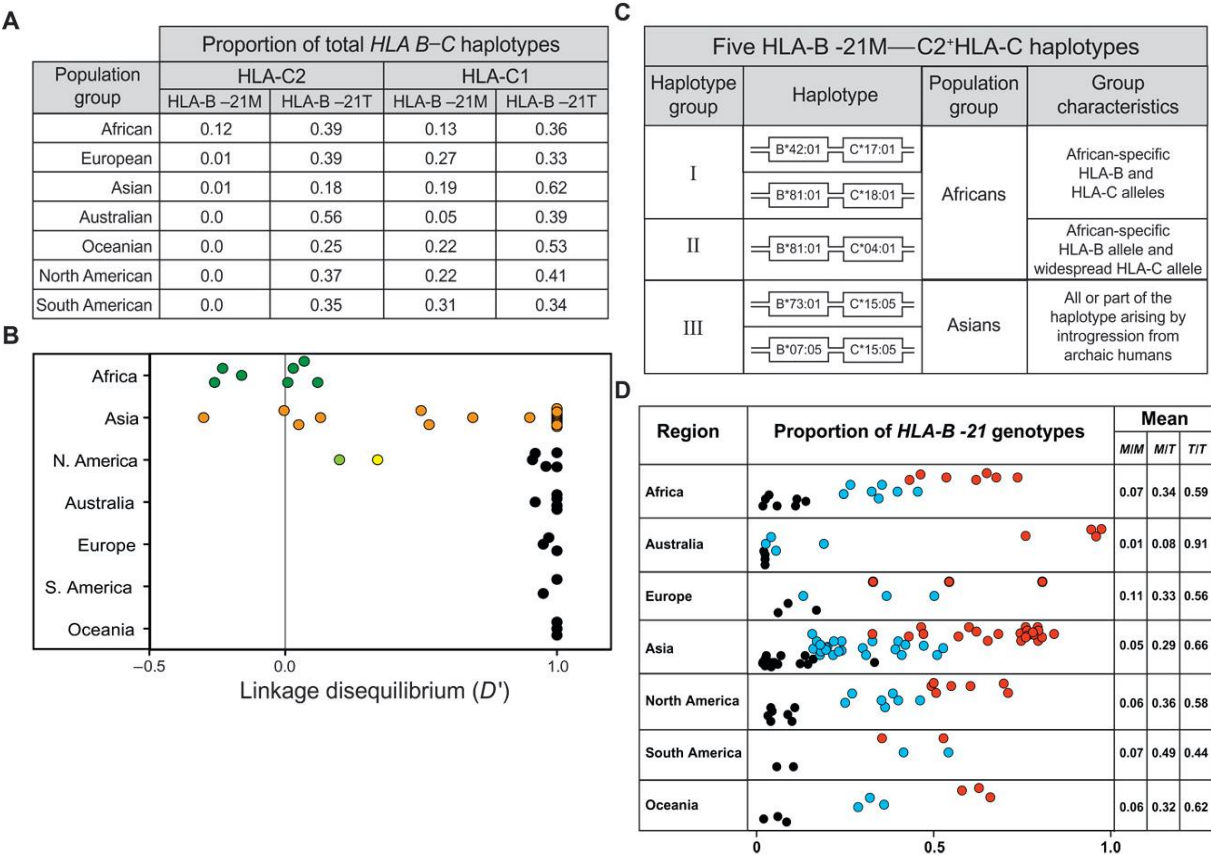
Figure 3. Alleles encoding –21M HLA-B and C2+HLA-C segregate on different haplotypes outside of Africa. C1/C2 dimorphism at position 80 of HLA-C and the –21M/T dimorphism of HLA-B define four HLA-B–HLA-C haplotypes. (A) The proportions of each haplotype in major human population groups (51 populations and 16,384 HLA haplotypes) were analyzed. (B) Plots of the LD (*D′*) between the HLA-B and HLA-C dimorphisms: Africans (dark green circles), Asians (orange circles), admixed U.S. populations of African ancestry (light green circles), Asian ancestry (yellow circles), and all other populations (black circles). The haplotype frequencies used to calculate *D′* are given in fig. S1. (C) Characteristics of the five haplotypes that encode –21M HLA-B and C2+HLA-C. (D) Frequencies of the three –21 HLA-B genotypes in major population groups: –21T/T homozygotes (red circles), –21M/T heterozygotes (blue circles), and –21M/M homozygotes (black circles) (8192 genotypes were analyzed). *Figure and figure legend taken from Horowitz et al. 2016.

23

This study also reported a highly significant increase in HLA-E expression in M/T vs. T/T donors. However, the second copy of -21M HLA-B only produced a minor further increase in HLA-E expression, indicating that the important difference is between donors who have -21M HLA-B and donors who have not. Accordingly, they concluded that the level of HLA-E expression fixed by peptides derived from HLA-A and -C is particularly sensitive to the presence and absence of -21M HLA-B. Another strength of this study was the attempt to functionally characterise the impact of the HLA-B -21 dimorphism. The overarching hypothesis that HLA-B haplotypes segregate individuals into those biased for NKG2A education, through the preferential supply of peptides enabling HLA-E surface expression, was also explored.

It was found that cells from T/T donors performed less strongly in education assays where antibody-dependent cellular cytotoxicity (ADCC) was used to stimulate IFN-γ and degranulation (measured by CD107a), especially when -21M was analysed in combination with other KIR receptors. ADCC assays measure intrinsic NK functionality. This is achieved by first using an antibody to target and coat the cell surface of a target cell. These antibodies are then recognised by NK-cell Fc receptors, which undergo cross-linking, resulting in degranulation and cytolysis of the target cells.

Lastly, it was reported that phenotypically more diverse NK cell populations (characterised by combinations of 35 cell surface markers) were found in association with HLA-B -21. Remarkably, NKG2A+ cell populations displayed significant diversity where individuals displayed between 337 and 989 different phenotypes. In general, the NKG2A^{+} NK cells of M/M donors displayed a greater phenotypic diversity than those of T/T donors, with M/T donors being the most diverse of all three of the SNP variants (the difference between M/M and M/T did not reach statistical significance). Also, the number of -21M alleles expressed by an individual also seemed to determine the number of KIR receptors they expressed. Furthermore, -21M displayed a clear and consistent association with a decrease in size of the NKG2A+ cell population.

d. NKG2A in disease

One indicator that NKG2A may be important in certain conditions came in the context of human immunodeficiency virus (HIV). Early work had found that the combination of HLA-Bw4 homozygosity and KIR3DS1 epistasis influenced progression to acquired immunodeficiency syndrome (AIDS) (Carrington 1999). A previous study of the role of HLA-B in HIV control (Flores-Villanueva 2001), which associated the control of HIV-viremia and protection from progression to AIDS with HLA-Bw4 homozygosity, was reanalysed. In the new

study (Yunis 2007), the number of individuals who were *T/T* in the group of HIV controllers was higher than in the groups that progressed to AIDS. This suggests that methionine-mediated up-regulation of HLA-E leads to NK inhibition and T cell interactions in the effector phase, resulting in inhibition of killing and a more favourable environment for progression to AIDS.

In addition, a recent large-cohort study has also suggested that the NKG2A-HLA-E pathway has a role in HIV. By analysing almost 10,000 HIV+ individuals, it was found that elevated HLA-A levels resulted in poorer control of HIV. This association was attributed to a greater availability of HLA-A-derived peptides for HLA-E expression, leading to greater NK cell inhibition. Interestingly, the negative effect of HLA-A expression on HIV viremia was worsened when in combination with methionine at position -21, and that therapeutic targeting of this pathway by blockade of the NKG2A receptor may lead to improved disease outcomes (Ramsuran 2018) by removing the 'brakes' on the innate immune system and optimising response to disease – in a way similar to how immune checkpoint inhibitors work in immunotherapy of cancer. This research, and others like it, has recently added fuel to a rapidly expanding field of research that aims to ascertain the clinical value of inhibiting certain elements of the immune system. The aim of this is to achieve greater functional responses to disease states such as cancer and viral infection. Some of these approaches will now be discussed.

1.5 Immune checkpoint inhibition

A comprehensive genome-wide bioinformatics search has revealed that there are likely to be more than 300 integral membrane proteins that contain at least one ITIM domain in humans (Daëron 2008). Despite this prevalence, or perhaps because it is so widespread, there are few therapeutic strategies aimed at targeting these receptor pathways. Both NKG2A and KIR2DL1 receptors exert strong inhibitory effects through the pathways previously discussed. It is also clear that NK cell activation is key to many immunological defence mechanisms. This has led investigators towards the natural question of whether blocking such pathways may result in an enhanced NK cell effector function, a process known as checkpoint inhibition.

Immune checkpoint inhibition is a rapidly growing field in cancer therapy with NKG2A (Creelan 2019) now joining more established targets such as PD-1 and cytotoxic T-lymphocyte antigen-4 (CTLA-4) (Haanen 2015). The notion that checkpoint inhibition can unleash and enhance immune responses in humans has been well evidenced. Indeed, the 2018 Nobel Prize for Medicine was awarded to two scientists (Allison and Honjo) who pioneered work in this

field. In 1996, it was first shown that anti-tumour activity in mice could be improved by anti-CTLA-4 therapy (Leach 1996), where earlier work had also identified PD-1 as a 'brake' on the immune system which could be removed to enhance effector function (Ishida 1992). One of the original key drugs used in this approach was a fully human monoclonal antibody Ipilimumab, which was used to target CTLA-4 in patients with advanced melanoma (Hodi 2010). This important clinical trial in over 600 patients with previously treated metastatic melanoma showed an improvement where patients receiving Ipilimumab plus gp100 (a glycoprotein peptide vaccine) displayed a median overall survival of 10.0 months, versus 6.4 months among patients receiving gp100 alone. CTLA-4 is constitutively expressed by FOXP3-expressing regulatory T cells (Tregs), and is upregulated by CD8+ T cells in response to activation, such as tumour activity. Its mechanism of action involves inhibiting T cell receptor (TCR) signal transduction by binding to TCRζ (an amplification module in the TCR signalling cascade) and inhibiting tyrosine phosphorylation after T cell activation (Lee 1998c).

Other well-established drugs in the class of checkpoint inhibitors are Pembrolizumab (a humanized IgG4 monoclonal antibody to PD-1) and Nivolumab (a fully human IgG4 monoclonal antibody to PD-1). PD-1 is expressed on the cell surface of T cells, and in general protects against autoimmunity by promoting apoptosis (programmed cell death) of antigen-specific T cells residing within lymph nodes and also contributes to reducing apoptosis in Tregs, which leads to an increased regulation of immune responses (Francisco 2010). Its ligand, programmed death-ligand 1 (PD-L1), is expressed by immune cells, including NK cells, and is often upregulated in response to IFN-γ. The PD: PD-L1 pathway is critical for the termination of immune responses (Hu 2019). Targeting this pathway has been shown to be effective in clinical trials of patients with various malignant conditions including non-small cell lung carcinoma, urothelial bladder cancer, relapsed or refractory Hodgkin's lymphoma and melanoma (Darvin 2018).

Of relevance to this project, blocking antibodies specific for both NKG2A and KIR2 antibodies have recently been developed. Blockade of inhibitory KIR receptors has also been explored, mainly in cancer settings. The first-in-class monoclonal antibody Lirilumab exhibits anti-KIR2DL-1, -2 and -3 cross-reactivity (Romagné 2009). Whilst there has been some evidence in pre-clinical studies to support its safety profile and KIR occupancy capability in various malignancies (Vey 2018), results from initial monotherapy clinical trials have shown that there appeared to be no clinical benefit in terms of leukaemia free survival in acute myeloid leukaemia (Vey 2017). Combination therapy with other chemotherapy agents (e.g. Azacitidine) continues to be explored however (Yalniz 2018).

One of the earliest studies that aimed to evaluate the effect of acute NKG2A blockade used a combination of human and mouse studies. This study (Li 2013) attempted to ascertain the role of NKG2A and its ligand in the response to chronic hepatitis B virus infection (HBV), where this orthohepadnavirus is a major cause of chronic hepatitis, liver cirrhosis, and hepatocellular carcinoma (Liu 2007). Interestingly, they initially found that levels of NKG2A were reduced in patients displaying inactive chronic HBV, when compared to active disease. This suggested that NKG2A could be inhibiting the response to infection. Next, they found that blocking either components of the NKG2A-HLA-E pathway resulted in increased peripheral NK cytotoxicity *in vitro*, in patients with active CHB. This was achieved by using either an anti-HLA-E antibody (clone MEM-E/07), or an anti-human NKG2A antibody (clone Z199). Finally, they used anti-NKG2A/C/E (clone 20d5) or an anti–Qa-1 antibody (clone 6A8.6F10.1A6) to do the same in HBV carrier mice, and found that both modes of blockade resulted in increased viral clearance. This was shown to be NK-dependent, as in mice where NK cells were depleted using anti-AsGM1 (As-GM1 is a glycolipid expressed by NK cells, and T cells in response to viral infection), this effect was absent.

Specific blockade of NKG2A through checkpoint inhibition restores the cytotoxicity of NK cells and T cells against HLA-E expressing targets in chronic lymphoid leukaemia *in vitro* (McWilliams 2016) and in phase II clinical trials targeting squamous cell carcinoma (Andre 2018). Monalizumab is a specific humanized anti-NKG2A antibody (Andre 2018) that has been shown to enhance effector function of both T-cells and NK cells. Initial justification for its potential efficacy was provided *in vitro* by showing that NKG2A checkpoint inhibition occurred through Fc-blocking mechanisms, and that such blockade could restore NK cytotoxicity against HLA-E expressing targets in a chronic lymphoid leukaemia setting (McWilliams 2016). A more recent study has also shown that NK cell-knockdown of NKG2A also results in increased anti-tumour activity towards HLA-E expressing tumour cells *in vitro* (Kamiya 2019). Encouragingly, when used in combination with Cetuximab (a monoclonal antibody commonly used to treat bowel cancer by targeting epidermal growth factor receptors), phase II clinical trials have shown a 31% objective response rate in previously treated squamous cell carcinoma (Andre 2018). Unleashing anti-tumour effects of both NK cells and T cells reportedly mediated this clinical improvement, whereas another report has shown potential when blocking NKG2A-expressing T cells in cancer vaccination (van Montfoort 2018).

An obvious question raised by the previously described checkpoint inhibition data is – can the same strategies be used to optimise immune cell responses in the context of pregnancy? This is important for two reasons; i) pregnancy does not preclude one from malignant disease, and shouldn't act as a barrier to treatment where delays in initiating therapy could be fatal, and ii) the enhancement of immune cell effector function may be helpful in preventing or treating certain non-malignant disorders of pregnancy e.g. pre-term labour, pre-eclampsia. Finally, there is obviously a significant question of risk of teratogenicity (abnormalities in fetal physiological development) to the fetes when such medications are administered systemically to pregnant woman.

There have been three case reports that go some way to answering this question. Whilst there has been one report that Ipilimumab administration in Cynomolgus monkeys lead to increased poor pregnancy outcomes, including stillbirth (FDA 2015), there have been no clinical trials in humans. Anti PD-1 therapy is currently listed as 'Category D' by the U.S. Food and Drug Administration (FDA), which is described as 'There is positive evidence of human fetal risk based on adverse reaction data from investigational or marketing experience or studies in humans, but potential benefits may warrant use of the drug in pregnant women despite potential risk'. However, two cases of metastatic melanoma in pregnant women being successfully treated with double immune therapy aimed at T cells (Nivolumab plus Ipilimumab) have been reported with successful live births. These cases also reported good neonatal outcomes and an absence of significant maternal adverse effects (Burotto 2018; Xu 2019). A further case has been reported where Ipilimumab monotherapy was used to treat metastatic melanoma alongside IL-2 in early pregnancy, with a successful and uncomplicated delivery (Mehta 2018). Whilst the overall risk vs. benefit profile of such therapy in pregnancy needs to be further evaluated, these reports provide early promise for their potential safety.

Clearly, the ability to block NK inhibition may enhance effector phase response by unleashing NK cytotoxicity is a potential area for great therapeutic development in cancer patients. However, there are states of physiology, e.g. pregnancy, where the function of tissue-resident NK cells may not rely upon degranulation and target cell elimination. To consider the role of NK cells in pregnancy, and how their functional role may be uniquely adapted to their cellular environment, it is worth considering how normal NK mechanisms may be operating at the maternal-fetal interface.

1.6 Immune cells in human reproduction

a. Rejection of allogenic tissue

Ever since Peter Medawar's famous essay discussing the immunological paradox of pregnancy (Medawar 1953), researchers and clinicians have been aiming to delineate how the semi-allogenic fetus is tolerated. Medawar's pioneering research discovered that tolerance to transplanted skin from a genetically different individual could be induced in very young animals, therefore opening up the possibility of accepting allografts. Having worked with skin grafts to treat large burns in World War II soldiers, he also mused on the question as to – how does a fetus displaying non-self antigens evade maternal immune response and rejection, hence comparing the fetus to a semi-allograft.

To best answer this question, it is important to briefly understand the key discoveries, which led to our current understanding of transplantation genetics. A landmark paper, considered by many as perhaps the most important piece of Immunological research ever, underpins many of our current theories. Sir Frank MacFarlane Burnet (later awarded a joint-Nobel prize with Peter Medawar in 1960), an Australian virologist better known for his contributions to Immunology, initially published his work alone, however with the assistance of co-author Frank Fenner, republished a revised 142-page report entitled 'The Production of Antibodies', some eight years later (Burnet & Fenner 1949). This paper described how every T- and B-lymphocyte (T lymphocytes had not been discovered yet) expresses a single receptor for a specific foreign antigen, and that these are produced through random gene rearrangement in fetal life (the genetic principle for the generation of antibody diversity was confirmed in later work by Susumu Tinegwa, who was also awarded the Nobel Prize in 1987). Necessarily, lymphocytes expressing receptors for fetal self are deleted to prevent autoreactivity, and the vast majority of mature lymphocytes never encounter their specific antigen. Those that do, specifically B-lymphocytes, undergo selection and produce many copies of themselves, the theory underpinning clonal expansion.

This initial 1941 theory by Burnet and colleagues was soon proven correct by some of Peter Medawar's work in skin transplantation, briefly mentioned above. Broadly speaking, when working at the Burn Unit of Glasgow's Royal Infirmary, Medawar and colleagues soon noticed that all skin grafts failed, and recognised this as likely to be a rejection seeded in immunological responses. Medawar returned to his studies in Oxford in 1944, and used a rabbit model of transplantation to prove this theory, that it was immune cells at the heart of skin graft rejection (Medawar 1944). His next key discovery, in 1953, was also a landmark study. With his colleagues Leslie Brent and Rupert Billingham, he inoculated mouse fetuses of

strain A with donor strain B splenocytes *in utero*. It was reported that as adults, the A survivors of the B inoculation would only accept skin grafts from the donor B strain, and not others (Billingham 1953). This showed that skin-graft rejection was not inevitable, and that tolerance could be induced. This work was supported by important work which further described the specificity of antibody production by individual 'plasma cells' isolated from rats immunized with both *Salmonella typhi* and *Salmonella adelaide* (Nossal 1958).

In parallel, in the 1960's, research into bone marrow transplantation paved the way for a role for NK cells in transplantation based on missing-self recognition (Kärre 1986). This alternative theory suggested that rejection of non-self wasn't solely mediated through the presentation of MHC-associated antigenic proteins to specific lymphocyte receptors, as it is the case for T cells. This was because this theory, in part, didn't explain how cells lacking MHC expression could also be identified and eliminated. The seminal study by Kärre and co-authors used mice and MHC-deficient tumour cells to show that NK cells are the likely effector cells and were programmed to identify cells expressing reduced or absent self-MHC (Kärre 1986). This was reported on the basis that murine lymphoma cells with no H-2 (murine MHC) were less malignant in inoculated syngeneic hosts than the same lymphoma cells that instead did express MHC. This phenomenon was found to be non-adaptive, and therefore not likely to be controlled by T- or B- lymphocytes, implicating NK cell action. One important cell type, which does not express MHC, is erythrocytes (red blood cells), yet they appear to evade elimination by NK recognition of missing-self. This is achieved through a separate receptor-ligand pathway, where expression of CD47 by erythrocytes is protective. CD47 is expressed on all cells, and serves as the ligand for the inhibitory receptor signal regulatory protein alpha (SIRPα), key to inhibiting the activity of macrophages. Recipient mice quickly eliminate RBC's from *Cd47*^{-/-} mice, providing evidence that CD47 acts as a RBC marker of self (Oldenborg 2000). As NK cells are not known to express SIRPα (Kim 2008), it is possible that RBCs evade the missing-self response because they also lack ligands that would engage activating receptors on NK cell surfaces.

A number of theories have since been proposed to solve how these pathways operate in the context of pregnancy. One way in which these pathways differ is highlighted by the unique MHC expression repertoire of EVT. HLA-A, -B and –C are expressed by almost all nucleated cells. Most peripheral cells express HLA-A and HLA-B at high levels, in contrast to HLA-C which is lowly expressed (around 10% of that seen in HLA-A and –B), possibly as a result of faster mRNA degradation resulting in low mRNA: protein levels (McCutcheon 1995). Taken alongside the evidence that very few CD8+ T cells are restricted by HLA-C (Matthews 2008),

and that T cells are present in small numbers in early pregnancy (Moffett 2004), it is suggestive that T cells play minor roles in the recognition of EVT. In contrast to peripheral cells, fetally-derived placental cells in early pregnancy display a completely different array of MHC molecules on their cell surface. Primary villous trophoblast cells do not express any HLA, whereas EVT have been shown to express HLA-C, trophoblast-specific HLA-G and HLA-E. Additionally, unlike most peripheral nucleated cells, EVT do not express HLA-A, HLA-B or HLA-DR (an MHC class II molecule, which also serves as a T cell receptor ligand) in physiological states of pregnancy (Apps 2009).

Conversely, uterine NK cells express a number of receptors capable of recognising these ligands expressed by EVT, including numerous KIR which binds HLA-C, Leucocyte immunoglobulin-like receptor subfamily B member 1 (LILRB1) which binds all MHC class I, and NKG2A which binds HLA-E. These data point towards a dominance of NK cell-EVT interactions in early pregnancy, over other immune pathways. Ultimately, EVT express maternal antigens and therefore avoid 'missing-self' elimination, but also do not express MHC molecules typically associated with initiating a T cell response to allogenic material. Taken together, these data go some way to explaining why EVT are tolerated by the maternal immune system, as T cells do not display any obvious recognition capability.

There is a more plausible case to be made for the role of antigen presenting cells (APCs e.g. macrophages, dendritic cells) in pregnancy. Alongside NK cells, macrophages are the most abundant immune cell at the maternal – fetal interface in early human pregnancy (King 2000). Whilst their function is yet to be understood, their presence suggests a possibility for *indirect* recognition of trophoblast by T cells, through the presentation of their molecules by APCs. It has been suggested that Dendritic cells (DC) may contribute to maternal tolerance of semi-allogenic tissue in pregnancy through the production of IL-10, which is known to be important for the generation of Tregs (Blois 2007), and more generally, to induce a tolerogenic type of immune responses.

b. Uterine immune cells

It has long been established that immune cells may play a key role in human pregnancy. It was important to precisely characterise when, during a natural menstrual cycle or pregnancy, immune cells operate. Various members of the Department of Pathology at the University of Cambridge carried out a lot of this work. In 1987, endometrial stromal granulocytes were identified as members of the large granular lymphocyte (LGL) family, and reported to be prominent in late luteal phase human endometrium (Bulmer 1987). Important other early

studies showed that NK cells in the non-pregnant endometrium displayed a marked increase in numbers by the time the implantation window arrived, during the secretory phase of the menstrual cycle. This suggested a role for LGLs in promoting trophoblast invasion, which was likely to be under hormonal control (King 1989). This fitted coherently with earlier findings that lymphoid cells were at large in the early placental bed (Bulmer 1984).

Interestingly, soon after, it was found that these decidual LGL cells exhibited NK activity against the K562 cell line, but did not exhibit cytolytic activity against early pregnancy trophoblast cells (King 1989). Importantly, it was shown soon thereafter that these decidual LGL cells were capable of lysing fetal fibroblasts and JEG-3 choriocarcinoma cells when stimulated by interleukin 2 (IL-2) (King 1990; King 2000). Identification of the common NK cell surface receptor, CD56, brought the scientific field closer to recognising LGL cells as NK cells. Through phenotypic analysis, it was shown that decidual LGLs express CD56 at much higher densities (almost 22x higher) than their peripheral counterparts, but are negative for CD16, suggestive of a distinct NK subgroup with tissue-specific adaptations (King 1991; King & Loke 1991) including the production of important cytokines such as GM-CSF (Jokhi 1994).

Many studies have since described, in detail, the anatomical location and phenotypic characteristics of human uNK. However, one standout paper describing the functional capabilities of human uNK cells was published in 2006 (Hanna 2006). This study reported a general phenotype of chemokine production, supporting a 'peaceful' model for immune cells in the decidua. More specifically, a previous gene expression analysis by microarray comparing blood and uterine NK cells revealed a striking transcriptional profile characterised by transcripts encoding angiogenic factors and endothelial mitogenic stimulants including vascular endothelial growth factor (VEGF) and placental growth factor (PLGF) (Koopman 2003). Additionally, several genes encoding chemokines such as IL-8, interferon-inducible protein (IP)-10 and CCL5 (RANTES) were also reported. Furthermore, these factors were expressed in much higher concentrations by uNK when compared to peripheral blood NK cells (pbNK), when stimulated by IL-15.

A more recent attempt to characterise the functional capacity of uNK, and specifically to identify the subtypes within them, has added further insight to these tissue-resident cells (Vento-Tormo 2018). This was achieved through single-cell RNA sequencing analysis of uterine cells from early pregnancies. A key finding was the presence of three major subsets of dNK cells (termed dNK1-3), all with distinctive phenotypic identifiers and immunomodulatory and chemokine profiles. It was found that dNK1 cells express higher levels of KIR capable of

binding HLA-C ligands, and is the only subset expressing the LILRB1 receptor that recognises the trophoblast-specific HLA-G with high affinity. In addition, dNK3 expressed NKG2A at low levels when compared to the other subsets. These findings point towards a recognition/response to EVT role for dNK1, and have been internally validated by finding corroborating protein expression through mass cytometry (Huhn 2020).

The previously discussed mechanisms by which EVT avoid triggering harmful maternal immune responses was also described by Vento-Tormo and colleagues (Vento-Tormo 2018). They showed that dNK1 cells expressed high levels of the anti-inflammatory Serine protease inhibitor Kazal-type 2 (SPINK2). Similarly, they also reported that the gene for the anti-inflammatory lipocortin I protein, ANXA1, was expressed at high levels by dNK2 and dNK3. Finally, they show that EVT express programmed death-ligand 1 (PD-L1) in the decidua basalis, the maternal uterine layer where the trophoblast invades, which acts as a checkpoint inhibitor to down modulate the activation of T cells through PD-1.

Much of the clinical and scientific emphasis on how immune cells contribute to human reproduction has focussed on NK cells. However, it is important to also consider the other cellular populations present in the uterine stroma, which contribute to the immune milieu in early pregnancy. It is beyond the scope of this thesis to comprehensively discuss all of these cells, however, a final notable pathway will be briefly discussed now. Regulatory T cells (Tregs) are a T cell subgroup known to play a role in the prevention of autoimmunity by maintaining tolerance to self-antigens, and have been implicated in human pregnancy as a potential part of the mechanism providing tolerance to fetal antigens (Zenclussen 2006). Having been shown to be higher in the decidua of human pregnancies collected after *induced,* compared to *spontaneous,* abortions (Sasaki 2004), they have also been associated with pregnancy success in mice, where their absence led to a failure of pregnancy caused by immunological rejection (Aluvihare 2004; Samstein 2012). However, given the role played by Tregs in other tissues, it is not excluded that Tregs may play tissue homeostatic roles in the decidua too (Panduro 2016)

A discussion of the immunological aspects of the fetal–maternal relationship in pregnancy would not be complete without mentioning rhesus incompatibility, commonly known as Haemolytic Disease of the Fetus and Newborn (HDFN). The understanding of this condition has its roots in adult-adult blood transfusion however, where a case report in 1939 famously described an unexpected transfusion reaction in a recipient from an ABO-group matched donor (Levine 1939). A woman in her first pregnancy suffered a stillbirth, thought to be due to HDFN, and unfortunately also suffered from post-partum haemorrhage (PPH). As her husband

was blood group O, she was transfused some of his blood. What was surprising was that she suffered a reaction, where the isoagglutination observed in her blood (antibody-mediated clumping of cells) was reported to have been potentially caused by a potential unknown RBC antigen.

This antigen, known as rhesus factor, was subsequently confirmed using animal experiments in 1940 (Landsteiner & Wiener 1940). It soon became clear that if mothers were sensitised to fetally-derived rhesus factor in pregnancy (a rhesus negative mother and a rhesus positive father) through the mixing of blood (potential caused by abdominal trauma, placental separation and at delivery) it could cause the production of anti-Rhesus IgG antibodies in the maternal circulation. These antibodies can cross the placenta and cause a severe antibody-mediated reaction to fetal RBCs in future pregnancies (if the rhesus incompatibility persists). This is almost always caused by the D variant of fetal rhesus antigen (RhD), although others can occur rarely. These types of reactions cause complex morbidity to the fetus *in utero*, who often go on to develop reticulocytosis (increased numbers of immature RBCs), anaemia, heart failure (known as hydrops fetalis) or even intrauterine death. The modern obstetric practise of screening every mother for their rhesus type, and treating them with anti-D antibodies after sensitising events to ensure that fetal RhD antigens are 'mopped up' prior to the maternal system being able to generate their own antibodies, is extremely effective and has protected millions of pregnancies over the past few decades.

c. Immunogenetics of human pregnancy

Having discussed some of the basic premises upon which our understanding of reproductive immunology lies, more specific biological interactions between the mother and fetus will now be examined. Alleles of the maternal KIR2DL1 gene, which is present in most individuals and encodes an inhibitory NK receptor present on about 40% uNK, are associated with increased risk of pre-eclampsia (Hiby 2004). This initial work perhaps provided the very foundation for which a significant amount of research has been performed since. In this landmark study, DNA from 200 pregnant women with preeclampsia, and from 201 matched women who had normal pregnancies, was genotyped for KIR-2DL1, 2DL2, 2DL3, 2DL5, 2DS1, 2DS2, 2DS3, 2DS4, KIR1D (2DS4 allele with a 22-bp deletion), and 3DL3, alongside genotyping for HLA-C to ascertain whether individuals were C1+HLA-C or C2+HLA-C. Significantly, mothers lacking most or all activating KIR (AA genotype) when the fetus possessed C2+HLA-C, were at increased risk of preeclampsia (odds ratio 2.38, n = 109 pregnancies). Of further interest was that this remained true when the mother herself also had C2+HLA-C. This provided strong evidence to support

the notion that neither non-self nor missing-self discrimination are key components of maternal-fetal interactions in human pregnancy.

In contrast, maternal KIR2DS1, KIR2DS4 and KIR2DS5, which are present in a fraction of individuals and encode activating uNK receptors, are associated with decreased risk of pre-eclampsia (Hiby 2010; Kennedy 2016; Nakimuli 2015). These associations are also often stronger in combination with fetal C2+HLA-C, known to be expressed by the invading extravillous trophoblast (EVT), and capable of ligating both inhibitory KIR2DL1 and activating KIR2DS1, KIR2DS4 and KIR2DS5. This epidemiological evidence suggests the working hypothesis that combinations of maternal KIR and fetal HLA-C impede placentation through excessive uNK inhibition, whereas a background of uNK activation is associated with protection from pre-eclampsia (Moffett & Colucci 2015). This hypothesis is supported by experimental studies in mice, where some aspects of the pathology, such as fetal growth restriction and insufficient vascular remodelling, are recapitulated in mice in which uNK are strongly inhibited (Kieckbusch 2014).

In order to effectively use animal models to recapitulate states of growth restriction or poor placentation, it is important to understand how these disease states manifest clinically in humans, and how they are detected. By understanding how certain imaging modalities relate to the underlying placental and/or fetal pathophysiology, one is better equipped to design animal models and assays where clinical translatability may become possible. Some of the key clinical approaches to detecting *in utero* pathology in human pregnancy will now be discussed.

1.7 Fetal growth restriction in humans

a. Screening of fetuses

In human pregnancy, fetal growth restriction (FGR) (also commonly known as intra-uterine growth-restriction, IUGR) can loosely be defined as a condition where the fetus fails to reach its genetically pre-determined growth potential *in utero* (Bettiol 2019). It is a serious clinical condition, and is one of the most important risk factors for stillbirth (defined as a baby delivered with no signs of life known to have died after 24 completed weeks of pregnancy) (Royal college of Obstetricians and Gynaecologists, RCOG, 2010). Stillbirth is surprisingly common, with 1 in 225 pregnancies in the UK affected, which is the equivalent to 9 cases every day.

Whilst a number of acute and chronic conditions can give rise to FGR, a generally accepted screening tool to measure growth *in utero* is to simply measure various fetal anatomical

components through ultrasound, and to plot the resultant estimated fetal weight (EFW) on a growth chart comprised of centiles. Commonly used growth centile reference standards were developed by using combinations of fetal biometry parameters to predict fetal weight. For example, the Hadlock formula was developed by prospectively collecting fetal biometry data and actual birthweights in 167 fetuses (Hadlock 1984). Despite this seemingly small and homogenous reference sample, this population remains the gold-standard reference population across most centres in the UK and US today.

The Hadlock formula estimates fetal weight by incorporating measurements of the fetal skeleton (femur length, FL), abdominal circumference (AC) and head circumference (HC). A variant of the Hadlock formula also include a measurement of bi-parietal diameter (BPD) alongside FL, AC and HC (Hadlock 1985). Other similar formulas include the Shepard formula (BPD and AC) (Shepard 1982), Woo formula (BPD, AC and FL) (Woo 1985) and the Higginbottom formula (AC only), among others.

A simple screening tool used to detect those fetuses at risk of FGR is to investigate all babies who classify as small-for-gestational age (SGA). SGA is usually defined as all fetuses who fall below the 10th centile of estimated fetal weight of the reference population. This classification was originally introduced in 1995 by the World Health Organization (WHO) (de Onis 1996). However, it is known that the majority of the fetuses who fall into this category simply represent healthy but small (i.e. constitutionally small) babies, who may have parents with short stature. Diagnosing all fetuses below the 10th centile as FGR would likely lead to a large number of false-positives and increased the risk of unnecessary and potentially harmful medical intervention.

Whilst the 10th centile of expected fetal weight has its uses, as a stand-alone test it is not sufficient. Indeed, this approach alone is unlikely to prevent all cases of stillbirth occurring after 32 weeks gestation, as the majority of these fetuses are not small for gestational age (Vasak 2015). In addition, it is also useful to consider the possibility of FGR in any fetus who is dropping down growth chart centiles of EFW, a term described as *reduced growth velocity,* whether they are below the 10th centile or not. Indeed, it has been shown that fetuses displaying reduced growth velocity in the third trimester of pregnancy often bare the hallmarks of placental insufficiency at birth, even if they are born within 'normal' birthweight ranges (MacDonald 2017). With both these clinical scenarios in mind, it has become important to develop non-invasive imaging tools capable of discriminating healthy SGA and pathological

FGR fetuses within all those below the 10th centile of EFW, and also in those displaying reduced growth velocity.

A number of ultrasonographic indices are currently in clinical use to achieve this end, and these are often used in combination, and as part of the broader clinical picture in each pregnancy. One key parameter used is the assessment of growth *symmetry*, where those fetuses displaying asymmetric growth are more likely to be suffering FGR than those symmetrical fetuses. It is generally believed that symmetrical growth is desirable as it is suggestive of an even distribution of fetal resources (e.g. oxygen, glucose) throughout the body. Compensatory measures do exist within human fetuses where placental function may not be optimal. Of most significance is the fetal compensatory mechanism commonly known as 'brain sparing', which will be discussed at length below.

Combining ultrasonographic measurements with maternal serum biomarkers to identify at-risk fetuses is an exciting area of research in this field. Many serum candidates have been postulated recently, with the soluble fms-like tyrosine kinase 1:placental growth factor (sFLT1:PlGF) ratio initially providing promising results (Gaccioli 2018). More recently (Sovio 2020), the ratio between two pairs of metabolites - (1-(1-enyl-stearoyl)-2-oleoyl-GPC (P-18:0/18:1) and 1,5-anhydroglucitol) and (5α-androstan-3α,17α-diol disulfate and N1,N12-diacetylspermine)- predicted FGR at term with almost twice the discrimination capability as the initial Gaccioli et al. study.

Another candidate has recently emerged by using sophisticated mouse models. Delta-like homologue 1 gene (DLK1), also known as fetal antigen 1 (FA1) and pre-adipocyte factor 1 (PREF1), plays a crucial role in adipose homeostasis (Smas 1993). It is the product of an imprinted gene that is predominantly expressed from the paternally-inherited chromosome during fetal development. Produced by fetal tissue, this transmembrane protein undergoes cleavage by extracellular proteases, where its soluble form reaches high levels in maternal circulation towards the end of pregnancy. It is known to be produced predominantly by fetal tissue in pregnancy, however, the placenta also produces a certain amount. It was also shown that in the absence of fetally-derived DLK1, the maternal fasting response is impaired (Cleaton 2016). Of interest to this project, this study also found that maternal circulating DLK1 levels in mice predict embryonic mass, and can differentiate healthy SGA from FGR in a human cohort. It was this finding that led me to test the hypothesis that *Klrc1*^{-/-} dams would display reduced DLK1 as a result of reduced embryonic mass and FGR in their fetuses.

b. Cerebral redistribution and the fetal circulation

Fetal cerebral distribution (or brain sparing) is defined as a low middle cerebral artery (MCA) pulsatility index (PI) on Doppler ultrasound (Morales-Rosello 2015). Middle cerebral artery Doppler velocimetry is a non-invasive method employed to assess resistance to blood flow in the fetal brain vasculature during pregnancy (Romero 2015). Pulsatility index in this artery is calculated by subtracting the end diastolic velocity (EDV) from the peak systolic velocity (PSV) and then dividing by the time averaged (mean) velocity (TAV): *PI = (PSV - EDV) / TAV*. During normal pregnancy, this value is expected to increase initially before decreasing as gestation advances, especially after 28 weeks. However, a particularly low MCA-PI is suggestive of cerebral redistribution. This is due to the fact that vasodilation of the MCA results in an increased EDV and increased cerebral blood flow, which drives the PI down.

Additionally, measures of blood flow within the fetal umbilical cord can be used to try to predict or diagnose cases of FGR. Human fetuses are supplied with oxygen-rich blood from the placenta via the umbilical vein. This vessel enters the fetus through the umbilicus and connects with the ductus venosus that, in turn, supplies the inferior vena cava. Oxygenated blood eventually reaches the right side of the fetal heart in the right atrium. Here, a right-to-left shunt occurs where oxygenated blood passes through a hole between the right and left atrium, known as the foramen ovale, and resultantly bypasses the pulmonary circulation. Oxygenated blood reaches the left atrium via the foramen ovale and is then pumped to the fetal brain and vital organs via the aorta. This hole is only supposed to be a feature of fetal physiology, and should close after birth when pressure in the left atrium exceeds that in the right atrium due to a decrease in pulmonary system pressure. Throughout infancy this closure is usually sealed by fibrous adhesions. A condition known as patent foramen ovale occurs when this hole persists into childhood and adult life, and can often need surgical intervention (Alp 2001).

Not all the fetal blood passes through the foramen ovale however, and as a result a second right-to-left shunt is also required. Where blood from the right atrium bypasses the foramen ovale and enters the right ventricle, it is first pumped out towards the lungs via the pulmonary arteries. However, another communicating hole called the ductus arteriosus (or ductus Botalli) exists which channels this oxygen-rich blood directly into the aorta in order to be pumped to the brain and remaining fetal circulation. Again, a persistent ductus arteriosus can be problematic after birth. In normal pregnancy, the ductus arteriosus is maintained by high circulating levels of the prostaglandin E2, produced by the ductus arteriosus itself and the

placenta (Olley 1981). At birth prostaglandin levels significantly drop, and spontaneous closure of the ductus arteriosus normally occurs.

Finally, some of the blood pumped out of the aorta reaches the fetal internal iliac arteries, and exits the fetal body via the umbilicus as the umbilical arteries, where they eventually reach the placenta in a deoxygenated state ready for removal of waste products such as CO_2, and re-oxygenation. As such, the umbilical artery pulsatility index (UAPI) is thought to be a reliable surrogate marker/indicator of placental pathology. The proposed mechanism for this suggests an underlying placental pathology that leads to a reduced villous surface area (e.g. poor development of peripheral placental villi) that results in an increased UAPI secondary to a reduction in umbilical artery EDV (Geipel & Gembruch 2009). Indeed, UAPI has been found to be associated with IUGR and pre-eclampsia. In normal pregnancies, the UAPI should start high and decrease as gestation advances. Where a raised PI is caused by reductions in EDF characterised by either absent end diastolic flow (AEDF) or reversed end diastolic flow (REDV), a clear association with perinatal mortality and morbidity exists (Bekedam 1990).

As discussed so far, both UAPI and MCA-PI can be useful diagnostic and predictive markers of placenta-related pregnancy complications. However, when used in combination they may be even more sensitive. The cerebroplacental ratio (CPR) – calculated as a ratio between the UAPI and the MCA-PI – has been shown to correlate more accurately with pregnancy complications effecting fetal outcome, including fetal acidosis, than the individual constituents of the ratio (Bahado-Singh 1999; Gramellini 1992). Other studies have highlighted its importance in identifying compromised fetuses *in utero* (Prior 2013; Sabdia 2015).

As well as serving as a reliable predictor of *in utero* feto-placental pathology, cerebral redistribution has also potential long-term sequelae for affected individuals. In fetuses born at term, a birthweight below the 10th centile is an independent predictor of the presence of brain abnormalities related to underdevelopment of major structures, as detected by magnetic resonance imaging (MRI) (Egaña-Ugrinovic 2013; Sanz-Cortez 2015). The importance of antenatal cerebral redistribution in downstream neurological development has been further evidenced. In one study of term SGA babies, the presence of a normal antenatal MCA-PI in small fetuses was associated with normal neurodevelopmental outcomes, when compared to AGA babies also born at term (Eixarch 2008). Furthermore, an additional study showed that adverse neurodevelopment at one year of age was associated with a raised CPR *in utero* (Rep 2008).

The relationship between FGR, cerebral/umbilical blood flow and brain volume has also recently been explored. One interesting study of term pregnancies found that, in small fetuses, an abnormal UA/MCA pulsatility index ratio was associated with reduced total brain volume and cerebral volume (as measured through fetal brain MRI), when compared to those fetuses with no evidence of cerebroplacental redistribution (Maunu 2007). This supports the notion that altered cerebral blood flow in the antenatal period may lead to post-natal neurological sequelae through aberrations in neurodevelopment.

Finally, the relationship between antenatal fetal brain volume and femur length has also been explored. In one study of 203 normal pregnancies between 20 and 40 weeks gestation, the authors used three-dimensional ultrasound to generate reference ranges for brain volume. In doing so, they were able to correlate brain volume with other parameters of fetal growth such as HC, AC and FL, among others. They found that brain volume was highly correlated with all other standard biometric measures of fetal growth, and suggested that brain volume could be incorporated into the clinical assessment and evaluation of fetal growth *in utero* (Chang 2003). In a further small-scale clinical study, it has also been shown that fetal brain volume measured by 3D ultrasound is smaller in fetuses suffering from severe FGR, when compared to normally grown fetuses (AGA) of an equivalent gestational age (Businelli 2015). This broad association between reduced brain volume and FGR may not be wholly surprising however, as most organ volumes / tissue compartments are likely to be reduced in smaller fetuses. What is of interest, however, is the ratio of brain volume to other fetal organs in growth restriction. One way of accurately measuring the effect of FGR on organ development is by weighing fetal organs post-mortem. Indeed, post-mortem brain: liver weight ratio is often used as a marker of nutrition status in fetuses for diagnosis of FGR. For example, in SGA fetuses, those with obvious placental pathology (diagnosed histologically) had higher brain: liver ratios when compared to other SGA fetuses (Man 2016).

c. Fetal growth and symmetry

In addition to the blood flow velocimetry techniques described above, fetal wellbeing can also be assessed through the ultrasound measurement of fetal growth, growth velocity and growth symmetry. It is worth considering that fetal growth *per se*, as opposed to vascular flow parameters, is seen by some as potentially more useful in identifying FGR as it represents the end-point of a pathophysiological process, as opposed to a subset of it or a causal factor (Sovio 2015). By creating ratios of standardised fetal anatomical compartments, growth symmetry can be assessed. A standard measurement of the fetal head is taken by measuring the head circumference (HC) during ultrasound, where the measurement is taken on an axial plane that

incorporates visualisation of the thalami and cavum septum pellucidum. This can be combined with a measurement of the fetal abdominal circumference (AC), which again is measured in an axial plane, where identification of the fetal stomach, portal sinus and umbilical vein serve as anatomical landmarks for the appropriate level of the upper abdomen. Finally, femur length (FL) is measured when the femur is orientated horizontally (where possible) along its longest possible width.

One of the initial fetal responses to a poorly functioning placental unit is a reduction in abdominal circumference, likely secondary to a reduction in fetal liver size. Resultantly, the fetal HC/AC ratio has been shown to be useful in detecting FGR in human pregnancy. In the original landmark study of this technique, the HC/AC ratio was measured in 568 normal pregnancies from 17 to 41 weeks. The ratio steadily declined from week 17 onwards (i.e. HC becomes relatively smaller as pregnancy advances), until an even sharper drop after 29 weeks to a mean value of 0.96 at 40 weeks gestation. Of note, around 5% of these fetuses were classified as SGA (in this study this was defined as being on or below the 5th centile fetal weight, after corrections made for fetal sex and maternal parity), and interestingly, all were found to display HC/AC ratios above the mean of the normal range (Campbell & Thoms 1977).

The importance of AC in detecting FGR has recently been highlighted by a large, prospective cohort study of over 4000 nulliparous women, known as the Pregnancy Outcome Prediction (POP) study in our Department. There have been few, if any, studies of this power in modern Obstetrics, so this report marks a significant advancement in our understanding of the ultrasonographic determinants and predictors of FGR. By using a composite outcome of neonatal morbidity where one or more of; i) metabolic acidosis, ii) 5 minute Apgar scores or iii) admission to the neonatal intensive care unit (NICU) were used, this study found that estimated fetal weight of <10th centile was only associated with the risk of neonatal morbidity if the fetal AC growth velocity was in the lowest decile. Indeed, in the 172 affected fetuses where both the EFW and AC growth velocity were <10th centile, the relative risk for neonatal morbidity was 17.6 (Sovio 2015).

Furthermore, fetal femur length is often used as a measure of skeletal development during ultrasonography, and has also been shown to correlate with FGR when found to be reduced. A 2012 study went further to delineate this relationship. In this study 156 fetuses with isolated short femur were compared to a control group of 637 fetuses who displayed normal femur length. All fetuses were beyond the 20 weeks' gestation, and fetal outcome measures in this study included SGA, FGR, abnormal UA Doppler studies, trisomy 21 (Down's syndrome) and

skeletal dysplasia. This study reported that of all the fetal outcomes measured, isolated reduced FL behaved as a good diagnostic test for SGA and FGR (Morales-Roselló 2012).

d. Maternal uterine artery

The maternal uterine arteries supply blood to the uterus and most major organs of the female reproductive system. There are two, one on the left and one on the right. They enter the pelvis and eventually cross over the distal ureter. In humans, they branch from the internal iliac artery (anterior division), which itself branches from the common iliac artery. The uterine arteries give off branches to four downstream arteries. These include the vaginal artery, the ovarian artery, the tubal artery and the ureteral artery. Once the main uterine artery reaches the myometrium (smooth muscle wall) of the uterus, it branches into the arcuate arteries supplying the myometrium, and then importantly, the radial arteries that eventually give rise to the spiral arteries. These supply the endometrium and intervillous space in the placenta during pregnancy (Clark 2018). During ultrasonography in pregnancy, a reliable anatomical landmark for identification is the segment of the vessel that crosses anteriorly to the external iliac artery.

In human pregnancy, when measured at the end of the second trimester, uterine artery pressure measurements are used to predict pre-eclampsia and FGR. In this screening test, only high-risk patients (e.g. previous pre-eclampsia, chronic hypertension, low pregnancy associated plasma protein A, PAPP-A) are screened. A large-scale meta-analysis which included 74 studies of pre-eclampsia (total 79,547 patients) and 61 studies of intrauterine growth restriction (total 41 131 patients) found that raised pulsatility index and the presence of 'notching' (a characteristic waveform pattern found in the diastolic phase) best predicted the development severe pre-eclampsia in all pregnancies. However, in the presence of risk factors, a raised resistance index was a better predictor of FGR than other indices used in Doppler ultrasonography (e.g. pulsatility index), which showed moderate – low predictive value (Cnossen 2008).

In mice however, whilst the uterine artery plays a similar functional role, differences in the maternal blood supply to the utero-placental unit in pregnancy exist when compared to humans (Figure 4). Advances in our understanding of these anatomical differences have largely been due to improvements in micro-scale imaging modalities such as micro-commuted tomography (micro-CT) and micro-ultrasound (micro-US). A key 2016 paper used micro-CT to determine the vascular anatomical changes that occur at various time-points of murine pregnancy, specifically in the CD-1 strain of mice. They found that the uterine arteries directly

give rise to radial arteries in both uterine horns where the arcuate artery (present in humans and rats) is absent. The radial arteries are then classified into either pre-myometrial (preferentially supplying blood to the myometrium) or pre-placental. The pre-placental subtypes start as primary pre-placental arteries and differentiate into secondary vessels, which supply the downstream maternal canals and spiral arteries (Rennie 2016). Interestingly, this micro-CT technique has recently been applied to murine placental tissue and offers an exciting avenue of investigation for studying placental structural aberrations in states/models of pregnancy disease (De Clercq 2019).
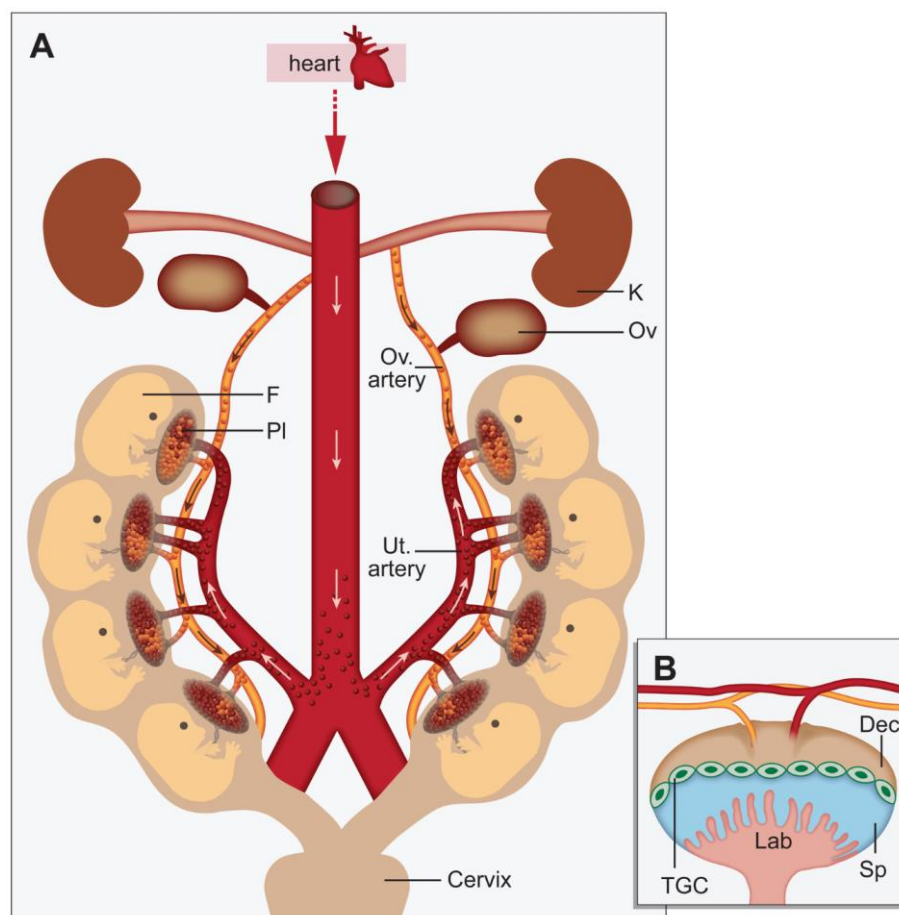

Figure 4. Hemodynamics of maternal arterial supply in the mouse pregnancy. (A) Diagram of mouse uterine horns and their arterial blood vessels in the gestation period after placentas have formed (g.d. 10.5 to term). The results demonstrate that each placenta can be perfused from two maternal arteries. F Fetus, K Kidney, Ov Ovary, Pl Placenta, Ut Uterine. (B) Schematic diagram of mouse placenta. Dec Decidua, Sp Spongiothrophoblast, TGC Throphoblast Giant Cells, Lab Labyrinth. *Image and legend adapted from Raz 2012.

There have been few studies examining the functional role of the uterine arteries in murine pregnancy, and few still that have measured blood flow velocimetry through ultrasound Doppler. The study utilising micro-CT to measure murine gestational haemodynamic changes

by Rennie et al. outlined some of the key changes that occur in terms of vessel diameter, which ultimately impacts on vascular resistance and blood flow. They showed that spiral arteries in mice gradually increase their luminal diameter as pregnancy advances, but that the biggest change occurs between gestational day (g.d.) 9.5-11.5. Uterine arteries also increase their vessel diameter as pregnancy advances, with a significant widening occurring immediately, between implantation and g.d. 5.5. The uterine artery diameter then remains stable until after significant spiral artery remodelling has taken place, and from g.d. 13.5 it then rapidly increases until the end of pregnancy.

One study looked at the impact of angiotensin-converting enzyme 2 (ACE2) genetic deletion, known to cause reduced fetal weight at late gestation, on maternal hemodynamics in mouse pregnancy. They found that ACE2-KO dams displayed an unusual pattern of reduced uterine artery resistance index (associated with a reduction in peak systolic velocity) in combination with FGR and placental hypoxia (Yamaleyeva 2015). Another interesting study aimed to characterise the developmental changes that occur in the murine uterine artery, again in CD-1 mice. They found that both peak systolic velocity (PSV) and end diastolic velocity (EDV) increase as pregnancy advances, which resulted in a resultant decrease in resistance index from implantation towards term. Furthermore, an early diastolic notch was found in early pregnancy, but this was absent after g.d. 14.5 (Mu 2006).

Finally, when embarking upon a project designed to use experimental models to inform and enhance the understanding of basic biology and human disease, it is important to understand the advantages and disadvantages of animal research. One of the mainstays of basic scientific research into pregnancy, and immunology, in recent decades has been the mouse model. Below is a brief discussion of the history of using mouse models in general, and specific examples that are of particular relevance and use to this project.

1.8 Mouse models

a. Humanised mouse models of disease

Humanised mice can include any mice that carry functioning human tissue, cells or genes. Despite the obvious convenience in using these animals that are relatively cheap and easy to house, and have a short reproductive cycle, there are many physiological differences that exist between mice and humans, not least within their immunological system. For example, mice, unlike all other mammalian species, lack a functional Toll-like receptor 10 (TLR10), which serves to down-regulate inflammation in human cells (Jiang 2016). Inter-species variations have led to the need for the development of animal models where human genes / gene

products can be functionally characterised. A key early step in this process was the development of IL-2 receptor common gamma chain (IL2rg^{null}) mice, which lacked high-affinity receptors for a wide range of cytokines, and were immunodeficient (Cao 1995; DiSanto 1995). This mutation could then be combined with other mutations in key elements of the immune system such as Prkdc^{scid} (also known as scid) or recombination activating gene-1 or -2 (Rag1^{null} or Rag2^{null}). These mice were severely immunodeficient and lacked functional features of both the innate and adaptive immune systems (Colucci 1999). These mice were advantageous because, when they became humanised, e.g. by injection of human peripheral blood leucocytes, their physiological responses more closely recapitulated human biological processes than any other previous mouse model (Walsh 2017).

Of relevance to this field, there are mice transgenic for KIR and HLA genes, that is, these genes are inserted at the embryonic stem cell stage and incorporated into the background genetic strain and bred to achieve germline transmission. These include HLA-A2.1 transgenic mice that were used to study T cell responses in a model of hepatitis virus (HCV) (Shirai 1995), HLA-B27 transgenic mice that were used to study spondyloarthritis (Sesma 2003) and HLA-Cw3 transgenic mice that were used to explore the innate function of the molecule itself (Dill 1988). Of course, expression of these human MHC molecules in mice may be made more insightful and interesting when expressed in combination with their cognate human receptors. One study was able to combine a double knock-in to measure the effects of co-expression of HLA-Cw3 and KIR2DL2 on NK cells (Van Bergen 2013). Interestingly, alternative approaches can also include a reductionist system where the endogenous mouse MHC is knocked out, and human HLA-Cw3 and KIR2DL3 are inserted as a single receptor-ligand system (K^{b}D^{b}KO-TgKIR/HLA) (Sola 2009). In this approach, the combination of HLA-CW3 and KIR2DL3 had an educational effect upon the NK cells, restoring the recipients' ability to reject target cells in vivo, whereas single transgene knock-in mice were unresponsive. Also, in this study, the authors were able to block this pathway using a monoclonal antibody (1-7F9, Lirilumab – a fully human monoclonal antibody that recognizes KIR2DS1/S2/L1/L2/L3) to provide evidence for the potential efficacy of the drug in cancer therapy.

This informative study led to further developments in the field, assisted by humanised mice. Using a KIR2DL3 transgenic mouse that lacks T- and B- cells, but not NK cells (Rag1KO-Tg KIR), Lirilumab was trialled in an attempt to impair inhibitory signalling alongside anti-CD20 therapy. It was reported to enhance NK cell function *in vitro* and improve *in vivo* response to murine lymphoma through anti-KIR activity, and is currently undergoing clinical trials in humans (Kohrt 2014). Despite the success of humanised mouse models in the context of

immunology and cancer therapy, almost no data has been reported which utilises these systems to investigate human pregnancy. This could be for a number of reasons, including difficulties encountered when providing evidence of stable protein expression of transgenes in mouse trophoblast cells.

b. Mouse models of pregnancy

Mouse pregnancy differs from human pregnancy in many ways. But some striking similarities also exist. The most significant similarity lies in their shared features of placental structure. First defined as the "apposition or fusion of the fetal membranes to the uterine mucosa for physiological exchange" the placenta is key to all aspects of pregnancy and fetal growth (Burton & Jauniaux 2015). Mouse placentae, like those in humans, rats and many other species, are classified as haemochorial and discoid in shape. Placentae of this type are generally characterised by a barrier between the maternal and fetal circulation that allows for the exchange of nutrients, oxygen and waste products, where under normal conditions, the two blood systems never physically mix. In these instances, maternal blood comes into direct contact with the fetal chorion when blood leaves the spiral arteries and enters the intervillous space, bathing the fetal villous tree (labyrinth in mice) in blood. In many cases of haemochorial placentation, invasion of fetal trophoblast cells into the uterine wall is also a common feature (Soares 2018). It should be noted however that the depth of trophoblast invasion in murine pregnancy is relatively shallower than that observed in human pregnancy (Soares 2017). Other key similarities between murine and human pregnancy are the presence of early gestation uterine NK cells which help to remodel spiral arteries and the fact that a certain degree of invasion of maternal tissue by fetal cells occurs (by EVT in humans and Giant cells in mice).

Other types of placentation include endotheliochorial and epitheliochorial. The former is found in many carnivores, including cats and dogs, and put simply, consists of a system where the fetal chorion comes into contact with the endothelial lining of the supplying maternal vasculature. In contrast, epitheliochorial placentae, seen in ruminants and pigs, are characterised by a barrier consisting of maternal vascular endothelium and uterine epithelium between maternal blood and the fetal chorion (Prabhudas 2015). Comparing the placental types in terms of evolutionary advantage is complex, but in general, placental evolution seems to have occurred in a convergent manner in vertebrates. Some suggest however, that possible advantages of the non-invasive placentae seen in the epitheliochorial type, include the reduction of exposure to the maternal immune system (suggested by some to be potentially hostile) and less potential damage / haemorrhage at the time of fetal delivery (Roberts 2016).

Obviously, significant differences between the two species occur in all aspects of anatomy, physiology and disease, and a few of those relevant to pregnancy will be briefly discussed below. Primarily, mice always have bicornuate uteri consisting of a left and right horn, where multiple concepti can implant and develop. This leads to a higher fertility rate, with an average number of live births (litter size is approx. 7 in C57BL/6 mice, versus approx. 2.5 births per human pregnancy globally). Anatomical uterine abnormalities, including bicornuate uteri do exist in humans, but are rare, where the vast majority of women display a single uterine cavity and display a multiple birth rate of around 1 in 65 births (twins, triplets or more), although it is worth mentioning that this figure has risen over recent years due to the increased use of assisted reproduction technologies such as *in vitro* fertilisation (IVF). A key difference between mouse and human pregnancy at the molecular level is that murine spiral artery remodelling appears to be reliant upon IFN-γ, a cytokine not thought to be of physiological importance in human gestation.

One of the leading laboratories in this field of scientific research has been Anne Croy's group in Canada, although there have been many significant contributors. Many landmark papers have arisen from her and her collaborators over the years, as well as the extremely comprehensive and well-known textbook 'The Guide to Investigation of Mouse Pregnancy', which she co-edited (Croy 2014). Early work first identified uterine NK cells between g.d. 5-7 which were reactive with the lectin Dolichos biflorus agglutinin (DBA), suggesting that these cells gain surface expression of N-acetylgalactosamine (a terminal carbohydrate which DBA has a specificity towards) (Stewart and Webster 1997), where later work suggested that DBA was also a good marker for NK cells which had homed to the decidua (Zhang 2009). This early work was soon followed by reports that aimed to characterise their functional role in pregnancy. It was soon shown that uNK acquire cytoplasmic granules (Peel 1989) containing perforin (Parr 1991), among others, and that IFN-γ was a key product of this cell-type (Platt and Hunt 1998: Ashkar and Croy 1999). In a further attempt to characterise their role in pregnancy, time-course histological studies were reported in due course. In mice with no NK cells (*Rag2$^{-/-}$ IL2rg$^{-/-}$*, discussed above), decidual integrity was reportedly compromised at g.d. 6 (Greenwood 2000), before an absence of spiral artery remodelling due to NK deficiency was observed at g.d. 9-10 in another study elegantly comparing *Rag2$^{-/-}$IL2rg$^{-/-}$* (lacking T, B and NK cells) with SCID mice (NK sufficient) (Guimond 1998).

1.9 THESIS OUTLINE

The specific hypotheses and aims of each project within this PhD will be discussed in the appropriate chapter sections.

In brief, this PhD aims to delineate the mechanisms whereby NKG2A contributes to NK education and pregnancy success through basic scientific assays and clinically translatable micro-imaging modalities in mice. It also aims to investigate how this pathway may influence human pregnancy and conditions such as pre-eclampsia.

A further project aiming to produce a humanised mouse model of pregnancy to gain further mechanistic insight into the previously described KIR2DL1 / C2+HLA-C paradigm, will also be described.

CHAPTER I

The role of NKG2A in pregnancy
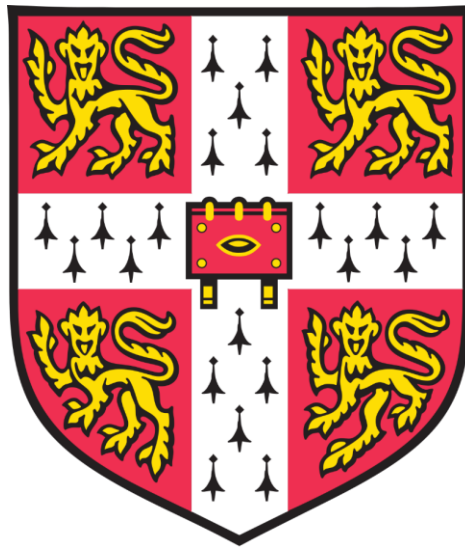
2.0 CHAPTER I – THE ROLE OF NKG2A IN PREGNANCY

2.1 PREFACE

This chapter represents the majority of the experimental work performed during this PhD. It is, therefore, the largest chapter and contributed all of the data to the manuscript entitled '*NKG2A educates uterine NK cells to optimise pregnancy in humans and mic*e' that is currently in the editorial process at *Immunity* journal. As a result, data analysis and experimental work for this project is ongoing and is expected to continue beyond this PhD.

2.2 HYPOTHESIS

Approximately 95% of human uNK cells are NKG2A+ (versus approximately 50% in peripheral blood). NKG2A+ uNK cells recognise HLA-E expressed by both maternal cells in the decidua and by invading fetal EVT. However, the contribution of NKG2A to uNK cell education and how this may contribute to reproductive fitness is unknown. Whilst NKG2A-KO (*Klrc1$^{-/-}$*) mouse models have pointed towards a protective role for NKG2A in response to viral infection, pregnancy outcomes have not been reported in these mice.

It is predicted that the presence of NKG2A on cell-surfaces, or the provision of its functional ligand, will confer a functional benefit to uNK in wild-type mice and humans, through enhanced NK cell education. It is also predicted that the genetic deletion of this receptor will lead to poor pregnancy outcome in mice.

2.3 AIMS

1. Characterise the NKG2A- Qa1^b expression pattern in pregnancy in C57BL/6 mice
2. Ascertain the contribution of NKG2A to NK cell education in general, and in early pregnancy
3. Investigate the relationships between NKG2A education and fetal growth in murine pregnancy outcomes. Specifically, I will investigate NKG2A deletion in a *Klrc1$^{-/-}$* mouse model – this will include experiments which are designed to delineate changes in maternal vascular adaptation, placental transcriptome and fetal growth
4. Measure the effect of NKG2A blockade on fetal growth in C57BL/6 mice
5. Genotype a human pre-eclampsia cohort for HLA-B-21 SNP to assess the role of the NKG2A pathway to human pregnancy disease

2.4 ACKNOWLDGEMENT OF CONTRIBUTIONS

All experimental work in this chapter was carried out by NS, except for the following:

- Delia Hawkes helped in with general animal husbandry, setting-up of matings, vaginal plug checking, collection of fetal and placental weights and assisted in anaesthesia of mice undergoing ultrasound.
- For spiral artery stereology, some of the serial sections were cut by James Warner at the Histology Core dept. Addenbrooke's Hospital.
- After collection of serum, the DLK1 ELISA was performed by Keith Burling at CBAL, Addenbrooke's Hospital. He also provided help with the methodology section for this assay, which can be found below.
- After RNA extraction, RNA sequencing and initial DEG analysis was run by Cambridge Genomic Services (CGS), Dept. of Pathology, University of Cambridge. Stephanie Wenlock (CGS) helped perform this analysis and provided some of the figures/legends found below.
- Keturiah Smithson at the Dept. of Zoology, University of Cambridge, physically scanned the fetuses for micro-CT analysis.
- Chris Cardinal and Delia Hawkes assisted in anaesthetising / recovering mice for Micro-ultrasonography experiments.

3.0 CHAPTER I – METHODOLOGY

3.1 Mice

Mice used for flow-cytometry were bred at the University of Cambridge Central Biomedical Service (CBS, pathogen-free), others were either bred at CBS or the University of Cambridge Combined Animal Facility (CAF). All mice were housed according to U.K. Home Office guidelines. Mouse experiments were approved by the University of Cambridge Ethical Review Panel and carried out in accordance with Home Office Project Licence PPL 70/8222. C57BL/6 mice were purchased from Charles River, UK (CBS) or Envigo, UK (CAF). Mice with a targeted *Klrc1* deletion generated on a C57BL/6 background (*Klrc1$^{-/-}$*) (Rapaport 2015) lacking NKG2A were a kind gift from the Helmholtz-Zentrum München institute. For pregnancy experiments, 8-14-week-old female mice were introduced to males with detection of an early morning copulation plug representing embryonic (E) / gestational day (g.d.) 0.5.

3.2 Genotyping

***Klrc1$^{-/-}$* strain**

The following 25 µl recipe was used to determine copy number for the *Klrc1* allele: DNA 5 µl, oligos 2.5 µl, 10x Taq buffer 2.5 µl, dNTPs (10 mM) 0.5 µl, Taq polymerase 0.25 µl, H$_2$O 9.25 µl Primer 1 (Rev) NKG2A 64181 2.5 µl, Primer 2 (Fw) NKG2A 63972 1.25 µl, Primer 3 (Fw) NKG2A 60665 1.25 µl. The following primer sequences were used: NKG2A 64181 5'-GCTGATTGCTGCTGTGTGTGCA-3'; NKG2A 63972 5'-CCTTGGACAATGAATACGAGTG-3' and NKG2A 60665 5'-ATGTTTCTCTTGGCAGCTG-3'. The following PCR cycle was used: Denaturation; 94°C for five minutes. Annealing and elongation; 35 cycles of (94°C for 30 seconds, 60°C for 30 seconds, 72 °C for 30 seconds). End; 72°C for five minutes. Hold indefinitely at 20°C.

***B2m$^{-/-}$* strain**

The following 20 µl recipe was used to determine copy number for the disrupted *B2m* allele: DNA 1 µl, H$_2$O 6 µl, primer OIMR0160 1 µl, primer OIMR0184 1 µl, primer OIMR0185 1 µl, REDTaq® ReadyMix™ (Sigma-Aldrich, MI, US) 10 µl. The following primer sequences were used: *B2m* Mutant 5'-TCTGGACGAAGAGCATCAGGG-3' (OIMR0160); *B2m* Common 5'-TATCAGTCTCAGTGGGGGTG-3' (OIMR0184), and *B2m* Wildtype 5'-CTGAGCTCTGTTTTCGTCTG-3' (OIMR0185). The following PCR cycle was used: Initial denaturation 98°C for 5min, 40 x (denaturation 98°C for 5s, annealing at 98°C for 5s, exlongation 72°C for 20s), final extension 72°C for 1 min.

Shp-1 conditional-KO strain

Two independent genotyping experiments were performed in order to ascertain the presence of alleles relating to SHP-1 and Cre-recombinase.

***Ptpn6f^flox/flox*:** For PCR, the following 20 μl recipe was used: DNA 1 μl, 2X PCR buffer 10 μl, Phire DNA Polymerase (Thermo Scientific, UK) 0.4 μl, H_2O 6.6 μl, primer OlMR9159 1 μl, primer OlMR9160 1 μl. The following primer sequences were used: OlMR9159 5'-ACCCTCCAGCTCCTCTTC-3' and OlMR9160 5'-TGAGGTCCCGGTGAAACC-3'. The following PCR cycle was used: Denaturation; 98°C for 5 minutes. Annealing and elongation; 40 cycles of (98°C for 5 seconds, 61.5°C for 5 seconds, 72°C for 20 seconds). End; 72°C for 1 minute.

NCR1-iCre: For PCR, the following 20 μl recipe was used: DNA 1 μl, 2X PCR buffer 10 μl, Phire DNA Polymerase 0.4 μl, H_2O 5.6 μl, primer 1 iCre 1 μl, primer 2 iCre 1 μl, primer 3(WT) 1 μl. The following primer sequences were used: iCre 1 (Fw) 5' GGAACTGAAGGCAACTCCTG '3; iCRE 2 (Fw) 5' GTCCATCCCTGAAATCATGC 3', and WT (Rev) 5' TTCCCGGCAACATAAAATAAA '3. The following PCR cycle was used: Denaturation; 98°C for 5 minutes. Annealing and elongation; 40 cycles of (98°C for 5 seconds, 63.1°C for 5 seconds, 72°C for 5 seconds). End; 72°C for 1 minute.

3.3 Tissue processing for flow cytometry

Whole uteri were processed according to previously described protocols (Collins 2009) using Liberase DH (Sigma-Aldrich, MI, US) to conserve the NKG2A epitope during enzymatic digestion (discussed in 4.0 Chapter I - Results). In brief, pregnant females underwent schedule 1 euthanasia by cervical spine dislocation which causes lethal trauma to the spinal cord, where cortical function is absent some 10 seconds after (Cartner 2007). The abdomen was then sprayed with 70% ethanol, before entry to the peritoneal cavity was achieved with sharp dissection. Whole uteri (including implantation sites) were identified and dissected before peri-uterine mesometrial fat was removed. Care was taken to ensure cervical tissue and any ovarian tissue was also removed. The uterine horns were then placed in 1 ml ice-cold Hank's balanced saline solution (HBSS) with calcium and magnesium (HBSS/$Ca^{2+}Mg^{2+}$ 1x, from 10x solution diluted in distilled water, Gibco, Thermo Fisher Scientific, MA, US) in Bijou tubes and placed on ice before being transported from the animal facility to the laboratory. Laboratory conditions were consistent for all FACS experiments, where air conditioning was always turned on at the same temperature for the duration of tissue processing and cell labelling, and artificial lighting was kept to a minimum when using light-sensitive fluorescently-labelled antibodies.

Uterine tissue dissociation protocol 1:

- Once in the laboratory, each implantation site was opened through a transverse incision of the uterine wall overlying the amniotic cavity, using Tweezerman scissors. Fetal tissue was then identified and removed, leaving the uterine smooth muscle, MLAP and decidua for processing. Remaining uterine tissue was weighed using a microscale on those occasions where absolute cell numbers were also being evaluated.

- Uterine tissue was finely minced in 1 ml ice-cold HBSS/Ca^{2+}Mg^2 1X in Bijou tubes, using Tweezerman scissors, before being placed in a water bath at 37°C to warm up. The presence of calcium is important because collagenase (present in Liberase mixes) requires it for its enzymatic activity.

- Next, Liberase DH 0.1 WU/ml (stock 13 WU/ml) for tissue digestion and cell liberation, plus DNaseI 30 μg/ml (stock 20mg/ml) to minimize the presence of free-floating DNA fragments and cell clumps, were added to the Bijou tube in 3 ml of warmed (37°C) HBSS/Ca^{2+}Mg^2 1x. This 4ml solution was then vortexed before being placed inside a pre-warmed oven, at 37°C. The tissue was then agitated on a rotator for 30 minutes to encourage tissue dissociation.

- The contents of the Bijou were then poured into a 15 ml Falcon tube (Fisher Scientific, UK). The original Bijou tubes were then washed out with 10 ml ice-cold 1X phosphate buffered solution without calcium or magnesium (PBS, Gibco, Fisher Scientific, UK) and 5 mM Ethylenediaminetetraacetic acid (EDTA) (PBS/EDTA) and added to the Falcon tube. The lack of calcium at this stage helps to inhibit the action of Liberase to prevent harmful over-digestion. EDTA is also important once the tissue has started to dissociate as it acts as a chelating agent and binds calcium to prevent the binding of cadherins between cells (this can only occur in the presence of calcium). This reduces the clumping together of cells that may subsequently be lost at filtration in later steps.

- The partially dissociated tissue in solution is then centrifuged at 1500 rpm for 10 minutes at 4°C. The supernatant was discarded, and the cell / tissue pellet was re-suspended in 10ml 37°C PBS/EDTA. This solution was then incubated for a further 15 minutes in an oven at 37°C, with agitation to facilitate mechanical tissue dissociation.

- Next, using the plunger of a syringe, the tissue was forced through 70 μm cell strainer (Falcon, Fisher Scientific) into a 50 ml Falcon tube. The filtration membrane was then washed repeatedly to ensure all cells passed into the tube into a total volume of 50 ml PBS. This suspension was then centrifuged at 4°C for 10 minutes at 1500 rpm.

- The supernatant was discarded, and the remaining pellet disrupted before being re-suspended in 8 ml of 40% Percoll solution (Sigma-Aldrich, MI, US). The 40% Percoll / cell solution was then slowly overlaid onto 5 ml of Percoll 80%, with care being taken

to ensure a clear demarcation between the two solutions was achieved. Percoll is a non-toxic colloidal silica coated with polyvinylpyrrolidone used to perform isopycnic separation, also called buoyant or equilibrium separation. During centrifugation, a density gradient is created within cell solutions because cells are separated on the basis of their density as they move until their density matches the surrounding Percoll medium. In this process, dead cells and debris will migrate to the surface of the tube, lymphocytes will form a ring at the interface between the 40% and 80% Percoll solutions, and RBC will pellet at the bottom of the tube. Specifically, in these experiments, Percoll centrifugation was performed at 850 G speed for 20 minutes, at room temperature. Importantly, the deceleration speed of the centrifuge was as slow as possible to avoid mixing of the isolated lymphocyte ring (speeds: acceleration 5, break 1).

- The top layer was discarded to avoid contamination when collecting deeper solutions. Next, using a plastic graduated pipette dropper, the leucocyte ring was extracted and passed into a 50 ml Falcon tube. Once the entire ring was removed, the falcon tube was filled up to 50 ml with ice-cold PBS 1X, and centrifuged at 1500 rpm for 5 minutes.

- Next, erythrocyte elimination was performed using a lysis buffer. 10X PharmLyse™ (BD Biosciences, NJ, US) was diluted with distilled water to create a 1X concentration. This ammonium chloride-based lysing reagent works by causing cell swelling and lysis, as ammonia permeates RBC membranes and causes a disequilibrium of the ammonium-ammonia balance, resulting in a net influx of ammonium-chloride. After the supernatant was discarded, 3 ml of 1X PharmLyse™ to disrupted pellets, and incubated for 3 minutes at room temperature, swirling the tube halfway through. The reaction was stopped by filling the Falcon tube to 50 ml with PBS 1X, and centrifuged for 10 minutes at 1500 rpm.

- The supernatant was discarded, and the pellets resuspended in 10 ml PBS 1X. This cell solution was then re-filtered through a 70 μm cell strainer, as before. Again, the filtration membrane was washed through (10 ml only this time) and centrifuged for 5 minutes at 1500rpm.

- The supernatant was discarded, and the pellet was resuspended in FACS buffer (1L PBS 1X/ 1% bovine serum albumin/ 0.1% sodium azide). The bovine serum albumin is added in order to prevent heterophilic antibody interference, where these endogenous proteins can bind animal antigen and cause both false positives and false negatives in downstream FACS analysis. Sodium azide was added to act as a preservative for antibodies.

- Finally, live cells were counted using a haemocytometer (Neubauer, Germany). I created a 1:1 preparation of cell suspension: trypan blue, and loaded 15 μl into the haemocytometer. Trypan blue is used in order to identify dead cells. As an azo dye, it works by being impermeable to cell membranes, and therefore only being taken up by dead cells where cell membranes have been compromised. Light microscopy was then used to count all cells in all four large outer squares. A minimum of 100 cells was counted, where possible. The following calculation to ascertain cell numbers/ml of cell suspension was used, where a dilution factor of 2 and 1 large square volume was 0.0001ml:

Cells / ml = $\left(\frac{no.of\ cells\ in\ 4\ large\ squares}{4}\right) \times 2 \times 10^4$

Uterine tissue dissociation protocol 2: When phenotyping knockout mouse cells, it is important to establish if there is any effect on the development of cells of interest. As a result, calculating precise cell numbers per gram of tissue or uterus is important. One issue with using a lymphocyte gradient is that there is potential for the loss of cells when doing so. Thus, for certain experiments, no gradient was used, but all other steps in the dissociation protocol remained the same.

Splenic tissue dissociation protocol: whole spleens were processed as per tissue dissociation protocol 1 if being directly compared to uterine tissue. However, in stand-alone experiments, the enzymatic tissue dissociation and extended mechanical dissociation steps were not necessary. Therefore, the following shortened protocol was used:
- Whole spleens were finely minced in 1 ml ice-cold HBSS/$Ca^{2+}Mg^2$ 1X in Bijou tubes, using tweezerman scissors
- Minced splenic tissue was then filtered. Using the plunger of a syringe, the tissue was forced through 70 μm cell strainer (Falcon, Fisher Scientific) into a 50 ml Falcon tube. The filtration membrane was then washed repeatedly to ensure all cells passed into the tube, into a total volume of 50 ml PBS 1X. This suspension was then centrifuged at 4 °C for 10 minutes at 1500 rpm.
- The supernatant was discarded, and the pellet resuspended in 10mls of PBS 1X and filtered through a 70μm cell strainer, again the membrane was washed, and the falcon tube topped up to 50mls with PBS 1X. The tubes were centrifuged at 1500rpm for 10 minutes.
- Red cell lysis was then performed as above, with 3ml of 1X Pharmlyse buffer per sample. Tubes were centrifuged at 1500rpm for 10 minutes.

- Cells were resuspended in 10mls FACS buffer and counted in the same way as described above. Due to the higher cell yield and need for greater dilution to make counting of cells accurate, the following calculation was used:

Cells / ml = $\left(\frac{no.of\ cells\ in\ 4\ large\ squares}{4}\right) \times 2 \times 10^4 \times 10$

3.4 NK education assays

Uterine *in vitro* activation assay protocol

- Uterine tissue was processed at g.d. 9.5 as described above for tissue dissociation protocol 1, where leucocytes were enriched on an 80%/40% Percoll, gradient prior to stimulation.
- 24-well plates were coated with anti-NK1.1 by adding 6ul of anti-NK1.1 antibody (PK136, Biolegend, CA, US) to 300μl of sterile PBS 1X in order to achieve a concentration of 20μg/ml. The plates were left overnight at 4 ℃.
- The following day, the residual PBS was removed.
- Next, cells were added to pre-coated wells in 500μl complete media at 37 ℃ (RPMI 1640, 10% Fetal calf serum, 1X Penicillin /Streptomycin. Cells were incubated with either anti-NK1.1 antibody + 1μl protein transport inhibitor (PTI) (added after 1 hour) or 1μl PTI only, at 37 ℃. Anti-CD107a antibody, at a dilution of 1/200 (2.5μl) was added at the start of the incubations.
- After 9.5 hours of stimulation, the cells were aspirated from the wells and the wells washed 2-3 times with PBS. The cells were transferred into Eppendorf tubes and spun down to create a pellet, before being transferred into 96-well plates for staining.

Splenic *in vitro* activation protocol

This experiment was performed in a similar way to the Uterine *in vitro* activation assay protocol described above. However, the incubation was only for 4 hours, as per previous protocol within the laboratory. Furthermore, the concentration of coated anti-NK1.1 antibody used was 20μg/ml.

***In vivo* rejection assay protocol**

Whole spleens were collected from donor *B2m*^{-/-} and C57BL/6 females, mechanically processed and stained with Carboxyfluorescein Diacetate Succinimidyl Ester (CFSE) for 20 minutes at 37°C. A 50:50 suspension of *B2m*^{-/-} (5mM CFSE) and C57BL/6 (0.5mM) splenocytes were injected into recipient mice and spleen harvested 48 hours later. The ratio of CFSE+:CFSE- cells was ascertained through flow cytometry.

3.5 FACS antibody labelling of cells

This protocol was kept consistent between all experiments, irrespective of the dissociation protocol employed.

- Approximately 1×10^6 cells per well were plated on u-bottom 96-well Falcon polystyrene microplates (Fisher Scientific, UK), in 200µl of FACS buffer, and centrifuged at 1500rpm for 3minutes. The supernatant was discarded and the plate gently vortexed.

- Next, 25µl of Truestain (Biolegend, CA, US) anti CD16/32 (Fc block) was added at a dilution of 1/50, for a final dilution of 1/100 when the antibody mix is added. Fc block is necessary as CD16 (FcγIII) and CD32 (FcγRII) are expressed on NK cells, DC's, macrophages, T cells, B cells and other immune cells. By using Truestain it is possible to block these sites in order to prevent non-specific binding of antibodies, thus preventing false positive signalling in FACS analysis. The cells were incubated in Fc block for 10 minutes at RT, on the bench side.

- 25µl of the extracellular target antibody cocktail were added to each well, and mixed thoroughly with the Fc block suspension. The dilutions of specific antibodies used in each panel can be found below. The antibodies were diluted in BD Horizon brilliant stain buff (BD Biosciences, NJ, US), the precise ingredients of which are not publicly available. However, this buffer is designed to reduce Fluorescent dye interactions which may cause staining artefacts significant enough to impact on data interpretation. 25µl FACS buffer was added to unstained control wells and single-stain viability controls. All wells were incubated for 20 minutes on ice, in the dark.

- 200µl of PBS 1X was added to each well before centrifugation of the plate at 1500rpm, for 3 minutes. Supernatants were discarded, and the plates were gently vortexed.

- Next, 200µl of fixable viability dye was added to all wells, except the unstained control well, to which 200µl of PBS 1X was added. These dyes distinguish live cells from dead cells based on cell membrane integrity and access to available amines, and are specifically designed to preserve their staining pattern throughout fixation. For this step, the wells were incubated for 30 minutes in the dark, on ice.

- The plates were centrifuged for 3 minutes at 1500rpm. The supernatants were discarded, and the plates gently vortexed. All wells were resuspended in 200µl FACS buffer, and centrifuged for 3 minutes at 1500rpm. The supernatants were discarded and the plates gently vortexed.

- All wells were then resuspended in 200µl fixation/permeabilisation buffer, made from 3:1 ratio of fixation/permeabilisation buffer diluent: fixation/permeabilisation buffer concentrate (both eBioscience, Thermo Fisher Scientific, MA, US). This buffer both is used to cross link, stabilize, and fix the cell membrane, whilst simultaneously reversibly

permeabilising the cell membrane, in order to allow intracellular antibodies to enter the cells and reach their epitope targets e.g. nuclear transcription factors. The cells were incubated with fixation/permeabilisation buffer for 45 minutes.

- The cells were next washed through a 3-minute centrifugation at 1500rpm. The supernatant was discarded and the plates were gently vortexed.

- Permeabilisation buffer 1X was made by diluting 10X Permeabilisation Buffer (eBioscience, Thermo Fisher Scientific, MA, US) in distilled water. All wells were resuspended in 200µl permeabilisation buffer 1X and centrifuged for 3 minutes at 1500rpm. Supernatants were discarded, and the plates were gently vortexed.

- Where appropriate, the cells were next resuspended in 50µl intracellular antibody cocktail (antibodies diluted in permeabilisation buffer 1X). This incubation lasted 30 minutes, and was performed at room temperature, in the dark. The dilutions of specific antibodies used in each panel can be found below.

- After incubation, 200µl of permeabilisation buffer 1X was added to each well. The plates were then centrifuged for 3 minutes at 1500rpm, the supernatants discarded, and the plate gently vortexed.

- Cells were stored at 4 °C in PBS + EDTA (1/250) to help reduce clumping, until acquisition.

Compensation panels

- Each of the fluorophores in the panel was used as a single-stain control, alongside the unstained cells and the single-stain viability stain cells in order to create a compensation matrix. A single stain-compensation control means just that, where instead of the entire cocktail of antibodies being used in the well, only one of the antibody-fluorophore conjugates is used. I used UltraComp ebeads (Invitrogen, Thermo Fisher Scientific, MA, US) which will bind any mouse, rat or hamster antibody. These polystyrene microspheres also contain a negative population in the mixture, which is completely unreactive to all antibodies.

- I added 1µl of antibody to 50µl of Ultracomp ebeads in U-bottom 96-well plates. These were left for 20 minutes in the dark.

- Next I added 200µl of PBS 1X and centrifuged the plate at 1500rpm for 3 minutes. The supernatant was discarded and the plate gently vortexed. The beads were stored at 4 °C in PBS + EDTA (1/250) to help reduce clumping, until acquisition.

3.6 Antibody panels for flow cytometry

Panel 1 – Enzyme cleavage of NKG2A testing

	Target	Antibody clone	Fluorophore	Dilution	Laser	Channel
Extracellular	CD45	30F11	BUV379	1:200	UV	379/28
	NK1.1	PK136	PE-CF594	1:100	Yellow	610/20
	NKp46	29A1.4	PerCP-ef700	1:50	Blue	695/40
	NKG2A (B6)	16A11	APC	1:100	Red	670-14
Viability	Live/dead	-	ef780	1:1000	Red	780/60

Panel 2 – Leucocyte phenotyping of *Klrc1*^{-/-} strain

	Target	Antibody clone	Fluorophore	Dilution	Laser	Channel
Extracellular	CD45	30F11	BUV379	1:200	UV	379/28
	CD3	17A2	BV785	1:50	Violet	780/60
	CD8a	53-6.7	BV605	1:100	Violet	605/12
	CD19	1D3	BUV739	1:100	UV	710/50
	CD11b	M1/70	BV650	1:100	Violet	655/8
	NK1.1	PK136	PE-CF594	1:100	Yellow	610/20
	NKp46	29A1.4	PerCP-ef700	1:50	Blue	695/40
	NKG2A (B6)	16A11	APC	1:100	Red	670/14
	CD49a	Ha31/8	PE	1:200	Yellow	582/15
Intracellular	EOMES	Dan11mag	BV450	1:100	Violet	450/50
Viability	Live/dead	-	ef780	1:1000	Red	780/60

Panel 3 – Myeloid phenotyping of *Klrc1*^{-/-} strain

	Target	Antibody clone	Fluorophore	Dilution	Laser	Channel
Extracellular	Ly6C	AL-21	FITC	1:200	Blue	530/30
	CD11c	HL3	PerCP-Cy5.5	1:50	Blue	695/40
	CD80	16-10A1	PE	1:100	Yellow	582/15
	Siglec-F	E50-2440	AF647	1:50	Red	670/14
	CD45.1	30-F11	AF700	1:100	Red	730/45
	MHC-II	APC-f750	M5/114.15.2	1:400	Red	780/60
	Ly6G	1A8	BV605	1:50	Violet	605/12
	CD11b	M1/70	BV650	1:100	Violet	655/8
	F4/80	BM8	BV785	1:100	Violet	780/60
Viability	Live/dead	-	ef450	1:1000	Violet	450/50

Panel 4 – NKG2A/C/E expression testing

	Target	Antibody clone	Fluorophore	Dilution	Laser	Channel
Extracellular	CD45	30F11	BUV379	1:200	UV	379/28
	NK1.1	PK136	PE-CF594	1:100	Yellow	610/20
	NKp46	29A1.4	PerCP-ef700	1:50	Blue	695/40
	NKG2A/C/E or isotype control	20d5	FITC	1:200	Blue	530/30
Viability	Live/dead	-	ef780	1:1000	Red	780/60

Panel 5 – Qa-1^b testing

	Target	Antibody clone	Fluorophore	Dilution	Laser	Channel
Extracellular	CD11b	M1/70	BV650	1:100	Violet	655/8
	NK1.1	PK136	PE-CF594	1:100	Yellow	610/20
	NKp46	29A1.4	PerCP-ef710	1:50	Yellow	780/60
	CD3	17A2	BV785	1:50	Violet	780/60
	CD45	30F11	BUV379	1:200	UV	379/28
	NKG2A/C/E	20d5	PerCP-e710	1:200	Blue	695/40
	Qa-1^b or isotype control	6A8.6F10.1A6	PE	1:50	Yellow	585/15
	CD19	1D3	BUV739	1:100	UV	710/50
Viability	Live/dead	-	ef780	1:1000	Red	780/60

Panel 6 – Splenic *in vitro* activation assay

	Target	Antibody clone	Fluorophore	Dilution	Laser	Channel
Incubation	CD107a	1D4B	FITC	1:200	Blue	530/30
Extracellular	Ly49I	YLI-90	PE	1:200	Yellow	585/15
	CD49b	DX5	PE-CF594	1:150	Yellow	610/20
	NKp46	29A1.4	PerCP-ef710	1:50	Blue	695/40
	CD3	17A2	BV785	1:50	Violet	780/60
	CD45	30F11	BUV379	1:200	UV	379/28
Biotin	NKG2A/C/E	20d5	-	1:50	-	-
Streptavidin	Biotin	-	BV650	1:200	Violet	655/8
Viability	Live/dead	-	ef780	1:1000	Red	780/60
Intracellular	IFN-γ	XMG1.2	APC	1:100	Red	670/14

Panel 7 - Uterine *in vitro* activation assay

	Target	Antibody clone	Fluorophore	Dilution	Laser	Channel
Incubation	CD107a	1D4B	FITC	1:200	Blue	530/30
Extracellular	Ly49I	YLI-90	PE	1:200	Yellow	585/15
	NKp46	29A1.4	BV605	1:12.5	Violet	605/12
	CD3	17A2	BV785	1:50	Violet	780/60
	CD45	30F11	BUV379	1:200	UV	379/28
	NKG2A/C/E	20d5	PerCP-e710	1:200	Blue	695/40
	CD19	1D3	BUV739	1:100	UV	710/50
	CD11b	M1/70	BV650	1:100	Violet	655/8
Viability	Live/dead	-	ef780	1:1000	Red	780/60
Intracellular	IFN-γ	XMG1.2	APC	1:100	Red	670/14

Panel 8 – NKG2A blockade

	Target	Antibody clone	Fluorophore	Dilution	Laser	Channel
Extracellular	NK1.1	PK136	PE-CF594	1:100	Yellow	610/20
	NKp46	29A1.4	BV605	1:12.5	Violet	605/12
	CD3	17A2	BV785	1:50	Violet	780/60
	CD45	30F11	BUV379	1:200	UV	379/28
	NKG2A/C/E	20d5	FITC	1:200	Blue	530/30
	CD19	1D3	BUV739	1:100	UV	710/50
	CD11b	M1/70	BV650	1:100	Violet	655/8
Viability	Live/dead	-	ef780	1:1000	Red	780/60

3.7 Spiral artery stereology

Pregnant females were sacrificed followed by tying-off the uterine arteries to minimize bleeding (Kieckbusch 2015). One uterine horn per mouse was dissected at random. These were fixed for 6 hours in cold 10% formalin before being stored in cold 70% ethanol. Horns were then processed and mounted in paraffin.

Serial sections were cut 7μm apart. Slides underwent haematoxylin and eosin staining through the following cycle: Xylene 10 minutes (x2), 100% ethanol 5 minutes (x2), 95% ethanol 2 minutes, 70% ethanol 2 minutes, brief wash ddH20, Harris haematoxylin 8 minutes, wash with running water 5 minutes, 1% acid-alcohol 30 seconds, wash running tap water 1 minute, lithium carbonate 30 seconds, wash running tap water 5 minutes, 95% ethanol 10 dips, eosin 30 seconds, wash running tap water 5 minutes, 95% ethanol 5 minutes, 100% ethanol 5 minutes (x2), xylene 5 minutes (x 2).

Sections were then mounted in xylene-based mounting medium and slides scanned at 40x using a Nanozoomer slide imager and analysed using NDP.View2 software (Hammatsu Photonics, Japan). Arterial remodelling was assessed in the central 2/4 of the decidua basalis on sagittal sections to avoid inclusion of veins that have been shown to be more peripherally located. For each implantation site, five circle-shaped vessels were measured in triplicate (three sections 49μm apart from each other). Spiral artery wall/lumen area was measured with the assessor blinded to maternal genotype.

3.8 Immunohistochemistry

Following the detection of differences between strains in the H&E analysis, the same implantation sites underwent immunohistochemical analysis of smooth muscle actin expression, as previously described (Boulenouar 2016). In brief, paraffin sections were initially deparaffinised and rehydrated through the following steps: Xylene (5 minutes x 3), 100% ethanol (10 minutes x 2), 95% ethanol (10 minutes x 2), ddH20 (5 minutes x 2). Next, epitopes underwent citrate buffer heat-induced epitope retrieval for 3 minutes (2.94g of 294.1g/mol sodium citrate in 1L ddH20 – pH titrated with 32% HCL), then placed on ice to cool. Slides were then washed in still ddh20 for 5 minutes, 3 times. Peroxidases were then quenched using 3% hydrogen peroxidase (250μl of 30% hydrogen peroxidase in 2.5mls ddH20). Next, each section was incubated in 300μl of mouse on mouse (MOM) blocking kit (Vector lab, MKN-2213) for 30 minutes, in order to block endogenous mouse IgG. Next, MOM was removed and sections were incubated at RT with 300μl mouse anti-human SMA (Dako, Agilent, CA, US: M0851) at a concentration of 1:100, or PBS for control sections. For secondary retrieval, 300μl

MOM biotinylated anti-mouse IgG reagent (Vector kab, MKB-2213) was applied for 10 minutes, then sections were washed in PBS 3 times before being incubated with 300µl ABC kit (Vector lab, PK6100) for 30 minutes. The final labelling step was performed by adding 300µl DAB (Sigma-Aldrich, MI, US, D4168) for 45 seconds before submerging sections in H20, and being counterstained in 50% for 1-minute haematoxylin. Sections were then processed in the following steps: 2 minutes in running water, 15 dips in lithium carbonate, 2 minutes in running H20, 95% ethanol for 10 seconds, 95% ethanol for 10 seconds, 100% ethanol for 10 seconds, xylene for 10 seconds (x 3). Finally, sections were mounted and scanned as per the H&E stereological analysis above.

3.9 High frequency micro-ultrasound measurements

Upon detection of a vaginal mucus plug to confirm mating, each female was assigned a unique ear notch ID code. At g.d. 14.5 mice were anaesthetised using isoflourane (4% induction dose, 2.0-1.5% maintenance dose) plus oxygen (1 L/min) and placed on a heat mat, as previously described (Zhang and Croy 2009; Greco 2013). Temperature was monitored via a rectal probe, and respiratory rate was monitored by an animal technician throughout the procedure. The total procedure time was approximately 30 minutes. Hair removal cream (Nair) was applied to the pregnant abdomen for 2 minutes with the dam supine, then fur was removed using an applicator. Warmed coupling gel was applied to the ultrasound probe. In all cases, a *Vevo 2100* micro-ultrasound machine (FUJIFILM Visualsonics, ON, Canada) was used with a MS500D transducer probe.

For identification of uterine arteries, dorsally recumbent dams were placed head down at approximately 30 degrees to encourage uterine horns away from the scanning window. The uterine artery branches from the common iliac artery, before passing laterally past the utero-cervical junction. When scanning, the maternal bladder was first identified in B-mode, then the probe was moved supero-laterally in colour doppler mode to identify the anatomical location where the uterine artery changes colour from blue to red. This is indicative of a change in blood flow from *towards* the probe, to *away* from the probe. Just distal to this juncture provides a reliable and identifiable landmark from which all Doppler indices were recorded. This is the location where the uterine artery routes latero-ventrally to supply the arcuate arteries to each uterine horn.

Single uterine arteries were identified in virgin mice to minimise anaesthetic exposure, whereas both were measured (and averaged) in pregnant mice to control for variable numbers of concepti in each uterine horn. Peak systolic velocity (PSV) and End Diastolic Velocity (EDV)

were recorded over 3 cardiac cycles, and averaged. Resistance index was calculated as (PSV/(PSV-EDV) (Arbeille 1983).

For scanning of fetuses, dams were placed back at 0 degrees. Again, orientation began at the maternal bladder. Working supero-laterally, implantation sites were identified and orientated in B-Mode, whereas colour Doppler was used to identify blood vessels. One fetus per uterine horn was analysed. This was not necessarily the first fetus to be identified, as often fetal positioning prevented accurate recordings of umbilical pressure indices. Umbilical arteries were identified in one random fetus per uterine horn, per dam. No umbilical EDV was present at g.d. 14.5, which has reassuringly also been reported in CD-1 fetuses (Hernandez-Andrade 2014). Umbilical artery pulsatility index in humans is often used to predict pathological fetal growth *in utero* (Cnossen 2008). However, this calculation relies on a diastolic velocity value, which isn't present in the C57BL/6 mouse at this gestation, as previously discussed. Thus, only peak systolic velocity was recorded, which alone, has not been reported to correlate with adverse pregnancy outcomes in human pregnancies (Kessous 2014).

For all measures, blood flow velocity data was retrieved in PW Doppler mode (40MHz frequency, 10 kHz PRF, Doppler angle of insonation <40 degrees). The ultrasound operator was blinded to the mouse strain as, fortunately, all strains matched for coat colour.

3.10 Micro-CT measurement of fetuses

Fetuses were collected at g.d. 18.5 and processed through previously established protocols (Wong 2012; Wong 2013). Briefly, fetuses were fixed in 4% paraformaldehyde for 24 hours at 4°C, then stored in PBS / 0.02% sodium azide at 4°C, before undergoing hydrogel hybridisation. Hydrogel solution was made using the following reagents: (ice-cold 4% (wt) PFA, 4% (wt/vol) acrylamide (Bio-Rad, Mississauga, ON, Canada), 0.05% (wt/vol) bis-acrylamide (Bio-Rad, Mississauga, ON, Canada), 0.25% VA044 Initiator (Wako Chemicals USA, Inc., Richmond, VA, USA), 0.05% (wt/vol) saponin (Sigma-Aldrich, MI, USA) and PBS.

Each fetus was incubated in 20ml hydrogel for 72hours at 4°C, to allow the hybridisation of hydrogel monomers into the tissue. Samples were then degassed to remove oxygen (inhibits polymerisation), before being placed in a 37°C water bath for 3 hours. Polymerisation was considered complete if gel had hardened after this period. Fetuses were then carefully removed from their encasing gel, and submerged in 50 ml stock 0.1 N iodine standard solution (Fisher Scientific, SI86-1) for 24 hours on a rocker, at RT. Finally, fetuses were removed from iodine

and washed for 1 hour in PBS. Each fetus was then mounted in 1% agarose within a Bijou tube, prior to scanning.

Fetuses were scanned in a *Nikon XT 225 micro-CT* at the Department of Zoology, University of Cambridge (pixel length was fixed at 14.7 microns) within 1 week of collection. For initial scans and optimisation, the voxel (3D pixel) length was always adjusted to provide the highest resolution for each sample. For *Klrc1*$^{-/-}$ comparisons however, the pixel length was fixed at 14.7 microns for every fetus. Image stacks were processed in Amira 6.3 (*FEI*) software for all 3d measures and femur lengths used in ratios with 3d measures, whereas ImageJ (Schneider 2012) free software was used for initial 2d measures. Brain volume was manually segmented through voxel intensity threshold selection to visualise organ boundaries. Brain volume segmentation included olfactory lobes, cortices, cerebellar and medullae (segmented at superior aspect of spinal cord). Femur length was measured along the diaphysis, from the distal tip of the medial condyle to the proximal tip of the femur head. Thymuses were segmented as whole organs.

3.11 DLK1 measurement

Pregnant dams at g.d. 15.5 underwent schedule 1 by carotid artery exsanguination, where maternal blood was collected, placed on ice, and then centrifuged for 15 minutes at 12000rpm. Serum was then aspirated and delivered to Keith Burling at the Core Biochemical Assay Laboratory (CBAL), Addenbrooke's Hospital. Here, a previously published protocol was used to determine DLK1 through a sandwich ELISA (Charalambous 2014). In brief, antibodies and standards were purchased from R&D Systems (BioTechne: Abingdon, UK). The capture antibody was a goat polyclonal (product code AF8277-SP), the detection antibody was a rabbit monoclonal (product code MAB8364-SP). The standard is recombinant mouse DLK1 (product code 8545-PR). The assay used was an in-house microtitre plate-based two-site electrochemiluminescence immunoassay using the MesoScale Discovery assay platform (MSD, Rockville, Maryland, USA). A standard-bind MSD microtitre plate was coated overnight with a polyclonal anti-DLK1 capture antibody diluted in PBS. After coating, the plate was washed three times with PBS/Tween using an automated plate washer and then blocked with MSD Blocker A. After blocking, 30μl of assay diluent plus 10μl standards, QCs and undiluted sample were added to the plate in duplicate. Two levels of QC were run at the beginning and end of each plate. After 2hrs incubation at room temperature on a plate shaker, the plate was washed three times with PBS/Tween. Rabbit monoclonal anti-DLK1 detection antibody was diluted in MSD Diluent 100, and added to the plate. After 1hr incubation at RT on a plate shaker and washing with PBS/Tween, Goat anti-Rabbit SulphoTAG (MSD) diluted in MSD Diluent 100 was added to the plate. The plate was incubated on a plate shaker for a further 30 minutes.

After another wash step, MSD read-buffer was added to all the wells and the plate was immediately read on the MSD s600 plate reader. Luminescence intensities for the standards were used to generate a standard curve using MSD's Workbench software package. Results for study samples and QCs were read off this standard curve. A concentrated solution of recombinant mouse DLK1 was diluted to prepare a series of calibrators. Lower limit of detection was 0.001 ng/ml (limited in-house data), and the upper limit of measurement was 10 ng/ml. Two quality control samples were run at the beginning and end of each plate.

3.12 RNA-sequencing

All g.d. 15.5 placentae were collected in RNALater (Thermo Fisher Scientific, MA, US) and stored at 4°C for 3-4 days, after corresponding fetal weight was recorded. One quarter (placental disc halved, and halved again) of each placenta was used for RNA extraction in the following process: tissue was homogenised in *RNA lysis buffer* (Zymo Research, CA, USA) for 2 x 20 seconds using an *MP FastPrep-24 Tissue and Cell Homogenizer* (Hyland Scientific, WA, USA). Genomic DNA was eliminated, and RNA was purified using standard RNAeasy Plus Universal Mini Kit (Qiagen, Hilden, Germany) columns and protocols. All fetuses were weighed immediately ex-vivo. Placentae from all 'Average' fetuses (those who were closest to their mean litter weight) were processed fresh, whereas all placentae from 'Small' fetuses (the fetuses with the lowest weight in their litter) were processed from frozen.

As both Average-B6 (Average fetus, C57BL/6 dam) and Average-KO (Average fetus, $Klrc1^{-/-}$ dam) placental groups were run from fresh tissue, and Small-B6 and Small-KO groups were run after a period of being frozen at -80°. In order to be confident in comparing RNA gene expression between frozen and fresh samples, I ran one placental sample twice, once fresh and once after being frozen. A small batch effect was detected, attributed to the freezing process. As a result, a batch correction for to all frozen samples using SVA software (Leek 2012) was applied.

All total RNA samples underwent initial quality control using a standard *Bioanalyzer* protocol (Agilent, CA, USA). Gel electrophoresis to check RNA quality and integrity was performed using RNA ScreenTape Analysis (Agilent, CA, US), with all samples achieving an RNA Integrity score (RIN[e]) of >8, the industry-accepted minimal value (Julian Bauer, verbal communication). This value is used to identify RNA degradation, which may occur in sample processing, and can be scored from 1-10. It is ultimately calculated through a proprietary algorithm which measures certain ratios of the ribosomal RNA (rRNA) 28s and 18s sample values, through gel electrophoresis.

All eukaryotic species contain mRNA that is polyadenylated. This Poly(A) tail consist of multiple adenosine monophosphates, and its addition is part of the process which produces mature mRNA for protein translation. It's position in the RNA is usually upstream of the coding region and the untranslated region (UTR), at the 3' end. This poly(A) tail can be used as a target to enrich total RNA samples, as other types or RNA e.g. rRNA, do not display it. Oligo-d(T)25 is covalently attached to a magnetic bead. When mixed with RNA samples, the Oligo-d(T) beads hybridise with poly-A tails on mRNA, which can then be isolated using magnetic separation.

The isolated mRNA was then used as a template to produce a complementary DNA (cDNA) library for downstream sequencing. These individual cDNA libraries were then quantified and assigned an individual sequence barcode to each DNA fragment, through the addition of individualised adapters. This means that each read contains both the fragment nucleotide sequence, and its sample identification barcode. This process is termed multiplexing. By pooling samples, it is possible to sequence large numbers of libraries simultaneously through a high-output machine.

The pooled samples were next sequenced on a NextSeq 500 system (Ilumina, CA, US). The loading concentration was 1.8pM, and *1% Phix* (Ilumina, CA, US), an adapter-ligated control library, was used also run. The kit used for sequencing was a *High Output* 75 cycle kit (Ilumina, CA, US). Strands were sequenced through base calling initially.   The samples were also run through quality control checks, trimmed to remove low quality bases and adapters, and mapped to the mouse genome (Dobin 2013). Mapped reads were counted to determine the level of expression in each gene using HTSeqCount (Anders 2015), counted reads were loaded into the edgeR package in R software (Robinson 2010), counts were filtered (using 5CPM), GC corrected using the CQN package (Hansen 2012) and normalised on a per comparison basis, then differential expression was determined using an edgeR generalised linear model, which took into account the batch effect and gender (Y-specific genes with sufficient placental expression used- *Rbmy*, *Uty*, *Ddx3*, *Zfy1*, *Eif2s3y*) of the samples being compared, by using SVA (Leek 2012). The p-values were corrected for multiple testing and finally sample clustering relationships (PCA) were analysed using the *R* package *DESeq2* (Love 2014).

All genes with an FDR <0.01 were considered to be DE, and were entered for functional pathway enrichment using a gene annotation and analysis resource (http://metascape.org). Terms with a p-value <0.01, a minimum gene count of 3, and an enrichment factor > 1.5 (the

enrichment factor is the ratio between the observed counts and the counts expected by chance) were collected and grouped into clusters based on their membership similarities.

3.13 Fetal and placental weight

After confirmation of schedule 1 of pregnant dams, fetuses were removed from their abdominal cavity within uterine horns, and placed on ice (first schedule 1 method). They were then removed from their uterine wall and amniotic cavity surroundings, and separated from their placentae at the umbilicus. Care was taken to ensure blood was not exsanguinated at this point. Next, individual fetuses were weighed using precision balance scales (Mettler Toledo), which were calibrated each day prior to measurements. Fetuses were then decapitated using Tweezerman scissors for their second schedule 1 method. Placentae were then separated from umbilical cord and removed from any surrounding membrane and fluid, an individually weighed.

3.14 NKG2A blockade

Sterile preparations of antibody or isotype control were diluted in PBS prior to transporting them to the lab. Pregnant mice at g.d. 6.5 were first placed inside a warming box to encourage peripheral vasodilation. They were then placed inside a restrainer to undergo tail vein injection, as per standard protocol. These mice were given a unique identification through ear-notching, and injected again 3 days later at g.d. 9.5. Mice were injected with a total of 10μg of either isotype or antibody, diluted in 50μl sterile PBS 1X.

3.15 Human Cohorts

UK cohort - details of selection criteria, DNA isolation and KIR/HLA-C genotyping have previously been reported for this cohort of women recruited from three UK hospitals (Hiby 2004; Hiby 2010) in Leeds, Cambridge and Oxford. Women aged between 17-45yrs old were recruited. In brief, pre-eclampsia was defined as new hypertension after week 20 of pregnancy (140/90 mm Hg), together with new proteinuria >300 mg/24hr.

For this cohort, I determined HLA-B -21 status through a maternal DNA polymerase chain reaction (PCR), followed by a restriction-enzyme digest. Briefly, *HLA-B* exon 1 was amplified using primers with the following sequences; forward 5′-TTCTAAAGTCCCCACGCACCCA-3′, reverse 5′-CCTCCCGGCAGAGGCCATTTCCCT-3′and 5′-CCTCCCYACAGAGGCCATTTCCCT-3′. The amplicon was digested using the *Nla*III restriction enzyme (NEB, Ipswich, MA). Sequenced controls were included in each set of digests. Bands were separated using QIAxcel

Advanced electrophoresis (Qiagen, Hilden, Germany) and visualised by QIAxcel ScreenGel l.5.0 software (Qiagen, Hilden, Germany).

3.16 Statistics

In general, Shapiro-Wilk test for normality (alpha = 0.05) was applied to all data sets except RNA-seq and fetal and placental weight. For comparison of means across 2 groups a parametric test was used if both groups passed normality testing. If either or both groups failed normality testing, a Mann-Whitney test was used. For multiple group comparisons, a one-way anova was used for normally distributed data with post-hoc t-tests corrected for multiple comparisons. All p-values are 2-sided, unless stated. ***For graphical data - unless a p-value is stated, assume the p-value for the statistical comparison shown is non-significant (>0.05)**. **Single data points on graphs represent single animals, e.g. one dam or one fetus, unless stated.**

Human case-control study - a Fisher's exact calculation of odds ratio (95% confidence interval) for pre-eclampsia and p value are given.

RNA-sequencing - the exact test edgeR approach was used to make pairwise comparisons between groups. These were then adjusted for multiple testing via the FDR (Benjamini-Hochberg) approach used by edgeR (Robinson 2010).

Mouse fetal and placental weight - where data can be skewed by the random effect of litter (e.g. fetal weight, placental weight), a mixed model was used to compare groups where condition (e.g. maternal genotype) was a fixed effect and litter was a random effect. Except for the NKG2A blockade experiment, litters containing 3 or less fetuses were excluded from all analyses.

For all statistical analyses, including parametric and non-parametric comparisons of groups, Fisher's Exact tests, Odds Ratios and normality tests, Prism v.8 (Graphpad, US) was used. The mixed model analyses were performed using SPSSv.25 (IBM, US). All error bars on graphs represent standard deviation (SD).

4.0 CHAPTER I – RESULTS

4.1 Mice colonies

NKG2A-knockout colony

I received two male and two female mice with the *Klrc1* deletion (*Klrc1*^{-/-}) as kind gifts from the Helmholtz-Zentrum München institute. In these mice, the first four exons of the *Klrc1* genomic locus were deleted. Importantly, they were created on a C57BL/6 genetic background. These mice were initially created and described by the Marco Colonna laboratory group at Washington University, Missouri, USA (Rapaport 2015).

These four founder mice were first genotyped by polymerase chain reaction (PCR) to confirm the presence of the deletion, and to ascertain allele copy number (Figure 5). For this experiment the PCR reagents and recipes, cycle protocols and primer sequences can all be found in 3.0 Chapter I - Methodology. All four mice were found to display homozygosity for the mutated form of *Klrc1*. These founder mice were bred together to produce offspring who were all *Klrc1*^{-/-} (F1 generation). Male F1 mice were kept and used either as stud males in future experiments or reserved for future breeding. Female F1 mice >6 weeks old were either used to further generate the colony or were mated with C57BL/6 mice as experimental females.
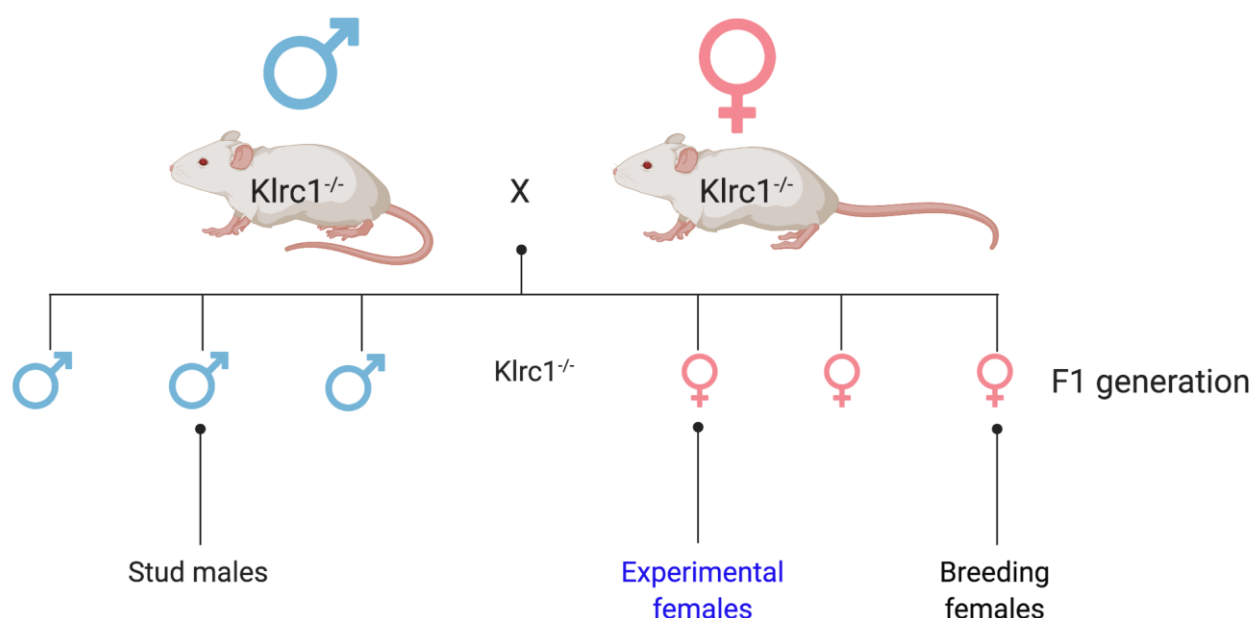
Figure 5. Breeding strategy used to generate *Klrc1*^{-/-} experimental females.

B2m-knockout colony

Founder mice of this strain were imported to our animal house prior to the commencement of this project. This *B2m*-KO strain (referred to as *B2m$^{-/-}$*), one of the earliest knockout strains ever made (Koller 1990), was created by disrupting the *B2m* gene in embryonic stem cells from the 129 mouse strain. The generated chimeras were then back-crossed onto a C57BL/6 background. The resultant mice completely lack MHC-I expression on all nucleated cells due to a disruption of the *B2m* gene, as MHC require *B2m* for cell-surface expression. The breeding strategy used to generate experimental females can be found in Figure 6. This approach was taken after verbal communication with a previous member of the lab (Jens Kieckbusch), who revealed that homozygotes for the deletion *(B2m$^{-/-}$)* are poor breeders, but it is unfortunately this precise genotype that is of biological interest. As a result, founder *B2m$^{-/-}$* were bred with C57BL/6 to create F1 heterozygotes for the deleted gene. These heterozygotes were then bred together to produce F2 litters with a mixture of offspring, where approximately 25% should be *B2m$^{-/-}$*. Again, females were either kept for future colony generation, or used as experimental animals. For this experiment the PCR reagents and recipes, cycle protocols and primer sequences can all be found in 3.0 Chapter I – Methodology.
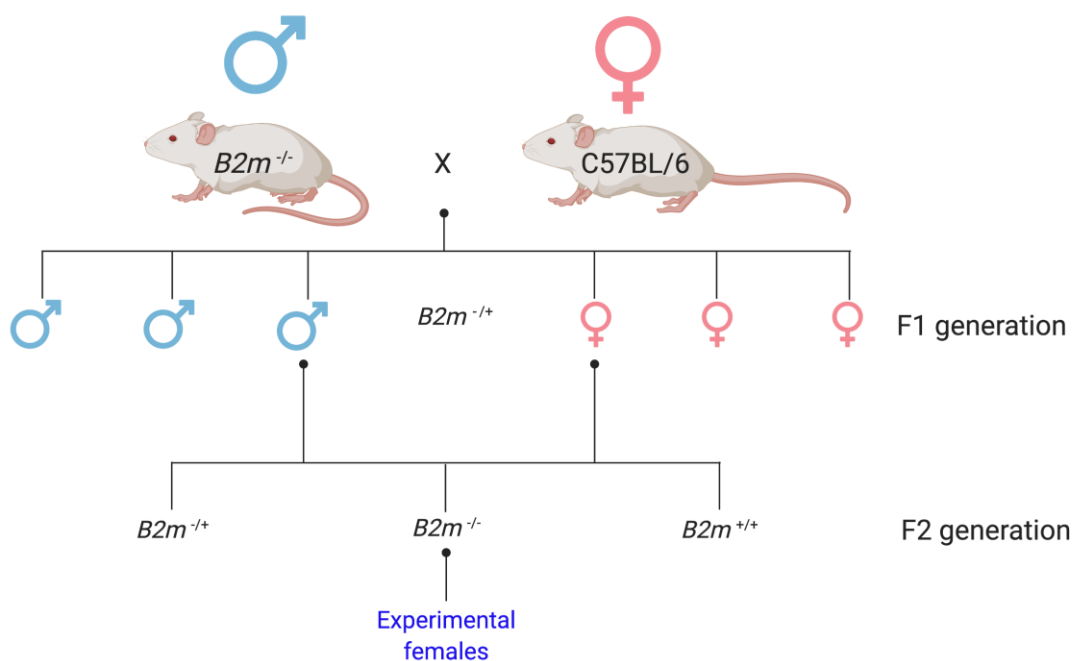
Figure 6. Breeding strategy used to generate *B2m$^{-/-}$* experimental females.

SHP-1 NK conditional knockout colony

Global deletion of MHC-I due to *B2m* deletion results in a lack of all MHC-dependent educating pathways, as no inhibitory receptors can be engaged. It also removes all other MHC-dependent

processes, whose role in physiology is both unclear and potentially vast. In addition, depending on the strain, these mice also lack some activating NK pathways, as MHC such as H2-D^d are capable of ligating certain activating receptors like Ly49D (George 1999). Fortunately, in C57BL/6 mice, the fact that none of their MHC class I molecules are known to be capable of engaging activating NK receptors as Ly49H is ligated by the virally encoded molecule M157 and C57BL/6 only express the *b* allelic variant of H2-D (H2-D^b).

Furthermore, the global deletion is obviously not NK-specific and results in a significant reduction in CD4- CD8+ T cells, which mediate cytotoxic T cell function. Whilst the relatively low number of cytotoxic T cells in uterine tissue in murine pregnancy is likely to represent a diminished role, their exact function is unknown. As a result, I wanted to create an NK-specific knockout of inhibitory pathways where I could better measure the effects of a lack of NK education. This approach uses a conditional KO line that deletes only in NK cells the *Ptpn6* gene coding for the SHP-1 phosphatase necessary for all ITIM-bearing inhibitory receptors. This approach has been discussed above (Viant 2014), and when used in C57BL/6 mice, takes advantage from the fact that no known MHC class I molecules are capable of engaging

There are two main site-specific recombination technologies used to produce cell-specific genetic knockouts in mice. These are termed the Cre-lox and FLP-FRT systems. The latter will be briefly discussed in chapter 2. The Cre-lox system works through a simple targeting pathway. Cre-expressing targeting vectors can be inserted into stem cells and designed where Cre-recombinase expression only occurs under certain genetic promoters, or in response to certain stimuli. For example, *Ncr1* (which encodes the cell-surface protein NKp46) is expressed in early immature NK cells, and remains constitutively expressed in NK cells throughout their life. NKp46 is expressed by NK cells and group 1 Innate Lymphoid Cells (ILC). The mouse strain used in this project, and described below, was created where Cre-recombinase is only expressed when under the Ncr1 promoter (Eckelhart 2011). This strain of mice is known as Ncr1-icre, where "i" stands for "improved", as the gene encoding the improved cre-recombinase was inserted into the Nkp46 locus (Narni-Marcinelli 2011). The original Narni-Marcinelli et al. paper describes good specificity of this cre-recombinase system, however efficiency of targeting was not reported and was not specifically determined in this project.

In addition, a different and complementary mouse strain needs to be created to allow for specific exon targeting in the offspring of the combined strains. Exon sequences of choice can be flanked by P1 bacteriophage sites known as LoxP sites. This chosen sequence or gene is then described as being 'floxed' (which stands for 'flanked by loxP sites'). When Cre-recombinase

and LoxP are simultaneously expressed within a cell, Cre-recombinase recognizes and binds to the first and last 13 base-pair sites of a LoxP site, forming a dimer. This dimer can then join to the other site, and form a tetramer. The Cre-recombinase then ligates both strands of DNA at the loxP sites, removing the exon of interest, and allowing the exposed ends of DNA to be rejoined by the DNA ligase which completes genetic recombination.

Our breeding strategy for this strain can be found in Figure 7. SHP-1 is encoded by the *Ptpn6* gene. I received mice who were homozygous for floxed *Ptpn6* (*Ptpn6^{flox/flox}*) as a kind gift from the Eric Vivier laboratory group in Marseilles. These mice were mated with mice homozygous for the *Ncr1-icre* gene (*Ncr1^{cre/cre}*), producing F1 offspring heterozygous for both transgenes (*Ncr1^{cre/wt}/Ptpn6^{flox/wt}*). Female F1 mice were then bred back to *Ptpn6^{floxflox-}* males in order to increase the chances of generating F2 mice of the desired genotype *Ncr1^{cre/wt}/Ptpn6^{flox/flox}*. This genotype was chosen as it allows for complete floxing of *Ptpn6* exons, whilst also reducing the expression of Cre-recombinase, which is known to display toxicity in high levels, due to the harmful ligation of illegitimate pseudo-LoxP sites (Semprini 2007). These pseudo-LoxP sites often bear little or no sequence similarity to the bactreriophage P1 LoxP element, and can be recognized by Cre-recombinase where catalysing recombination between DNA sequences can occur, even in mammalian cells *in vitro* (Thyagarajan 2000). The PCR reagents and recipes, cycle protocols and primer sequences for the genotyping used to confirm gene expression and allele copy number for this colony can be found in 3.0 Chapter I - Methodology.
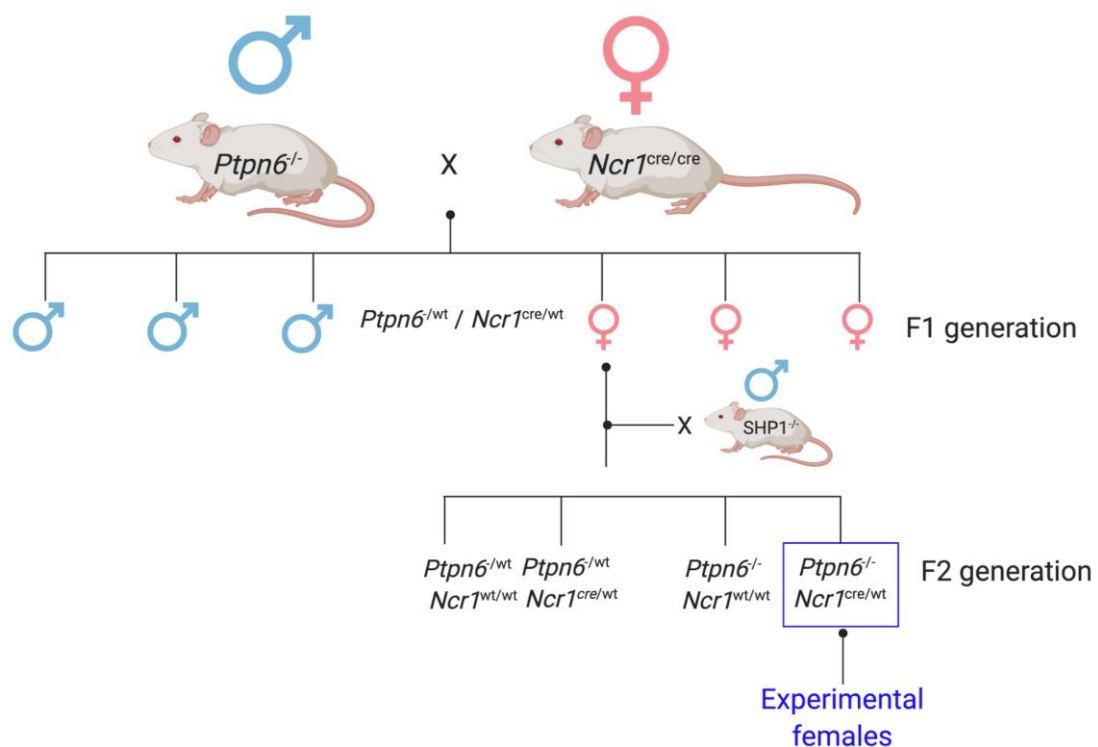
Figure 7. Breeding strategy used to generate *Ncr1^{cre/wt}/Ptpn6^{flox/flox}* (SHP-1 conditional knockout) experimental females.

4.2 Optimisation of NKG2A staining

In order to accurately characterise cell populations and measure absolute cell numbers, it is important to process tissue in order to maximise live cell yield, whilst also maintaining epitope integrity for antibody labelling in downstream fluorescence activated cell sorting (FACS). In the field of murine reproductive immunology this is particularly problematic, as many of the key tissue-resident immune cells lie in the mesometrial lymphoid aggregate of pregnancy (MLAp), which lies within two firm smooth-muscle associated uterine wall layers (Bilinski 2008). Combine this with the relatively low cell yield from individual murine maternal decidua in early pregnancy, and analysis of poorly represented cell populations is challenging.

Previous protocols to isolate decidual leucocytes used by members of our research group have been combined either with the more aggressive Liberase TM (Thermo Fisher Scientific, MA, US) (Collins 2009), or the weaker Liberase DH (Thermo Fisher Scientific, MA, US) (Doisne 2015), as part of the enzymatic digestion for tissue dissociation. Both these enzymes contain a purified mixture of the proteases collagenase I and collagenase II. They differ by their additional enzymatic constituents. Liberase TM also contains high levels of thermolysin, a metalloproteinase, whereas Liberase DH has additional dispase, a protease which cleaves fibronectin, collagen IV and collagen I.

I first tested whether the NKG2A epitope, pivotal to this project, was affected by the enzymatic protocol used. Details of the flow-cytometry panel (Panel 1) of fluorescently labelled antibodies can be found in 3.0 Chapter I – Methodology. Live, single splenocytes were selected based on their positive expression of CD45, NK1.1 and NKp46, as an efficient and simple strategy to identify NK cells (Figure 8a). I found that Liberase TM removed the NKG2A epitope almost entirely, as labelling of splenocytes with the NKG2A(B6) (antibody clone 16A11) led to almost zero positive events (Figure 8b), however Liberase DH completely preserved antigen-labelling, displaying similar levels to the mechanical-digestion only control. For details of the exact composition of tissue dissociation media and enzymatic volumes/concentrations, see 3.0 Chapter I – Methodology.

As a result of these findings, for future tissue dissociation I used Liberase DH only to preserve the NKG2A epitope, but in combination with the *Collins et.al* dissociation protocol. This new combination was used as the *Doisne et.al* (2015) dissociation protocol normally used with Liberase DH includes a leucocyte gradient step, which can bias the accuracy of cell number quantification needed to phenotype the *Klrc1*^{-/-} strain in pregnancy.

Flow cytometry using C57BL/6 splenocytes

A

B

Enzyme (lot)	Enzymatic constituent	Working conc.
PBS (no enzyme control)	-	-
Liberase DH (5401054001) Stock 13WU/ml	Dispase high	10μl/ml
Liberase TM (5401119001) Stock 26WU/ml	Thermolysin medium	20μl/ml
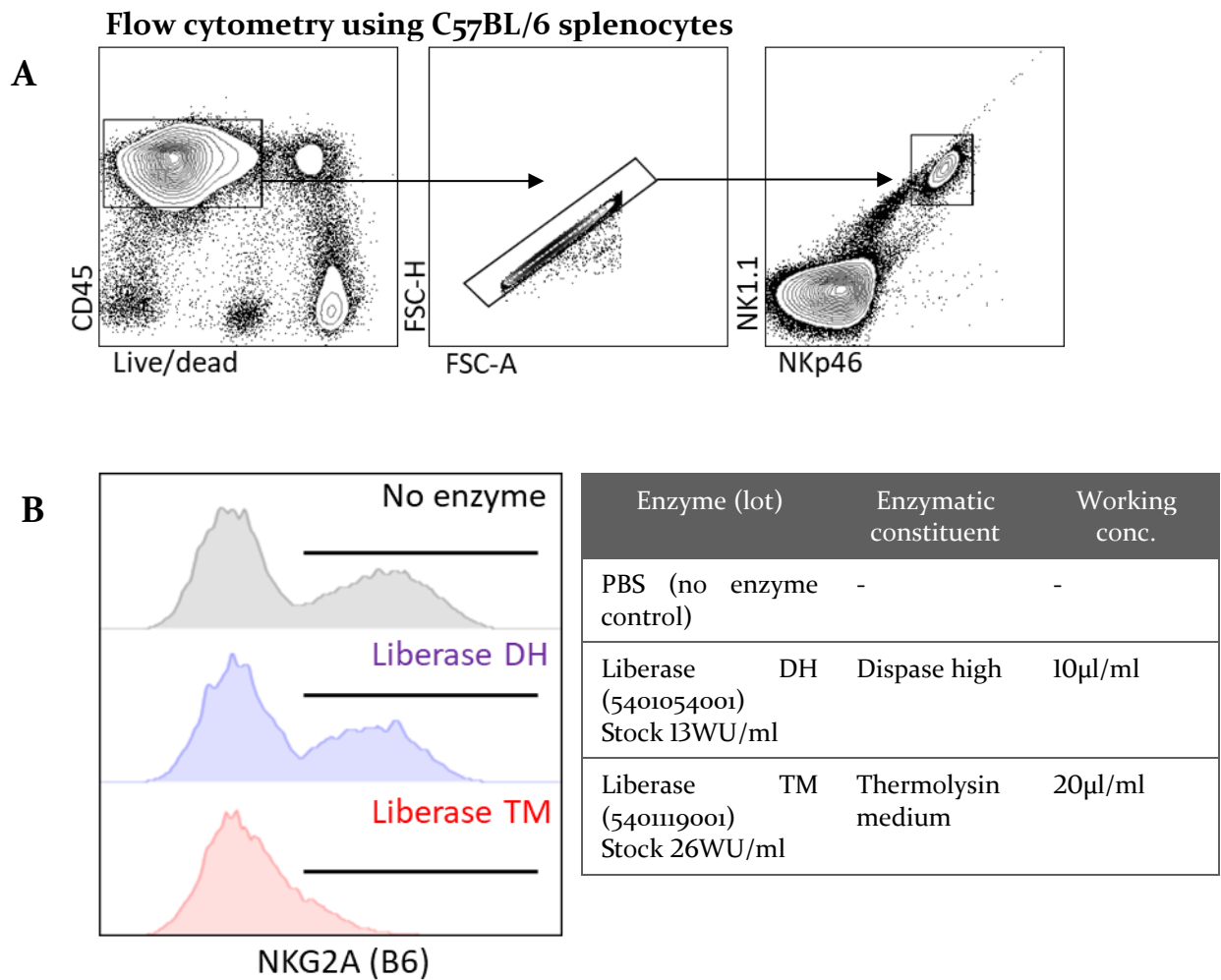
Figure 8. A) Flow cytometry gating strategy to identify splenic NK cells. B) Histograms to show representative NKG2A expression on NK cells, by enzymatic condition (left), with enzymatic constituents per condition (right). n = 5-6 animals, 2 technical repeats.

4.3 Phenotyping of *Klrc1*-/- *mice*

Next I needed to test the expression pattern of NKG2A in pregnancy, as it is clear that immune cell phenotypes are altered in this state. This was important as I needed to ensure that any phenotype I was modelling in the *Klrc1*-/- strain, and downstream experimental findings, were due to NK cell-specific abnormalities. Fortunately, a previous study of this mouse strain reported that NK cells from *Klrc1*-/- mice display normal maturation, cell surface receptor repertoires and cellular development (Rapaport 2015). However, some T cells express NKG2A when activated, an example being in head and neck tumours where NKG2A-expressing CD8+ T cells form a very distinct population of early activated tumour resident T cells (van Montfoort 2018). Thus, I needed to ensure that this did not also occur in early pregnancy, otherwise I might have confounding effects due to the expression of NKG2A on T cells.

I phenotyped the splenic and uterine immune landscapes in both *Klrc1*⁻ᐟ⁻ and C57BL/6 pregnant mice by designing flow cytometry panels to recognise NKG2A-expressing cell populations, and all major leucocyte and myeloid cell populations. I mated *Klrc1*⁻ᐟ⁻ females with C57BL/6 males, and compared them to control C57BL/6 females, also mated with C57BL/6 males. At g.d. 9.5, pregnant dams were culled, and uterine horns removed, tissue was digested, and cells were stained.

Antibody panels for leucocyte populations can be found in 3.0 Chapter 1 – Methodology – Panel 2. Gating strategies displayed in representative flow cytometry dot plots are also shown in Figure 9, based on previously published strategies (Filipovic 2018). Live single cells negative for the B- and T cell markers CD19 (Krop 1996) and CD3 (Zumla 1992), respectively, were attributed to the NK subgroup if they displayed the pan-leucocyte marker CD45 (Trowbridge 1994), medium-low levels of the integrin CD11b (Kim 2002), the NK/NKT surface antigens NK1.1 (Yokoyama & Seaman 1993) and NKp46 (Walzer 2007). In the mid-gestation mouse uterus there are three subsets of group 1 innate lymphoid cells (ILC) that express NKG2A. These are the conventional NK cells (cNK), uterine innate lymphoid cell 1 (uILC1) and tissue-resident (tr) uNK cells (TRuNK) (Doisne 2015; Filipovic 2018). These three subsets are characterised by the expression of the transcription factor Eomes and the surface marker CD49a. Subgroups were identified as TRuNK if they were positive for both the integrin CD49a and the transcription factor Eomes (Sojka 2014; Doisne 2015), uILC1 if they only expressed CD49a and cNK if they only expressed Eomes. Cytotoxic T cells were identified as being CD45, CD3 and CD8 positive (Ellemeier 1999).

Uterine horns were weighed and live cells counted prior to antibody staining. The absolute number of NK cells and CD8+ T cells, per gram did not differ between *Klrc1*⁻ᐟ⁻ and C57BL/6 dams in the uterus (Figure 10A). In addition, the representation of these cell types within the tissue (expressed as a percentage of cells) also did not differ (Figure 10B). This pattern was consistent for NK cells and T cells in the spleen. Gating strategies displayed in representative flow cytometry dot plots for splenic leucocytes are also shown in Figure 11, with their absolute cell numbers in Figure 12A and tissue representation in Figure 12B.

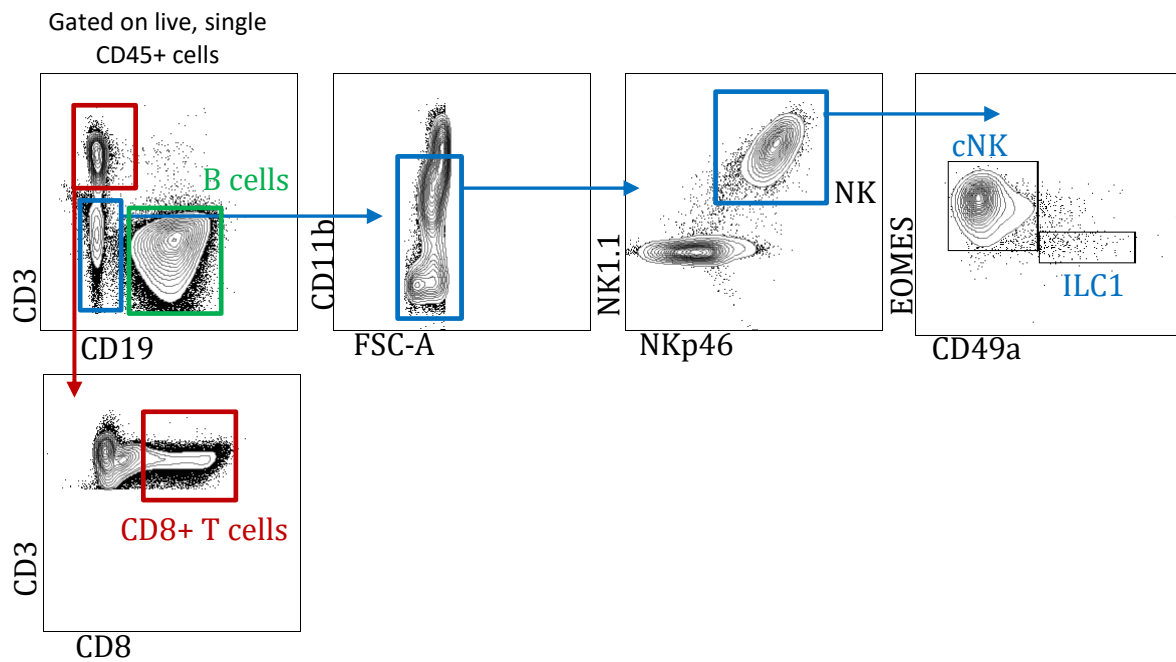**Flow cytometry using C57BL/6 uterine cells**
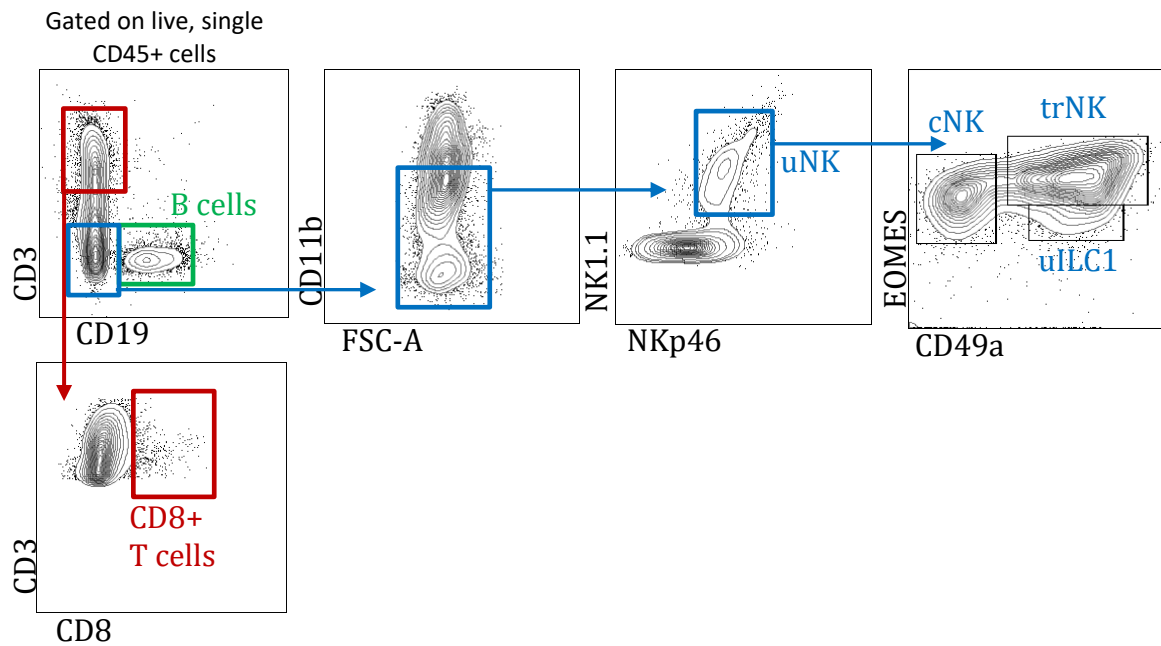
Figure 9. Representative flow cytometry gating strategy to identify leucocytes in uterine tissue at g.d.9.5, in C57BL/6 mice.

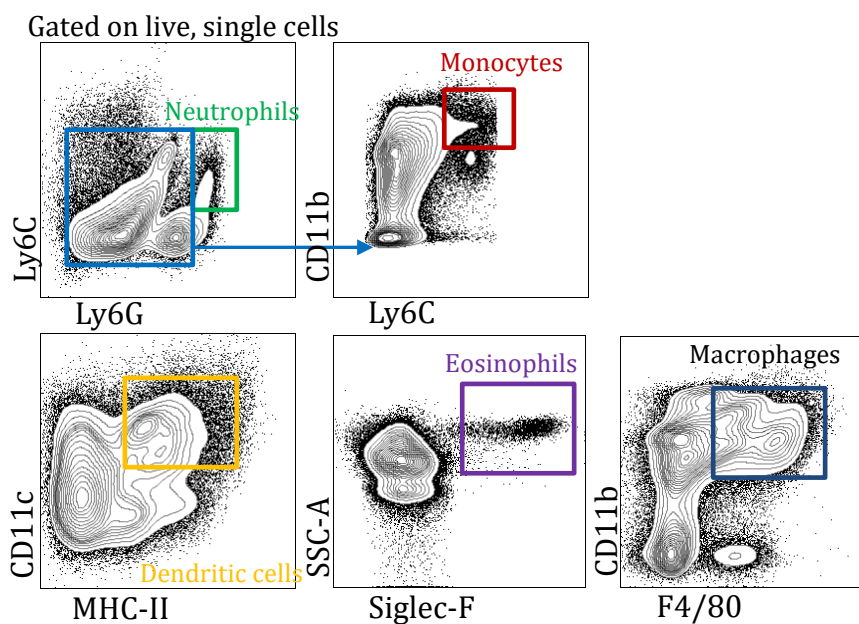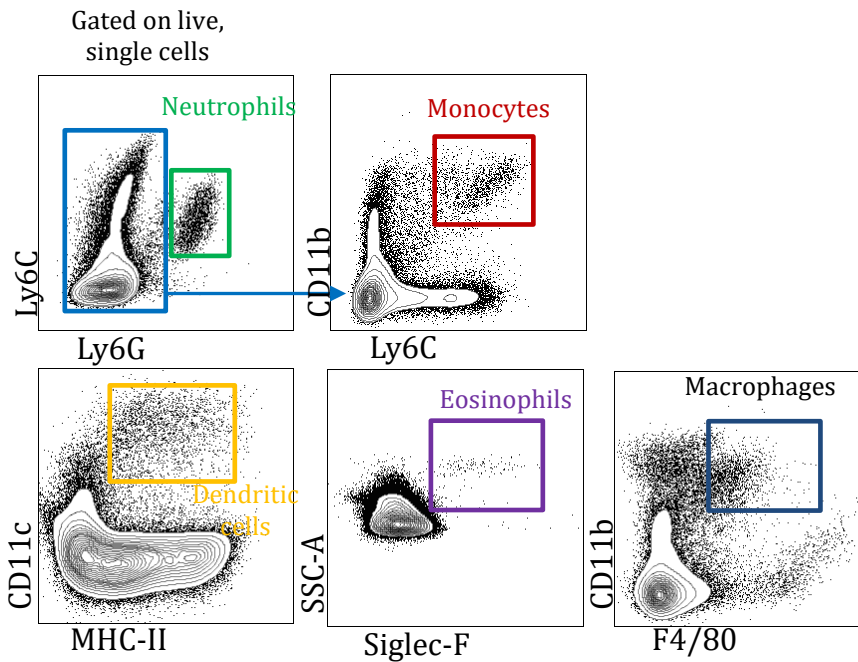**Flow cytometry comparing C57BL/6 and *Klrc1*^{-/-} uterine cells**
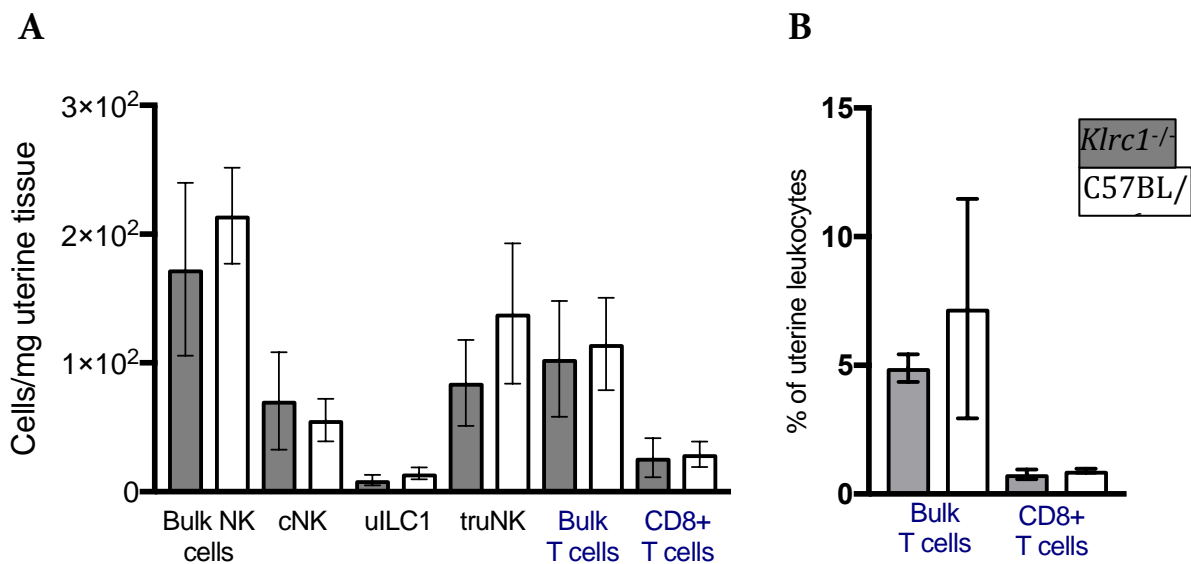
Figure 10. A) Absolute cell numbers/g of uNK and CD8+ T cells, and B) representation of NK cells and CD8+ T cells in uterine tissue at g.d. 9.5 (n= 4-5 mice per group, ANOVA, mean + SD). Grey bars indicate *Klrc1*^{-/-}, clear bars indicate C57BL/6.

Flow cytometry using C57BL/6 splenocytes

Figure 11. Representative flow cytometry gating strategy to identify leucocytes in splenic tissue at g.d. 9.5, in C57BL/6 mice.

Flow cytometry comparing C57BL/6 and *Klrc1*^{-/-} splenocytes
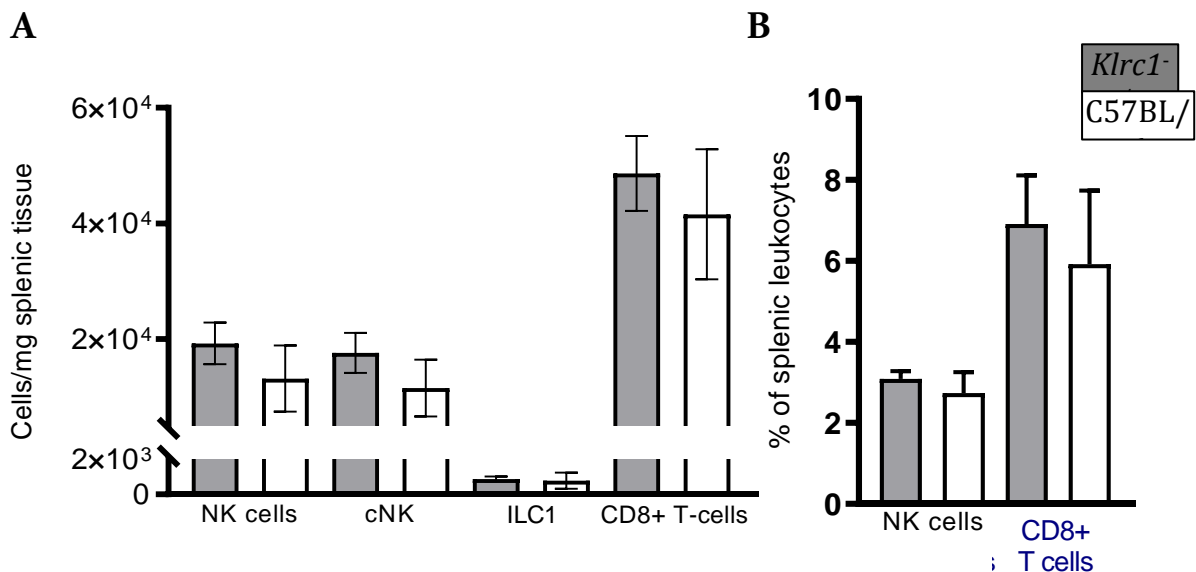
Figure 12. A) Absolute cell numbers/g of splenic NK and CD8+ T cells, and B) representation of NK cells and CD8+ T cells in splenic tissue at g.d. 9.5 (n = 4-5 mice per group, ANOVA, mean + SD). Grey bars indicate *Klrc1*^{-/-}, clear bars indicate C57BL/6.

In order to detect any effect of NKG2A deletion on the wider immune cell milieu, I also stained uterine and splenic cells for major myeloid cell groups. The antibody panel can be found in 3.0 Chapter I – Methodology – Panel 3, along with representative flow cytometry dot plots and gating strategy for each population in Figure 13A (uterus) and spleen Figure 14A (spleen). Cell

groups were identified through a gating strategy already established in the laboratory group. Live, CD45+, single cells were categorised as neutrophils if they expressed high levels of the antigen Ly6G. Monocytes were deemed to be Ly6G neg-low, CD11b high and highly expressed the antigen Ly6C. Dendritic cells were selected if they expressed high levels of both the integrin CD11c and MHC-II. Eosinophils were classified as expressing high levels of the cell-surface lectin siglec-F. Finally, macrophages were identified as being CD11b high, and high for the adhesion molecule F4/80. Again, there were no differences in absolute cell numbers between the two strains for any of the above-mentioned myeloid cell populations, in either uterine (Figure 13b) or splenic tissue (Figure 14b), in early pregnancy.

A   Flow cytometry using C57BL/6 uterine cells

B   Flow cytometry comparing C57BL/6 and *Klrc1*-/- uterine cells
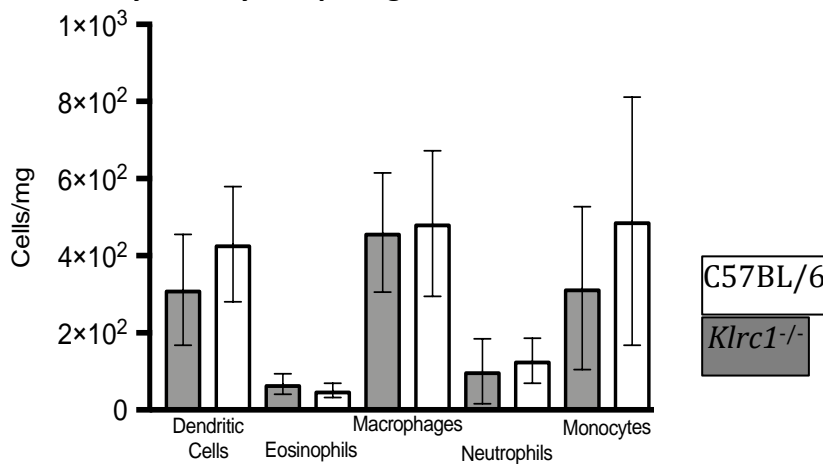
Figure 13. A) Representative flow cytometry gating strategy to identify myeloid cells in uterine tissue at g.d. 9.5, in C57BL/6 mice, and B) representation of various myeloid cell populations in uterine tissue at g.d. 9.5 (n = 4-5 mice per group, ANOVA, mean + SD). Grey bars indicate *Klrc1*-/-, clear bars indicate C57BL/6.

A Flow cytometry using C57BL/6 splenocytes

Gated on live,
single cells

B Flow cytometry comparing C57BL/6 and *Klrc1*^{-/-} splenocytes
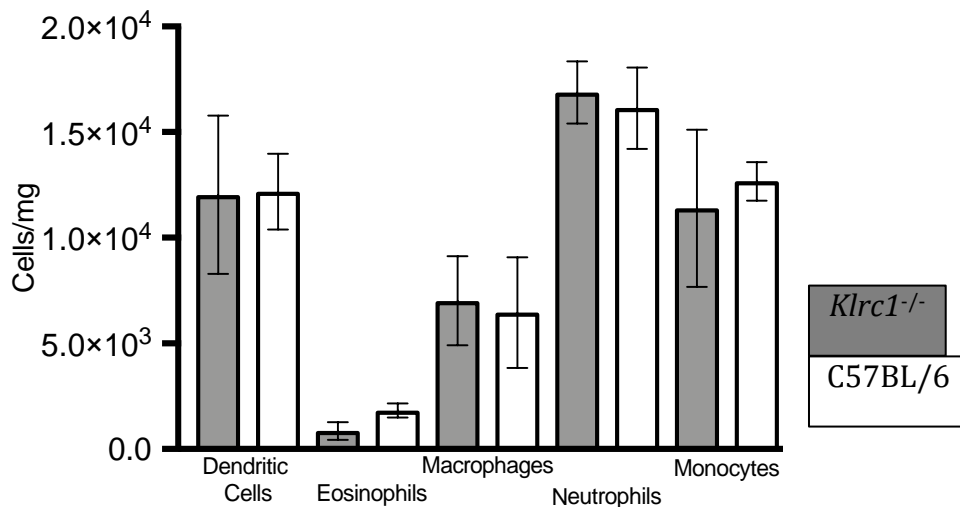
Figure 14. A) Gating strategy to identify myeloid cells in splenic tissue at g.d. 9.5, in C57BL/6 mice, and B) representation of various myeloid cell populations in splenic tissue at g.d. 9.5 (n = 4-5 mice per group, ANOVA, mean + SD). Grey bars indicate *Klrc1*^{-/-}, clear bars indicate C57BL/6.

4.4 NKG2A expression in pregnancy

NKG2A is expressed in a dimer with CD94, which can pair with other NKG2 receptors of the same family, called NKG2C and NKG2E, which also bind human HLA-E and mouse Qa1 and are activating. Many available antibodies (e.g 20d5) do not discriminate among NKG2A, NKG2C and NKG2E and stain them all, however the 16A11 clone of anti-NKG2A antibody is

specific for NKG2A only, and in mice is known as NKG2AB6. Most murine and human peripheral NK cells display a bi-modal expression pattern for NKG2A and some cells also express NKG2C or NKG2E. Unlike human NK cells, C57BL/6 mouse NK cells do not express activating NKG2C or NKG2E receptors in most conditions (Rapaport 2015). I needed to check that pregnancy did not upregulate or alter the cell-surface expression of these receptors, as this would act as a confounding factor for later experiments where a non-specific NKG2 antibody would be used to block the NKG2A epitope.

As expected, I found that both spleen and uterine mouse NK cells (Lin$^-$, CD45$^+$, CD11b$^{med-low}$, NK1.1$^+$, NKp46$^+$) were approximately 30-50% positive for NKG2A (Figure 15A) at g.d. 9.5. I also found that the number of positive cells did not change when staining splenocytes with either the NKG2A-specific antibody clone 16A11 (NKG2AB6) or the pan-NKG2 antibody clone 20d5 (NKG2A/C/E). This finding suggested a lack of NKG2-C or –E expression, but could not rule out the possibility that NKG2C and NKG2E are only ever expressed on the same, NKG2A+ cells.

To address this, next I mated both C57BL/6 females and *Klrc1$^{-/-}$* females with C57BL/6 males and labelled immune cells through FACS at g.d. 9.5. I confirmed that neither uNK or splenic NK cells express NKG2C or NKG2E at mid-gestation (g.d. 9.5), as cells from *Klrc1$^{-/-}$* mice do not stain with the antibody 20d5 that reacts with NKG2A, NKG2C and NKG2E (Figure 15B), for antibody panel see 3.0 Chapter 1 – Methodology – Panel 4. NKG2A is also expressed on activated CD8+ T cells, but at g.d. 9.5 there is no expression of NKG2A on (Lin$^-$, CD45$^+$, CD3$^+$) T cells in the uterus (Figure 16A). Therefore, in C57BL/6 mice, NKG2A is solely expressed on NK cells and not accompanied by other CD94-dependent NKG2 receptors in pregnancy.

The specific role of the three uNK subsets has yet to be delineated, however recent work suggests a pivotal role for trNK cells in promoting fetal growth (Fu 2017). I confirmed that the three subsets express NKG2A in early gestation (Figure 16B). This was important as it ensured that any phenotype found in the *Klrc1$^{-/-}$* strain could be attributed to NKG2A deletion, as all recognised uNK would normally be educated through this receptor.

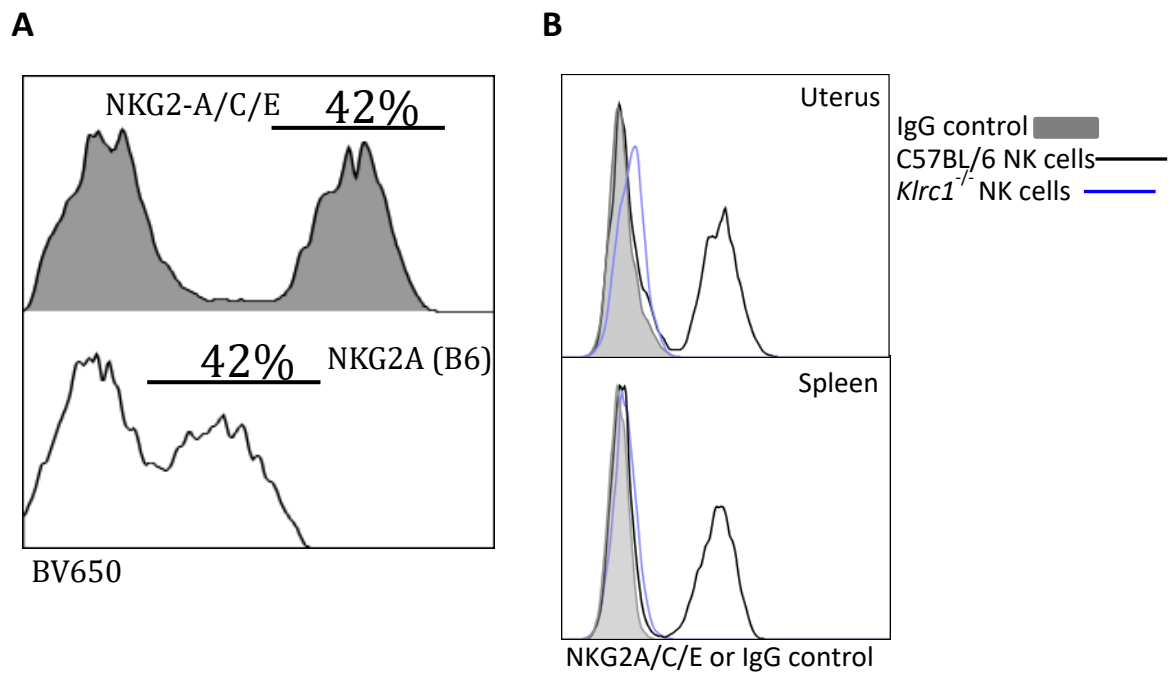## Flow cytometry using C57BL/6 and *Klrc1*^{-/-} splenocytes

A

B

Figure 15. A) NKG2-A/C/E vs NKG2A(B6) expression on splenic NK cells in C57BL/6 mice. **B)** NKG2-A/C/E expression on splenic NK cells from C57BL/6 and *Klrc1*^{-/-} mice (black line represents C57BL/6, blue line represents *Klrc1*^{-/-} and shaded area represents IgG control). Both experiments were performed at g.d. 9.5. 2-3 mice per experiment, 2 technical repeats.
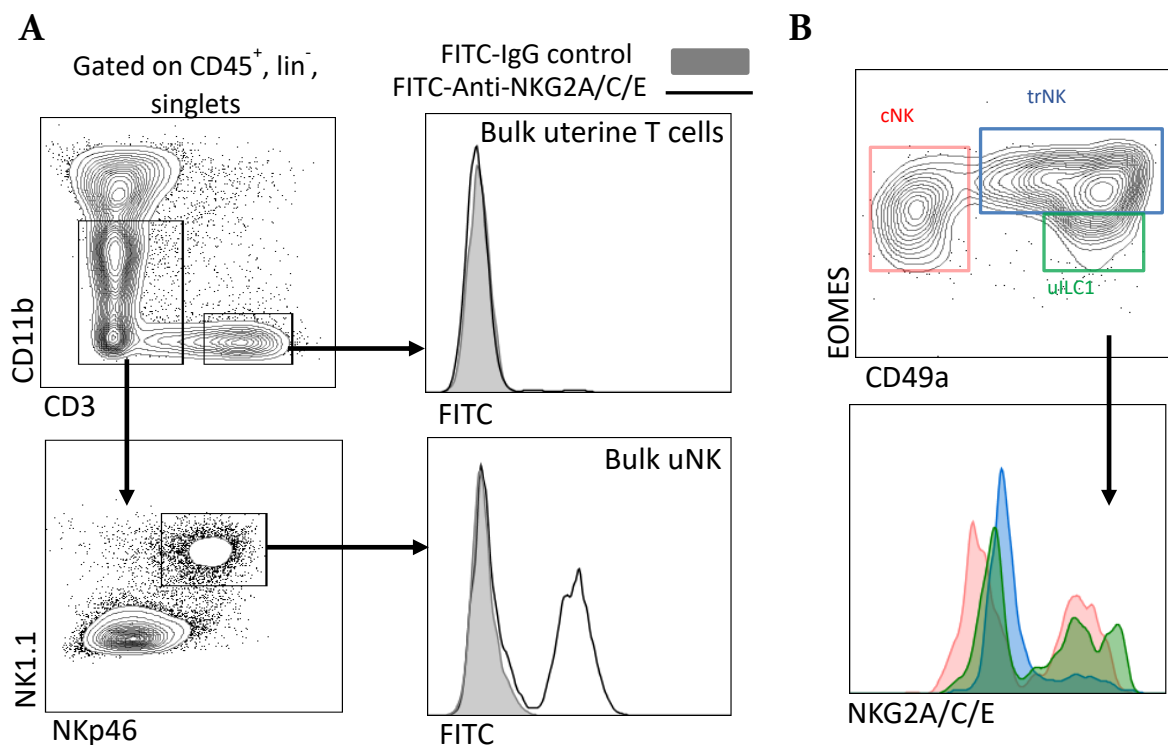
Flow cytometry using C57BL/6 splenocytes

A

B

Figure 16. A) NKG2A expression on uterine NK cells and T cells at g.d. 9.5. **B)** NKG2A expression on the three uNK subsets at g.d. 9.5. 2-3 mice per experiment, 2 technical repeats.

4.5 Qa-1^b expression in pregnancy

Having characterised the expression of the educating receptor, next I needed to ensure that its ligand was also present in early pregnancy. The NKG2A ligand Qa-1^b (the mouse equivalent of HLA-E) is a non-classical MHC-Ib molecule expressed on lymphocytes and other cells. It is not a strict orthologue of HLA-E due to differences in amino acid sequence, but it functions very similarly (Yeager 1997). Previous studies in our laboratory have shown that, unlike HLA-E, Qa-1^b is not expressed by mouse trophoblast, using a mouse trophoblast cell line (Madeja 2011). This is interesting, as placental extracts have been shown to express a number of genes for non-classical proteins (Ohtsuka 2008). Further studies using reverse transcriptase PCR (RT-PCR) went on to show that only H2-K and H2-D molecules are expressed by mouse trophoblast, and not any of the M, Q and T nonclassical gene families are found. This was validated at the protein level by using immunoprecipitation to identify cell surface proteins on mouse trophoblast, where a monoclonal antibody to *B2m* was used. They found no protein precipitated at a molecular weight compatible with non-classical MHC molecules (Madeja 2011).

I mated C57BL/6 females with C57BL/6 males and analysed decidual cells at g.d. 9.5. I found, as expected, Qa-1^b is expressed by uterine and splenic CD45+ leucocytes. The low-level expression of Qa-1^b found on the majority of cells was consistent with antibody manufacturer's data (Miltenyi Biotec, Bergisch Gladbach, Germany) and previous studies (Xu 2017). As NK education can occur in *-trans* through interactions with other cells, or in *–cis* through receptor-ligand binding on the same cell surface, I further analysed Qa-1^b expression in pregnancy (for antibody panel see Chapter 1 – Methodology – Panel 5). I found that leucocytes express Qa-1^b in both the spleen and uterus in pregnancy (Figure 17a). More specifically, I also found that T cells, B cells and NK cells all express low-levels of Qa-1^b in the uterus at g.d. 9.5 (Figure 17b), and could therefore all potentially provide educating signals in early gestation.

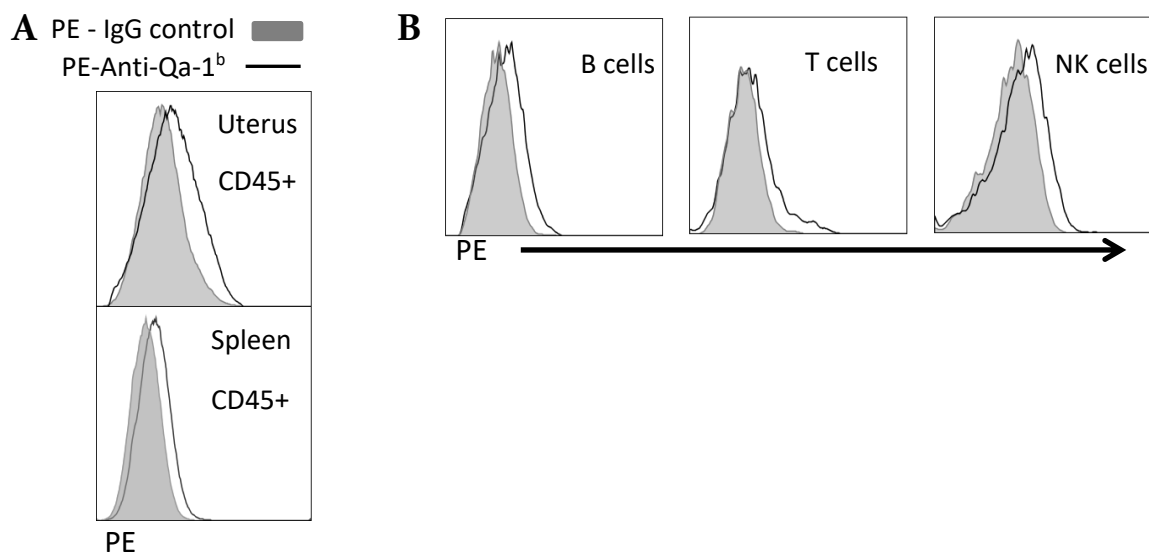## Flow cytometry using C57BL/6 splenocytes and uterine cells

A PE - IgG control ▆
PE-Anti-Qa-1^b ——

B

Figure 17. A) Qa-1^b expression on bulk leucocytes in the uterus (above) and spleen (below) at g.d. 9.5. B) specific expression of Qa-1^b on leucocyte subtypes in the g.d. 9.5 uterus. Black line represents anti-Qa-1^b and shaded area represents IgG control. 2-3 mice per experiment, 2 technical repeats.

4.6 NKG2A educates splenic NK cells *in vitro*

Having established the non-classical MHC receptor-ligand expression pattern in pregnancy, I next wanted to assess the impact of NKG2A on NK education. Whilst the focus of this project was on the impact of NKG2A in pregnancy, it was also important to test the significance of NKG2A to education in general. Indeed, the recruitment of peripheral NK cells to the uterus during pregnancy in still poorly understood, and it is possible that the cNK cells described in the uterus and very much resembling splenic NK cells, are recent immigrants from the blood. In order to investigate the role of NKG2A C57BL/6 mice, I was able to conduct paired analyses comparing NKG2A- and NKG2A+ NK cells. First performed in splenocytes, the FACS antibody panel used for this assay can be found in 3.0 Chapter I – Methodology – Panel 6. Having performed an NK1.1 cross-linking activation of NK cells in this experiment, I had to adjust the gating strategy slightly, as the NK1.1 epitope would not be a reliable positive selection marker for NK cells (Figure 18). Instead of NK1.1, I used the integrin CD49b (also known as DX5) which is expressed on the majority of NK cells, NKT cells and a minority of CD8+ T cells (Arase 2001).

For each tissue well incubated with anti-NK1.1, I also ran positive and negative controls for cell activation. Positive control wells had Phorbol 12-myristate 13-acetate (PMA) added, which activates protein kinase C, and the ionophore ionomycin which triggers the production of interferon. The addition of these factors results in cellular stimulation and a dramatic

upregulation of cytokine production. Untreated negative control wells simply had PBS added. This system enabled me to measure cytokine production in a dynamic range, where the results of NK1.1 cross-linking can be normalised to the intrinsic maximal functional output of cells from each individual mouse. This can be expressed in a specific production value, where the response was calculated as (A/B), where (A) = (% positive cells (of given readout e.g. CD107a) in response to NK1.1 activation – % positive cells in untreated) and (B) = (% cytokine positive cells in response to PMA/ionomycin.

Flow cytometry in vitro functional data using C57BL/6 splenocytes
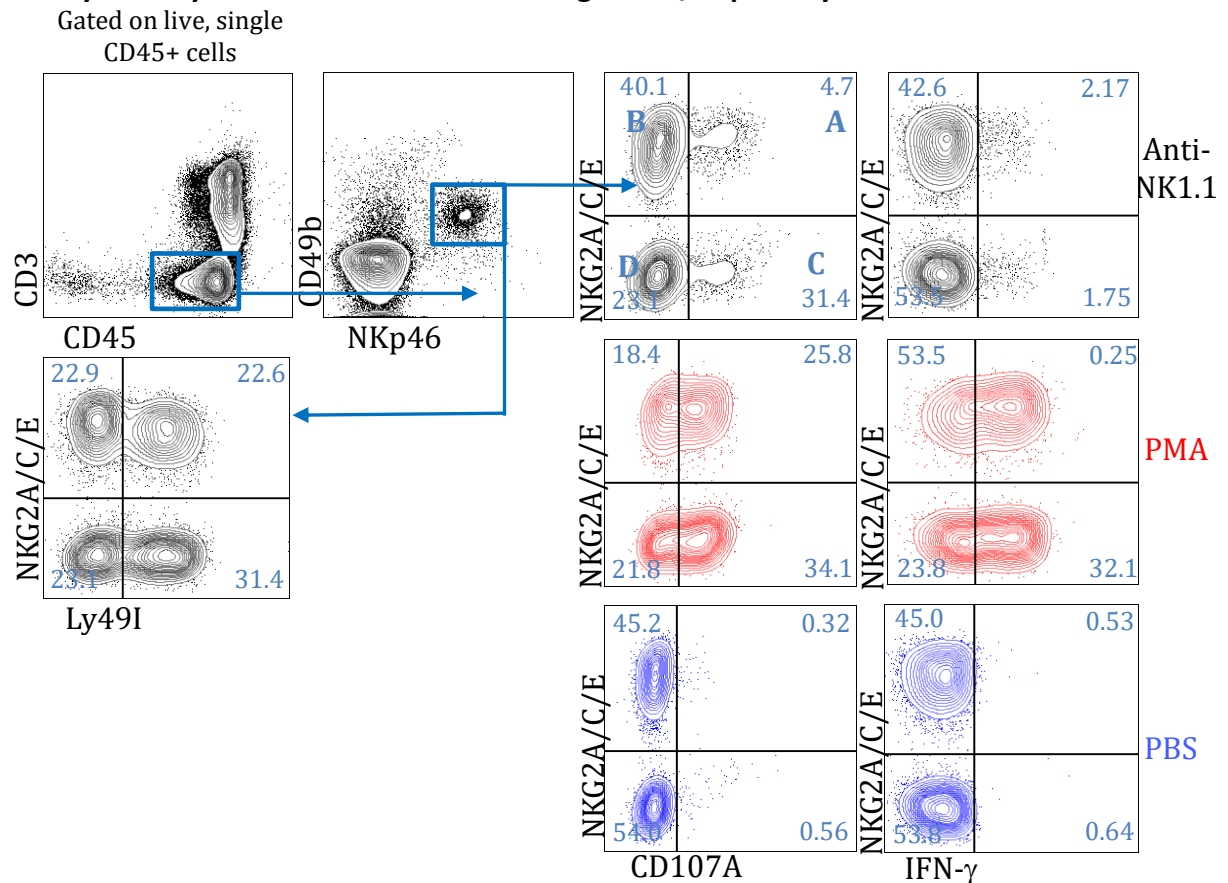
Figure 18. (Left panels) Representative flow cytometry gating strategy for splenocyte NK1.1 activation assay, with education subsets (bottom left), and functional responses (right panels), by condition. The anti-NK1.1 responses (top right) were used to draw quadrant gates for NKG2A vs. IFN-γ to produce licensing ratios in fig. 19B.

I found that NKG2A+ cells produced more IFN-γ and CD107a than their NKG2A- counterparts in every mouse tested (Figure 19A), when analysed as a paired comparison of specific production. The proportion of cells which upregulated functional readouts in response to activation was in keeping with previous reports of education assays in splenocytes. Representative flow cytometry dot plots of cellular responses to the three experimental conditions can be found in Figure 18. In a further analysis, I implemented what is referred to as "NK licensing ratio" (Jonsson & Yokoyama 2010), where a value of >1.5 suggests an educating effect. The "licensing ratio" describes the propensity of cells that are positive for a given marker

(e.g. NKG2A, Ly49-I) to produce IFN-γ relative to their negative counterparts, and is the result of dividing the percentage of positive NK cells that produce IFN-γ by the percentage of negative NK cells that produce IFN-γ. If the receptor does not mediate licensing, the licensing ratio is approximately 1 (usually 0.8–1.2). If the receptor mediates licensing, the licensing ratio will be over 1.5. This ratio was calculated in the following way:

$$\frac{a/(a+b)}{c/(c+d)}$$

a = (NKG2A+, IFN-γ+), b= (NKG2A+, IFN-γ-), c = (NKG2A-, IFN-γ+) and d= (NKG2A-, IFN-γ−)

A representative flow cytometry dot plot of where values for licensing ratios were derived can be found in Figure 18 in the functional response plots. The mean NKG2A licensing ratio for IFN-γ was 1.7, and for CD107a it was 1.4 (Figure 19B). In order to control for any education pathway heterogeneity introduced by other receptors between the NKG2A+ and NKG2A- subgroups, I measured the co-expression of the maturity marker CD11b and another self-specific educating receptor Ly49I Figure 19C. I found that the proportion of Ly49I+ cells was slightly lower in the NKG2A- subgroup, which may bias the results discussed above.

Flow cytometry in vitro functional data using C57BL/6 splenocytes
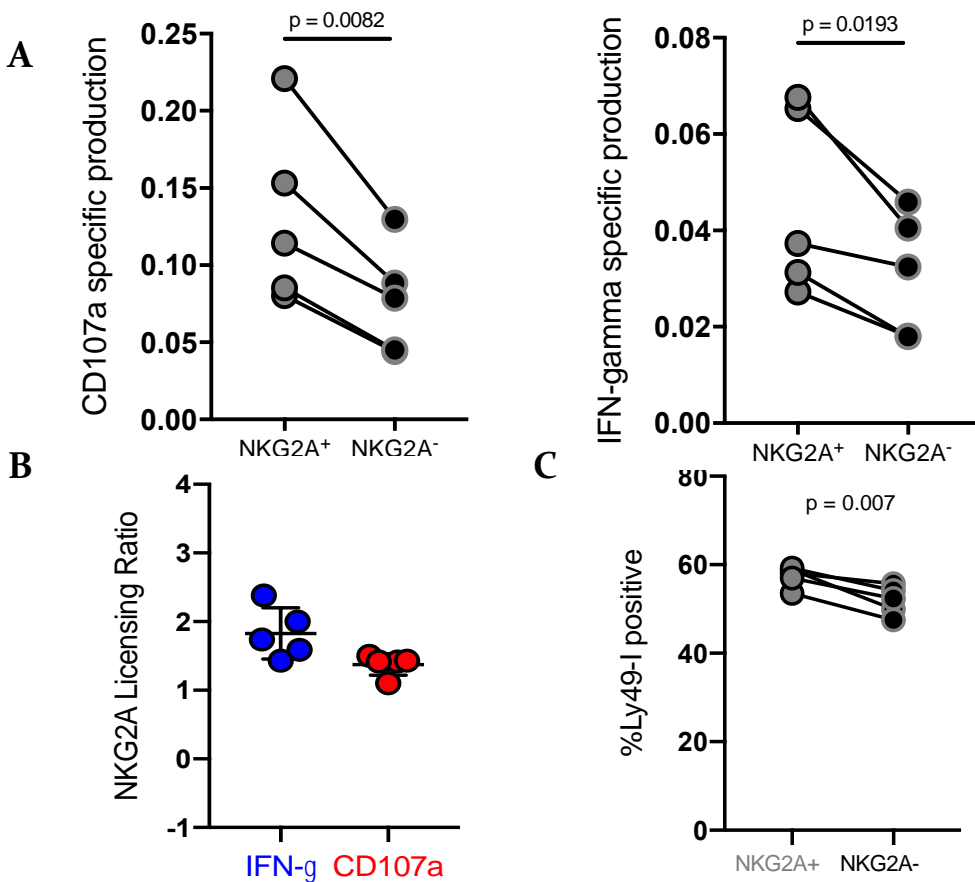
Figure 19. A) Specific production of CD107a (left) and IFN-γ (right) in response to NK1.1 cross-linking, by NKG2A subset, paired t-test. B) Individual NKG2A licensing ratios for each cytokine, calculated using A, B, C &* D in figure 18. For formula see above. C)

Comparison of percentage of each NKG2A subset which also express Ly49-I. Comparisons in A & C both paired t-test (sNK, splenic NK cells). Grey circles represent NKG2A$^+$ cells, black dots represent NKG2A$^-$ cells.

4.7 NKG2A educates NK cells to reject missing-self *in vivo*

Having established that NKG2A+ NK cells are functionally more responsive than NKG2A- NK cells in C57BL/6 mice, and that NK-and T-cell development is not altered in *Klrc1*$^{-/-}$ mice, I turned to the *Klrc1*$^{-/-}$ mice for further studies of systemic NK education. To test the contribution of NKG2A to peripheral NK cell education I used a standard *in vivo* assay based on rejection of MHC deficient *B2m*$^{-/-}$ haematopoietic cells (Höglund & Brodin 2010). This assay measures the ability of host NK cells to reject MHC-deficient transplanted leucocytes, in a classical illustration of the 'missing-self' recognition of NK cells. In this experiment, I harvested and counted MHC-sufficient splenocytes from C57BL/6 females and mixed them with MHC-deficient splenocytes from *B2m*$^{-/-}$ mice (a schematic can be found in Figure 20). The splenocytes from the *B2m*$^{-/-}$ mice were stained with CFSE at a 10x higher concentration than the normal cells to ensure the two populations could be easily segregated during FACS analysis. The primary cell suspension mixture was analysed by FACS and displayed approximately a 50:50 ratio of MHC+ and MHC- cells, as planned
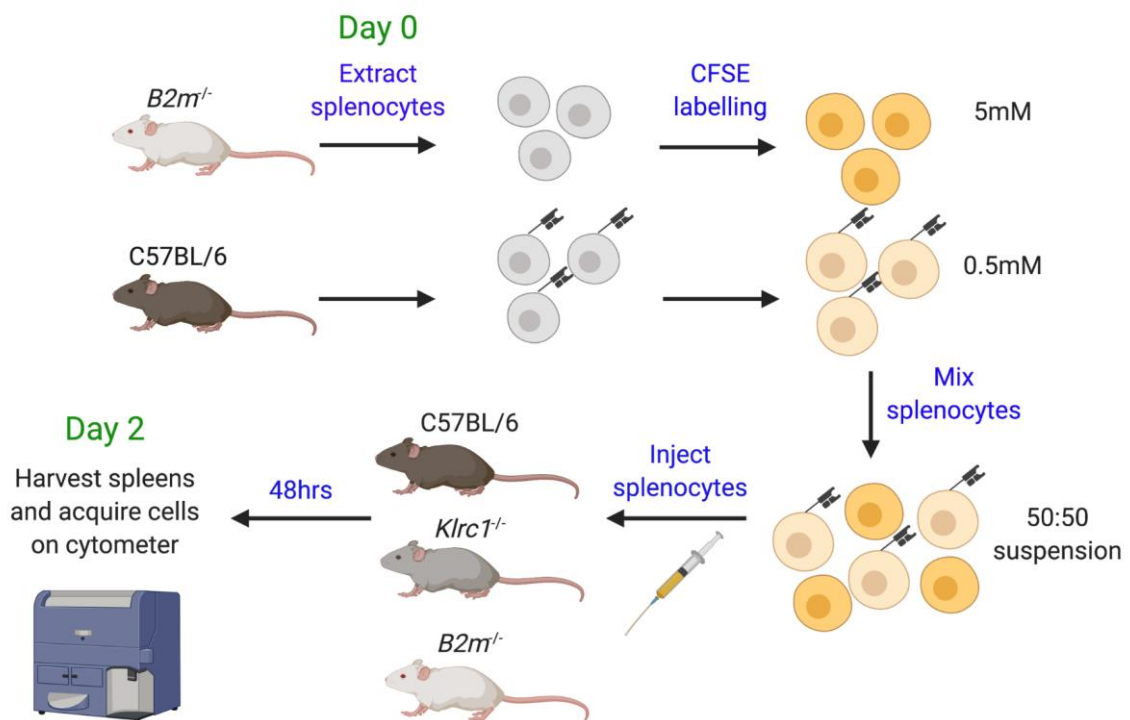
Figure 20. Schematic to represent *in vivo* rejection assay. Donor Splenocytes are harvested from *B2m*-sufficient and –deficient mice, labelled with CFSE, and then injected into mice strains of interest i.e. C57BL/6 controls, *Klrc1*$^{-/-}$ and *B2m*$^{-/-}$. Spleens are then harvested after 48hours to assess the number of *B2m*-deficient cells which have failed to be eliminated.

Under normal conditions, C57BL/6 mice should eliminate the majority of MHC-deficient but not MHC-sufficient donor cells within 48 hours, highlighting the exquisite ability of NK cells to discriminate between MHC-deficient and MHC-sufficient cells. As a result, at the end of the assay, the ratio between the two groups of cells is drastically changed to about 90:10 in favour of the MHC-sufficient cells. I found that $Klrc1^{-/-}$ mice were almost 50% less efficient than C57BL/6 mice. The percentage of MHC- cells dropped from approximately 50% at injection, to approximately 15% in C57BL/6 mice. However, in $Klrc1^{-/-}$ the percentage of MHC- donor cells still present within the spleen was approximately 30%, with the same injected ratio (Figure 21A). As a percentage of target cells eliminated, the C57BL/6 strain rejected around 70%, compared to only 35% in the $Klrc1^{-/-}$ strain. This analysis revealed a statistically significant reduction in an NK-cell function that is known to be directly dependent on MHC-education, as measured through the function of missing-self recognition (Figure 21B).

These data provide *in vivo* support to the *in vitro* splenocyte NK1.1 activation assay detailed above, confirming that NKG2A optimises NK cell education in the periphery of C57BL/6 mice. It is likely that the other educating pathways present e.g. Ly49 family receptors, provided some educational benefit to retain the low level of rejection seen in $Klrc1^{-/-}$ mice. As a validation of this *in vivo* approach, I performed the same experiment in *B2m*-KO mice. These mice are the gold standard as a model for no NK education (Kim 2005). When performing such experiments in this strain however, results should be interpreted with caution, due to the T cell phenotype discussed previously.

Like in $Klrc1^{-/-}$ mice, I found that a lack of educating pathways led to an inability to reject target cells in $B2m^{-/-}$ mice. All C57BL/6 mice rejected a proportion of their target cells, although not to the same degree as in the $Klrc1^{-/-}$ experiment discussed above. In contrast, only one of the $B2m^{-/-}$ mice was able to reject MHC-deficient cells, whereas the other four displayed a complete inability to recognise and eliminate target cells (Figure 21C). These data confirm that NK education is pivotal in the missing-self phenomenon, and that this assay is appropriately designed to detect *in vivo* education phenotypes.

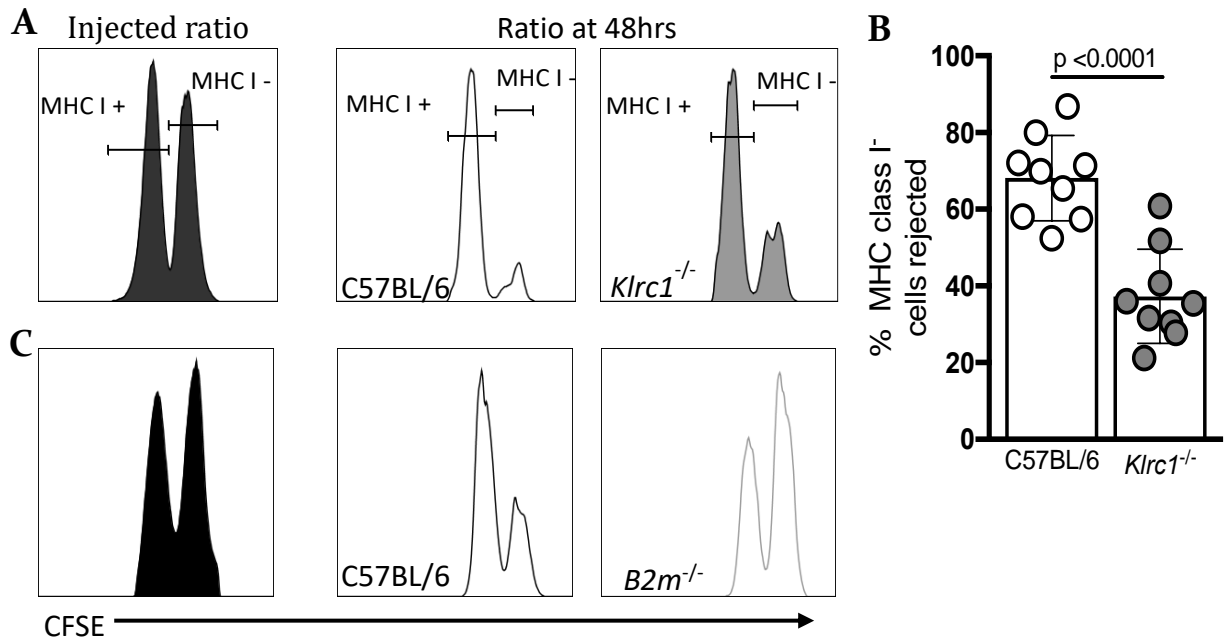**Flow cytometry in vivo rejection data using C57BL/6, *Klrc1*^{-/-} and *B2m*^{-/-} mice**

Figure 21. A) Representative flow cytometry histograms of injected ratios of donor MHC-I- and MHC-I+ splenocytes vs. ratios at 48hrs, *Klrc1*^{-/-} vs C57BL/6. B) Statistical comparison of rejection of MHC-I-deficient cells, by strain (t-test, mean + SD). C) Control experiment, identical to that shown in (A), with *B2m*^{-/-} vs C57BL/6 instead.

4.8 NKG2A educates uterine NK cells in early gestation

Having established a key role for NKG2A in peripheral NK cell education, and ensuring that I can recapitulate these findings *in vivo*, I next turned my attention to the context of early pregnancy. Our laboratory has previously published assays of education in uNK in C57BL/6 mice during pregnancy. In this study (Kieckbusch 2014), it was shown that the mean proportion of IFNγ-producing cells among Ly49C/I+ uNK at g.d. 9.5/10.5 was more than 1.5-fold higher than in their Ly49C/I–uNK counterparts, in C57BL/6 dams, indicating that maternal MHC educates uNK. It was also shown that there was no education from paternal MHC as Ly49A+ and Ly49A–cells were equally responsive in D8-mated C57BL/6 females, in which the trophoblast expressed the transgenic H-2D^d, a ligand for Ly49A. For the experiments in this project, I also chose the time-point of g.d. 9.5, when uNK cells are abundant in the maternal decidua and spiral artery remodelling is still not complete. This time-point also provides a cell yield large enough for individual mouse analysis, avoiding the necessity to pool tissue, which provides biases.

In mice, NK-cell produced IFN-γ is the key cytokine to remodel the uterine spiral arteries (Ashkar 2000), a necessary step for optimal placentation in both humans and mice. Production of IFN-γ through stimulation of activating-receptors is also the standard functional readout of both human and mouse NK education, together with degranulation, measured by expression of CD107a, as discussed previously. To quantify the contribution of NKG2A to uNK cell education in mice, I compared the % of IFN-γ and CD107a+ cells upon NK1.1 stimulation of NKG2A+ and NKG2A- subsets in C57BL/6 mice at g.d. 9.5.

I found that cell suspensions needed to be enriched for lymphocytes through a Percoll gradient prior to NK1.1 cross-linking. I discovered this as initial experiments using whole uteri were unsuccessful. This is likely to have occurred due to the low yield of live cells in a mechanically- and enzymatically -digested whole g.d. 9.5 uteri. Incubating these cell suspensions for 9 hours leads to almost complete cell death within the well, probably due to the release of cytotoxic factors from the high proportion of dead cells present at the beginning of the incubation.

Furthermore, I found that my activation protocol needed to be slightly adapted from that used in the splenocyte NK1.1 cross-linking described previously. For uterine tissue, I used a longer incubation period of 9.5 hours instead of 4 hours (Kieckbusch 2014). I also used 10μg/ml of plate-bound antibody, as opposed to 20μg/ml used in splenocyte activation. This slower and more 'gentle' activation of cells was sufficient to allow for a significant amount of cytokine production, whilst avoiding excessive cell death. I also found that adding PMA/ionomycin to uterine cell wells resulted in excessive cell death and debris over a 9.5 hour period, with downstream analysis not possible. As a result, the specific production calculation used in analysis of splenocytes could not be performed in uterine tissue.

Again, this analysis was performed in C57BL/6 mothers whose uNK can be split into two subgroups based on NKG2A expression. I mated C57BL/6 females with C57BL/6 males. At g.d. 9.5 I processed uteri as described previously, and incubated with either cell suspensions with either anti-NK1.1 or PBS (negative control) for 9.5 hours, before fluorescence cell labelling and FACS analysis (for schematic see Figure 22). The antibody panel can be found in in 3.0 Chapter I – Methodology – Panel 7, and gating strategy to identify uNK in Figure 23A. In keeping with previous attempts by members of the laboratory group (Jens Kieckbusch), individual analysis of cytokine production by all three uNK subgroups was not possible due to the low cell yield in this assay. Thus, all three subgroups groups were collated and termed 'bulk uNK'.

I found that uNK cells from all mice upregulated IFN-γ and CD107a in response to NK1.1 cross-linking, with minimal background production of these factors in the PBS-treated wells. Representative flow cytometric dot plots of these responses can be found in Figure 23B. Due to the negligible background production observed, negative control wells were used to set gates for positive events in functional readouts. This strategy was tested against an internal biological control for each mouse (CD19+ B cells) which are known to not produce either cytokine, and similar results were observed.
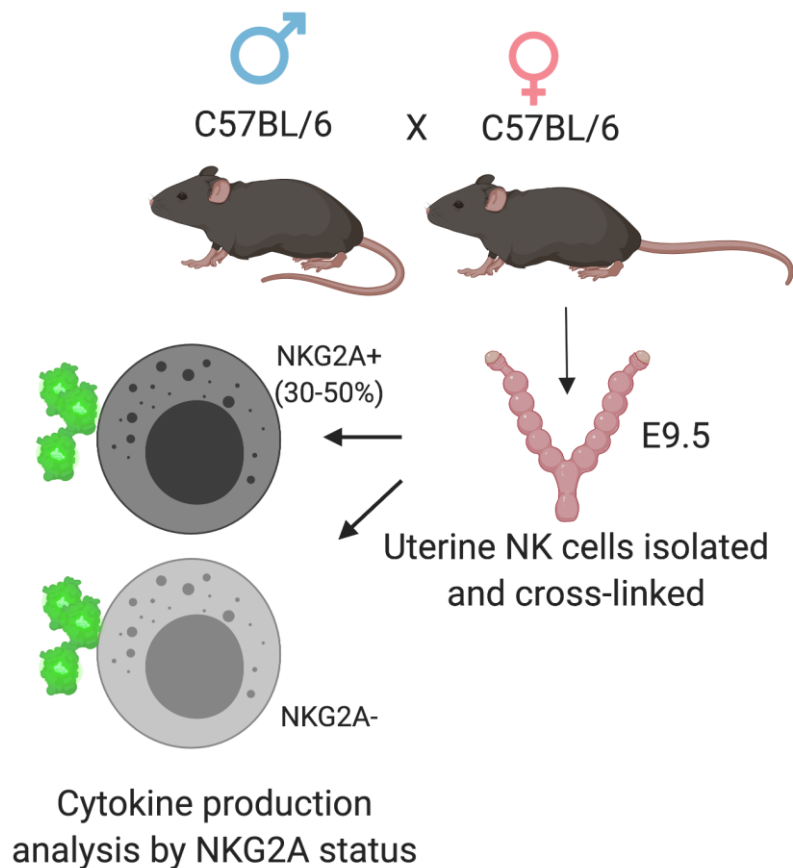
Figure 22. Schematic to show experimental design of uterine *in vitro* activation assay

Flow cytometry in vitro functional data using C57BL/6 uterine cells
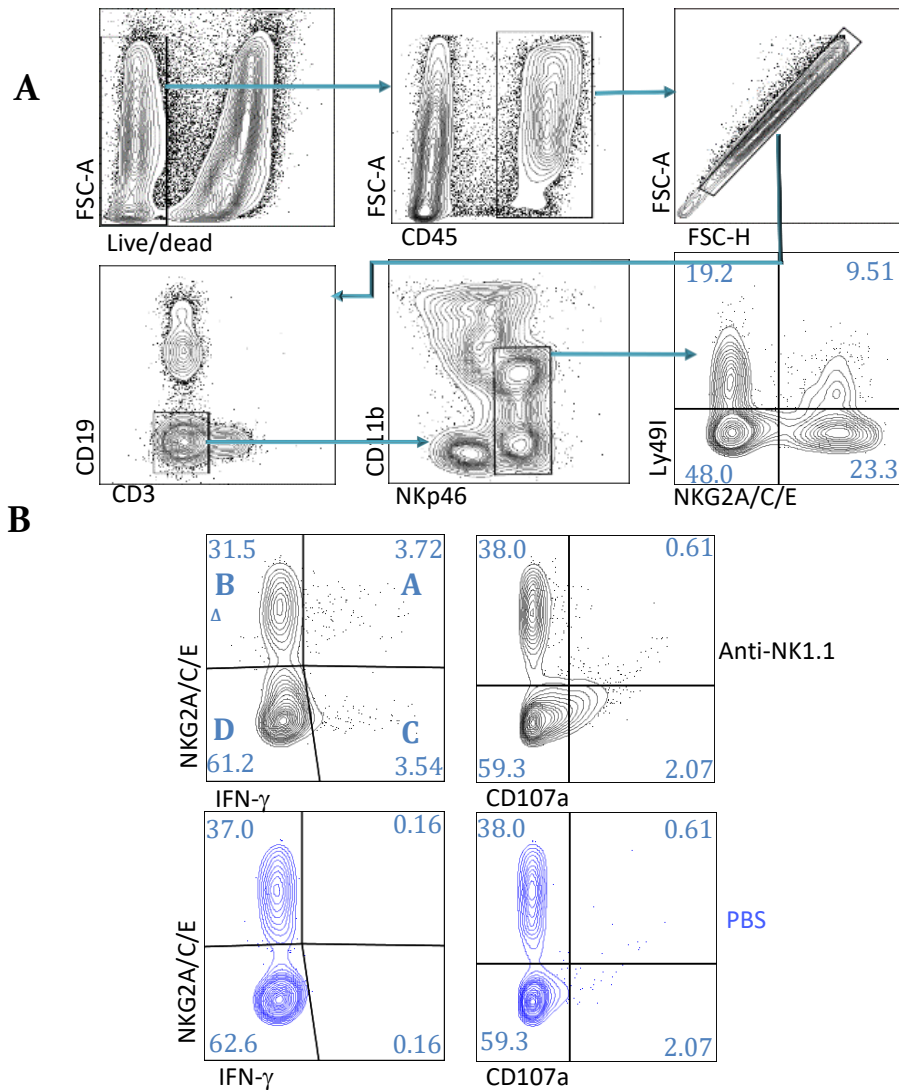
Figure 23. A) Representative flow cytometry gating strategy used to identify uNK education subsets at g.d. 9.5. B) Functional responses (IFN-γ left, CD107a right) in response to anti-NK1.1 and PBS (negative control) by NKG2A subset.

A paired analysis revealed that the % of IFN-γ producing cells at g.d. 9.5 was approximately 2-fold greater within NKG2A+ uNK cells than in NKG2A- uNK cells, where approximately 8-10% of uNK expressed the cytokine, compared to approximately 4-5% in the NKG2A- subgroup (Figure 24A). This enhanced response was mediated through an expansion of cells positive for IFN-γ, however, as mean IFN-γ expression *per cell* did not change when measured through geometric mean fluorescence intensity (GMFI, Figure 24B). These percentage differences, whilst small, are statistically significant and are also in keeping with previous findings in other studies of NK cell education (Kim 2005; Anfossi 2006). These data also recapitulate preliminary experiments performed on education-null $B2m^{-/-}$ mice in our laboratory group (Jens Kieckbusch, unpublished data), and represent biologically significant changes.

Like in the spleen, the specific educational effect of the NKG2A receptor in the uterus was confirmed through implementing the 'licensing ratio' (Jonsson & Yokoyama 2010). NKG2A was confirmed to independently educate uNK as it displayed a mean licensing ratio of approx. 2. This effect was not found for the degranulation marker CD107a however, where the licensing ratio was less than 1 (Figure 24C). Because Ly49 inhibitory receptors also educate NK cells, I measured the percentage of cells expressing Ly49I (one of the two self-specific educating Ly49 receptors in B6 mice) (Fernandez 2005) within NKG2A+ and NKG2A- subsets and found no significant differences, ruling out the potentially confounding effect of Ly49I education in the two subsets (Figure 25A). NKG2A is generally expressed in less mature NK cells and indeed the maturation marker CD11b was higher on NKG2A- NK cells (Figure 25B), suggesting that the increased IFN-γ response observed in the NKG2A+ cells was not due to maturity but rather to education.

Taken together these data indicate an important role for NKG2A in modulating NK education and mounting functional NK responses both systemically and in the uterus during pregnancy. They also confirm the suitability of NKG2A-deficient mice to model NK education in pregnancy.

Flow cytometry in vitro functional data using C57BL/6 uterine cells
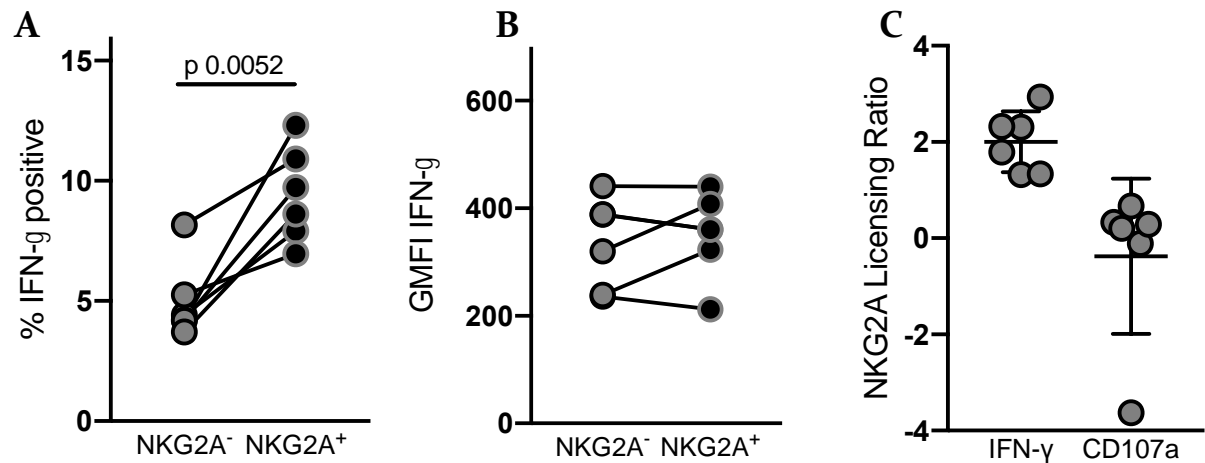
Figure 24. A) Comparison of % IFN-γ + cells, in response to NK1.1 cross-linking, by NKG2A subset, paired t-test. NKG2A+ value calculated by A/B, and NKG2A- values by C/D in figure 23B. B) GMFI of IFN-γ expression, by NKG2A subset. C) NKG2A licensing ratio for IFN-γ and CD107a calculated by using A, B, C & D in figure 23B, for formula see above.

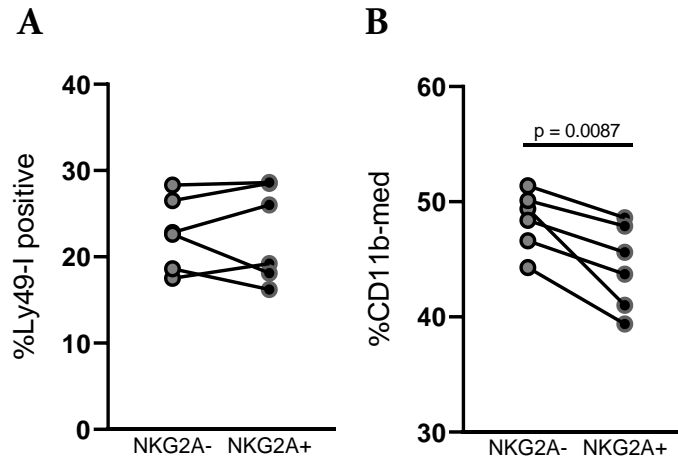**Flow cytometry in vitro functional data using C57BL/6 uterine cells**

Figure 25. A) %Ly49-I+ uNK cells, by NKG2A subset, paired t-test. B) %CD11b+ uNK cells, by NKG2A subset, paired t-test.

4.9 Spiral artery remodelling in *Klrc1*^{-/-} dams

Maternal uterine spiral arteries undergo transformation through the destruction of smooth muscle media in early pregnancy to allow optimal fetal nourishment (Lyall 2013). This process helps to establish appropriate placentation and in part relies upon uNK cells producing IFN-γ in mice (Ashkar 2000). I used established stereological techniques (Kieckbusch 2015) to measure whether the observed reduction in IFN-γ production in NKG2A-deficient uNK cells was associated with a defect in gestational maternal vascular adaptation in *Klrc1*^{-/-} dams. I measured spiral artery remodelling at g.d. 9.5 where uNK are prevalent in the maternal decidua, and where previous stereological techniques have been employed. I mated *Klrc1*^{-/-} females with C57BL/6 males, and compared them to control C57BL/6 female mated with C57BL/6 male pregnancies (schematic in Figure 26).

A representative g.d. 9.5 implantation site stained with haematoxylin and eosin (H&E) can be found in Figure 27A. This technique allows the identification of the fetus and amnion, the transformation zone, the maternal decidua and the MLAP. Under a higher magnification (Figure 27B), the thick-walled spiral arteries with erythrocytes present in their lumen, can be easily identified.
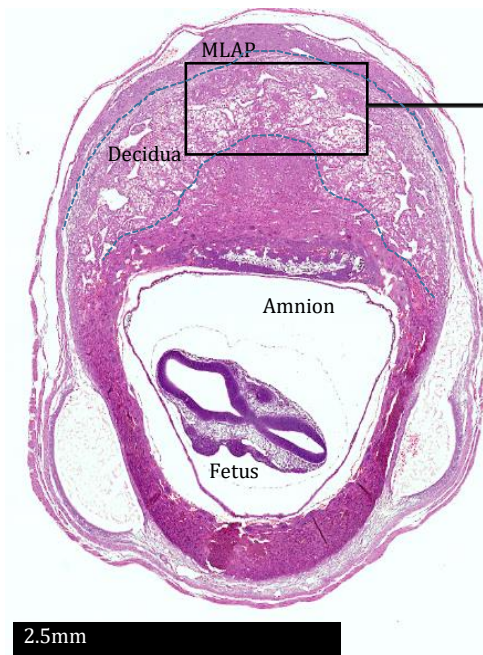
Figure 26. Mating strategy for spiral artery stereology experiment

A

B
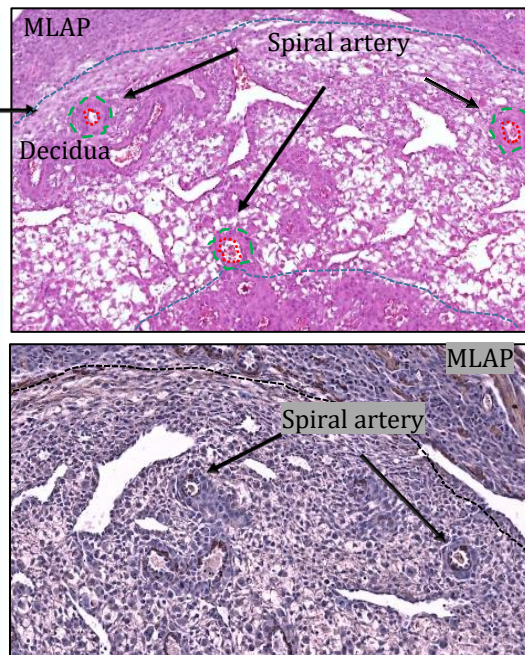
Figure 27. A) Representative section of g.d. 9.5 implantation site (IS), and B) stereological assessment of spiral arteries using H&E (top), and IHC (bottom) for smooth muscle actin (SMA, brown).
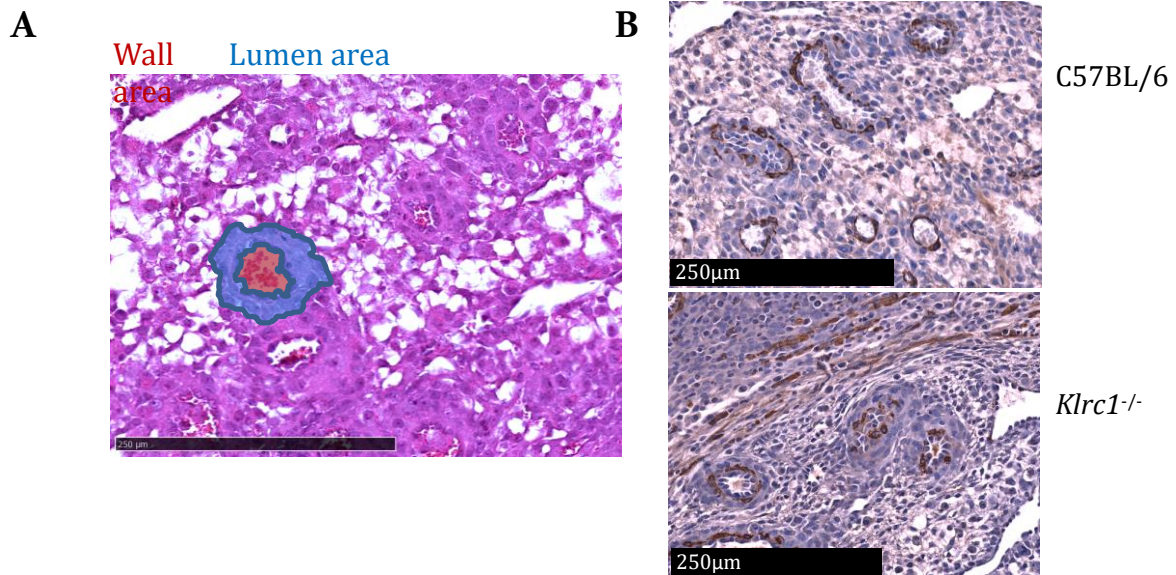
Figure 28. A) Representative section of g.d. 9.5 implantation site showing stereological assessment of spiral arteries using H&E (left) with red shading representing vessel lumen area, and blue shading representing vessel wall thickness. B) IHC for smooth muscle actin, by group (right SMA, brown).

Through quantitative stereological measurement in H&E stained sections (Figure 28A, I found that NKG2A is required for spiral artery remodelling. By measuring the spiral artery wall area (Figure 29A) and lumen area (Figure 29B), I calculated a wall: lumen ratio, which is indicative of vascular remodelling. *Klrc1*$^{-/-}$ dams exhibited a higher wall volume ratio (Figure 29C), which was driven by a thicker wall volume, not smaller lumen. This finding is suggestive of incomplete remodelling of the vessel wall.
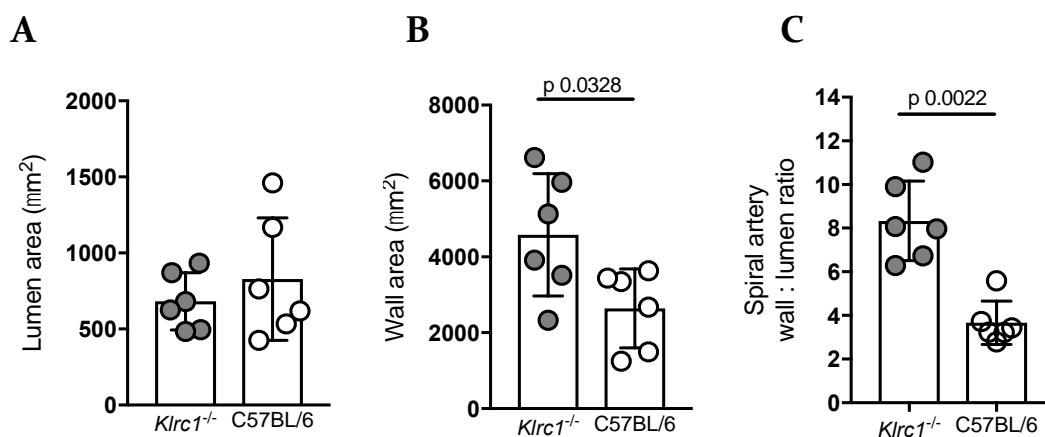

Figure 29. H&E staining. A) Spiral artery lumen area, vessel wall area B) and resultant wall: lumen ratio C) in C57BL/6 vs. *Klrc1*$^{-/-}$ dams at g.d. 9.5 (all t-tests). Each dot represents the mean of 15 different measurements from one implantation site (n = 2-4 mice per group).

Identification of spiral arteries in this technique can be biased towards blood vessels with thick walls, and measurement of wall and lumen area is subjective. In order to confirm the suggested biological process of a reduction in smooth muscle destruction in *Klrc1*$^{-/-}$ dams, I used

immunohistochemistry to validate the H&E findings. I used an antibody to identify the contractile protein smooth muscle-actin (SMA) in tissue sections from the same implantation sites measured with H&E.

SMA was found to be associated with spiral arteries in the maternal decidua at g.d. 9.5, as expected. Rings of SMA were found to line the inside of maternal vessels, where vascular smooth muscle cells are known to be present (Whitley 2010). Taken qualitatively, these sections appear to show that SMA is more prevalent around spiral arteries in *Klrc1*^{-/-} dams, when compared to C57BL/6 dams, suggesting that the remodelling process was incomplete in *Klrc1*^{-/-} dams (Figure 28B). However, when only using SMA as a marker of vessel wall boundaries through immunohistochemistry, one can generate quantitative data from these sections. Reassuringly, this further analysis on a smaller number of mice supported the H&E data, and found that vessel wall: lumen ratios were higher in *Klrc1*^{-/-} dams (Figure 30A-C)
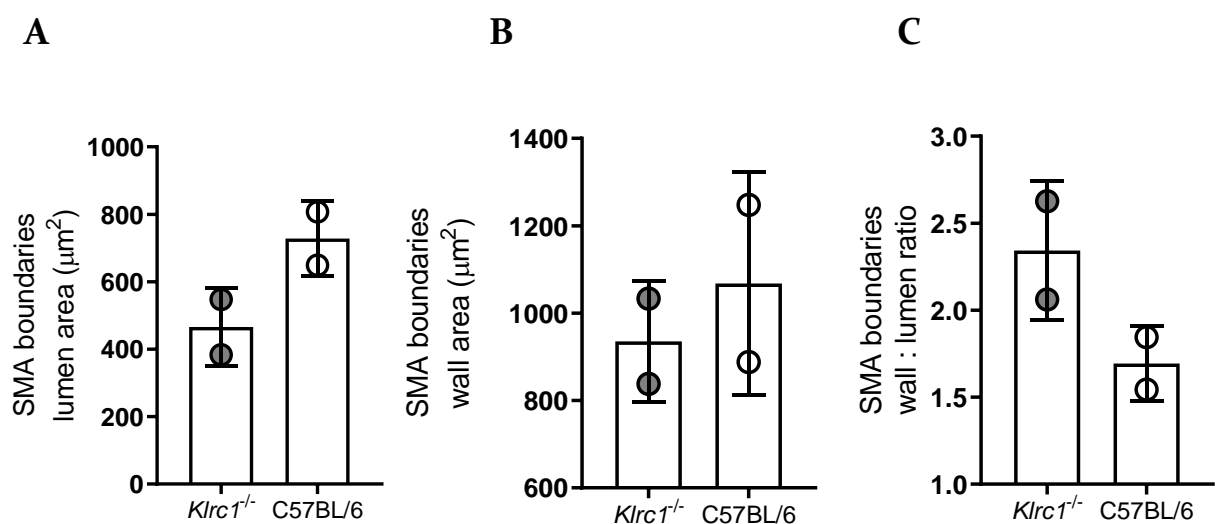
A **B** **C**

Figure 30. SMA Immunohistochemistry. A) Spiral artery lumen area, vessel wall area B) and resultant wall: lumen ratio C) in C57BL/6 vs. *Klrc1*^{-/-} dams at g.d. 9.5. Each dot represents the mean of 15 different measurements from one implantation site (n = 2 mice per group).

4.10 Micro-ultrasound of maternal uterine arteries

I next assessed whether the vascular maladaptation observed in the spiral artery remodelling assay may lead to other vascular changes in the maternal-fetal vascular unit. I chose to focus on the maternal uterine artery. I chose this artery because it is upstream of decidual spiral arteries, is used to predict early-onset pre-eclampsia in human pregnancies, and has been shown to be affected during pregnancy in a mutant mouse line lacking both NK cells and Mast cells (Meyer 2018). The technique used was ultra-high frequency micro-ultrasound Doppler, which provides a sensitive assessment of blood flow velocity in embryonic-size blood vessels.
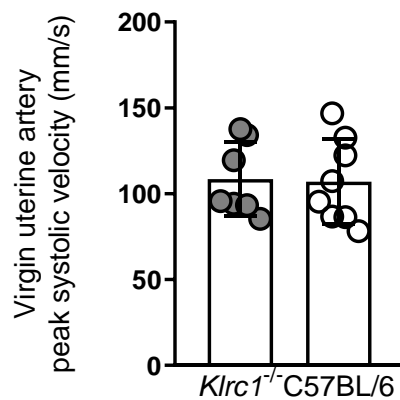
Representative images of micro-ultrasound assessment of dams can be found in Figure 30A. I first analysed pre-pregnancy single uterine arteries in virgin C57BL/6 and *Klrc1*^{-/-} females. Resistance index is a measure of pulsatile blood flow that reflects the resistance to blood flow caused by a vascular bed distal to the site of measurement, in this context the distal site would be the maternal decidua. When I analysed virgin mice, I found no difference in end diastolic velocity (EDV), peak systolic velocity (PSV) or resistance index (UARI) (Figure 31B-D) between *Klrc1*^{-/-} and C57BL/6 females. This was a reassuring finding as it confirmed no direct effect of *Klrc1*^{-/-} in vascular blood flow, meaning any phenotype found in pregnancy could be attributed to maternal adaptation, and not an underlying systemic phenotype.
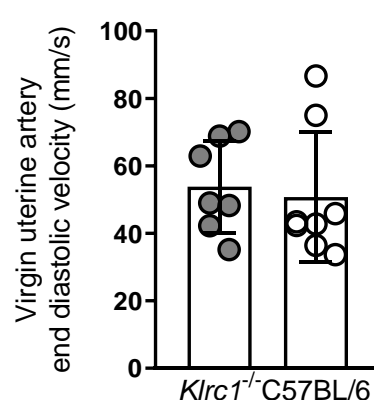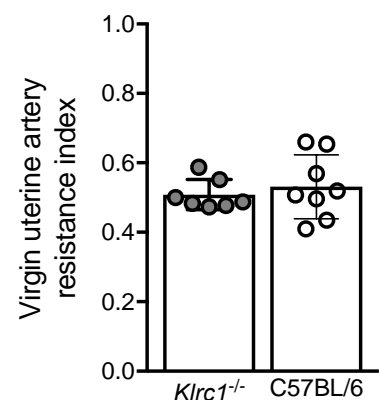
A
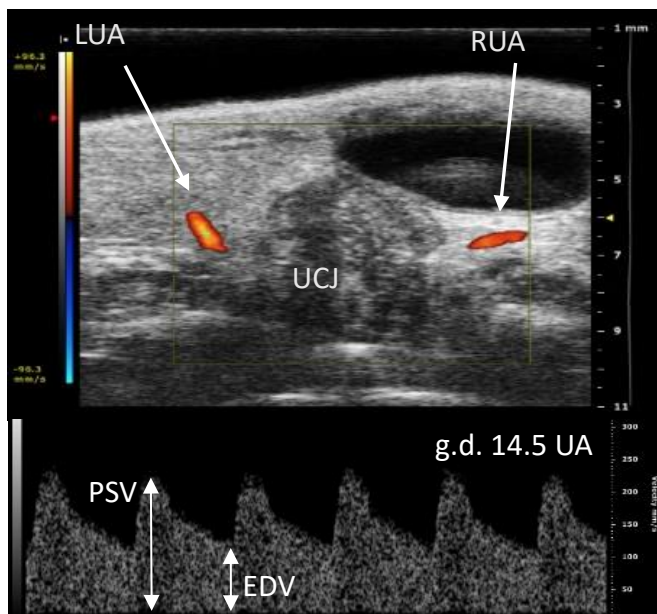
Uterine Artery Doppler in virgin mice

Figure 31. A) Representative micro-ultrasound colour Doppler image showing both uterine arteries (UA) lateral to the utero-cervical junction (UCJ), and PW Doppler waveform data of B) PSV, C) EDV and D) UARI comparisons in C57BL/6 and *Klrc1*^{-/-} virgin mice, by maternal strain. Error bars represent standard deviation.

I then performed a study on pregnant females, and analysed both of their uterine arteries at g.d. 12.5 in order to take into account any bias in the number of concepti in each uterine horn. This second time-point was used to detect any significant gestational difference in uterine artery blood flow between C57BL/6 and *Klrc1^-/-* mice, in early pregnancy. I did not expect to see a large difference in this analysis, as uterine artery dilatation does not significantly increase until after g.d. 13.5 in mice (Rennie 2016). This analysis at g.d. 12.5 was also an opportunity to optimise experimental conditions and ultrasound set-up in pregnant mice, where the presence of multiple concepti render identification of uterine arteries challenging. Data generated from this experiment should therefore be treated with caution. Finally, the sample size for g.d. 12.5 measurements was smaller than later studies, as unfortunately not all females were successfully mated. At g.d. 12.5 I found no difference in mean uterine artery PSV, mean EDV or UARI (Figure 32).
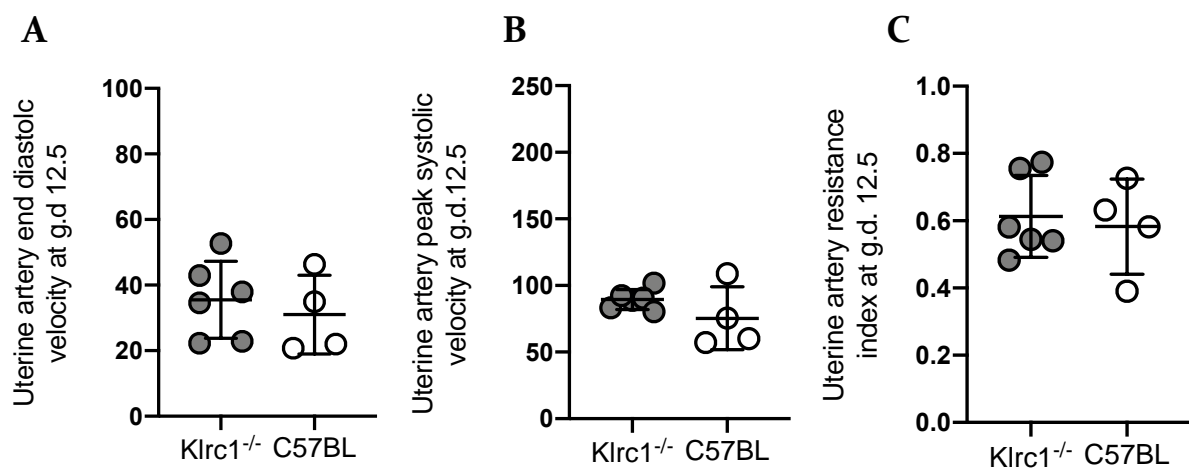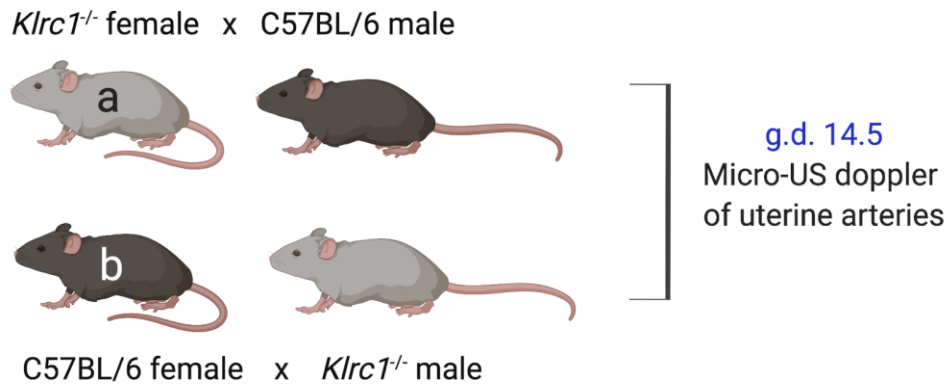
Uterine Artery Doppler at g.d. 12.5

Figure 32. PW Doppler values for A) PSV, B) EDV and UARI comparisons in C57BL/6 and Klrc1-/- pregnant g.d. 12.5 mice, by maternal strain. Error bars represent standard deviation.

In a new batch of females, I next analysed uterine artery blood flow at g.d. 14.5. This experiment was performed in genetically-matched pregnancies, where the study group consisted of *Klrc1^-/-* females mated with C57BL/6 males, and the control group was C57BL/6 females mated with *Klrc1^-/-* males (Figure 33A). I observed no difference in mean peak systolic velocity between *Klrc1^-/-* and C57BL/6 dams (Figure 33B) However, the end diastolic blood flow velocity was reduced in *Klrc1^-/-* dams (Figure 33C). This contributed to an increased mean resistance index (Figure 33D) in *Klrc1^-/-* dams, when compared to C57BL/6 dams. This finding at g.d. 14.5 resulted in an absence of the pregnancy-induced decrease in resistance index normally expected, when compared to the values obtained in the previously discussed virgin female groups (Figure 33E). Thus, to our knowledge, I provide the first evidence in mice that
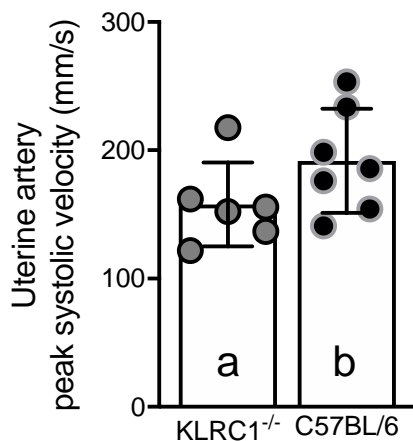
NK cell-specific alterations can result in uterine artery blood flow perturbations associated with reduced spiral artery remodelling.
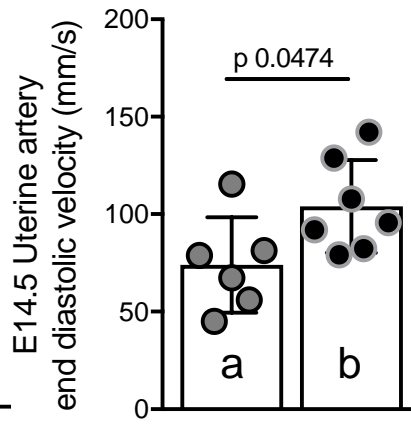
A

Klrc1-/- female x C57BL/6 male

g.d. 14.5
Micro-US doppler
of uterine arteries

C57BL/6 female x *Klrc1*-/- male

Uterine Artery Doppler at g.d. 14.5
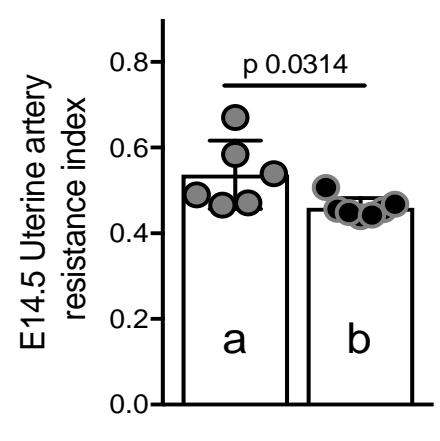
B

C

p 0.0474

D

p 0.0314

E
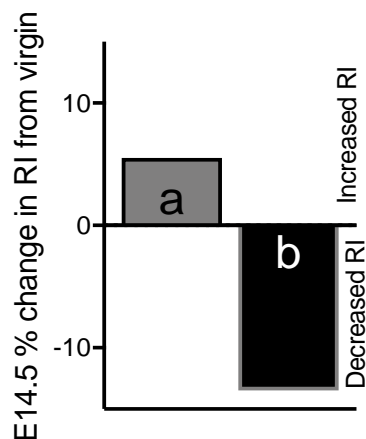
Figure 33. A) Outline of breeding strategy for ultrasound assessment of gestational vascular adaptation. B-D) UA PSV, EDV and UA RI comparisons, by group (error bars represent SD, lettering corresponds to figure 33A where grey dots represent *Klrc1*-/- dams, and black dots represent C57BL/6 dams) at g.d. 14.5, (t-test). E) Percentage change in RI from virgin to g.d. 14.5 (bars show mean change in RI from data shown in figures 31D and 33D). Error bars represent standard deviation.

4.11 Umbilical artery micro-ultrasound

Placental insufficiency is the likely underlying mechanism in most cases of fetal growth restriction (FGR) and pre-eclampsia. Human fetuses suffering from pathological FGR *in utero* display characteristic responses to an abnormal placental supply of nutrients and oxygen through a relative increase in middle cerebral artery blood flow, often associated with changes in umbilical artery pressure indices (Robson 2013).

Again, I compared the umbilical artery blood flow velocity in genetically-matched fetuses, who were all heterozygotes for the mutated form of *Klrc1*. These fetuses were grouped by whether they developed in C57BL/6 (control group) or *Klrc1*$^{-/-}$ (study group) mothers (Figure 34A). This assay was performed by applying to fetal vessels at g.d. 14.5 the same ultra-high frequency micro-ultrasound technique described above. I measured two fetuses per dam, where the probe was moved laterally from the maternal utero-cervical junction below the bladder, until an appropriately-positioned fetus was identified, once in each uterine horn.
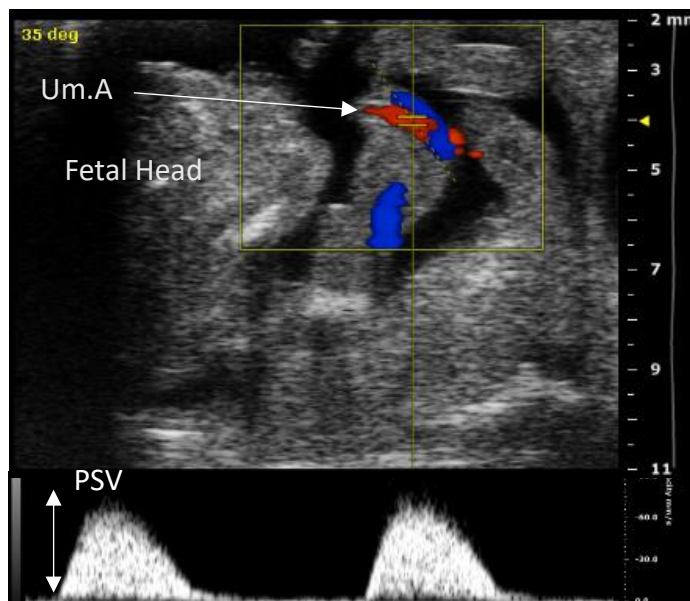
A representative micro-ultrasound image in colour-doppler mode displaying the fetal umbilical artery and vein can be found in Figure 34B. I found an absence of end diastolic velocity in fetuses at this gestation, in keeping with previous studies showing that this ultrasonic feature tends to develop at g.d. 15.5. However, I did find that fetuses from *Klrc1*$^{-/-}$ dams displayed a perturbed vascular response to developing in their high resistance *in utero* environment. This was characterised by a statistically significant reduction in peak systolic blood flow velocity in umbilical arteries analysed in fetuses from *Klrc1*$^{-/-}$ dams (Figure 34C). Blood flow velocity in umbilical veins was not measured, as its relevance to murine and human pregnancy is not yet clear.

The combination of an abnormally high resistance uterine blood flow, and abnormally reduced umbilical blood flow, represents sub-optimal vascular adaptation to pregnancy either side of the maternal-fetal interface, resting solely on the deletion of one NK receptor. To our knowledge, this is the first report of this nature in murine pregnancy, and closely recapitulates states of pathology in human pregnancy.
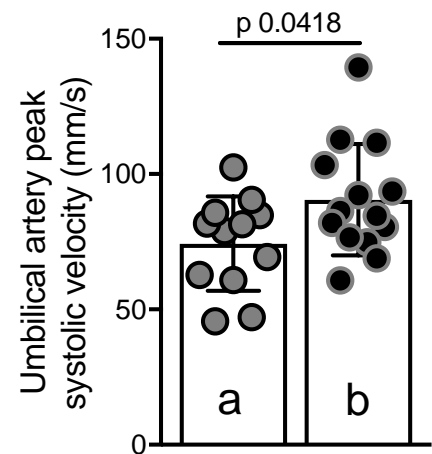
A
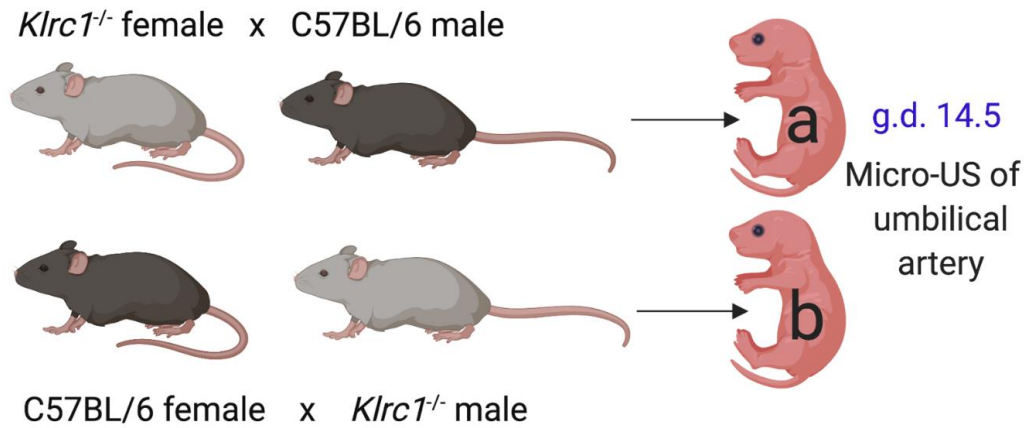
B

C

Figure 34. A) Breeding strategy to measure the effect of maternal NKG2A deletion on fetal growth restriction. B) Representative micro-ultrasound image of uterine umbilical artery (red, Um. A) and umbilical vein (blue) with Um. A waveform below (PSV = peak systolic velocity). C) Comparison of Um. A PSV at g.d. 14.5, by group (t-test). Error bars represent standard deviation.

4.12 Optimising Micro-CT analysis of fetal growth

Previous murine models of reduced fetal growth have simply reported fetal weight at a given pregnancy time point. These data are useful when comparing mean fetal weight from a model to a suitable control. However, it often does not give any indication as to whether the reduced fetal growth is caused by significant placental pathology, or whether it is representative of the type of pathological reduced fetal growth displayed by human FGR fetuses. Asymmetric fetal growth can also discriminate pathologically small fetuses (FGR) from small-for-gestational-age (SGA), but otherwise healthy fetuses, who also lie below the 10th centile of estimated fetal

weight (Sharma 2016). Accordingly, I chose to utilise a technology capable of analysing whole mouse fetuses at g.d. 18.5, where organ segmentation and measurement could be used to provide a sensitive assay of growth symmetry.

Having been taught the technique at the centre where it was first developed in g.d. 15.5 fetuses, the Mouse Imaging Centre at the University of Toronto, I first sought to validate this technique in g.d. 18.5 fetuses. There are a number of tissue processing and analysis steps in this protocol which may influence the final organ volume output. These became apparent during the first experiment where the optimisation was performed, prior to the main analysis in *Klrc1*$^{-/-}$ dams.

The first experiment done to validate this technique was performed at g.d. 15.5 in a mouse strain known to predispose fetuses to growth restriction. The strain *Rag2*$^{-/-}$*IL2rg*$^{-/-}$ mice (RAG2GC-KO) compound mutant mice (also called *Rag2*$^{-/-}$*γc*$^{-/-}$ mice) exhibit T-cell, B-cell and NK-cell deficiency. They lack the recombinase activating gene 2, which is essential for assembling antigen receptors in B- (Grawunder 1995) and T-cell (Wilson 1994) development. These mice also lack the common gamma chain shared by receptors for IL-2, IL-4, IL-7, IL-9, IL-15 and IL-21 that is essential for the growth and maturation of all lymphocytes, including NK cells (Wilson 1994).

I mated *Rag2*$^{-/-}$*IL2rg*$^{-/-}$ females with C57BL/6 males, and C57BL/6 females with C57BL/6 males. At g.d. 15.5 I found no difference in fetal weight between the two strains (Figure 35A-B). However, at g.d. 18.5 I found that *Rag2*$^{-/-}$*IL2rg*$^{-/-}$ females were twice as likely to produce fetuses below the 10th centile of the control group (Figure 35C-D), consistent with a potential late-onset growth restriction phenotype. Having established this, I used 2D micro-CT analysis of *Rag2*$^{-/-}$*IL2rg*$^{-/-}$ and C57BL/6 strains at g.d. 15.5 to see if I could detect any anatomical differences.

Fetal weight at g.d. 15.5

A
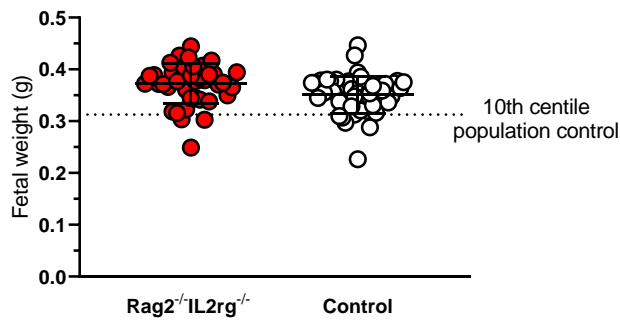
B
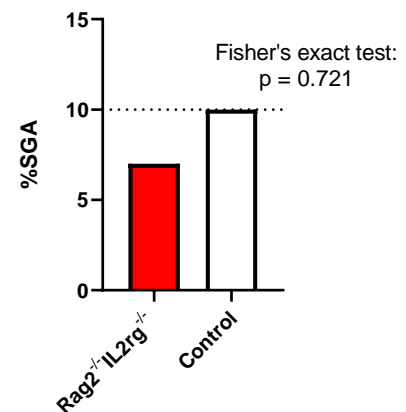
Fetal weight at g.d. 18.5

C

D
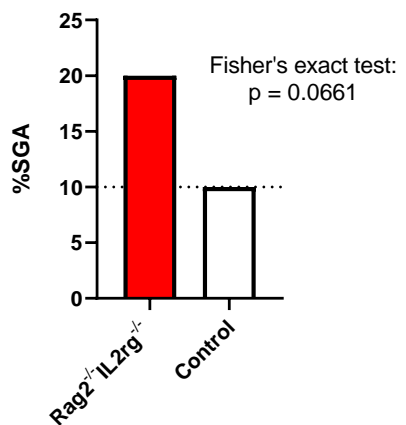
Figure 35. Fetal weight and %SGA comparison at g.d. 15.5 (A-B) and g.d. 18.5 (C-D) in C57BL/6 vs Rag2$^{-/-}$IL2rg$^{-/-}$ dams, mixed-model analysis for comparisons A&C. Error bars represent standard deviation.

In this analysis using *ImageJ* software, free to download online (Schneider 2012), I was able to identify three anatomical compartments based on femoral length, abdominal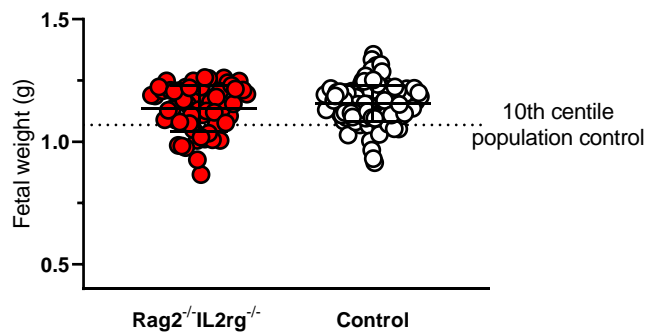 growth and brain growth commonly used in human ultrasonography. These were termed femur length, abdominal diameter and head diameter. I was able to consistently identify fetal anatomical landmarks to generate reproducible data and growth ratios. Head diameter was measured by taking an axial section through the fetal brain at the level of the 4th ventricle and measuring the widest diameter. Abdominal diameter was measured by taking an axial section through the abdomen at the level of both diaphragmatic bases and measuring the distance between the posterior vertebral border and the opposing abdominal wall. Femur length was measured by taking the longest point between the head of femur and the lateral condyle. Representative 2D images of the above can be found in Figure 36.
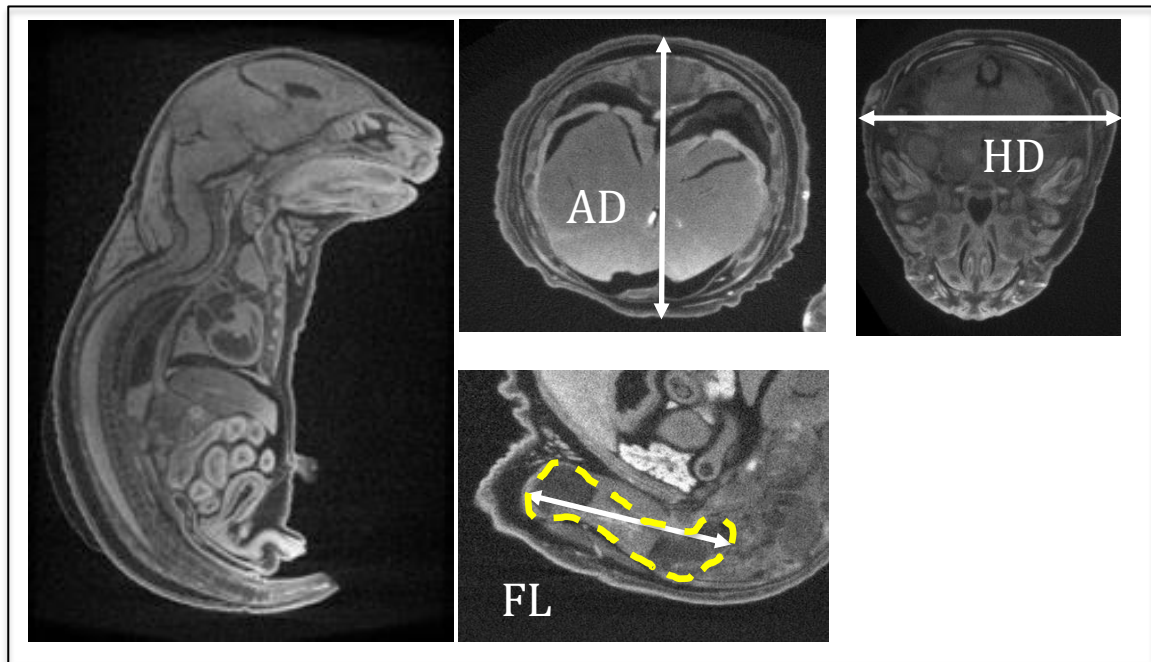
Figure 36. Representative 2D images of g.d. 15.5 C57BL/6 fetus, processed using *ImageJ* software. (Left) whole fetus in saggital plane, and representative images of abdominal diameter (AD), femur length (FL) and head diameter (HD).

I chose femur length as it represents skeletal development and displays consistent and reliable anatomical landmarks. It is also a good predictor of FGR in human pregnancies, when measured in the second half or gestation (Morales-Rosello 2012). I found shorter femur lengths and lower fetal weight: femur length ratios in the *Rag2$^{-/-}$IL2rg$^{-/-}$* strain at g.d. 15.5, when compared to C57BL/6 control dams. However, I found that head diameter and abdominal diameter did not significantly differ between the two groups at g.d. 15.5 (Figure 37A-D). Isolated reduced femur length is found in states of pathology in human pregnancy, as discussed previously. These data provided novel evidence that murine pregnancy may recapitulate some of the hallmarks of human pregnancy in terms of fetal anatomical development in adverse uterine environments.

Micro-CT analysis of fetuses at g.d. 15.5
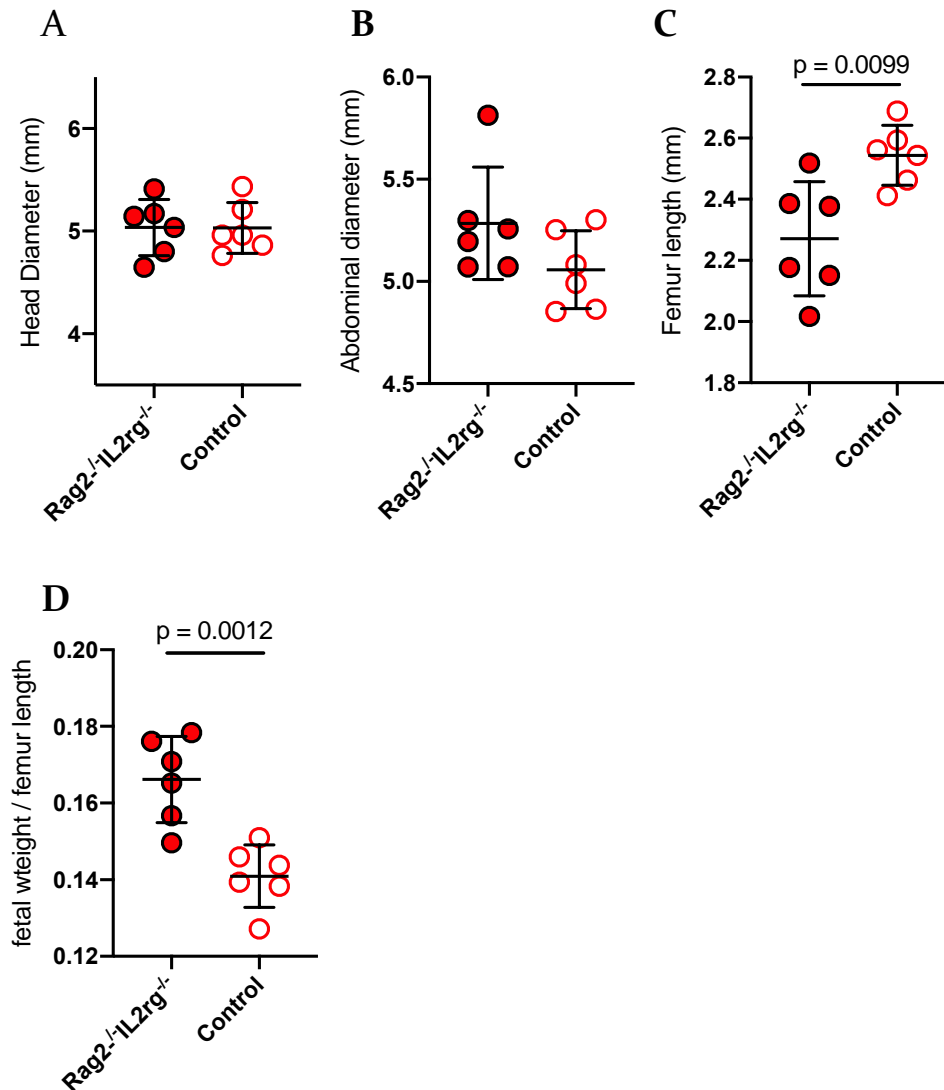
Figure 37. (A-D) Micro-CT comparison of head diameter, abdominal diameter, femur length and fetal weight/femur length at g.d. 18.5 in C57BL/6 vs Rag2$^{-/-}$IL2rg$^{-/-}$ dams, t-test. Error bars represent standard deviation.

Next, I sought to optimise this technique in g.d. 18.5 mice, where 3D analysis of fetuses could lead to a potentially more sensitive approach to detecting differences in organ development. Our lab had recently discovered that fetuses from innate lymphoid cell 2 (ILC2)-KO females crossed with C57BL/6 or interleukin 7 (IL7)-cre control males are growth restricted (Balmas 2018 – currently published in the open online repository ww.biorxiv.org, available at https://www.biorxiv.org/content/10.1101/348755v1). It was also observed through simple gross measurements on live animals that fetuses from these dams appeared to display smaller heads, consistent with a potential deficiency in neurological development. As brain development was of particular relevance to placental insufficiency and this project as a whole, the ILC2-KO strain was appropriate to optimise the methodology and assess the sensitivity of the analysis.

The mating, genotyping and selection of these mice were performed by our laboratory group member Elisa Balmas, as part of her PhD. I first confirmed, through 2D measurement, that head diameter in fetuses born from ILC2-KO dams was smaller when compared to genetically identical reverse cross controls at g.d. l8.5 (Figure 38A). This suggests that these mice may display a rare phenotype where the typical 'brain sparing' response to IUGR is lost. I then analysed these images in 3D, using *Amira* image rendering software. Femur length was visualised in 3D but measured in 2D, and was easily generated using the landmarks described for the *ImageJ* approach. I was also able to reliably measure total brain volume, by manually segmenting brain tissue to include the olfactory lobes, cortices, cerebellar and medullae (segmented at superior aspect of spinal cord). In support of the 2D data discussed above, I found that total brain volume was reduced in fetuses taken from ILC2-KO dams when compared to controls (Figure 38B) In addition, this abnormality appeared to be brain-specific as femur length was not affected resulting in a higher brain volume: femur length ratio in these offspring (Figure 38C-D).

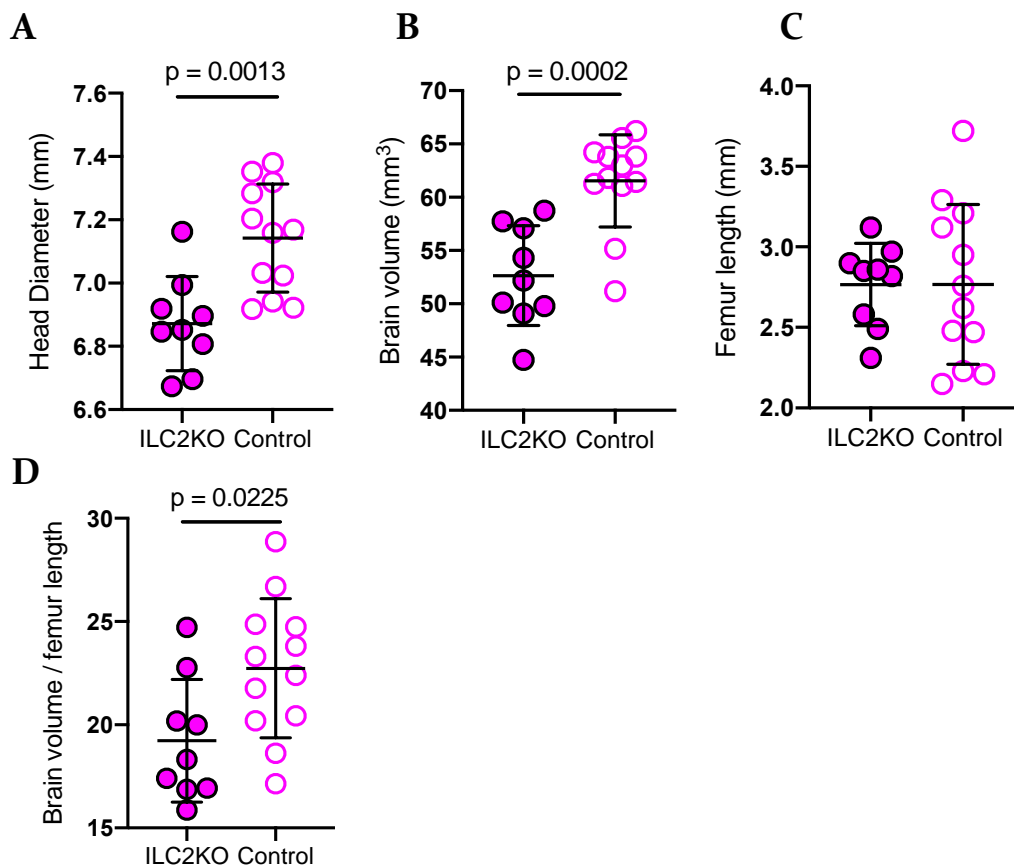**Micro-CT of fetuses at g.d. 18.5**

Figure 38. Micro-CT comparison of Head diameter measured in 2D A), brain volume and femur length measured in 3D (B-C) and brain volume/femur length at g.d. l8.5 in ILC2KO vs Control dams, t-test. Error bars represent standard deviation.

Some further qualitative data was gathered using this technique. A number of organs including the fetal thymus, lung, heart and liver were segmented out of whole fetuses to assess how efficiently and accurately organ boundaries could be identified for volume analysis (Figure 39). The effective segmentation of all of these organs was achieved. Some organs e.g. lung, were much more labour-intensive, however. Future application of these broader analyses may prove useful and relevant, but were not employed again in this project.

3D rendered Micro-CT organ segmentation
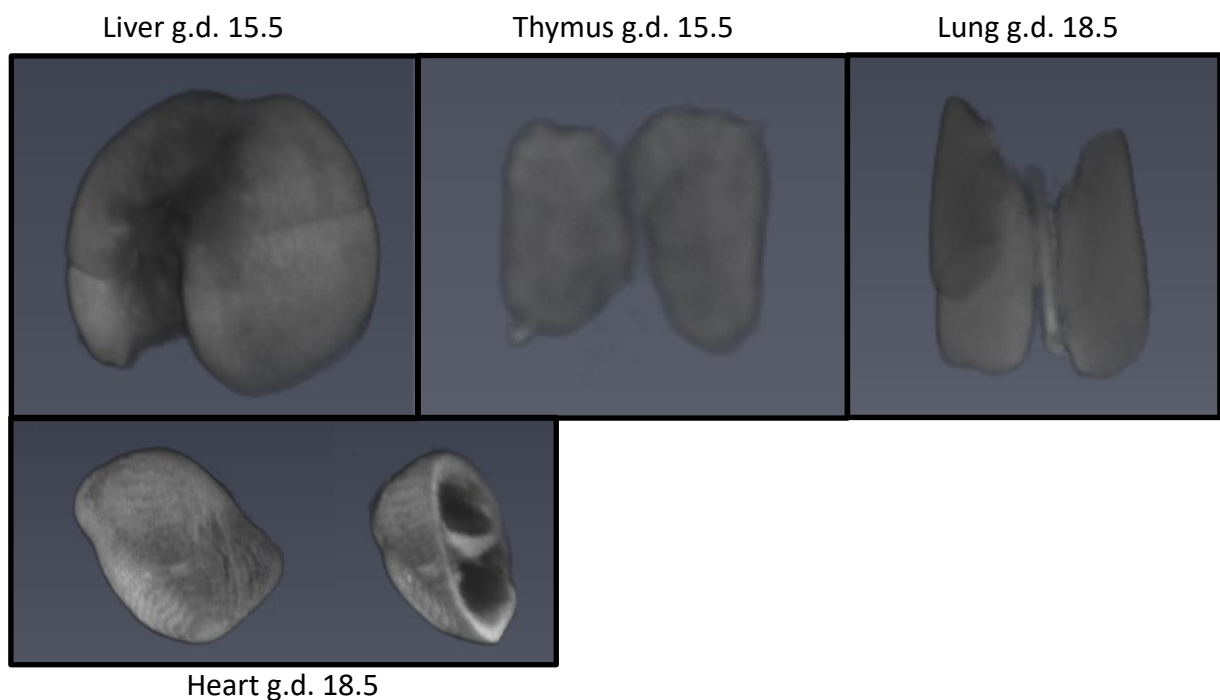
Figure 39. Representative images of 3D rendered Micro-CT analysed and segmented fetal organs, produced using Amira software.

The first experiment aimed at measuring any effect of NKG2A deletion on fetal growth symmetry revealed some potential experimental biases. All previous work comparisons of brain volumes between strains had revealed consistent and biologically plausible differences, with relatively small effect sizes. However, when comparing fetuses from C57BL/6 females x C57BL/6 males with and *KlrcI*$^{-/-}$ females x C57BL/6 males and their reverse-cross (C57BL.6 females x *KlrcI*$^{-/-}$ males), I saw large variation in 3D brain volume. Some brain volumes were almost three times larger than others. This appeared to be way outside of biological plausibility, and this large range was also present intra- and inter- groups being compared. Interestingly, 2D femur length measurements displayed normal and consistent values. This led to two possible explanations. Either there were tissue processing effects which were actually

shrinking or swelling the soft brain tissue prior to CT analysis, or there was a bias within the post-processing analysis.

After fixation, fetuses were stored at 4°C in PBS/0.02% sodium azide until hydrogel hybridisation and scanning. The addition of sodium azide should help avoid microbial contamination and stabilise the tissue to maintain its integrity, the possibility of defixation and tissue swelling could not be ruled out. Defixation occurs as formaldehyde fixation relies upon a chemical equilibrium. After time, the ionic constitution of PBS can alter (e.g. water loss through evaporation) and can affect the degree of fixation within the tissue. The length of time tissue was stored differed in this analysis due to unexpected delays with animal mating, and varied between 7 days and 4 months. However, I did not find a direct correlation between length of time in PBS, and brain volume. This must be interpreted with caution however, as the length of time in PBS was strongly linked to experimental group. This, to a degree, ruled out a tissue-processing bias as a cause of the large variation seen previously.

I next sought to address whether our scanning protocol or 3D analysis of micro-CT images was biasing results. A voxel represents a value on a grid in three-dimensional space, and can be visualised through direct volume rendering. Resolution of 3D images is measured in voxel length (x), where voxel size is equivalent to (x^3). Essentially, there are two ways to scan processed fetuses. One way is to opt for the lowest possible resolution, and the smallest voxel length with each fetus. The smaller the fetus/tissue, the lower the possible resolution. This is especially useful for qualitative data where one is seeking the highest quality image possible. Another approach is to scan all fetuses at the same resolution. An issue with this, is that you are limited by the size of your largest piece of tissue/fetus. This may result in sub-optimal scanning of smaller samples.

In this analysis, I opted to scan all samples at the lowest possible resolution. This resulted in a range of resolutions, with voxel length varying from around 7 microns, to 14 microns. Once extrapolated to 3D, these small changes can become significant. I contacted Professor John Sled, at the University of Toronto, who helped to develop this technique. He indicated that these differences are significant, and that whilst the 3D software includes voxel length in its volume calculation, this isn't enough to correct for other biases. It was suggested that changes in voxel size can hugely affect the visualisation of organ boundaries, and that these may result in large variations in volume measurements. In this experiment, I found a strong correlation between brain volume and voxel size, in keeping with this notion. This made the detection of any fetal growth changes influenced by maternal NKG2A deletion impossible (Figure 40).
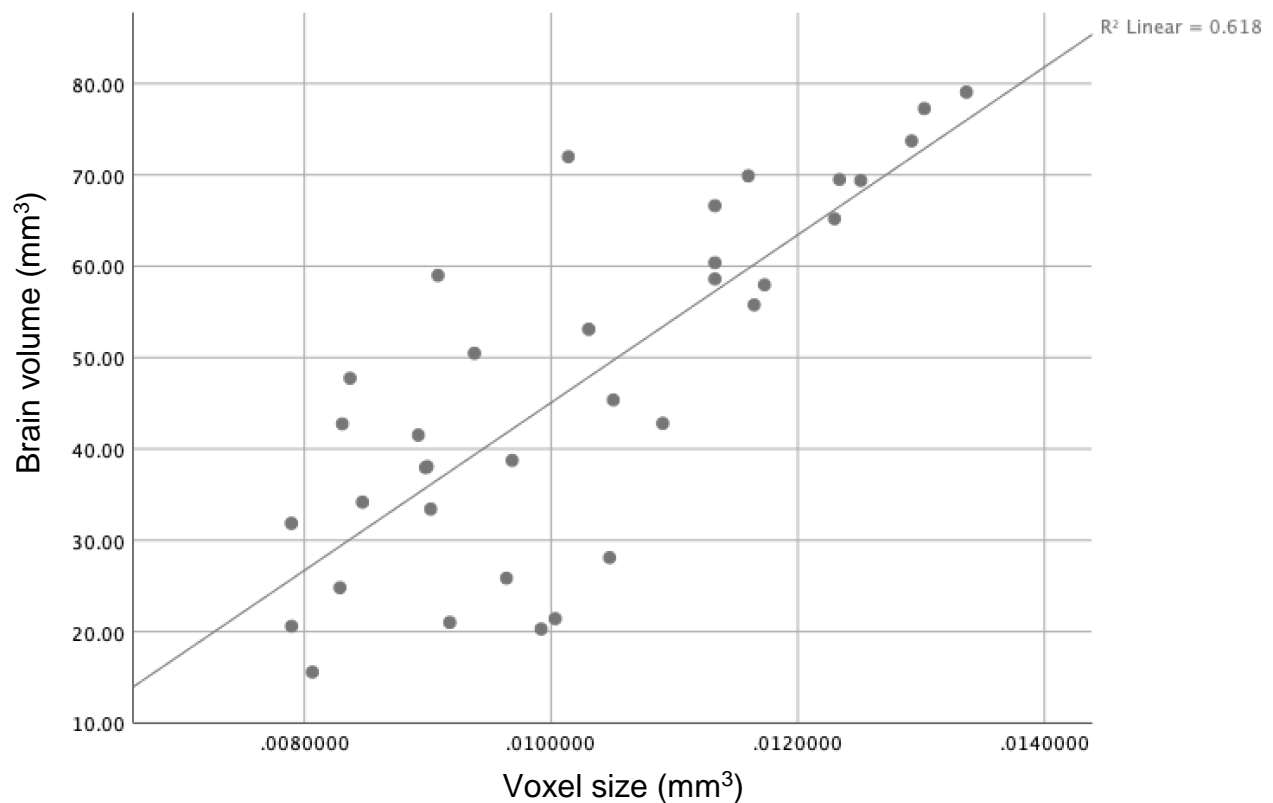
Figure 40. Brain volume plotted against voxel size for Micro-CT analysis, each dot represents one mouse, mixed strains. Created using SPSS software.

To address this, in part, I built a statistical model to account for the effect of voxel size in this analysis, using the statistical software package SPSS Statistics v.21 (IBM). Once this was applied, I was able to make a more accurate comparison. When comparing fetuses from *Klrc1*^{-/-} mothers, I found brain volume to be similar to that found in fetuses from C67BL/6 females x males. However, both of these groups displayed a greater brain volume than the *Klrc1*^{-/-} reverse cross fetuses (Figure 41A), but only the *Klrc1*^{-/-} comparison was statistically significantly difference (Figure 41B). It is important to note that all the fetuses used in these comparisons were of approximately an average weight for their litter, so these data weren't able to model for growth restriction per se. These initial experiments suggested that maternal Klrc1^{-/-} deletion may affect the brain development of offspring, and also helped to identify important technical issues which would need to be addressed in future experiments.

A

Estimates

Dependent Variable: bv

group	Mean	Std. Error	95% Confidence Interval	
			Lower Bound	Upper Bound
B6	49.149[a]	3.507	41.997	56.301
NKG2A–KO	50.782[a]	2.794	45.084	56.480
reverse cross	38.432[a]	3.829	30.623	46.241

a. Covariates appearing in the model are evaluated at the following values: pixel = .010225059.

B

Pairwise Comparisons

Dependent Variable: bv

(I) group	(J) group	Mean Difference (I–J)	Std. Error	Sig.[b]	95% Confidence Interval for Difference[b]	
					Lower Bound	Upper Bound
B6	NKG2A–KO	–1.633	4.458	1.000	–12.915	9.649
	reverse cross	10.716	5.248	.149	–2.566	23.999
NKG2A–KO	B6	1.633	4.458	1.000	–9.649	12.915
	reverse cross	12.350[*]	4.829	.047	.127	24.572
reverse cross	B6	–10.716	5.248	.149	–23.999	2.566
	NKG2A–KO	–12.350[*]	4.829	.047	–24.572	–.127

Based on estimated marginal means

*. The mean difference is significant at the .05 level.

b. Adjustment for multiple comparisons: Bonferroni.

Figure 4l. Output data from statistical model to normalise brain volume (bv) by voxel size. A) Adjusted means for all three groups (B6 = C57BL/6 x C57BL/6, NKG2A-KO = *Klrc1*^{-/-} females x C57BL6 male, Reverse cross = C57BL6 females x *Klrc1*^{-/-} males). B) Pairwise comparisons of all three groups.

4.13 NKG2A deletion in dams results in asymmetric fetal growth restriction

Given the vascular changes outlined previously, I hypothesised that placental function would be sub-optimal in fetuses developing in *Klrc1*^{-/-} dams, and that these fetuses would exhibit abnormal growth symmetry and developmental patterns. In order to address this, I designed an experiment to assess any potential effect on small fetuses specifically, as many fetuses in each litter are likely to achieve a normal growth potential and appear unaffected. Thus, randomly selecting fetuses is unlikely to be a sensitive enough approach, nor is only selecting fetuses who are an average representation of their litter with regard to fetal weight.

As I did for assessing maternal vascular adaptations, in the main micro-CT analysis I compared fetal growth in genetically-matched pregnancies, i.e. from (*Klrc1*^{-/-} females x C57BL/6 males) or from (C57BL/6 females x *Klrc1*^{-/-} males) pregnancies, where fetuses are genetically identical but develop in NKG2A-deficient or -sufficient uteri, respectively. As a result of the findings in the

optimisation experiments, all fetuses were scanned within 2 days of fixation, and all were scanned at the same resolution.

Within normal litters, there is significant intra-litter variation in the growth of individual fetuses, however the small fetuses in normal pregnancies are presumably healthy and not expected to have an asymmetric growth pattern or represent any pathology per se. As a result, analyses of small fetuses developing in C57BL/6 dams were not initially made. In contrast, I hypothesised that the haemodynamic defect I found in fetuses from $Klrc1^{-/-}$ dams at g.d. l4.5 would in fact be associated with subsequent asymmetrical growth pattern in the smallest g.d. l8.5 fetuses. Using micro-CT, I compared the smallest fetuses (Small) with the average-weight littermate fetuses (Average) in litters of $Klrc^{-/-}$ dams. The schematic of how I selected fetuses for the analysis can be found in Figure 42A, alongside fetal weights of selected groups (Figure 42B). Representative 3D images of organs measured can be found in Figure 43. These fetuses were then further compared to average-weight fetuses from genetically-matched pregnancies where the dams were C57BL/6. Small fetuses from C57BL/6 dams were not included in the comparison because they were not predicted to represent pathological growth. I found that, while femur length was smaller in the Small group (Figure 44A), brain volume was in fact not different between the two groups (Figure 44B), resulting in a higher brain volume: femur length ratio in the Small fetal group (Figure 44C).

A

B
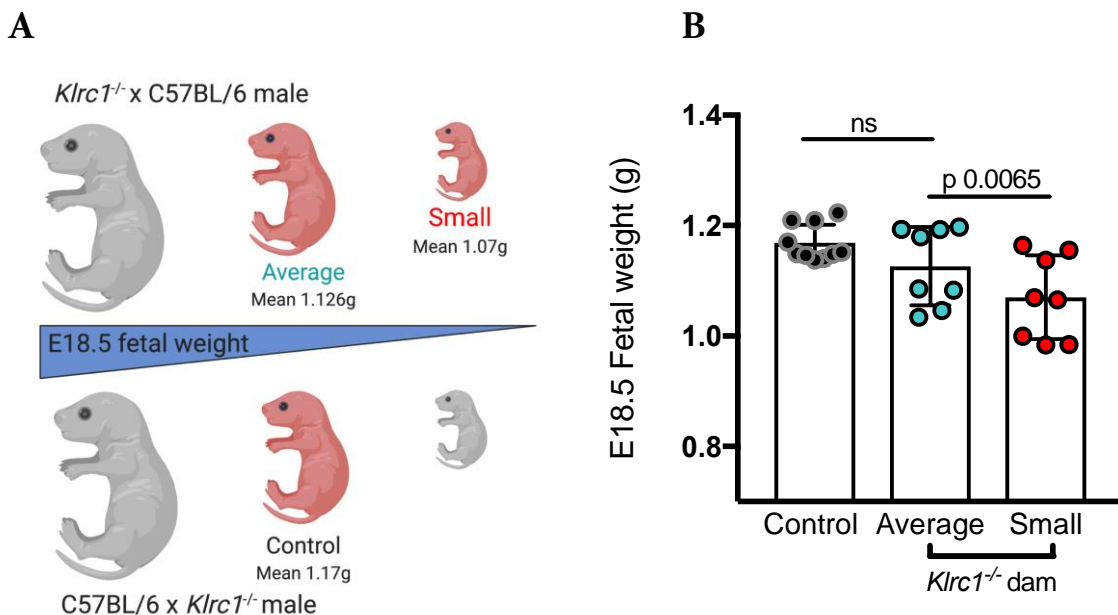
Figure 42. A) Schematic to show fetal selection for micro-CT analysis of growth symmetry, and B) comparison of fetal weights of selected groups (t-tests). Error bars represent standard deviation.
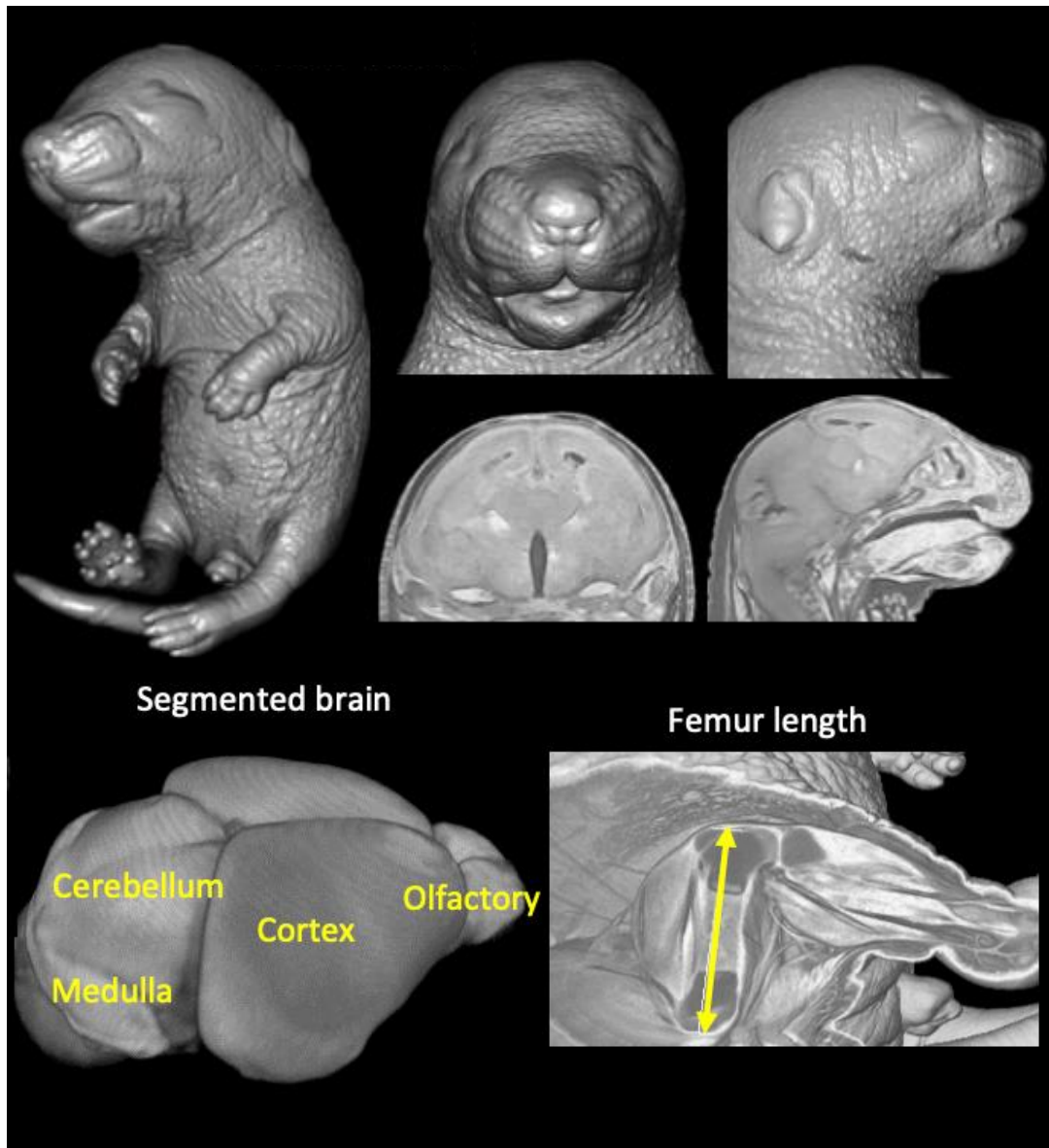
Figure 43. Representative 3D rendered images of C57BL/6 fetus at g.d. 18.5 showing (from top left, clockwise) whole fetus, fetal head through saggital and coronal plane, femur length and segmented whole brain
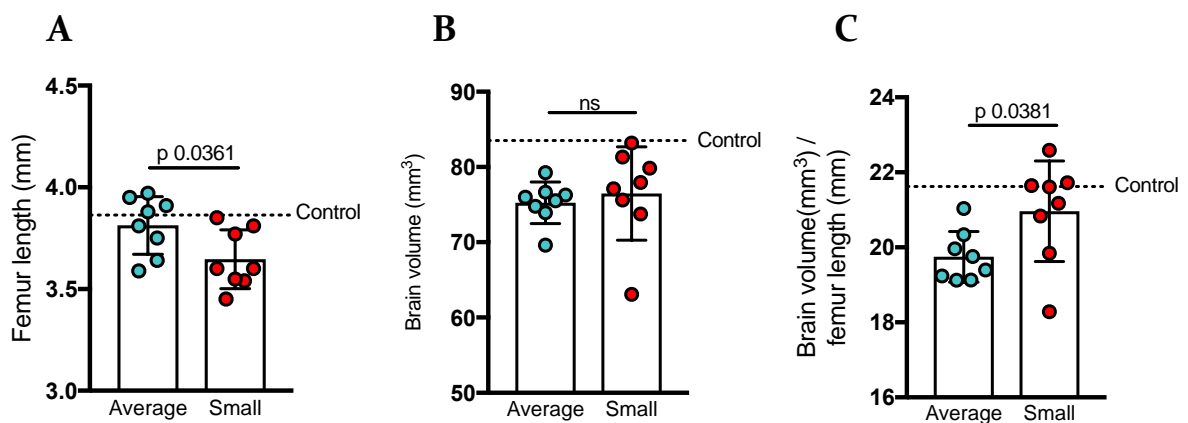
Figure 44. Comparisons of femur length A), brain volume B) and brain volume: femur length ratio C) by fetal group (n = 4-5 litters per group, t-test) in Klrcl$^{-/-}$ dams. Dotted line represents mean value for Average fetuses in C57BL/6 x *Klrcl*$^{-/-}$ pregnancies (controls). Error bars represent standard deviation.

4.14 Maternal DLK1 levels do not differ in *Klrc1*^{-/-} dams

The previously discussed finding that maternal DLK1 levels may potentially be able to discriminate between healthy SGA and FGR (Cleaton 2016) led me to test the hypothesis that *Klrc1*^{-/-} dams would display reduced DLK1 as a result of reduced embryonic mass and FGR in their fetuses.

I found that virgin *Klrc1*^{-/-} females displayed DLK1 levels comparable to C57BL/6 females (Figure 45A). This is not surprising, as the non-pregnant levels are very low and would not yet be influenced by any potential differences in fetal growth. I then mated *Klrc1*^{-/-} females with C57BL/6 males and compared the DLK1 levels to pregnancies where C57BL/6 females were mated with *Klrc1*^{-/-} males. This approach enabled me to specifically detect the influence of embryonic mass on maternal DLK1, as fetal genotypes were identical. I observed the expected increase in DLK1 from virgin to g.d. 15.5 (approx. 10-15-fold increase, Cleaton 2016), however the fold change from virgin was similar between groups, when normalised for litter size (Figure 45B).

A **B**

Figure 45. A) Total serum DLK1 in virgin mice, by group and B) fold change serum DLK1 from virgin n to g.d. 15,5, by group, normalised by litter size. Error bars represent standard deviation.

I found no difference between the two groups in terms of absolute DLK1 levels, and also when normalised for number of concepti and total embryonic mass (Figure 46).

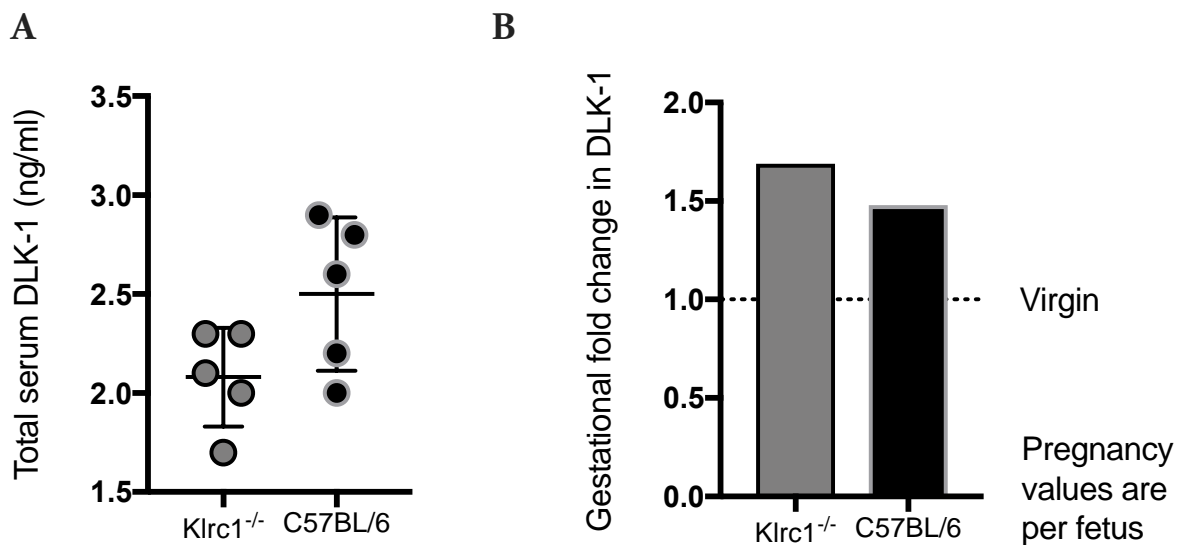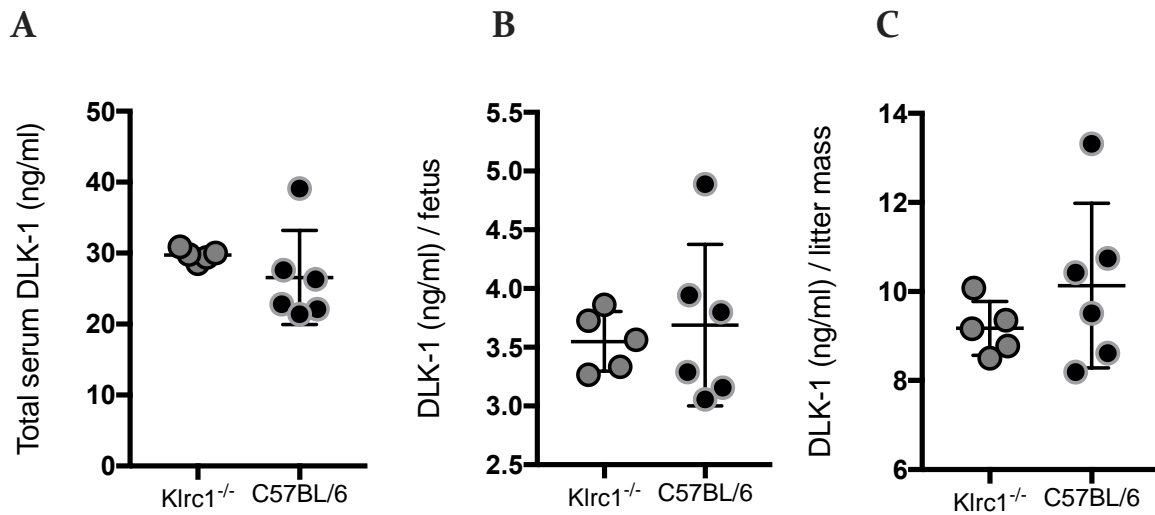**Figure 46. Maternal serum DLK1 levels at g.d. 15.5, by group, (A) absolute DLK1 levels, (B) DLK1 levels per fetus and (C) DLK1 levels divided by total embryonic mass. All non-significant, t-tests. Error bars represent standard deviation.**

4.15 Placental mRNA-sequencing experimental design and quality control

Our initial experimental plan was to screen for any global transcriptomic changes which may occur between average fetuses from each condition at g.d. 15.5 (e.g. the presence or absence of maternal NKG2A). This analysis was performed immediately, on ex-vivo fresh tissue. Between the two groups there were no differentially expressed genes. I therefore decided to further analyse groups, by segregating them according to their fetal weight. This is logical as maternal immune cell knockouts rarely affect the entire litter, but do expose fetuses to a higher risk of being SGA. As a result, if one is interested in measuring the effects of sub-optimal fetal growth in a certain condition, it is important to ensure those small fetuses are being selected and compared.

All placental samples from small fetuses were frozen after a period of storage in RNAlater. This meant comparing placentae that had undergone mRNA sequencing fresh, to those samples which had undergone a freeze-thaw cycle prior to analysis. All extracted RNA underwent initial analysis of yield and purity using a photospectrometer in our laboratory. Samples were then blinded and delivered to Cambridge Genomics Services (CGS, Cambridge, UK) on dry ice for mRNA-sequencing. Before the samples were run at CGS, they underwent further quality control checks using a Bioanalyzer. All samples across the four groups achieved a RIN score of >8, confirming the high quality and purity of the extracted RNA.

A minimum of 10 million mRNA reads are required from all pooled samples in order to proceed to later analytical steps. The average yield (per placental extract) of my fresh samples

was approx. 44 million, versus 35 million in the thawed samples, both providing ample mRNA reads for pooled analysis. Furthermore, each individual sample should contribute approximately evenly to the overall pooled read count, and ours did so (approx. 9% per placenta), however this distribution was slightly less consistent in the thawed group.

Next, the *per base sequence quality* was assessed. This is, ultimately, a reflection of the base nucleotide calling error rate at each position in the read. It is scored from 0-40, across the 75 base positions called by the TrueSeq Stranded mRNA (Ilumina, CA, US) library preparation kit used. The score reflects the error rate, where a score of 10 is equal to an error rate of 1 in 10, and is expected to decrease towards the end of reads due to a processing phenomenon known as 'phasing'. All 20 of the samples showed quality values above 30 in all positions, meaning they were of high quality (representative example is shown in Figure 47). In addition, all samples showed were measured for *per base sequence content*, which measures the proportion of the four DNA nucelotides Adenine (A), cytosine (C), Guanine (G) and thymine (T).The samples showed, as expected, a roughly even distribution of A, C, G and T across the base positions, with the expected drop off of A towards the end of the read which occurs with the trimming of adapters used in library preparation (Figure 48).
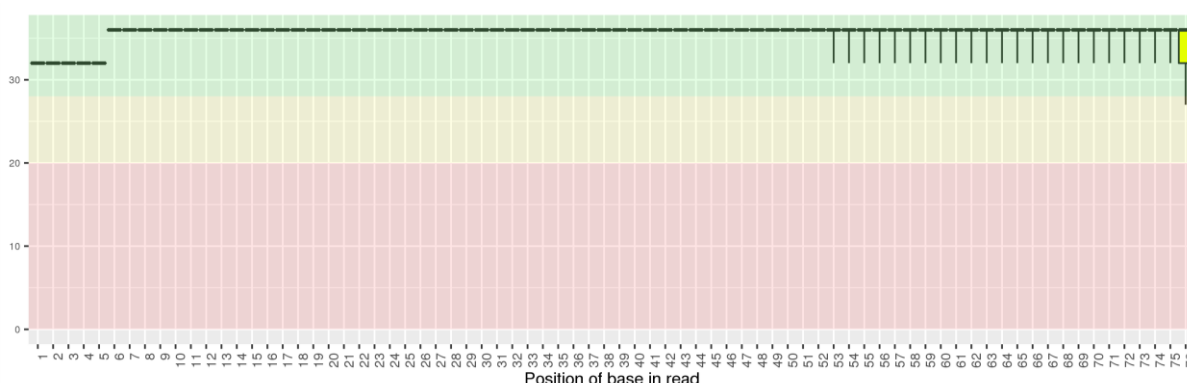
Figure 47. Representative boxplots of the distribution of quality values across the reads at each position. On the y-axis the values range from 0 to 40. A y value of 10 would mean a rate of 1 error in 10. Quality is normally expected to drop towards the end of the reads. As shown in the plots, the quality values across all 10 samples are above 30, meaning they are of high quality. *figure and legend produced by Stephanie Wenlock at Cambridge Genomic Services, Cambridge.
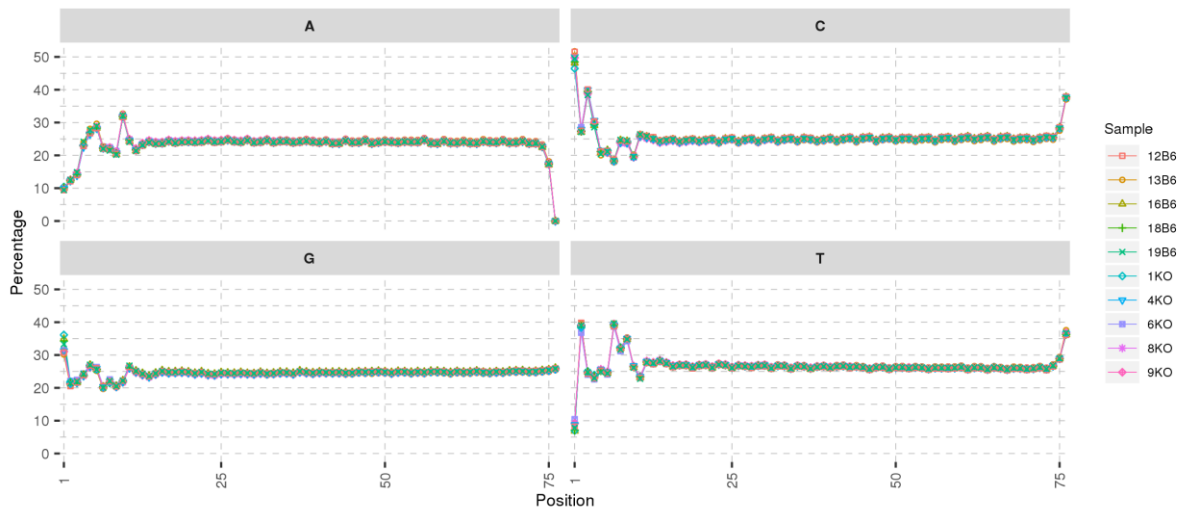
Figure 48. The per base sequence content plot shows the proportion of each of the four DNA nucleotides at each position across the reads, with sample ID colour-coded and shown on the right. The plot should in general show parallel lines across the x-axis, as seen here. It is common to see a drop in the proportion of A nucleotide at the end of the read due to trimming of adapters. *figure and legend produced by Stephanie Wenlock at Cambridge Genomic Services, Cambridge.

In addition, it is important to ascertain the per sequence guanine cytosine (GC) content for each sample. This is important as non-biased libraries should display a normal GC distribution, with distribution reflecting that of the overall GC content of the underlying genome. The mouse genome contains a GC content of approximately 50% (Romiguier 2010), and all the samples replicated this (Figure 49). This suggest a lack of contamination or enrichment bias in the placental cDNA library.
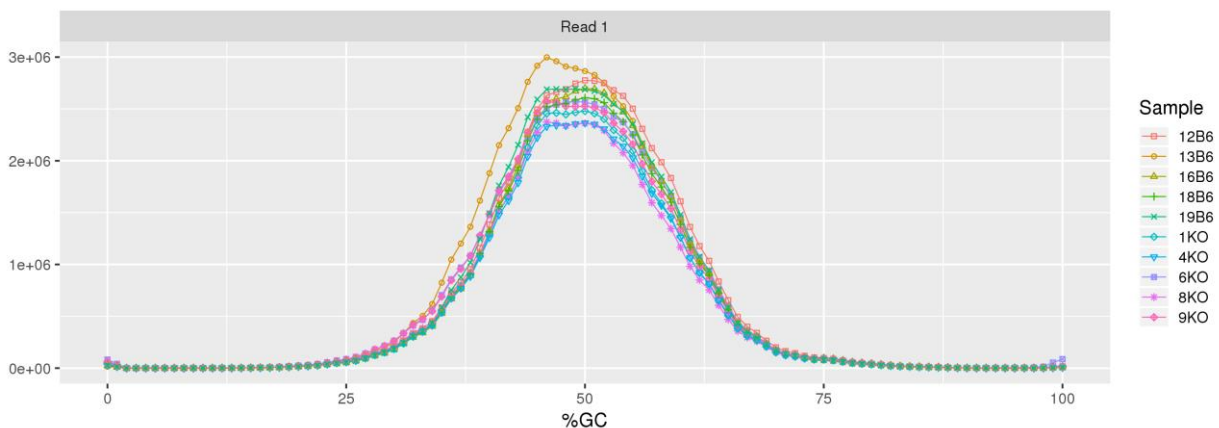
Figure 49. Per Sequence GC content. This graph shows a normal distribution of GC content, with distribution centred at the overall GC content of the underlying genome. *figure and legend produced by Stephanie Wenlock at Cambridge Genomic Services, Cambridge.

Before differential gene expression analysis can be performed, reads need to be trimmed. CGS used *TrimGalore v0.4.1.* to remove low quality base calls from the 3' end of the reads. Ilumina

sequencing adapters are used to barcode sequences, for forward and reverse primers and in binding sequences to allow immobilisation to the flowcell for bridge-amplification. The original DNA being read is downstream of the 5' primer, which means that the 5' adapter used will not feature in the sequenced read. Therefore, adapter removal involves the identification of adapter sequences attached to 3' ends of reads only. This was performed on all placental samples, and if after trimming, reads were less than 20 bases long, they were discarded to avoid adapter sequence contamination. The samples displayed an appropriate post-trimming read count when compared to raw reads. Furthermore, it was confirmed that the *per base sequence content* was not significantly affected by read trimming, with the expected decrease in Adenine proportion at the end of the read present, but all other base positions remained unaffected.

Next the total genetic coverage achieved through the steps undertaken in the initial processing and analysis was determined. Reads were mapped to the mouse reference genome (Ensembl Mus_musculus.GRCm38 (release 95). The number and percentages of uniquely mapped reads, the percentage of reads that mapped to multiple loci and the percentage of unmapped reads were checked and found to be within normal ranges. This is an important quality control check to in determining the non-specificity of reads, and is expected to yield a result of >85%. All of the 20 samples achieved a % uniquely mapped value of >85%. After this analysis, the multiple loci reads were removed in order to avoid false positives. In addition, the vast majority of the uniquely mapped reads that were inputted were found to be mapped to genes, and not other genomic locations or ambiguous locations. Finally, the number of genes detected in each sample was analysed. The average number was between 24,000-25,000, where the mouse is known to have around 25,000 exons, similar to the number found in humans.

4.16 Differential gene analysis

In order to accurately account for any effect of the freeze-thaw cycle, when running the second (thawed) batch of samples, I re-ran a placenta from the initial fresh group in order to have a biological replicate in both conditions. Gene expression was then compared between the two experiments in this individual sample, and a small effect on gene expression attributable to freezing was discovered. Using SVA software, this batch-effect was successfully corrected for by CGS.

Differential Gene Expression (DGE) analysis was performed using the counted reads previously described. In order to compare gene expression across groups, the R package edgeR [8] version

3.16.5 (R version 3.4.1) was used to create pairwise comparisons. The following is a broad and simplified version of the statistical pipeline used to produce a list of genes which were differentially expressed between placental groups:

1. Genes were filtered based on read counts, where the aim was to only keep genes in the analysis where at least half of the samples display a read count of greater than 5.

2. EdgeR software was used to calculate effective library sizes using trimmed mean of M-values (TMM) as a method to achieve normalisation. This accounted for sequencing depth and RNA composition of samples.

3. Removal of a systematic GC content and gene length bias by a smoothing function was performed using CQN bioconductor package version 1.24.0. This ensured there was no bias towards reads high in GC content.

4. Differential gene expression was performed. The exact test edgeR statistical analysis package to produce pairwise comparisons between all placental sample groups was used. Adjustment for multiple testing via the false discovery rate (FDR, Benjamini-Hochberg) approach was used by edgeR.

4.17 Maternal NKG2A regulates the placental transcriptome

I aimed to determine whether the pattern of defective placentation seen in fetuses of NKG2A-KO dams was associated with aberrant placental gene expression. Again, this was investigated by comparing placental gene expression in genetically-matched pregnancies, i.e. from ($Klrc1^{-/-}$ females x C57BL/6 males) or from control (C57BL/6 females x $Klrc1^{-/-}$ males) at g.d. 15.5. I aimed to characterise any differences resulting from the presence or absence of maternal NKG2A, but also to delineate transcriptomic changes between Average and Small fetuses in each maternal condition (for fetal weights, see Figure 50). This approach resulted in four study groups (1-4) and four comparisons used to detect any differentially expressed genes (A-D) (Figure 51 with sample-size based on previous studies (Chu 2016; Chu 2019).
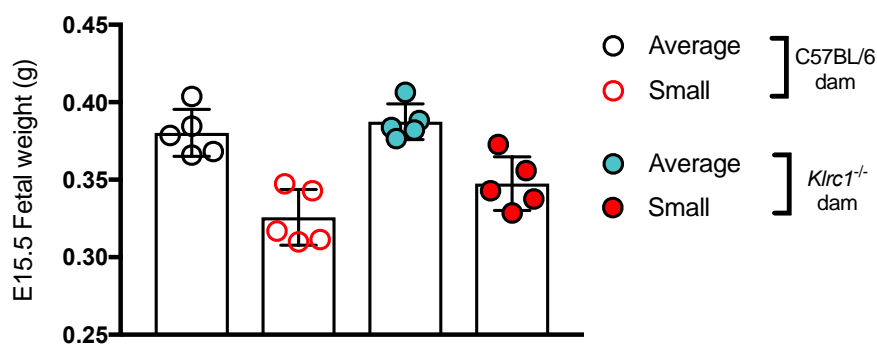

Figure 50. Fetal weight at g.d. 15.5 of those selected for placental RNA-sequencing, by study group (5 litters per maternal strain, 1 Small and 1 Average fetus per litter selected). Error bars represent standard deviation.

121

A

C57BL/6 X
Klrc1⁻/⁻ male

Klrc1⁻/⁻ X
C57BL/6 male

1. Average

A | 2

2. Small

C
3
DE genes

0
D

3. Average

407 | B

4. Small

B

Principal component analysis
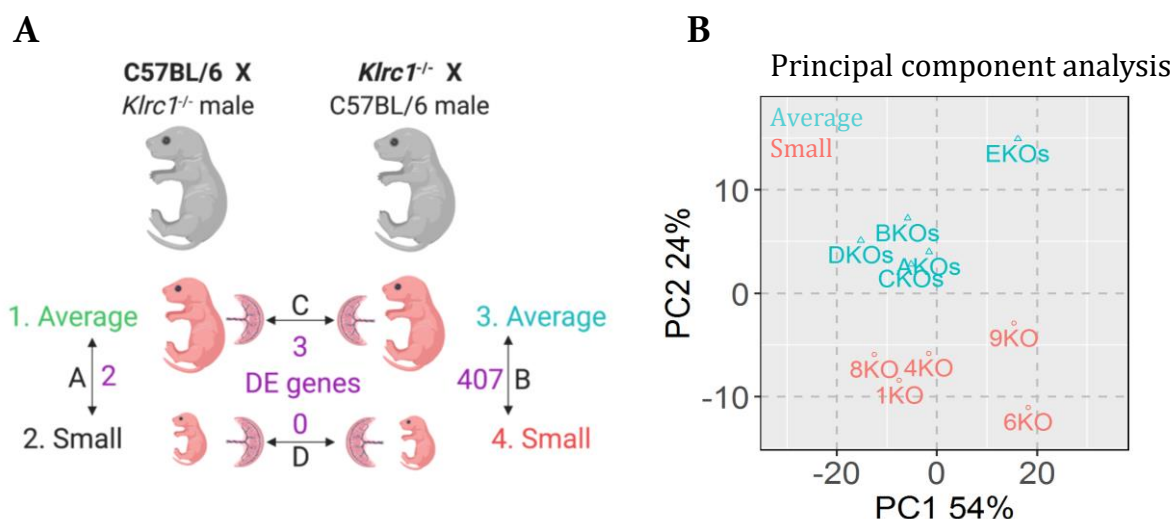
Average
Small

Figure 51. A) Placental selection (1 average and 1 small per litter, 5 litters per group), study groups and differentially expressed genes (purple), by comparison. B) Principal component analysis of comparison B, labelled by sample ID.

After adjustment for fetal sex (see methods), initial screening found that the comparison between placentae of Average and Small fetuses within B6 dams (comparison A) only indicated 2 differentially expressed (DE) genes. These were *Gm4130*, a heterogeneous nuclear ribonucleoprotein K pseudogene of unclear functional importance, and *Gpc3*, which encodes the protein Glypican 3 and also has no known role in the placenta. This finding is in keeping with my initial hypothesis that Average and Small fetuses developing in B6 dams are unlikely to be associated with any significant differences in placental function, as they are thought to represent normal variations in healthy litters. In striking contrast, the comparison between placentae of Average and Small fetuses within *Klrc1⁻/⁻* dams (comparison B) indicated 407 DE genes. Comparison C, which was between the placentae of Average fetuses in the two groups (comparison C) indicated only 3 DE genes, among which was *Ldoc1,* a gene important for normal placental cell differentiation/maturation (Naruse 2014). Comparison D, between placentae of Small fetuses in the two groups indicated no DE genes.

Further analysis was performed on comparison B only, that is between placentae of Average and Small fetuses within *Klrc1⁻/⁻* dams, where an NKG2A-deficient environment may cause FGR and abnormal placental gene expression. I found that previously reported mouse placenta housekeeping genes *Hprt*, *Gapdh*, *Actb*, *Ubc*, *Polr2a* and *Ywhaz* (Solano 2016) were stably expressed by all placentae, across both groups, suggesting that the comparison was not biased by variations in housekeeping genes (Figure 52). A principal component analysis (PCA) of gene expression in all placentae from comparison B revealed that fetuses segregated according to whether they were from the Average or Small group (Fig 5b). Next, I selected all 407 DE genes

(false discovery rate, FDR <0.01) and performed a gene functional annotation analysis in *Metascape* (Zhou 2019) to discover significantly enriched pathways (see methods). A total of 35 pathways were reported (Figure 53).
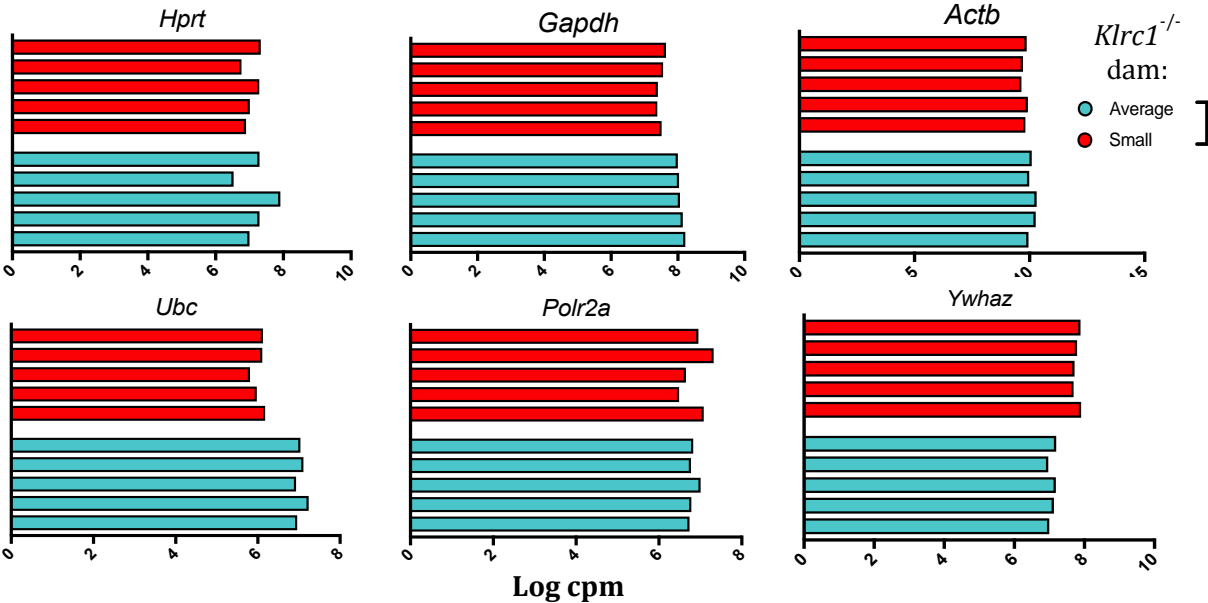
Figure 52. Comparison of placental housekeeping gene expression by group. T-tests, all non-significant comparisons.
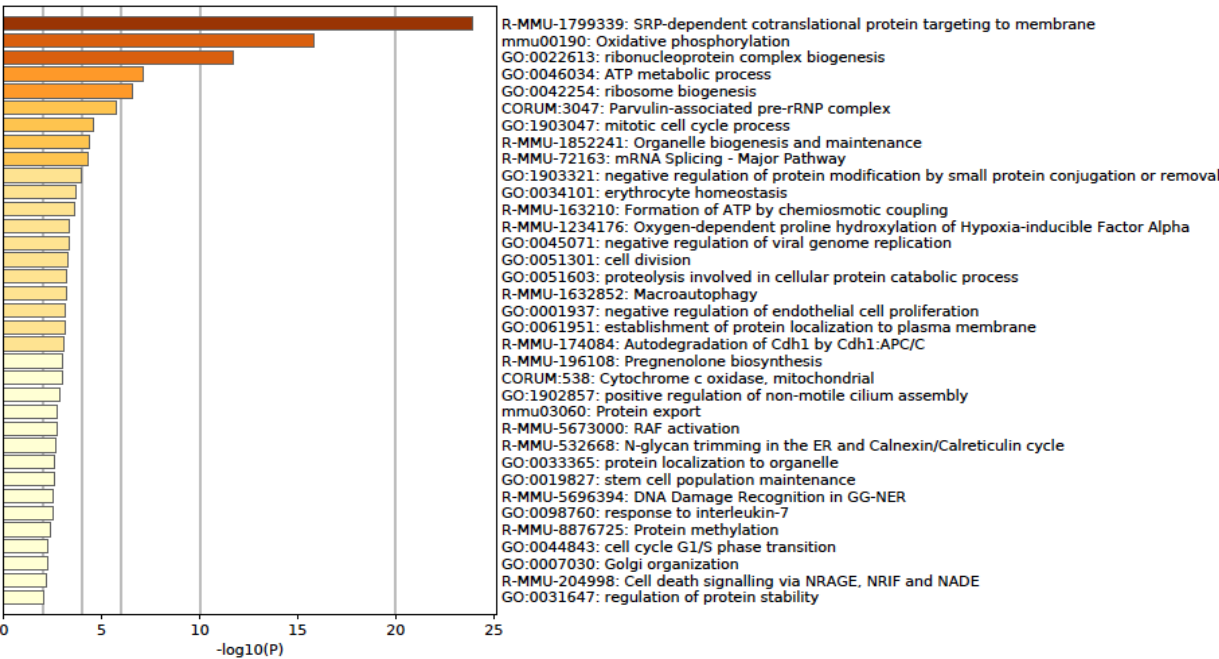
Figure 53. A) List of significantly enriched gene pathways from comparison B in figure 43A, figure produced at www.metascape.org.

The most enriched pathway involved genes relating to the control of protein translation to the endoplasmic reticulum (ER), which is yet of unclear significance to placental physiology, but has been implicated in pre-eclampsia and FGR mediated by ER stress (Yung 2008). In keeping with a model of placental stress, the gene pathway '*mmu-00190 Oxidative phosphorylation*' was

the second most enriched pathway. This was driven by 23 DE genes, many of which encode proteins within respiratory complex I of the electron transport chain, an enzyme key to aerobic respiration (Table 1). The additional enrichment of the pathway '*R-MMU-1234176: Oxygen-dependent proline hydroxylation of HIF*' also implicated placental oxygen delivery as a potentially aberrant pathway between the two groups. Additional dysregulated pathways identified in this comparison further suggested placental stress. The pathway '*GO:0001937 negative regulation of endothelial cell proliferation*' is of interest as placental endothelial cell injury/dysfunction, likely to be secondary to hypoxia, is suggested to be a key contributor to pre-eclampsia (Powe 2011). Other DE genes were associated with autophagy – which is activated by cell damage/death and can occur in response to hypoxia/reoxygenation in placental cells (Sagrillo-Fagundes 2019) – cell death signalling and DNA damage recognition.

Family	Gene ID	Log cpm Average-KO	Log cpm Small-KO	Log Fold Change	FDR
ATP synthase					
	Atp5e	5.815123925	4.15018509	-1.553201478	2.20E-13
	Atp5j2	6.983306359	6.109787171	-0.957445427	0.000170393
	Atp5g1	5.080761421	4.338976015	-0.745232202	0.005789358
ATPase					
	Atp6v1b2	6.81796796	6.462535958	-0.78211472	0.006027481
	Atp6v1d	6.426348	7.659270124	0.778001849	0.008892431
	Atp5k	5.441553139	4.621943725	-0.747621274	0.008999943
Cytochrome c oxidase					
	Cox7c	5.569164208	4.674609509	-1.316222345	6.78E-08
	Cox5a	6.41544931	5.789447861	-0.999180833	4.45E-07
	Cox11	3.67053083	2.580879872	-1.408052584	4.62E-07
	Cox7a2	6.737623926	6.15942184	-1.082597721	2.86E-06
	Cox7a2l	6.199046552	7.384075854	0.925573187	6.02E-05
NADH:ubiquinone oxidoreductase					
	Ndufa2	5.708653396	4.589017444	-1.466960747	5.50E-11
	Ndufa4	6.865181465	6.064238323	-1.348904889	7.93E-11
	Ndufs5	3.282085685	2.158076749	-1.356719644	0.000413499
	Ndufc1	4.10244161	3.106980694	-1.058348935	0.000511712
	Ndufs3	3.996133896	3.170933101	-1.012374127	0.00062626
	Ndufa7	5.576481751	4.804579458	-0.895835258	0.000640238
	Ndufa1	5.130481103	6.324465217	0.794828545	0.002032213
	Ndufs6	5.173595481	6.145980057	0.843958589	0.003234527
	Ndufb10	5.332236041	5.966417185	0.732011383	0.00349357
Ubiquinol-cytochrome c reductase					
	Uqcrb	5.626481556	7.498431723	1.326060402	8.07E-07
	Uqcrfs1	5.709817521	5.025158831	-1.075525139	9.98E-07
	Uqcr10	6.121566618	5.418151327	-0.932159229	7.88E-05

Table 1. Comparison of DE genes from enriched 'Oxidative phosphorylation' RNA-sequencing pathway by gene family, in comparison B. FDR p-values listed in far right column.

Finally, I sought to investigate whether this model of defective placentation highlighted DE genes previously reported to be important in placental function and fetal development in mice (Figure 53). I found the major regulator of mouse placental and fetal development, *Igf2* (Constancia 2002), and *Igf2bp* to be raised in placentae of Small fetuses from *Klrc1*^{-/-} dams, alongside a decreased expression of two genes from the prolactin gene family, *Prl7b1* and *Prl2c1*, which play a role in placental response to stress (Simmons 2008). Among DE genes were also *Bok* and *Isg15*, two genes related to innate immunity and inflammation and altered in a maternal diet-restriction model of FGR (Chu 2016). Furthermore, fetally- and placentally- derived endocrine signalling molecule *Dlk1*, which can discriminate healthy SGA from pathological SGA human fetuses and correlates with fetal mass in mice (Cleaton 2016), was reduced in placentae of Small fetuses from *Klrc1*^{-/-} dams.

Finally, within the top 50 highest fold-change increases in the Small-KO group were both *Bex1*, which plays an anti-apoptotic function in the rat brain (He 2018), and *Bex3*, which is important for neuronal differentiation and survival (Calvo 2015). This finding could provide further insight into some of the transcriptomic changes which play a role in the neurological injury and inflammation associated with FGR in humans (Baschat 2011).
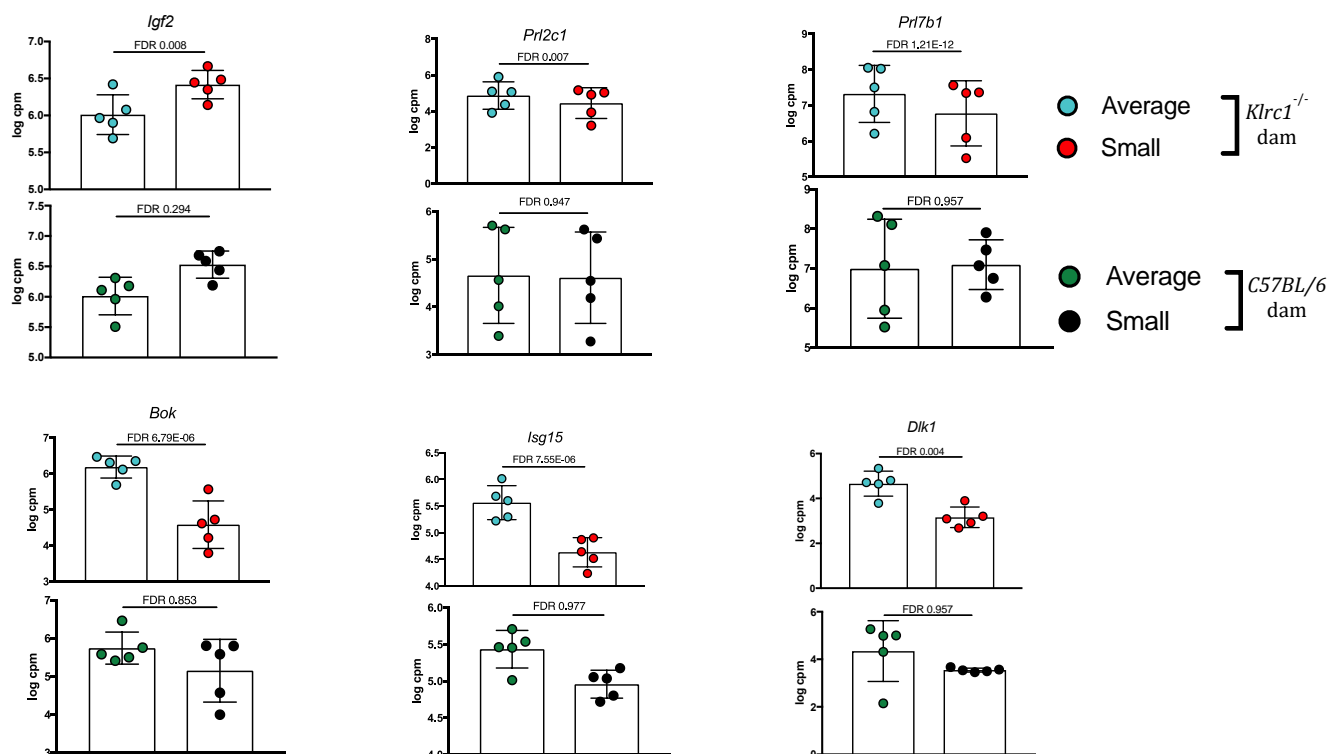

Figure 53. Comparison of normalised log counts per million (cpm) of selected genes from comparisons A (green and black dots, C57BL/6 dam) & B (blue and red dots, *Klrc1*^{-/-} dam) in figure 51A, by gene. Error bars represent standard deviation.

4.18 NKG2A regulates fetal growth through NK education, not inhibition

Finally, I tested whether the observed aberrations in both maternal and fetal hemodynamics as well as *in utero* asymmetric growth would result in sub-optimal fetal growth. First, I assessed the impact of the previously described pregnancy aberrations on fetal growth at g.d. 15.5. I found that maternal NKG2A status did not result in growth-restriction for the fetuses as genetically-matched fetuses were the same weight whether they developed in C57BL/6 or *Klrc1*^{-/-} dams (Figure 54). This was possibly due to the fact that any fetal growth abnormalities would have been caused by defective placental functioning, and fetal growth rapidly accelerates in the last few days of gestation in the mouse, placing large demands on the placenta for oxygen and nutrient delivery. For example, mean fetal weight in C57BL/6 fetuses is almost four times higher at g.d. 18.5 than at g.d. 15.5

Fetal weight at g.d. 15.5
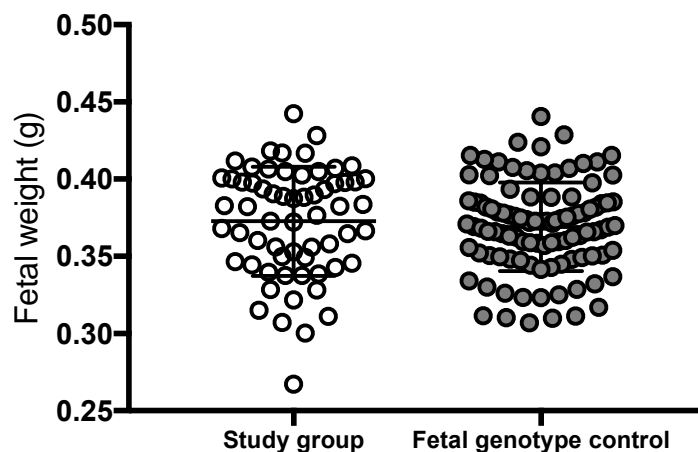
Figure 54. Comparison of fetal weight in *Klrc1*^{-/-} dams and controls at g.d. 15.5, by group. Mixed model analysis, non-significant. Error bars represent standard deviation. (n= 8-13 litters pre group).

In order to accurately assess whether late-onset growth restriction may be occurring in *Klrc1*^{-/-} dams, I compiled a control data set of mean fetal weight of g.d. 18.5 fetuses from (C57BL/6 males x C57BL/6 females) pregnancies. I then plotted the mean fetal weight of g.d. 18.5 fetuses from both (*Klrc1*^{-/-} females x C57BL/6 males) pregnancies and genotype control (C57BL/6 females x *Klrc1*^{-/-} males) pregnancies against the reference fetuses from (C57BL/6 x C57BL/6) pregnancies (for more information about each group, see Figure 55 for a breeding schematic, and Table 2 for further details regarding sample size) and found that only fetuses from (*Klrc1*^{-/-} females x C57BL/6 males) pregnancies displayed a significant reduction (Figure 56A). This suggested that reduced fetal growth was driven by maternal NKG2A deficiency.

Indeed, fetuses developing in NKG2A-deficient dams were not only smaller overall, but also almost three times more likely to be classified as SGA, whereas their fetal-genotype controls did not differ from the reference population (Figure 56B). The overall fetal weight reduction was not influenced by litter size (Figure 57A) and was absent at g.d. 15.5, consistent with a placentally-driven phenotype where exponential fetal-growth demands are not met in late-pregnancy in fetuses from (*Klrc1*⁻/⁻ females x C57BL/6 males) pregnancies. This finding was associated with normal placental size (Figure 57B), resulting in reduced fetal: placental weight ratio, which indicated reduced placental efficiency (Figure 57C).
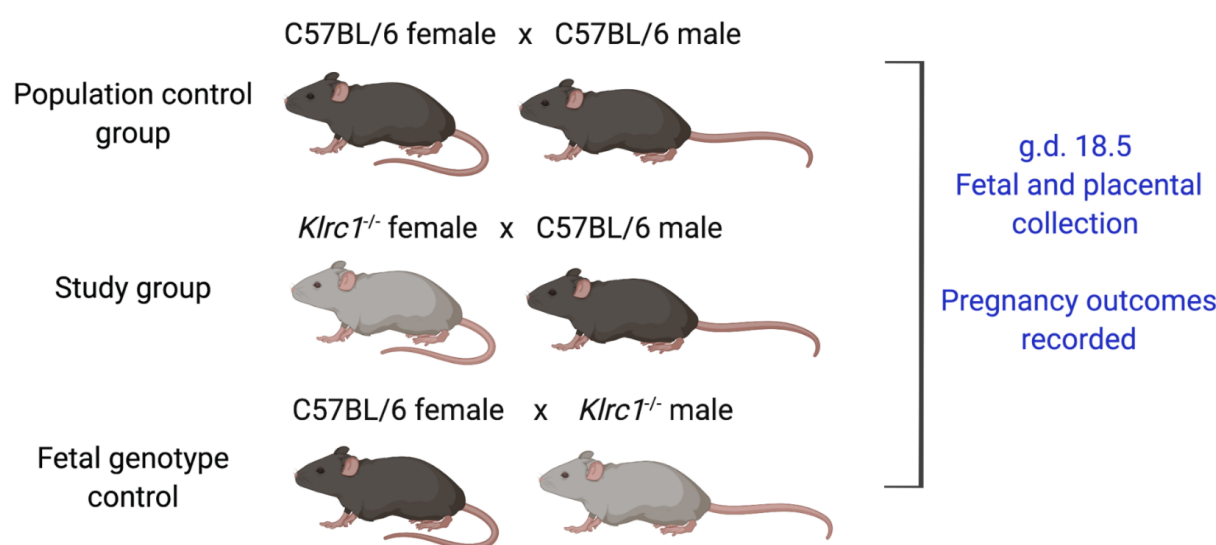
Figure 55. Schematic of breeding strategy to assess the role of maternal NKG2A deletion on fetal growth at g.d. 18.5

Group	Maternal strain	Paternal strain	Litters (n)	Fetuses (n)	Mean litter size
Population control	C57BL/6	C57BL/6	17	131	7.7
Study group	*Klrc1*⁻/⁻	C57BL/6	13	98	7.5
Fetal genotype control	C57BL/6	*Klrc1*⁻/⁻	10	70	7

Table 2. Group characteristics for g.d. 18.5 fetal weight comparison
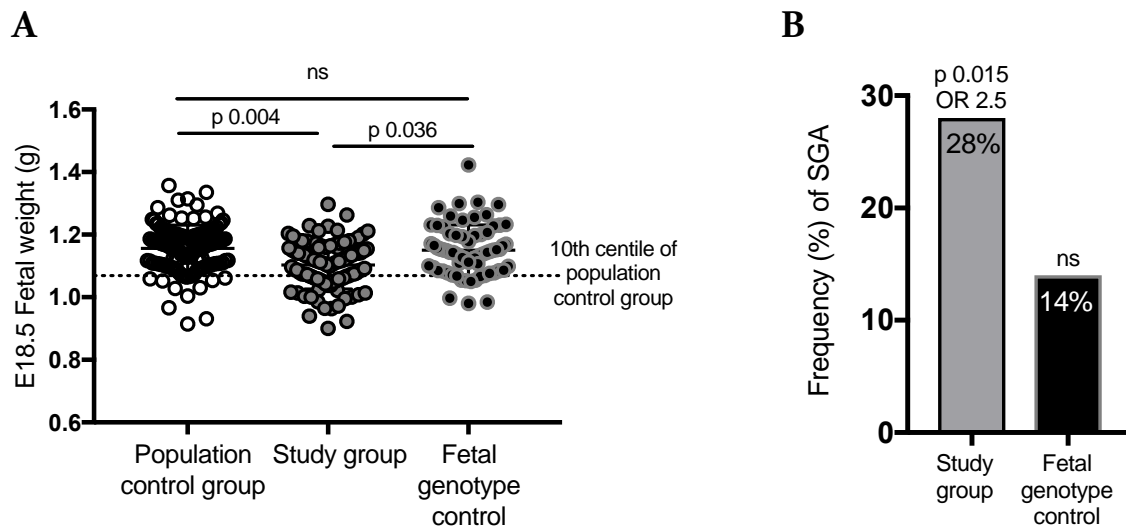
Figure 56. A) Comparison of fetal weight at g.d. 18.5, by group (Mixed model analysis). B) Frequency of SGA (%) in study group and fetal genotype control (Fisher's exact test, OR = odds ratio).
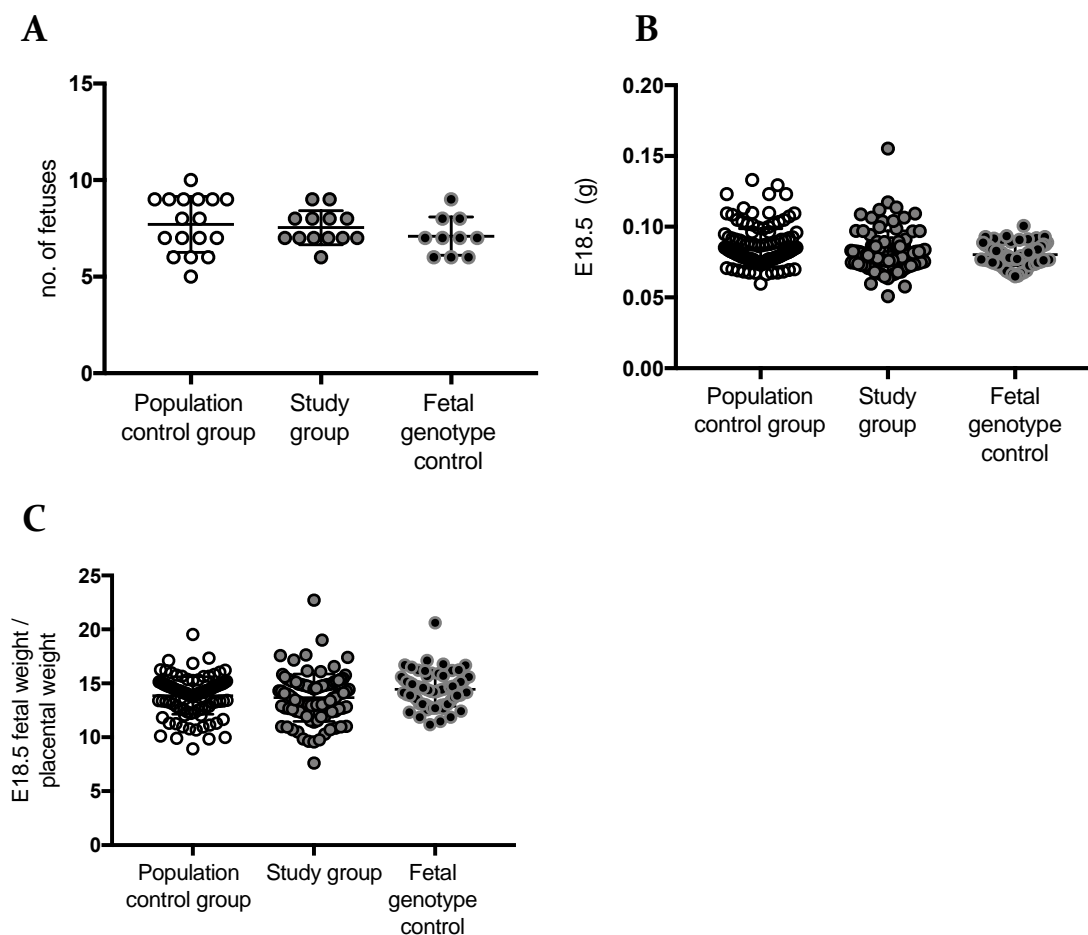
Figure 57. A) Litter size, B) Placental weight and fetal weight: placental weight ratios (C) at g.d. 18.5, by group (Mixed model analysis, all comparisons non-significant). Error bars represent standard deviation.

In order to assess the impact of NK education on fetal growth more broadly, I chose to investigate the effect of SHP-1 conditional knockout and *B2m* deletion on fetal growth. These experiments also potentially act as controls for mice lacking conventional NK educating pathways.

When mated with C57BL/6 males, dams with the conditional knockout of SHP-1 in NK cells displayed a reduction in fetal weight when compared to normal (C57BL/6 x C57BL/6, control) pregnancies (Figure 58A). However, when compared with control mothers who also expressed cre-recombinase (also as heterozygotes, cre-contol), there was no difference in fetal weight, as these dams also produced fetuses smaller than expected. Neither the presence of the conditional knockout, or the cre-recombinase alone appeared to have an impact on placental weight, placental efficiency or litter size, as these were similar in all three groups (Figure 58B-D).
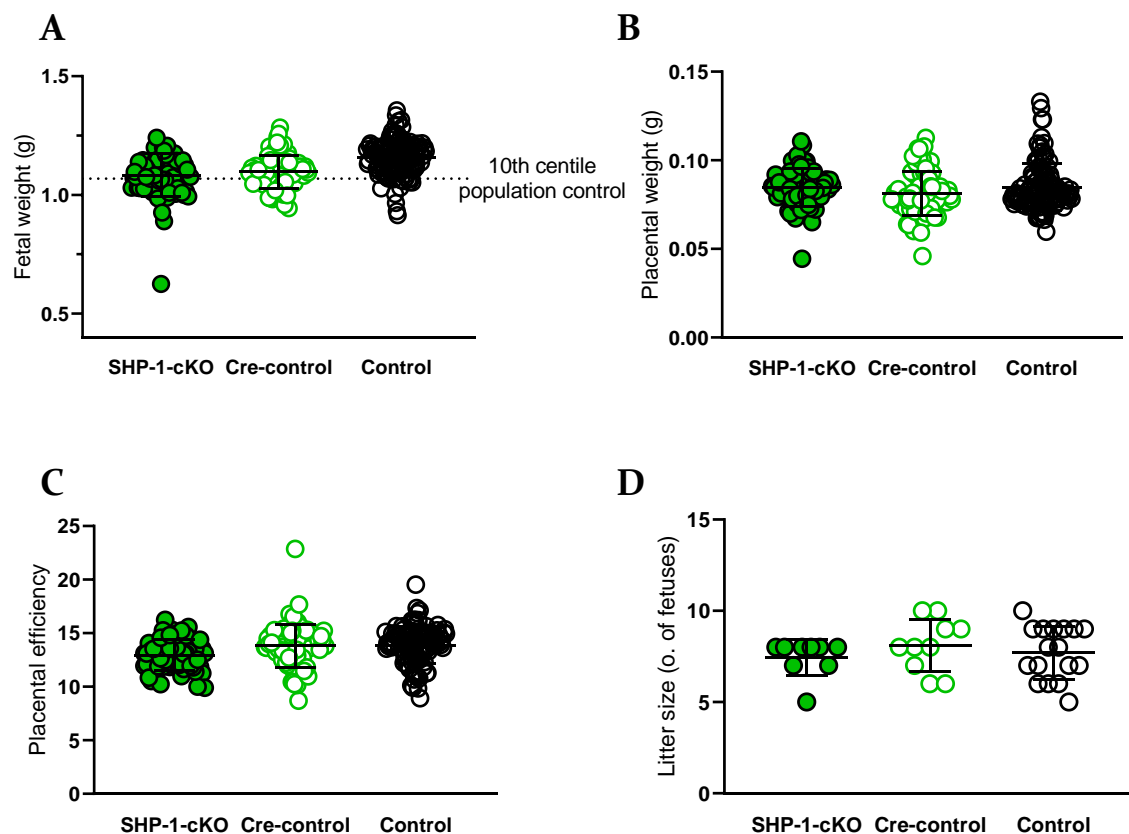
Figure 58. Pregnancy outcomes in SHP1-KO and control dams. Comparisons of A) Fetal weight, B) placental weight, C) fetal weight: placental weight ratios and D) litter size at g.d. 18.5, by group (mixed model analysis, all comparisons non-significant). Error bars represent standard deviation.

As previously shown by Jens Kieckbusch in our laboratory (unpublished data), it was confirmed that maternal *B2m* deletion had an impact on mean fetal growth. When $B2m^{-/-}$ females were mated with C57BL/6 males there was a significant reduction in fetal weight at

g.d. 18.5, and a significant increase in the numbers of fetuses born below the 10th centile of the control group (C57BL/6 females x C57BL/6 males). However, this phenotype was rescued when using a reverse cross control experiment (C57BL/6 females x $B2m^{-/-}$ males), indicating that, as for ($Klrc1^{-/-}$ females x C57BL/6 males) pregnancies, the fetal growth phenotype observed was likely being caused by the maternal environment, and not any effects of $B2m$ heterozygosity in the fetus.

4.19 Blockade of NKG2A in pregnancy

Like all educating receptors, NKG2A transmits inhibitory signals when ligated. My data so far indicated that NKG2A was exerting its control of fetal development through uNK education but did not exclude that NKG2A was exerting its control through the inhibition of uNK cells in early pregnancy. To uncouple the constitutive absence of NKG2A education from the acute lack of NKG2A inhibition, I performed immune checkpoint blockade experiments in which I acutely blocked NKG2A by injecting two doses of either the blocking monoclonal antibody 20d5 (Vance 1999) or an isotype-matched control antibody into pregnant B6 females at g.d. 6.5 and g.d. 9.5.

I chose these two time-points in pregnancy because the g.d. 6.5 to g.d. 9.5 window is when uNK are believed to exert their maximal function, and when both uterine vasculature remodelling and placenta formation begin (for more details regarding sample size see Table 3, and for schematic see Figure 59). The antibody panel used for this experiment can be found in 3.0 Chapter 1 – Methodology – Panel 8), whilst the gating strategy to identify uNK post-injection can be found in Figure 60A. The NKG2A epitope was 100% saturated in both uterine and splenic NK cells up to 3 days after injection (Figure 60B), providing evidence of sufficient NKG2A blockade for sufficient duration of pregnancy (at least up to g.d. 12.5). Although 2/11 dams treated with anti-NKG2A produced small litter sizes, the other 9 dams produced litters of normal size, indicating that acute lack of NKG2A inhibition may not lead to embryonic lethality/resorption in this context, unlike PD-1, CTLA-4 and Tim-3 blockade that cause fetal loss in mice (Guleria 2005; Wang 2019) (Figure 61A). Furthermore, fetal weight at g.d. 18.5 was the same across both treated and control groups (Figure 61B). Although I cannot formally distinguish between the acute effect of NKG2A blocking on education or on inhibition, the data are consistent with the possibility that it is NKG2A-derived *education*, and not early-gestation *inhibition* through NKG2A, which optimises fetal growth. Further experiments are ongoing to formally assess the effect of NKG2A blocking on NK phenotype and function, as well as on downstream consequences on uterine vascular adaptation to pregnancy

Group	Maternal strain	Paternal strain	Injected with	Litters (n)	Fetuses (n)	Mean litter size
Isotype control	C57BL/6	C57BL/6	10µg Isotype IgG2a (R35-95)	8	71	8.9
Antibody treated	C57BL/6	C57BL/6	10µg Anti-NKG2A/C/E (20d5)	11	78	7.1

Table 3. Group characteristics in NKG2A blockade experiment
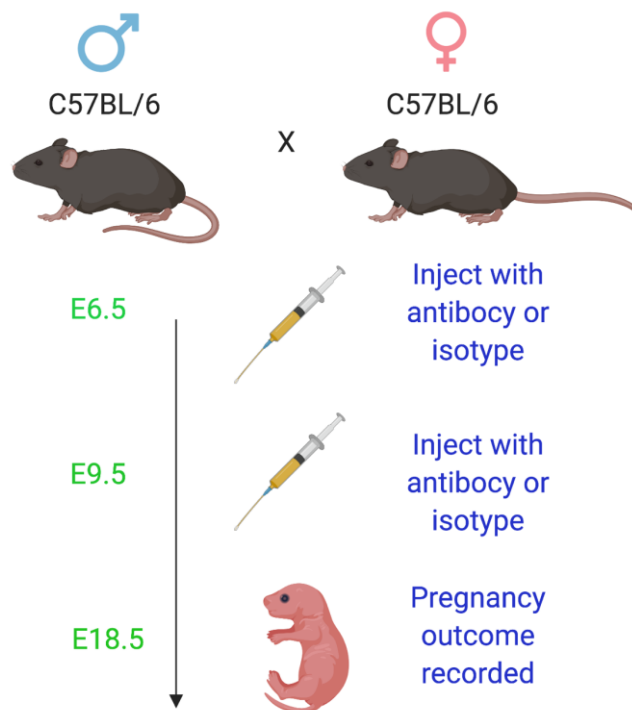
Figure 59. Schematic to represent the NKG2A blockade in early pregnancy experiment.
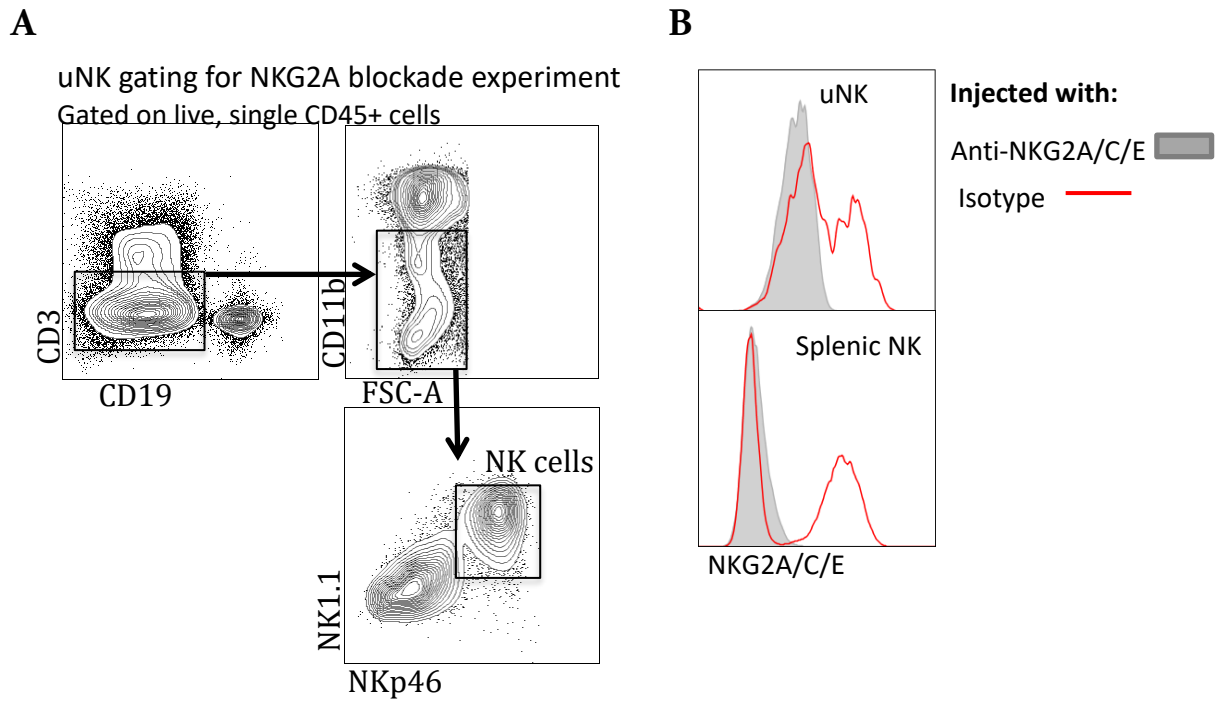
Figure 60. A) Flow cytometric gating strategy to identify uNK after injection. B) Representative histogram of NK cell NKG2A/C/E antibody labelling at g.d. 10.5 after either isotype or antibody injection in early pregnancy in (uNK above, splenic NK below)
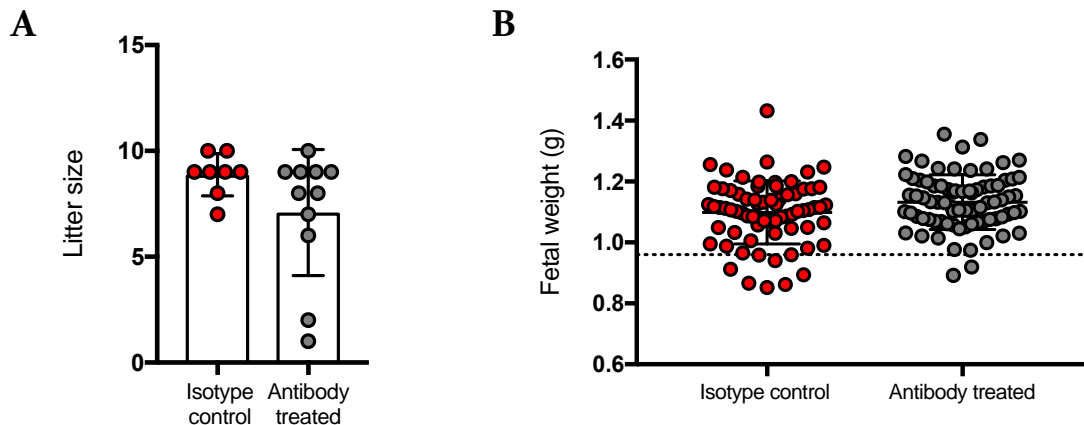
Figure 61. A) Comparison of litter size at g.d. 18.5, by condition (Mann-whitney-U test, each data point represents one litter, non-significant). B) Comparison of fetal weight at g.d. 18.5, by condition (Mixed model analysis, non-significant). Error bars represent standard deviation.

4.20 Educating NK genes protect against pre-eclampsia

The NKG2A inhibitory receptor, encoded by the conserved and invariable *KLRC1* gene, is present on 95% of human uNK cells and binds both maternal and fetal HLA-E. Its education potential is instructed by a dimorphism in the *HLA-B* gene, which separates the various HLA-B allotypes into either strong (*-21M/X*) or weak (*-21T/T*) NKG2A educators (Horowitz 2016), due to the ability of the leader peptide to promote high or low HLA-E expression, respectively. I tested the hypothesis that *-21M/X* women, who can educate NK cells through NKG2A better

132

than *-21T/T* women, are less likely to suffer from pre-eclampsia due to increased uNK education and functionality. To do so, I determined the *-21 HLA-B* status of 500 individuals from a previously characterised UK case-control study (n=250 vs. 250 controls) (Hiby 2004; Hiby 2010) (for genotyping see Figure 62A, for clinical characteristics see Chapter I Methodology section 3.15). In this cohort, neither fetal weight nor fetal outcome data was available. The population frequencies of *M/M (12%)*, *M/T* (43%) and *T/T* (45%) individuals were as expected, as was the linkage disequilibrium (LD) between *M/M* and C1+HLA-C (Horowitz 2016, Figure 62B).

Ethnicity can influence risk of pre-eclampsia, especially in non-hispanic black women, who are at greater risk of disease (Ghosh 2014). In this study, the prevalence of 'Black African', 'Black Caribbean' and 'Black Other' ethnicities were low, and the same across both *M/T* and *T/T* subgroups (4% vs. 4%). Also, no significant difference was found between *M/X* and *T/T* groups in the frequency of white (eastern or western) individuals (91% vs. 87%, not shown). Furthermore, multiple pregnancy also increases the risk of pre-eclampsia (Hernandez-Diaz 2009). Again, in this study, there was no statistical difference in the frequency of multiple pregnancies between *M/X* and *T/T* groups (3% vs. 2%).

C2+HLA-C expressed on fetal extravillous trophoblast (EVT) can predispose mothers to pre-eclampsia, whereas maternal expression by uterine cells may enhance uNK education through KIR2DL1 ligation. Accordingly, *M/M* individuals (n = 61) who do not express C2+HLA-C due to LD between HLA-B and C1+HLA-C allotypes, were removed from further analysis. This also removed any bias introduced by the fact that Bw4+HLA-B (a ligand for the educating KIR3DL1) is also almost never found in *M/M* individuals (Horowitz 2016). Overall, the presence of -21M did not significantly affect, by itself, the predisposition to pre-eclampsia (Table 4) (OR 0.84 [95%CI 0.58-1.23], p 0.39).

It has previously been shown in humans that uNK display educational receptor repertoires which are distinct from those found in peripheral blood NK cells (pNK), and that NKG2A improves functional responses when in combination with certain educating KIR, including KIR3DL1 (Sharkey 2015). I tested these *in vitro* findings by selecting all KIR3DL1+ mothers (n=304), and stratifying by *T/T* and *M/T*. Within this subgroup I found a significant reduction in pre-eclampsia in M/T individuals, who were almost half as likely to be sufferers (OR 0.62, [95%CI 0.39-0.98], p 0.0254, Figure 63A). This effect was independent of KIR2DS4 (in LD with KIR3DL1), as the frequency of individuals expressing the functional and protective

KIR2DS4^{wt} allele was equal in both subgroups (Figure 63B). This suggests that uNK cells benefit from NKG2A education, and can provide protection against pre-eclampsia.

In order to fully disentangle the impact of NK education on human pregnancy, it would be useful to compare women with no educating genetic pathways, to various populations expressing differing educating genotypes. However, almost all women carry the educating KIR2DL1 gene. Furthermore, women homozygous for C1+HLA-C (who cannot educate through KIR2DL1) carry an implicit bias where they are less likely to suffer pre-eclampsia driven by fetal C2+HLA-C expression because they can only transmit C1+HLA-C to their progeny. As a result, identifying truly uneducated individuals for comparison with other education genotypes is challenging.

I therefore performed a sub-group analysis of groups within all KIR2DL1+ / C2+HLA-C women, as a baseline level of NK education. I then analysed subgroups within this group, selected by the number of other educating genes those individuals expressed (non-independent groups). In support of my initial findings, I observed a pattern of decreasing frequency of pre-eclampsia with the addition of KIR3DL1 and -21*M/T*, but not -21*T/T* (Figure 64). These groups cannot be statistically compared as they are subgroups of each other, however the pattern is in support of my initial findings. These data support the notion that human pregnancy benefits from NKG2A education, however validation in independent cohorts would be beneficial. To our knowledge, this is the first immunogenetic data linking NK education to reproductive success in humans.

A

B
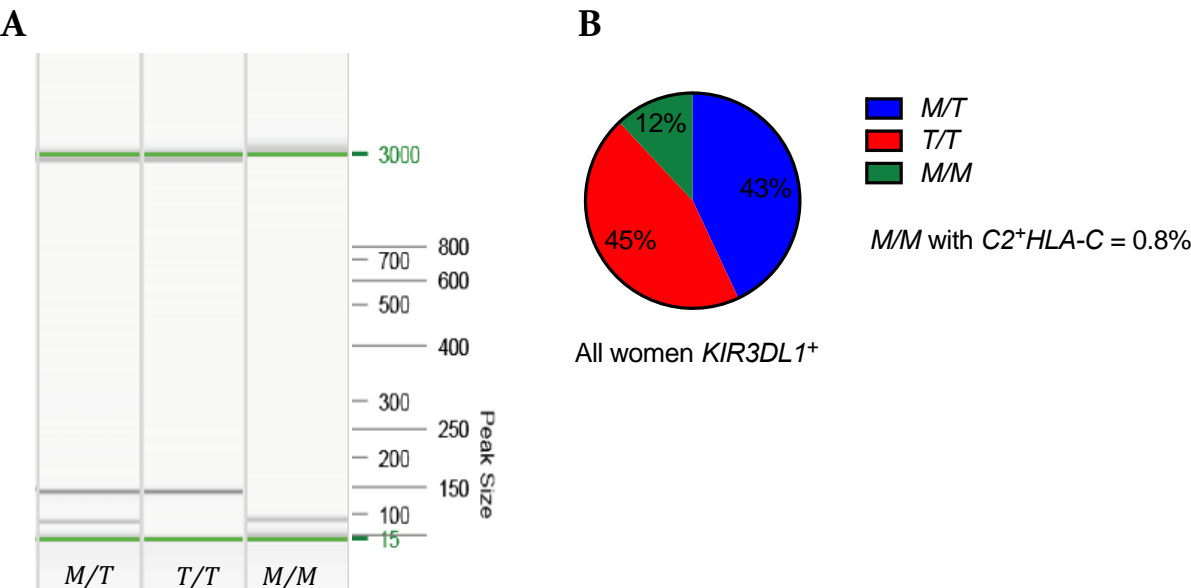
Figure 62 A). QIAxcel electrophoresis showing restriction enzyme PCR digestion products (grey bands) for M/T, T/T and M/M individuals (green bands indicate

reference markers). B) Graphical representation of *-21 HLA-B* allelic frequencies in the cohort.

	Pre-eclampsia (n)		
M/T (n/N)	*T/T* (n/N)	OR (95% CI)	Fisher's Exact
108/226	111//213	0.84(0.58-1.23)	0.39

Table 4. Table showing Fisher's exact test and relative risk of pre-eclampsia for *M/T* vs. *T/T* individuals in UK cohort.
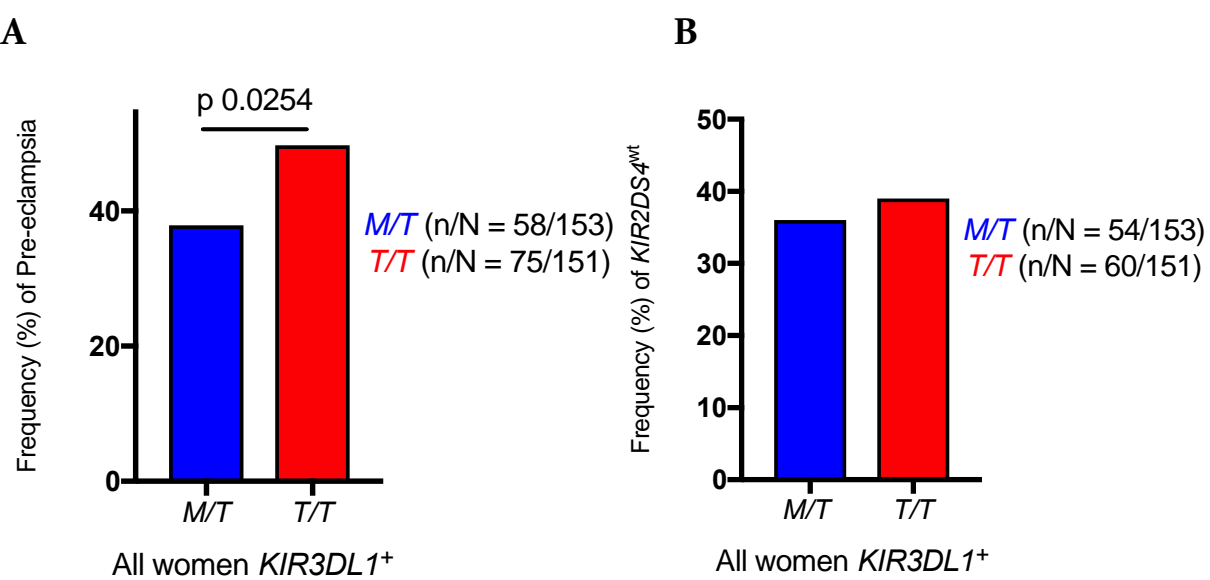
Figure 63. A) Frequency of pre-eclampsia in *KIR3Dl1+* women, by *HLA-B-21* status (Fisher's Exact test, one-sided. B) Frequency of the protective *KIR2DS4^{wt}*, by group (Fisher's exact test).
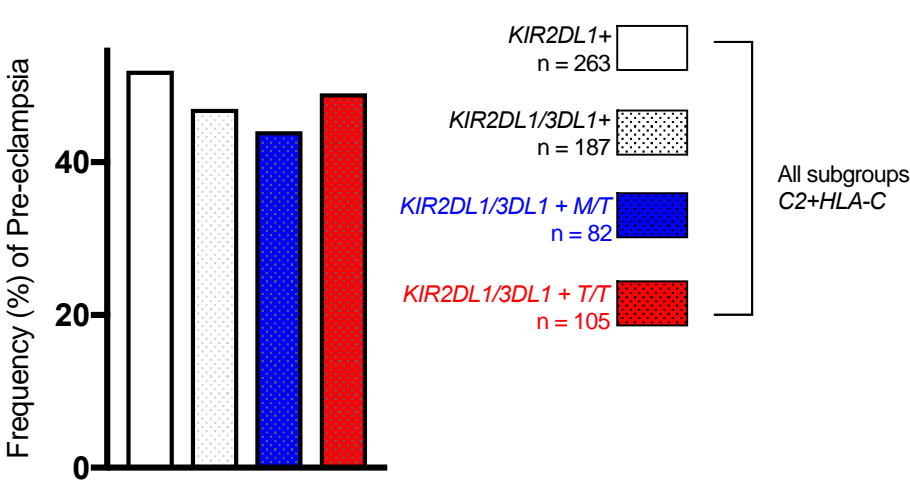
Figure 64. Frequency of pre-eclampsia in KIR2DL1+ / C2+HLA-C women, by education status (groups are non-independent).

5.0 CHAPTER I – DISCUSSION

To our knowledge, this project provides the first evidence that implicates NK education in physiology and that NKG2A regulates pregnancy outcome. By combining human immunogenetics data with functional studies in transgenic and C57BL/6 mice, I have shown that the inhibitory receptor NKG2A is important for uNK function, and its absence results in a number of perturbations to important physiological pathways in pregnancy.

Our finding that mothers who are able to educate through NKG2A in combination with KIR3DL1, are at decreased risk of pre-eclampsia, provides a novel insight into the immunogenetics that regulate this condition. It also supports the recently published notion that NKG2A and KIR work synergistically to educate NK cells and optimise their function (Zhang 2019). That this effect is seen without selecting for fetal C2+HLA-C expression, also adds weight to the notion that maternal immunogenetics profiling may eventually play a role in the prediction of pre-eclampsia, where early detection or risk stratification may lead to improved outcomes (Poon & Nicolaides 2014).

Two sets of ligands may engage with NKG2A on uNK cells. The first set is maternal HLA-E expressed on decidual cells, which is independent of pregnancy and educates NKG2A+ uNK cells in individuals who are -21M+HLA-B, which drives high HLA-E expression. The second set is fetal HLA-E expressed by invading EVT during pregnancy. The latter may contribute to both education and/or inhibition of NKG2A+ uNK cells. Data in mice exclude that fetal MHC molecules educate uNK cells (Kieckbusch 2014) and no evidence for that exists in humans either. Moreover, non-classical MHC molecules do not appear to be expressed by mouse trophoblast (Madeja 2011). Therefore, the mouse system is ideal to address the role of interactions between MHC molecules and inhibitory receptors on uNK cell education avoiding the confounding effect of these interactions on uNK cell inhibition contributed by fetal cells.

Using an NKG2A-KO mouse model, it was shown that NKG2A regulates the production of the important cytokine IFN-γ, but not degranulation. This is pertinent as human uNK are poorly cytotoxic (King 1989), but rather produce functionally important cytokines and chemokines (Hanna 2006). This supports previous findings which implicate NKG2A in NK education/function in C57BL/6 mice (Fernandez 2005; Yu 2009) and in human uterine tissue (Sharkey 2015). NKG2A is expressed in a heterodimer complex together with CD94 in both humans and mice. Using a CD94 KO model in 129/SvJ mice, in which NKG2A is not expressed, one study has shown a redundancy for NKG2A in NK education. However, the Ly49 receptor

repertoire of 129/SvJ mice differs from that of B6 mice, having more inhibitory Ly49 receptors that can educate NK cells, thus compensating for the lack of NKG2A-driven education (Orr 2010). My studies of $Klrc1^{-/-}$ dams in pregnancy provide multiple mechanisms for how NKG2A may contribute to improved pregnancy outcome. IFN-γ is a key regulator of decidual spiral artery remodelling in mouse pregnancy, and its production was reduced in NKG2A- uNK cells. Despite anatomical differences between human and murine utero-placental tissues, the observed association of reduced spiral artery remodelling with increased uterine artery resistance in $Klrc1^{-/-}$ dams, is in keeping with established human studies of placental insufficiency where FGR and disorders of gestational hypertension are common (Olofsson 1993; Sagol 1999).

In addition, it was found that variations in gene transcription occurred within placentae of $Klrc1^{-/-}$ dams and not within placentae of C57BL/6 dams, despite variations of fetal weights in both groups and despite both sets of placentae having the same genetic make-up. Moreover, no gene expression changes occurred between the placentae of small fetuses in $Klrc1^{-/-}$ and B6 dams. This suggests that the NKG2A-deficient environment is perturbed and causes transcriptomic changes in placentae of small fetuses that require to adapt to achieve normal fetal growth. The finding of enriched gene pathways associated with aerobic respiration and hypoxia fits the model that placental hypoxia/reoxygenation leads to oxidative stress and may be a key pathophysiological determinant of pre-eclampsia (Hung 2002). DE of genes between placentae of Small and Average fetuses within $Klrc1^{-/-}$ dams was associated with a pattern of late-onset asymmetric growth in Small fetuses later in pregnancy. This pattern is further evidence of chronic hypoxia leading to placental insufficiency (Fleiss 2019) in these fetuses. This is pertinent as it is these fetuses who are more likely to suffer from neurobehavioral problems in the neonatal and postnatal period in humans (Tolsa 2004; Eixarch 2008; Oros 2010).

In this project, I also show that fetuses developing in $Klrc1^{-/-}$ dams display a lower mean body weight at the end of gestation and are more likely to fall below the 10th centile of a control population, than genotype-matched controls. This finding was independent of placental weight and supports the evidence that NKG2A is required for the optimal delivery of nutrients and oxygen to the fetal circulation. I also provide data suggesting that this process might be governed by NKG2A education, not inhibition, as blocking the NKG2A receptor with a monoclonal antibody in early pregnancy had no effect on fetal weight. If confirmed, this would be the first *in vivo* data, to our knowledge, to discriminate between these two physiological processes.

It is interesting that the fetuses of both the *Klrc1*^{-/-} and the *B2m*^{-/-} dams were at risk of being SGA, but not the mice from the conditional-SHP1-KO. The SHP-1 KO mouse should lack all known ITIM-dependent inhibitory pathways, and therefore the vast majority of known inhibitory NK pathways. However, the relative contributions of maternally-derived NK cell inhibition in pregnancy (i.e. a transient loss of activation potential), that may well be functional, is simply not known and could bias these results. Furthermore, cre-recombinase can significantly alter promoter activity, and can also reduce mammalian cell proliferation and induce chromosomal abnormalities (Loonstra 2001; Schmidt-Supprian 2007). That growth-restriction was found in control dams, heterozygous for cre-recombinase but lacking a lox-P target, suggests that the overall impact of this genetic insertion may have been masking any underlying phenotype caused by the SHP-1 conditional knockout. The cre-recombinase was not a feature of either the NKG2A-knockout, or the *B2m*-knockout models. If this presumed effect of the cre-recombinase is confirmed, it may be important as it could affect all mouse models involving Ncr1-specific KO of other target genes.

That *Klrc1*^{-/-} dams displayed normal DLK1 levels when compared to controls is also interesting. The DLK1 predicts embryonic mass in mice. However, the hypothesis that fetuses developing in NKG2A-deficient dams prone to FGR would exhibit a lower serum level, was disproved. A possible explanation for this is that, as shown in the fetal weight data, only approximately 30% of fetuses in *Klrc1*^{-/-} dams display a growth potential below the 10th centile of the control population. Indeed, the majority of fetuses are normally grown in this model. This significant, yet not global prevalence of SGA, may have been too subtle to be detected in maternal serum DLK1 levels which represent a cumulative total from all fetuses who contribute to it.

As previously discussed, the sex differences at large between the RNA-sequencing groups should be addressed in future work, and certainly represent a limitation when interpreting this data. Placentae were selected on the basis of the weight of their corresponding fetus, in order to model the specific placental causes of growth restriction in the perturbed maternal environment. It wasn't until after selection, tissue processing and RNA sequencing that it became clear that there were differences in gender distribution between the groups. Nearly all the 'small' fetuses in both experimental groups were females (the group from C57BL/6 mothers contained 1 male and 4 females, and all 5 of the 'fetuses from the *Klrc1*^{-/-} group were female), whereas nearly all of the 'average' fetuses in both groups were males (4 males vs. 1 female in both groups). It is unclear why this is the case, although it may reflect the gender dimorphism

which is thought to be present in response to stress *in utero* (Rosenfeld 2015) and may affect brain development (Wheelock 2019).

This problem could be addressed in a number of ways. Although the previously described adjustment for fetal sex may have gone some way to control for this, it is not ideal, and almost certainly would not eliminate all bias. By genotyping future placental tissue for the presence of Y chromosomes, it would be possible to select an equal balance of placentae from males and females, prior to RNA extraction and sequencing. In doing this, the sample size of all groups could also be increased which would add more statistical power for DEG expression. If performed successfully, RNA expression analysis by RT-qPCR could be performed to validate the sequencing data, and to provide confidence in performing downstream validation of results at the protein level. Other further potential experimental work for this project could include single-cell RNA sequencing of uNK subsets to assess the specific transcriptional effects of NKG2A absence and presence in C57BL/6, and to assess the effects of deletion in *Klrc1*^{-/-} mice. Furthermore, using the same monoclonal antibody utilised in the *in vivo* NKG2A blockade experiments to investigate the cellular functional effects of acute checkpoint inhibition *in vitro* would be useful.

In an attempt to detect asymmetrical growth patterns in FGR fetuses, I compared small fetuses to average fetuses born from *Klrc1*^{-/-} dams. In the control group, I only selected average fetuses, as I did not expect the small fetuses to represent any significant pathology, as all fetuses developed in 'normal' conditions. In hindsight, the analysis of small fetuses from control dams should have also been performed as it would have shown any baseline differences present in normal, but small and healthy murine fetuses. Whilst I predict, since 50% of SGA human fetuses display normal and symmetrical growth, that these mice will not display the asymmetry observed in the fetuses from *Klrc1*^{-/-} dams, it cannot safely be ruled out at this stage.

Increasing the sample size of the human cohort pre-eclampsia study and validating the finding in an independent cohort would also be beneficial and may provide more sensitivity and statistical power to detect NKG2A: KIR gene interactions. There is the possibility of accessing a large cohort dataset at the Sanger Institute, Cambridge, where the -21 SNP has been typed in a pre-eclampsia study. Another interesting area to expand this work in to would be to include an analysis of birthweight, according to the presence of threonine or methionine at HLA-B -21. This could be combined with also looking for the effect of alleles which effect HLA-E expression (there are 2 alleles, one of which enhances cell surface expression), to fully

investigate all components of this pathway which may influence pregnancy outcome. This work could be combined with functional assays in human uterine NK cells, where the specific effects of NKG2A, or the HLA -21 dimorphism, could be analysed in genotyped cohorts. An advantage of this approach would be the ability to measure functional outputs with known physiological roles in early human gestation, such as VEGF.

One of the strongest findings in this study was the reduction in spiral artery remodelling seen in the *Klrc1*$^{-/-}$ dams, when compared to C57BL/6 dams. The effect size was greater than that seen in the fetal weight comparison, which would be expected, as by late-gestation many other factors (e.g. number of concepti, maternal nutrition etc.) would have contributed to overall fetal nourishment and growth. Whether the observed lack of arterial remodelling was caused by a lack of education, or a lack of acute inhibition, would be interesting to address. One way this work could be continued would be to block the NKG2A receptor pathway in early pregnancy, as described above, and re-perform the spiral artery stereology assay.

Finally, the obvious limitations when extrapolating murine data to a human context cannot be ignored in this project (discussed in 1.0 Introduction). However, it was possible to combine the animal model findings with clinical human data, which appear to support each other. Furthermore, the use of clinically translatable imaging techniques in this project provide new insights into murine pregnancy, and lend credibility to the conclusions drawn from the data.

The current screening tools used to predict pre-eclampsia are poor, and the vast majority of cases present for the first time to clinicians having never undergone any specific screening (e.g. uterine artery Doppler). Instead, Obstetricians rely heavily upon the detection of antenatal hypertension and proteinuria in the community, through sporadic visits to the midwife or General Practitioner throughout pregnancy. It is also incumbent upon pregnant women to present to hospital settings if they feel certain symptoms, which are often subjective in nature (e.g. headache, visual disturbances), in order for diagnoses to be made. As a result, this often results in late diagnoses when maternal morbidity secondary to uncontrolled hypertension is more likely, and harder to control. In such instances, delivery of preterm fetuses is often necessary to prevent potentially fatal eclamptic seizures, with the associated increased risks of prematurity to the fetus representing a significant burden of this condition. It is for this reason that research in this field should include attempts to develop strategies to better develop potential predictive markers of disease, whether they be immune genetic profiling, improved placental imaging in early pregnancy, clinical algorithms or maternal biomarkers of placental disease.

CHAPTER II

A humanised mouse model of pregnancy

6.0 CHAPTER II – A HUMANISED MOUSE MODEL OF PREGNANCY

6.1 PREFACE

This experimental work carried out in this chapter was all performed in the first 18 months of the PhD, and thus is the smallest experimental section of this thesis. Once the data described below was collected and analysed, and the *Klrc1*$^{-/-}$ mouse colony was established and available for experimentation, this project was given less priority.

6.2 HYPOTHESIS

It is predicted that in pregnancies where transgenic male mice expressing C2+HLA-C are mated with transgenic female mice expressing KIR2DL1*003, excessive inhibition of uNK in early pregnancy will result in reduced fetal growth at g.d. 18.5.

6.3 AIMS

1. Successfully create humanised mouse colonies as described above
2. Confirm protein expression of KIR2DL1 on uNK cell surfaces in KIR2DL1-tg mice, and C2+HLA-C on cell surfaces of trophoblast of HLA-Cw6-tg fetuses
3. Provide evidence of functional effects of uNK inhibition through the KIR2DL1: C2+HLA-C pathway
4. Measure the effect of this uNK receptor-ligand interaction on fetal growth

6.4 ACKNOWLEDGEMENT OF CONTRIBUTIONS

All experimental work in this chapter was carried out by the author, except for the following:

6.5 BACKGROUND

As discussed previously (Introduction), there are a number of maternal immunogenetic profiles, and maternal/paternal genetic combinations that appear to contribute to reproductive success in humans. Of note, the combination of maternal KIR AA genotype (the presence of two KIR A haplotypes) and paternal C2+HLA-C appears to predispose pregnancies towards pre-eclampsia (Colucci 2017).

There are two well-described haplotypes for KIR genes, simply termed KIR A and KIR B (Parham 2005). Individuals can therefore be classified as KIR AA, KIR AB or KIR BB. The KIR A haplotype is represented by a consistent arrangement of predominantly inhibitory genes, while many B haplotypes exist through varying numbers of additional activating genes (Hollenbach 2012). Consisting of only seven genes, KIR A haplotypes contain three framework genes which are constitutively found in all individuals, and three inhibitory KIR genes. KIR2DS4 is the only activating KIR found on the KIR A haplotype, and is nearly always non-functional, at least in Europeans (Moffett 2016). Two KIRs bind to C2+HLA-C ligands, the inhibitory KIR2DL1 and the activating KIR2DS1. As KIR2DS1 is not present on the KIR A haplotype, but is a feature of KIR B haplotypes, it is likely that the previously described combination of KIR A and C2+HLA-C in poor pregnancy outcome is being driven by the inhibitory action of KIR2DL1 (Moffett 2016). Conversely, in European women, the presence of a KIR2DS1-containing KIR B haplotype confers protection when in combination with paternal C2+HLA-C, as the strong inhibitory signal from KIR2DL1 is overridden by this activating signal (Hiby 2010; Moffett 2016). A figure containing the genetic contents of the two KIR haplotypes, and their cognate ligands, can be found in Figure 65.

Of the 26 KIR2DL1 alleles currently known, three are typically found on KIR A haplotypes. These are known as KIR2DL1*003, *002 and *001. The dominant allele found in KIR B haplotypes is known as KIR*004 (Huhn 2018). For this study, the 003 allele of KIR2DL1 (KIR2DL1*003) was chosen as it is known to bind strongly to C2+HLA-C (Blokhuis 2017).

Like KIR, many HLA-C alleles exist. In the context of pregnancy, the HLA-C ligands for KIR on trophoblast cells can be divided into two groups, C1+HLA-C and C2+HLA-C. These two groups are defined by a dimorphism at position 80 of the α1 domain, where C1 displays asparagine and C2 displays lysine (Hilton 2012). It is worth noting that HLA-G, exclusively expressed by EVT, acts as a ligand for KIR2DL4, LILRB1 and LILRB2 receptors on natural killer (NK) and other cells (Li 2009), however it is beyond the scope if this thesis to discuss these interactions fully. Of all the C2+HLA-C alleles, the highly expressed HLA-C*0602 (also designated, and referred

to in this thesis as, HLA-Cw6) allotype, that binds strongly to KIR2DL1*003 (Hilton 2015), was chosen for this project.
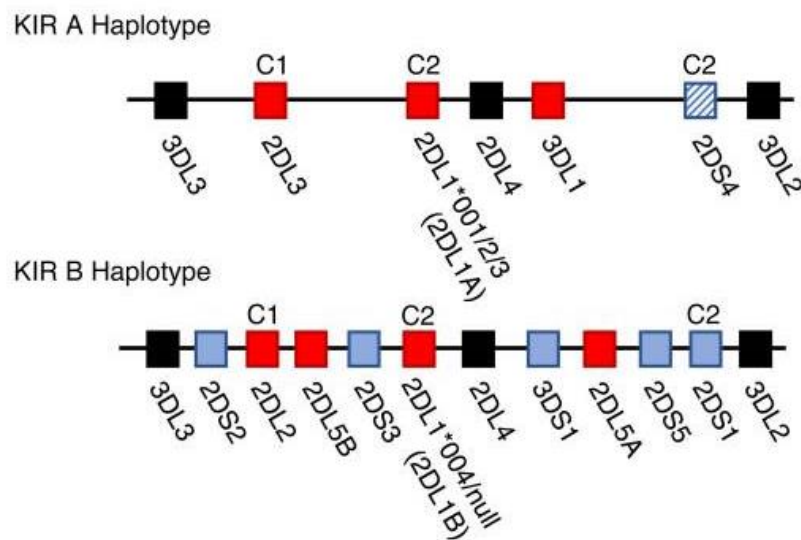
Figure 65. Representative KIR A and B Haplotypes. Cognate HLA-C ligands are depicted above their receptor. Framework genes (present in all common haplotypes) are shown in black, activating KIR in blue and inhibitory KIR in red. *Figure and legend taken from Huhn et al. 2018.

Despite the extensive published work that has characterised the genetic associations between KIR, HLA and pregnancy, the physiological mechanisms at large in this paradigm remain poorly understood. Understanding the cellular perturbations that may occur in these cases is challenging, as most of these pregnancies will continue to a gestation where fetal viability is reached. This has meant that experimental work is usually confined to either the analysis of *ex vivo* pregnancy tissue from first trimester termination of pregnancies, or miscarriages where, by their very nature, the tissue being studied cannot be assumed to be representative of normal physiology. This has meant an over-reliance on the analysis of maternal genotypes through DNA sampling, and their correlation with pregnancy outcomes such as fetal weight, recurrent miscarriage and pre-eclampsia. This project was designed to address this issue in a reliable animal model, and to provide evidence to test the previously described genetic association studies in humans.

7.0 CHAPTER II – METHODOLOGY

7.1 Generation of humanized mice

Mouse embryonic stem cells (mESC) transgenic for either KIR2DL1*003 (KIR2DL1*003-tg) or HLA-Cw6 (HLA-Cw6-tg) were generated at Babraham Institute (for full targeting vectors, see below). In brief, 1×10^7 ES cells were electoporated with 20µg of purified linearized targeting vector. 24 hours post electroporation the medium was changed and Geneticin (G418) selection was added to final concentration of 200µg/ml. Medium containing G418 was changed on a daily basis for the following 8 days. Next, 200 clones from each targeting condition, KIRR2DL1 or HLA-Cw6, were picked and screened using long range PCR for the correct insertion into the Rosa26 locus. The clones were then expanded for Southern blot before the final QC of karyotyping and sequencing of all functional domains of the best clones.

The mESCs were injected into C57BL/6 –Tyr (albino) blastocysts and transferred into pseudo-pregnant surrogate mothers. Chimeric offspring positive for the transgenes were then used to establish founder colonies.

7.2 KIR2DL1 and HLA-Cw6 targeting

For a targeting vector schematic, see Figures 66 and 67. For KIR2DL1, the gene was inserted downstream of a loxP-flanked stop codon in order to inhibit transcription outside of the appropriate cre-recombinase-containing cells (NK cells). Downstream of the KIR2DL1, an FRT-flanked selection cassette was inserted in order to identify transgene-positive cells following antibiotic selection. The following cDNA sequences were used in generating the KIR2DL1 targeting vector for electroporation:

ATGTCGCTCTTGGTCGTCAGCATGGCGTGTGTTGGGTTCTTCTTGCTGCAGGGGGCCTGGCC
ACATGAGGGAGTCCACAGAAAACCTTCCCTCCTGGCCCACCCAGGTCGCCTGGTGAAATCAG
AAGAGACAGTCATCCTGCAGTGTTGGTCAGATGTCATGTTTGAACACTTCCTTCTGCACAGA
GAGGGGATGTTTAACGACACTTTGCGCCTCATTGGAGAACACCATGATGGGGTCTCCAAGGC
CAACTTCTCCATCAGTCGCATGACGCAAGACCTGGCAGGGACCTACAGATGCTACGGTTCTG
TTACTCACTCCCCCTATCAGGTGTCAGCTCCCAGTGACCCTCTGGACATCGTGATCATAGGT
CTATATGAGAAACCTTCTCTCTCAGCCCAGCTGGGCCCCACGGTTCTGGCAGGAGAGAATGT
GACCTTGTCCTGCAGCTCCCGGAGCTCCTATGACATGTACCATCTATCCAGGGAAGGGGAGG
CCCATGAACGTAGGCTCCCTGCAGGGCCCAAGGTCAACGGAACATTCCAGGCTGACTTTCCT
CTGGGCCCTGCCACCCACGGAGGGACCTACAGATGCTTCGGCTCTTTCCATGACTCTCCATA
CGAGTGGTCAAAGTCAAGTGACCCACTGCTTGTTTCTGTCACAGGAAACCCTTCAAATAGTT
GGCCTTCACCCACTGAACCAAGCTCCAAAACCGGTAACCCCCGACACCTGCACATTCTGATT

GGGACCTCAGTGGTCATCATCCTCTTCATCCTCCTCTTCTTTCTCCTTCATCGCTGGTGCTCC
AACAAAAAAAATGCTGCGGTAATGGACCAAGAGTCTGCAGGAAACAGAACAGCGAATAGCG
AGGACTCTGATGAACAAGACCCTCAGGAGGTGACATACACACAGTTGAATCACTGCGTTTTC
ACACAGAGAAAAATCACTCGCCCTTCTCAGAGGCCCAAGACACCCCCAACAGATATCATCGT
GTACACGGAACTTCCAAATGCTGAGTCCAGATCCAAAGTTGTCTCCTGCCCATGA.

Figure 66. Schematic (above) and map (below) of KIR2DL1*003 targeting vector with restriction sites indicated. Produced by Dominik Spensberger.

For HLA-Cw6, the gene was inserted in conjunction with a green fluorescent protein (GFP)-coding gene, with a gene sequence for a self-cleaving peptide (P2A) separating the two sequences. This would allow for GFP to be exclusively expressed when HLA-Cw6 was expressed, but both proteins should form independent and separate entities upon cleavage. Downstream of this was a Lox-P flanked selection cassette, as described above. The following cDNA sequences were used in generating the HLA-Cw6 targeting vector for electroporation:

ATGCGGGTCATGGCGCCCCGAACCCTCATCCTGCTGCTCTCGGGAGCCCTGGCCCTGACCGA
GACCTGGGCCTGCTCCCACTCCATGAGGTATTTCGACACCGCCGTGTCCCGGCCCGGCCGCG
GAGAGCCCCGCTTCATCTCAGTGGGCTACGTGGACGACACGCAGTTCGTGCGGTTCGACAGC

147

GACGCCGCGAGTCCGAGAGGGGAGCCCCGGGCGCCGTGGGTGGAGCAGGAGGGGCCGGAG
TATTGGGACCGGGAGACACAGAAGTACAAGCGCCAGGCACAGGCTGACCGAGTGAACCTGC
GGAAACTGCGCGGCTACTACAACCAGAGCGAGGACGGGTCTCACACCCTCCAGTGGATGTA
TGGCTGCGACCTGGGGCCCGACGGGCGCCTCCTCCGCGGGTATGACCAGTCCGCCTACGAC
GGCAAGGATTACATCGCCCTGAACGAGGACCTGCGCTCCTGGACCGCCGCGGACACGGCGG
CTCAGATCACCCAGCGCAAGTGGGAGGCGGCCCGTGAGGCGGAGCAGTGGAGAGCCTACCT
GGAGGGCACGTGCGTGGAGTGGCTCCGCAGATACCTGGAGAACGGGAAGGAGACGCTGCAG
CGCGCGGAACACCCAAAGACACACGTGACCCACCATCCCGTCTCTGACCATGAGGCCACCCT
GAGGTGCTGGGCCCTGGGCTTCTACCCTGCGGAGATCACACTGACCTGGCAGCGGGATGGC
GAGGACCAAACTCAGGACACCGAGCTTGTGGAGACCAGGCCAGCAGGAGATGGAACCTTCC
AGAAGTGGGCAGCTGTGGTGGTGCCTTCTGGAGAAGAGCAGAGATACACGTGCCATGTGCA
GCACGAGGGGCTGCCAGAGCCCCTCACCCTGAGATGGGAGCCATCTTCCCAGCCCACCATCC
CCATCGTGGGCATCGTTGCTGGCCTGGCTGTCCTGGCTGTCCTAGCTGTCCTAGGAGCTGTG
ATGGCTGTTGTGATGTGTAGGAGGAAGAGCTCAGGTGAAGGAGGGAGCTGCTCTCAGGCTG
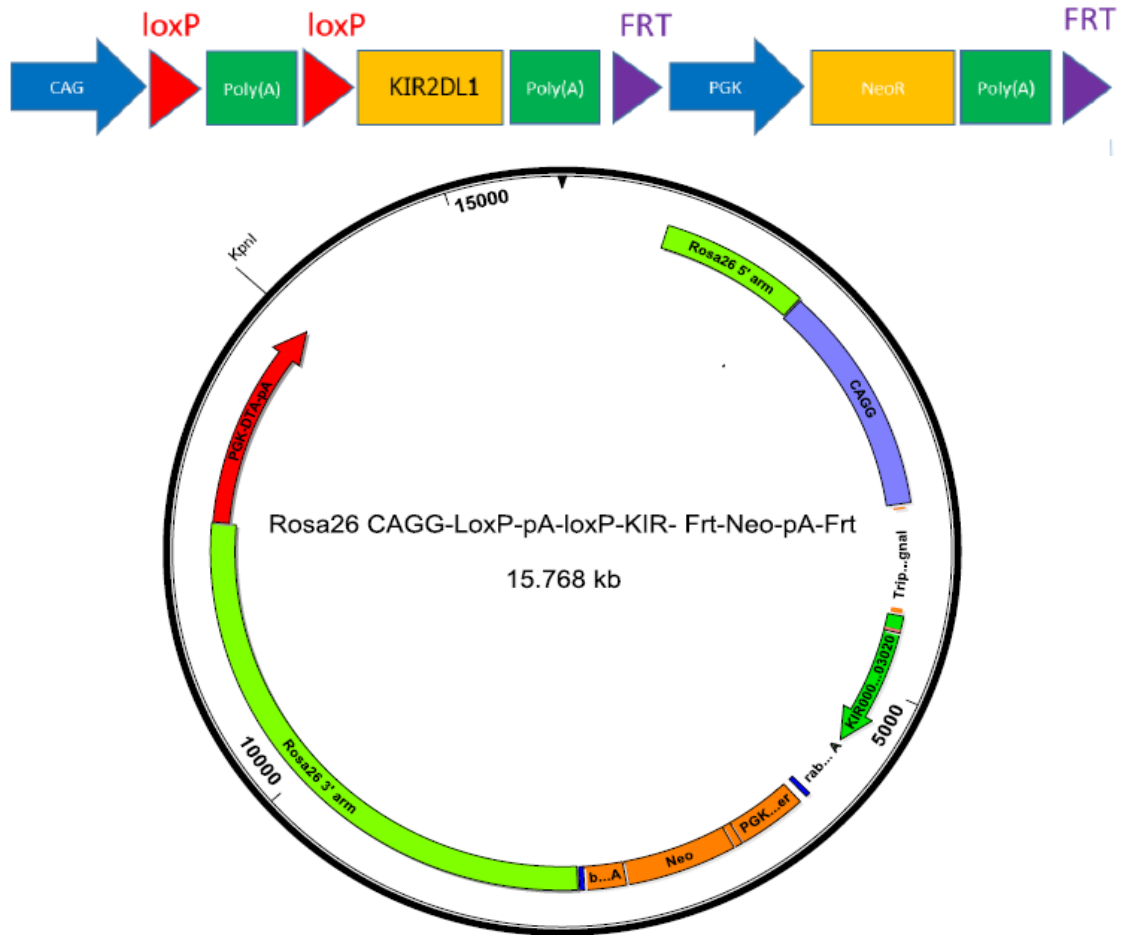CGTCCAGCAACAGTGCCCAGGGCTCTGATGAGTCTCTCATCGCTTGTAAAGCCTG.
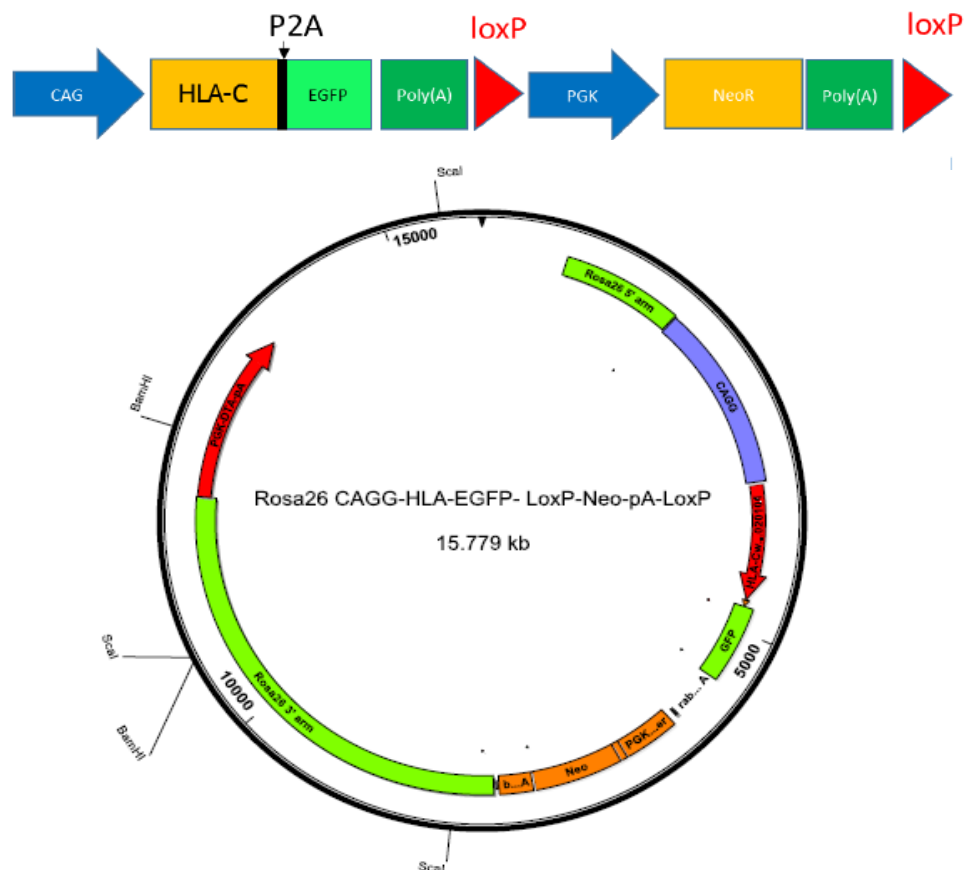
Figure 67. Schematic (above) and map (below) of HLA-Cw6 targeting vector with restriction sites indicated. Produced by Dominik Spensberger.

7.3 PCR for genotyping transgenic mice

KIR2DL1*003

The following PCR recipe was used; 2.5µl ddH$_2$0, 10µl 2x Phire buffer, 0.5µl Phire enzyme, 5µl diluted DNA, 1µl each Fw and Rv primer. The following primers were used; Rev 5' *AGCGGACCACTTTAGTCTTCT* '3 amd Fw 5' *GACGATTGGTACAAGTACG* '3. The following PCR cycle was used; Initial denaturation 98°C for 5min, 40 x (denaturation 98°C for 5s, annealing at 98°C for 5s, exlongation 72°C for 20s), final extension 72°C for 1 min.

HLA-Cw6

The same PCR recipe and PCR cycle was used, with the following primers; Rev 5' *GAAGTAGAGTCACCCGATGC* '3, Fw 5' *GACGATTGGTACAAGTACG* '3.

Rosa26

The same PCR recipe and PCR cycle was used, with the following primers; Rev wt 5' CACACCAGGTTAGCCTTTA 3', Fw 5' TGTTATCAGTAAGGGAGCT 3'.

7.4 Flow cytometry antibody panels

Panel 9 – HLA-C functional assay

	Target	Antibody clone	Fluorophore	Dilution	Laser	Channel
Extracellular	CD107a	H4A3	BV650	1:100	Violet	655/8
	CD14	M5E2	BV510	1:100	Violet	525/50
	CD19	HIB19	BV510	1:100	Violet	525/50
	CD3	HIT3a	PE-Cy 5.5	1:200	Yellow	710/70
	CD4	OKT4	BV510	1:100	Violet	525/50
	CD56	HCD56	PE_Dazzle	1:100	Yellow	610/20
	KIR2DL1	REA284	APC vio770	1:20	Red	780/60
	KIR2DL1/S1	EB6	PE-Cy7	1:20	Yellow	780/60
	NKG2A	REA110	APC	1:50	Red	670/14
Viability	Live/dead		Aqua	1:100	Violet	525/50

Panel 10 – KIR2DL1 expression

	Target	Antibody clone	Fluorophore	Dilution	Laser	Channel
Extracellular	CD45	30F11	BUV379	1:200	UV	379/28
	CD3	17A2	BV785	1:50	Violet	780/60
	NK1.1	PK136	PE-CF594	1:100	Yellow	610/20
	CD19	1D3	BUV739	1:100	UV	710/50
	NKp46	29A1.4	PerCP-ef710	1:50	Blue	695/40
	KIR2D/Isotype	HP-MA4	APC	1:100	Red	670/14
Viability	Live/dead	-	Ef450	1:1000	Violet	450/50

Flow cytometry tissue processing

When PBMCs were analysed, the following protocol was used:

- Whole blood was sampled from mice by tail vein venepuncture and collected in heparinised tubes and placed on ice.
- The blood then underwent red cell lysis (PharmLyse, BD Biosciences, NJ, US) twice, as previously described.
- Cells were then centrifuged and resuspended in FACS buffer.
- Cells were counted using a Neubauer chamber and plated for antibody labelling, as previously described.

7.5 Mouse serum exchange

Spleens were removed from euthanized C57BL/6 or HLA-Cw6$^{+/-}$ mice. Where splenocytes were used, the tissue dissociation (named Splenic tissue dissociation protocol) protocol listed in 3.0 - Chapter I – Methodology was used, without enzymatic digestion. Splenocytes were then incubated in either RPMI (Gibco) or RPMI + 10% Human Serum (HuS, Sigma-Aldrich, MI, US) for 5 hours, at 37°C (Bernabeu 1984). Cells were then fixed and stained for flow cytometry analysis.

7.6 Generation of mouse embryonic fibroblasts (MEFs) for lentiviral transfection

- Pregnant dams were sacrificed as described previously, at g.d. 14.5. Whole embryos were removed from surrounding uterine tissue, detached from placentae and placed in ice cold sterile PBS 1X.

- Brain tissue and all red tissue (organs such as spleen, heart, liver etc.) was then removed, and the organ-free embryos were placed into fresh sterile PBS. Embryos were minced in a small amount of cold PBS 1X using a syringe in a 10cm dish.

- 0.05% Trypsin/EDTA was added to the tissue, then all tissue was transferred into a 50ml falcon tube.

- 15 ml warm 0.05% Trypsin/EDTA was added to the falcon tube. DNaseI 30µg/ml was added next, and the tissue left at 37°C for 30 min with agitation.

- A further 15 ml warm 0.05% Trypsin/EDTA was added to the falcon tubes, along with a further DNaseI 30µg/ml. Again, the tissue was left to agitate at 37°C for 30 min.

- This above was repeated one more time (three times in total. After the 30 minute agitation the tissue fluid suspension was divided fluid into 4 50ml falcon tubes. Falcon tubes were then filled up with 3% Dulbecco's modified eagle media (DMEM).

- Falcon tubes were centrifuged for 5 min 1300rpm, and most of the supernatant removed.

- Liquid was filtered through a 100µm filter and centrifuged again for 5 min at 1300rpm. Supernatants were removed again, and the cells resuspended in 40 ml 3%DMEM.

- Cells were counted using a Neubauer chamber

- 25 Million cells per 15 cm dish were seeded, and 3% DMEM added to make a 30ml total volume per dish

- 1 day later: Change medium

- 4 days later: cells were split 1:4

- 3 days later: cells again split 1:4

- 3 days later (when confluent): cells were Trypsinized and counted prior to downstream application.

Previously generated mouse embryonic fibroblasts (MEFs) from BALB/c mice were used to optimize experimental conditions. Approximately 4×10^4 MEFs were seeded in flat-bottom 96-well plates in 100µl DMEM (Sigma-Aldrich, MI, US) + 3% fetal calf serum, without antibiotics. Pre- packaged lentiviral plasmid particles containing either red fluorescent protein, human B2M or blank vectors (G&P Biosciences, CA, US) were added at multiplicity of infection (MOI) of either 2 or 10, once cells were 70% confluent at 24hrs. Cells were liberated 4 days later by adding 100µl *accutase* (Sigma-Aldrich, MI, US) for 15 minutes plus a further 100µl for another

15 minutes. Cells were then stained as per usual flow cytometry protocol (above) before analysis through flow cytometry.

7.7 HLA-Cw6 functional assay

Whole blood was sampled from C57BL/6 or HLA-Cw6$^{+/+}$ mice by tail vein venepuncture and collected in heparinised tubes. The blood then underwent red cell lysis (PharmLyse, BD Biosciences, NJ, US) twice. The cells were then incubated with peripheral blood cells from genotyped human donors at an effector target ratio of 10:1. Anti-CD107a antibody was added at the start of the co-culture along with Golgiplug and Golgistop (BD Biosciences, NJ, US) which was added after 1 hour. After either 4- or 24-hours cells were stained and analysed by flow cytometry.

7.8 Immunohistochemistry for HLA expression on trophoblast
Anti-GFP immunofluorescence

7um sections were prepared as previously described for spiral artery stereology (3.0 Chapter I – Methodology). For De-wax and hydration, the following protocol was used; Xylene, 5 minutes at RT (x3), EtOH 100%, 10 minutes at RT (x2), EtOH 95%, 10 minutes at RT (x2), ddH2O, 5 minutes at RT (x2). For antigen retrieval, slides underwent boiling for 10 minutes at 95°C in fresh citrate buffer (pH 6.0) and then underwent incubation with either pronase or protease k for 10 minutes at RT. For staining, sections were washed in PBS 1X for 5 minutes at RT (x2), blocked non-specific sites in PBS with 5% goat serum for 1 hour at RT, incubated with Rabbit-anti GFP Polyclonal antibody conjugated with AlexaFluor 488 (Thermo Fisher Scientific, MA, US. Ref: A-21311, final concentration of 10 ug/ml) diluted in PBS with 5% goat serum. Finally, slides were washed in PBS (1X) for 5 minutes at RT (x3) and mounted with Vectashield Hardset and DAPI (Vector Lab, Ref: H-1500) and coverslipped.

Anti-HLA-C immunofluorescence

The same De-wax and hydration protocol as above. For antigen retrieval, slides underwent boiling for 10 minutes at 95°C in fresh citrate buffer (pH 6.0). For staining, slides were washed in PBT (1X) for 5 minutes at RT (x2). Blocking of non-specific sites in PBS with 5% goat serum for 1 hour at RT was performed. Incubation with Rabbit Polyclonal Anti-HLA-C antibody - Extracellular domain (Abcam, Cambridge, UK, Ref: ab193432, final concentration 100μg/ml), ON at 4°C. Rabbit Isotype IgG at the same final concentration (Dako, Agilent, CA, US, Ref: X0936) was used as a matched negative control. Both antibodies were diluted in PBT (1X) with 5% goat serum. Slides were next washed in PBT (1X) for 5 minutes at RT (x3) and then incubated with either Goat Anti-Rabbit IgG H&L Alexa Fluor488 (Abcam, Cambridge, UK,

ab150081, final concentration 5 ug/ml) or Goat Anti-Rabbit IgG H&L Alexa Fluor647 (Abcam, Cambridge, UK, ab150083, final concentration 5 ug/ml). The incubation was for 2 hours at RT. Both antibodies were diluted in PBT (1X) with 5% goat serum. Finally, slides were washed in PBT (1X) for 5 minutes at RT (x3) and mounted with Vectashield Hardset with DAPI (Vector Lab, Ref: H-1500) and coverslipped.

Anti-HLA immunostaining (HRP)

The same de-wax and hydration protocol as above was followed. For antigen retrieval, slides underwent boiling for 10 minutes at 95°C in fresh citrate buffer (pH 6.0). For staining; quenching of peroxidase activity was performed using ddH20 with 3% hydrogen peroxide (Thermo Fisher Scientific, MA, US, Ref: H/1800/15). This incubation was for 30 minutes at RT. Next slides were washed in Tris-buffered saline, 0.1% Tween 20 (TBST 1X) for 5 minutes at RT, twice. Blocking of non-specific sites in TBST with 5% goat serum for 1 hour at RT was performed next. Incubation with Rabbit Polyclonal Anti-HLA-C antibody - Extracellular domain (Abcam, Cambridge, UK, Ref: ab193432, final concentration 100μg/ml), ON at 4°C was next performed. As a matched negative control, Rabbit Isotype IgG at the same final concentration (Dako, Agilent, CA, US, Ref: X0936) was used. Both antibodies were diluted in Antibody Diluent (Cell Signaling, MA, US, Ref: 8112). Slides were washed again in TBST (1X) for 5 minutes at RT (x3) before being incubated with horseradish peroxidase (HRP) Rabbit Signal Stain boost detection reagent (Cell Signaling, MA, US, Ref: 8114) for30 minutes at RT. Slides were again washed in TBST (1X) for 5 minutes at RT (x3). Finally, slides were expose to 3,3'-diaminobenzidine (DAB) (Cell Signaling, MA, US, Ref: 8059) until browning occurred. At this point, the reaction was stopped using ddH20. For dehydration and cleaning the following protocol was used; EtOH 95%, 10 seconds at RT (x2), EtOH 100%, 10 seconds at RT (x2), Xylene, 10 seconds at RT (x3). Finally, slides were mounted with DPX mountant (Thermo Fisher Scientific, MA, US. Ref: LAMB/DPX) and coverslipped.

8.0 CHAPTER II – RESULTS

8.1 Generation of humanized mice colonies

Initial work was carried out by Dominik Spensberger at the Babraham Institute. Details of cDNA sequences, targeting vectors, electroporation and clone selection for both strains can be found in 7.0 Chapter II – Methodology. In brief, I received transgenic blastocysts, where the transgenes had initially been inserted into mouse embryonic stem cells (mESCs) from C57BL/6 mice (brown coat colour), and these MESCs had then been inserted into a blastocyst of the B6(Cg)-Tyrc-2J/J strain (albino C57BL/6). Mice from B6(Cg)-Tyrc-2J/J strain carry a mutation in the tyrosinase gene, meaning that their usual dark pigment is completely absent from skin, hair and eyes in homozygotes (Hughes 2007). These chimeric blastocysts were then injected into B6(Cg)-Tyrc-2J/J recipient surrogate dams. As expected, chimeras born displayed both coat colours (see Figure 68).

Figure 68. Photographs of chimeric male mice, KIR2DL1*003 (left) and HLA-Cw6 (right), used as breeders for germline transmission.

Males displaying 80% coat-colour chimerism were then chosen and mated with B6(Cg)-Tyrc-2J/J females to produce F1 offspring. The aim of this step is to achieve germline transmission of the transgene, so that all offspring will express the gene of interest. High percentage coat-colour chimerism increases the likelihood of achieving this, however it is no guarantee that the transgene will be present in the germ line tissue (spermatozoa in males, oocytes in females). A total of 15 pups with coat-colour chimerism were born and genotyped for the HLA-Cw6-tg strain, 6 of which were positive for the transgene. An F1 male and female were then crossed to produce F2 offspring and tested for allele number. For the KIR2DL1 strain, a total of 268 pups with coat-colour chimerism were genotyped, with 8 pups positive for the transgene. For both HLA-Cw6-tg and KIR2DL1*003-tg strains, genomic DNA from the original embryonic stem cells were used for positive controls initially, and primers for the Rosa26 locus were used to identify allele number (C57BL/6 as positive controls). Again, F2 generations were immediately produced and genotyped and displayed a Mendelian pattern of inheritance. These results show

that the transgenes are stable within the colonies, and are reliably transmitted through the germline. For PCR recipes see 7.0 Chapter II – Methodology, and for PCR results see Figure 69.
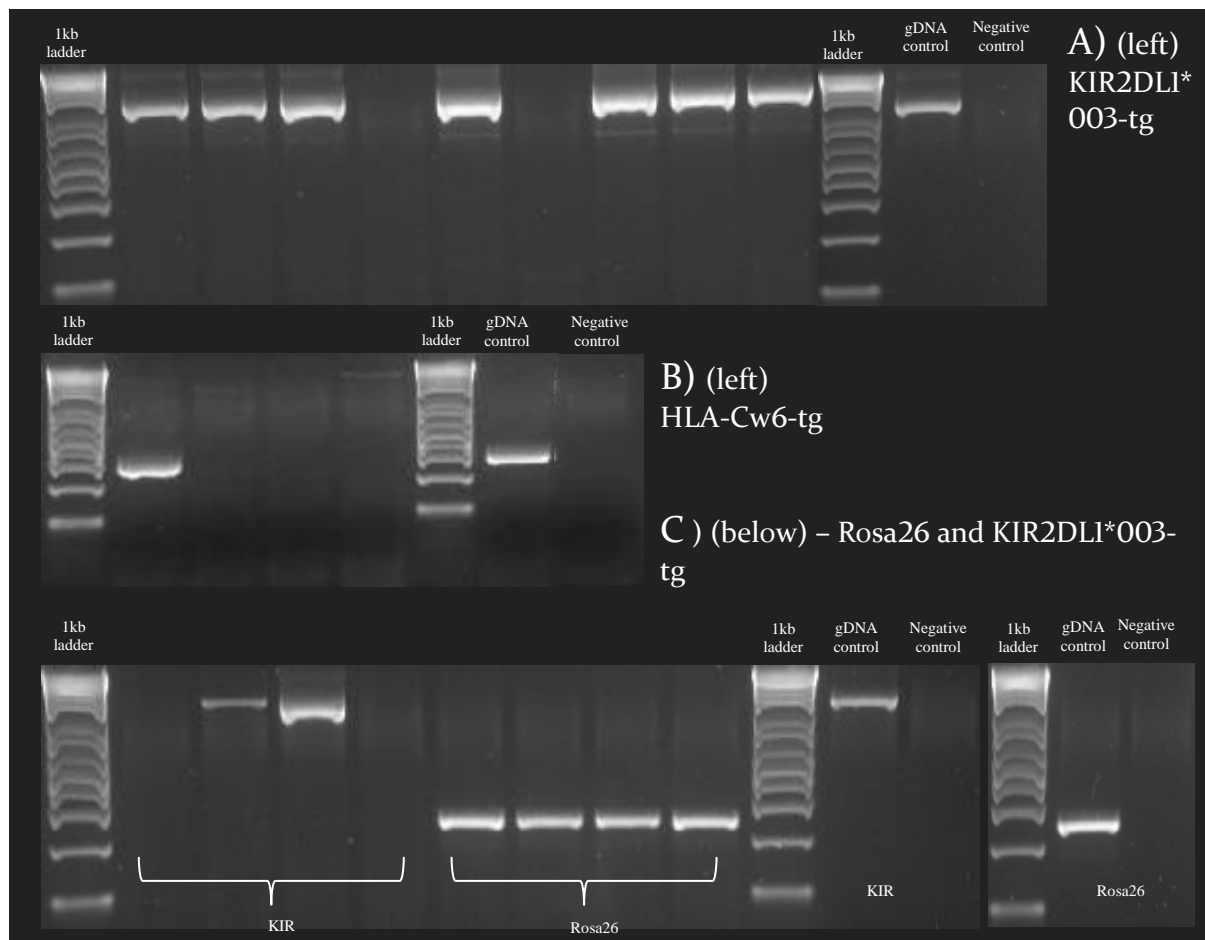
Figure 69. Representative images of Agarose 2% gel (UV transillumination) PCR products. A) (top row) results for KIR2DL1*003-tg showing 2 mice absent for the transgene. B) (middle row) results for HLA-Cw6-tg, showing 1 mouse positive for the transgene. C) (bottom row) combination of Rosa 26 and KIR2DL1*003-tg results in order to ascertain allele copy number.

8.2 C2+HLA-C protein expression

In the initial targeting vectors, the HLA-Cw6 transgene was inserted alongside a GFP protein-encoding sequence in order to aid identification of positive cells in downstream applications, i.e. the presence of GFP should always indicate the simultaneous expression of the HLA-Cw6 protein. This gene was inserted into the Rosa26 genetic locus. First identified in 1991 (Friedrich and Soriano 1991), this locus is ubiquitously expressed in embryonic and adult tissues in mice. Due to the high frequency of gene-targeting events observed at this locus in MESCs, it is an ideal candidate to integrate a transgene of interest for stable expression in mice, and has become a popular gene promoter since its discovery.

Primary flow cytometric analysis of peripheral blood mononuclear cells (PBMCs) taken from F2 HLA-Cw6$^{+/+}$ and HLA-Cw6$^{+/-}$ mice confirmed the expression of GFP in all cells from homozygotes and heterozygotes in an allele-dependent manner, with C57BL/6 mice showing zero expression (Figure 70). For this experiment, mutant GFP/HLA-Cw6 co-expressing 721.221 cells were used as positive controls.

GFP   HLA
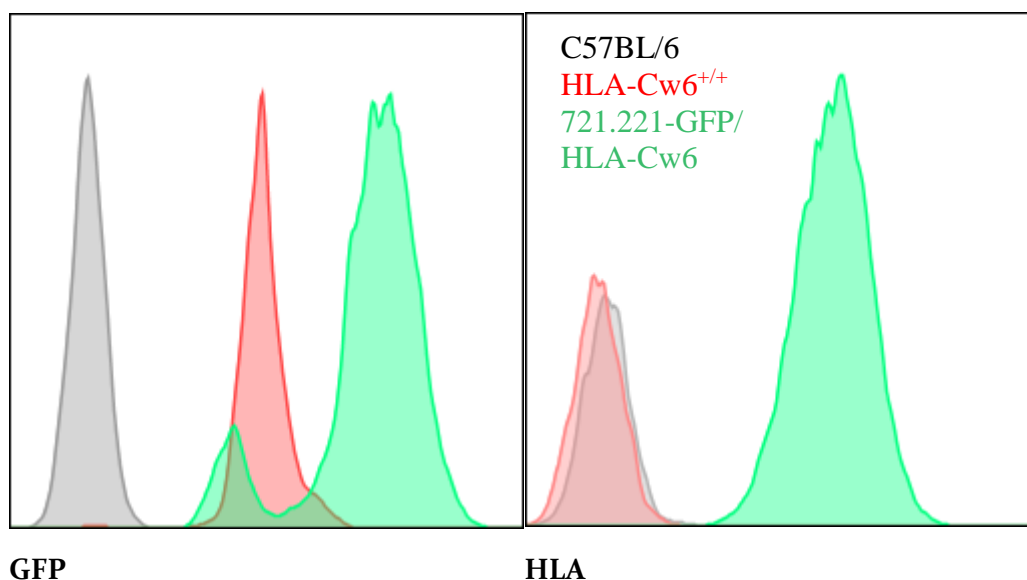
Figure 70. Representative flow cytometry histograms of GFP (left) and HLA (right) expression. Grey and red histograms represent PBMCs from C57BL6 and HLA transgenic mice, respectively. Green histograms represent 721.221-CW6 cells as a positive control for both proteins (n= 3 mice per experiment, 2 technical repeats).

W6/32 is a purified anti-human HLA-A/-B-/C antibody, whereas B1.23.2 is a monoclonal antibody which recognizes HLA-B and –C. In all mice tested, surface staining for HLA-C in HLA-Cw6$^{+/-}$ mice was only able to detect minimal cell surface expression with the W6/32 or B1.23.2 antibody clones (Figure 71A, data shown is for B1.23.2) where freshly isolated and genotyped human PBMCs were found to express these markers at high levels, as expected. The antibody panel simply consisted of a viability marker and the two clones mentioned above, so isn't shown. This led to the question as to whether sufficient C2+HLA-C protein was able to reach the cell surface, as this process would be reliant upon its cleavage from the GFP protein and it's binding with the endogenous mouse *B2m* molecule. Intracellular staining for HLA-B/C did indeed reveal expression at a higher level than that found at the cell surface (Figure 71B), albeit with a higher background in the C57BL/6 strain. For antibody panels please see 7.0 Chapter II – Methodology.

A Extracellular   **B** Intracellular

Mean GMFI: C57BL/6 = 37.46
HLA-Cw6$^{+/-}$ = 117.04
Fold change: 3.12

Mean GMFI: C57BL/6 = 68.32
HLA-Cw6$^{+/-}$ = 253.25
Fold change: 3.71
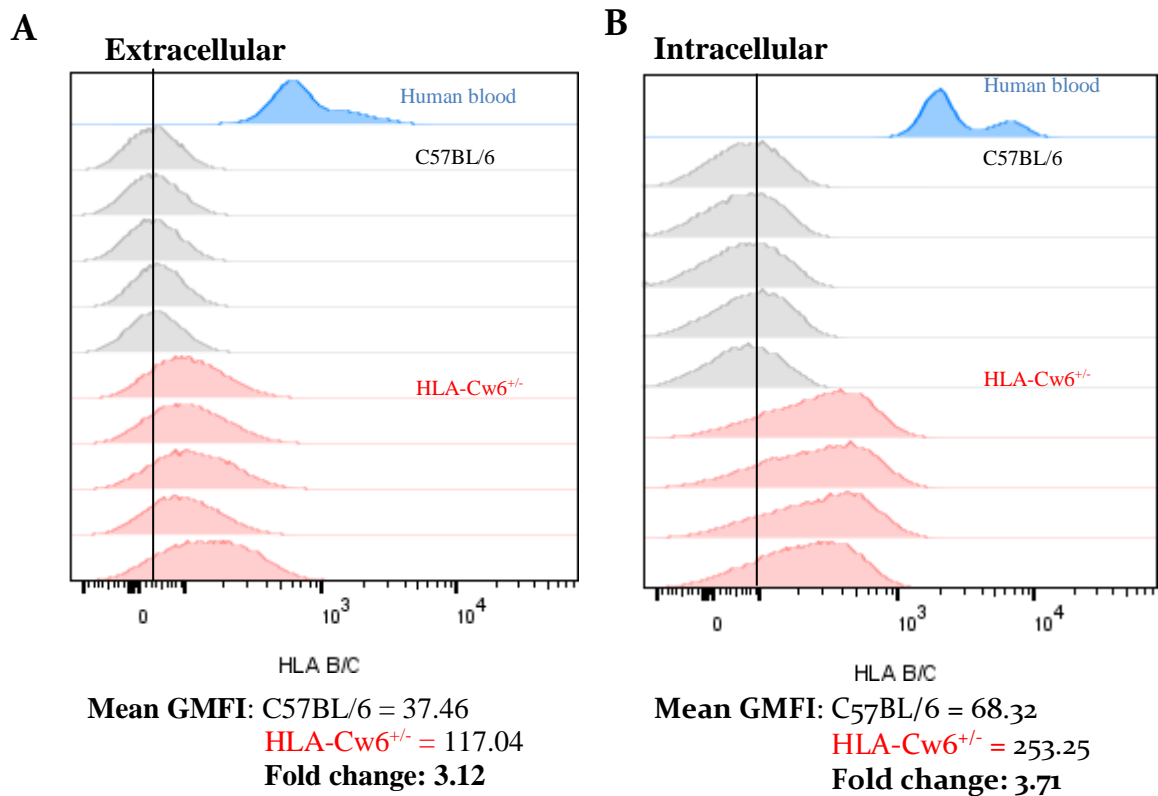
Figure 71A. Histograms of flow cytometry experiments to show HLA-B/C epitope detection on PBMCs isolated from C57BL/6 (grey) and HLA-Cw6$^{+/-}$ (red) mice both extracellularly A) and intracellularly B), with GMFI listed below. Blue histogram represents human PBMCs, as a positive control.

8.3 Serum exchange of human B2M

As previously discussed, B2M is a highly conserved polypeptide which is non-covalently associated with the heavy chain of the MHC class I antigens. Its presence is of vital importance in both humans and mice, as its synthesis is required for expression of the HLA-A/B and H-2K/D heavy chains at the cell surface. In order to address the question as to whether the murine B2M was sufficiently folding with the transgenic human HLA-Cw6 gene product, I attempted a simple but proven method of serum exchange of B2M. Two previous studies had suggested that this could solve the issue of surface expression. Firstly Bernabeu et al. (Bernabeu 1984) showed that both B2M from fetal calf serum (FCS, bovine B2M) or human serum (HuS, containing human B2M) could exchange with murine B2M on the cell surface when cultured together. Furthermore, another study using HLA-A3-, HLA-B7-, and HLA-Cw3-transfected cells cultures in the presence of murine B2M showed that these hybrid human-mouse molecules displayed structural modifications of both light and heavy chains. However, serological reactivity with W6/32 was restored when B2M was replaced by the human equivalent (Ferrier 1985).

As a result, splenocytes from C57BL/6 and HLA-Cw6$^{+/-}$ mice were next analysed after incubation with or without human serum. This was performed to detect any increase in C2+HLA-C cell surface expression after a period of potential serum exchange between human and mouse B2M. As a control, RPMI without human serum was used as a culture medium to detect any background increase in HLA-C expression that may occur as a result of the incubation process. Again, cells isolated from HLA-Cw6$^{+/-}$ mice displayed strong GFP expression when compared to C57BL/6 mice (Figure 72A). The antibody panel simply consisted of a viability marker and the two clones mentioned above, so isn't shown. When cultured in human serum (HuS), a slight increase in the level of HLA-B/C detection was found in the HLA-Cw6$^{+/-}$ cells when compared to RPMI (Figure 72B). However, this effect was also seen in the C57BL/6 strain. This suggests that this phenomenon was likely to be caused by the HuS incubation protocol itself (Figure 72C), and not due to serum exchange of B2M upregulating HLA-C cell surface expression.
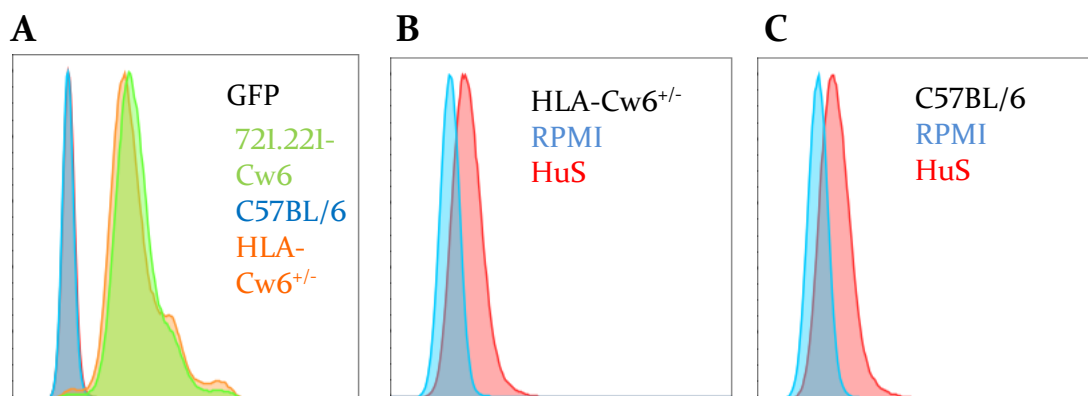
Figure 72. A) Representative flow cytometry histograms showing GFP expression on 721.221-Cw6 cells (green) and cells isolated from C57BL/6 (blue) and HLA-Cw6$^{+/-}$ mice (orange). Histograms to show the effect of human serum on HLA-C expression in cells isolated from HLA-Cw6$^{+/-}$ (B) and C57BL/6 (C) mice.

8.4 Functional assay of HLA-Cw6+ cells

As the endogenous expression of HLA-C is generally low in human cells, it was important to check the functional capability of HLA-Cw6-expressing cells from the HLA-Cw6-tg mice, irrespective of their cell surface expression. This was achieved by co-culturing cells from C57BL/6 and HLA-Cw6$^{+/+}$ mice with genotyped human NK cells, known to express the receptor KIR2DS1. If the effector cells express C2+HLA-C they should bind KIR receptors on target cells and cause an activating response, measured through CD107a release.

I gated on human NK cells (CD56^{Bright}, CD14-, CD19-, CD3-, CD4- . For gating strategy see Huhn 2018) as per published protocols (for antibody panel see 7.0 Chapter II – Methodology –

Panel 9). Unfortunately, the HLA-Cw6^{+/+} cells showed no difference in eliciting CD107a expression in KIR2DS1+ NK cells after 4 hours of incubation. In contrast, positive control 721.221-Cw6 cells were able to elicit an increase CD107a response from KIR2DS1+ NK cells, which was negated by the presence of 2DL1, as expected. These responses were independent of NKG2A expression (Figure 73), which provides a strong inhibitory signal potentially capable of overriding any signaling from C2+HLA-C. Overall these results indicate that one cannot have confidence that HLA-Cw6 gene expression in cells isolated from HLA-Cw6-tg mice results in the translation of a functional cell-surface C2+HLA-C protein.
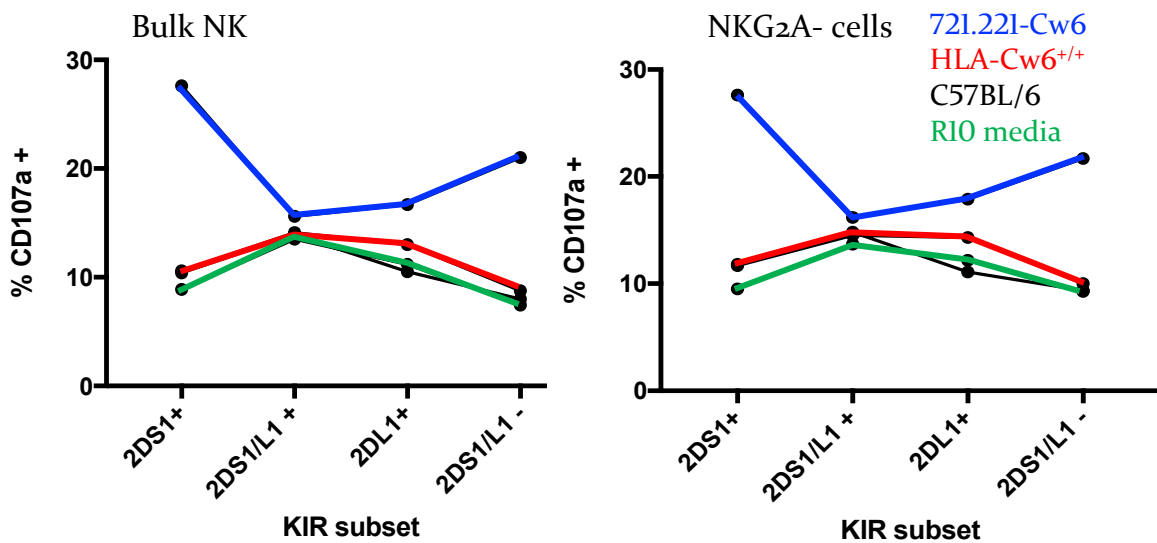
Figure 73. Human NK cell degranulation in response to the effect of various target cells, by KIR subset in bulk NK cells (left) and NKG2A- only cells (right). Blue lines represent 721.221-Cw6 cells, whereas cells isolated from C57BL/6 and HLA-Cw6^{+/-} mice are shown in black and red, respectively, R10 media negative control culture conditions are represented in green.

8.5 Lentiviral transfection of Human B2M

In light of the results of the functional assays, a further attempt to increase cell surface expression of the HLA-Cw6 molecule was attempted. As the human serum exchange assay had failed to increase surface expression of HLA-C, I hypothesized that adding the human B2M gene to dividing cells may restore the expression of the HLA-C. A lentiviral plasmid system was used to attempt this, for full details of the vector see 7.0 Chapter II – Methodology. In brief, a plasmid containing the human B2M gene under a strong cytomegalovirus promoter was chosen for integration into the MEF genome through transfection. Mouse embryonic fibroblast cells (MEFs) were generated by mating HLA-Cw6^{+/+} males with C57BL/6 females, and collecting the fetuses at g.d. 13.5. As a result, all MEFs generated were HLA-Cw6^{+/-}. Seeding cells at 2 x 10^4 per well and culturing for 6 days yields sufficient live cell numbers for

downstream analysis (Figure 74A). Lentiviral packaged blank vector (negative control) transduction had little impact on cell viability at MOI of 2 and 10, as compared to MEFs only cultured in growth media, when cells were counted. Initial transduction attempts to induce cell surface expression of human B2M and increase the expression of HLA-B/C at MOI of 2 and 10 were unsuccessful, as downstream flow cytometry analysis of liberated cells showed them to be unreactive with the anti-HLA-B/-C antibody clone B1.23.2 (Figure 74B). The antibody panel simply consisted of a viability marker and the two clones mentioned above, so isn't shown. Of note, the positive control red fluorescent protein vector was also not identifiable by flow cytometry, suggesting a possible error with the transduction process itself (Figure 74C).

MEF transduction with Lentiviral system

Figure 74. A) Representative flow cytometry to show viability of MEFs following seeding at 2 x 10^4/well, at a MOI of 10. B) Flow cytometry histograms to show HLA-B/C and RFP (C) detection following lentiviral transduction, with blank gene control vectors in grey, below.

8.6 HLA-Cw6 expression by trophoblast

If low-level C2+HLA-C expression is to induce inhibition of uNK in pregnancy through KIR2DL1 ligation, its expression by trophoblast cells is clearly paramount. Interestingly, previous attempts at demonstrating HLA-C expression in murine trophoblast by collaborators in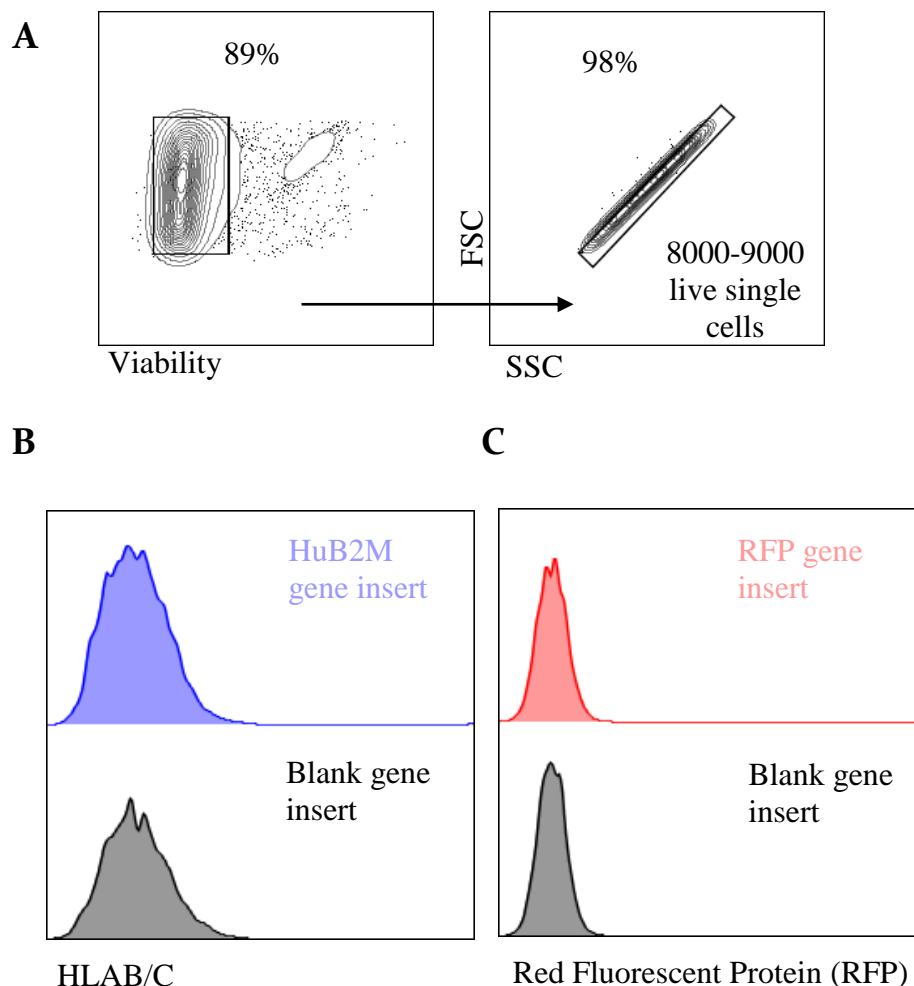 Oxford have been unsuccessful (unpublished data), and to our knowledge, has never been published before. The approach to achieve this was again by mating HLA-Cw6$^{+/+}$ males with C57BL/6 females, and analyzing the resultant implantation sites at g.d. 9.5 through various histological approaches. This is because there is as yet no established flow cytometry technique capable of detecting the very few numbers of trophoblast present in an implantation site. However, by sectioning implantation sites one is able to visualize the fetal and junctional zone cells where trophoblast will be present.

At g.d. 9.5 a number of immunohistochemical techniques were used to identify HLA-C+ trophoblast cells. Through the direct visualization of GFP positive cells using immunofluorescence microscopy, through the use of fluorescently labelled anti-GFP antibodies, through targeting HLA-C with fluorescently labelled antibodies and through the direct antigen labelling of HLA-C targets using horseradish peroxidase for identification, no evidence of HLA-C expression by HLA-Cw6$^{+/-}$ fetal or trophoblast cells could be confirmed.

8.7 KIR2DL1 protein expression

Once gene expression had been established, protein expression of KIR2DL1 was analysed next. In order to achieve this, C57BL/6 mice who were bred to also express Ncr1-icre (*Ncr1$^{cre/WT}$*) and used as biological negative controls. Protein expression in these mice was compared to transgenic mice of genotype *KIR2DL1$^{flox/flox}$/Ncr1$^{cre/WT}$*. All mice transgenic for KIR2DL1 also contained a stop codon which prevented the gene from being transcribed. However, these mice were mated with Ncr1-icre expressing mice. In the offspring of these mice, the cre-recombinase should target and remove the stop codon previously preventing KIR2DL1 expression, in cells where Ncr1 is strongly expressed. For the antibody panel used to assess the conditional expression of KIR2DL1, see 7.0 Methodology – Chapter II – Panel 10). The gating strategy used to identify NK cells in this experiment can be found in Figure 75A. The reactivity of the anti-KIR2D antibody was confirmed in a genotyped human donor (Figure 75B). Lack of expression in cells not expressing Ncr1 (T cells and B cells) was also confirmed. Finally, the conditional and strong expression of KIR2DL1 in the peripheral NK cells of the KIR2DL1*003-tg mice was confirmed (Figure 75C).
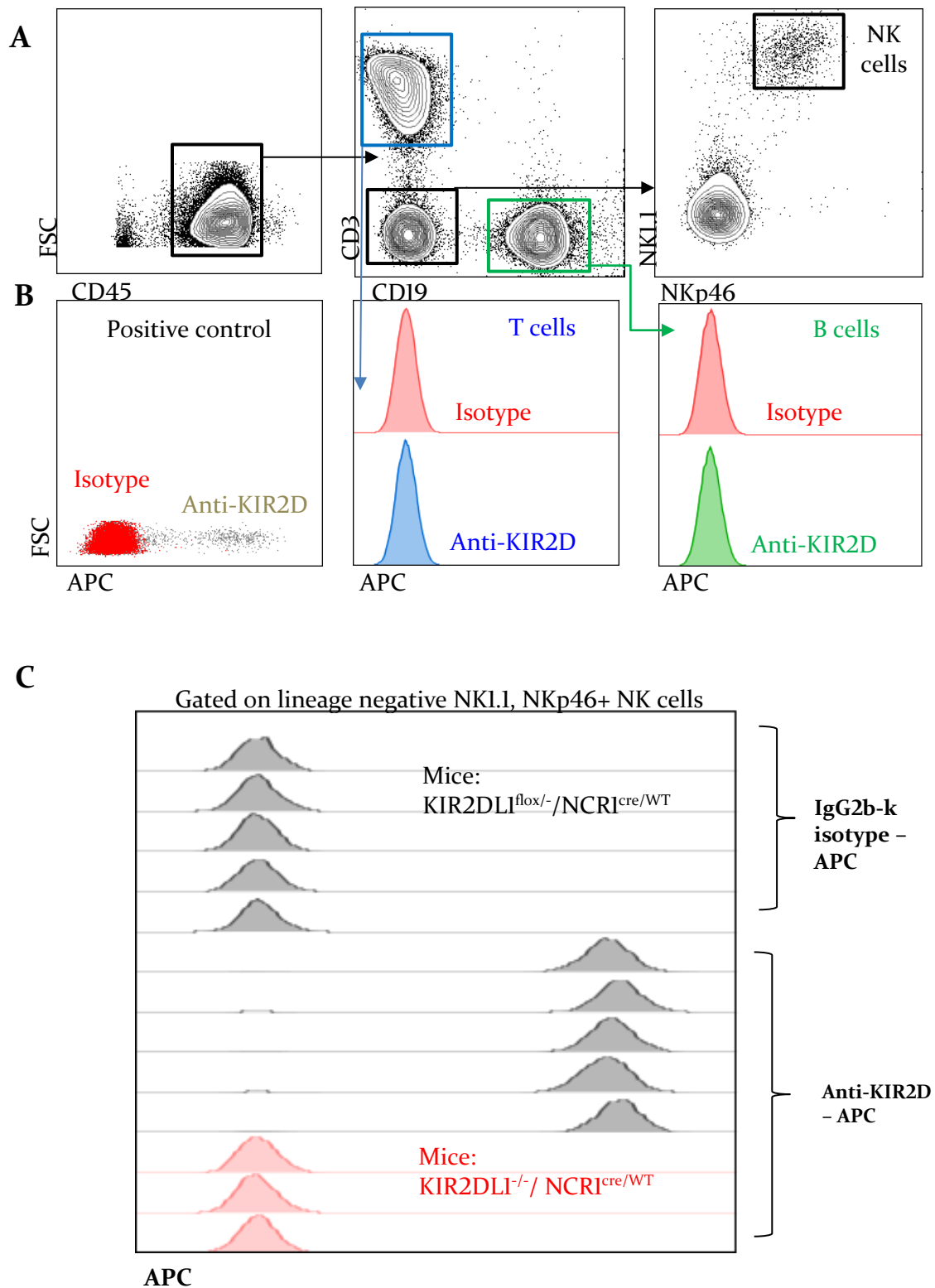
Figure 75. A) Gating strategy to identify NK cells through flow cytometry, B) detection of KIR2D targets in human cells as a positive control, with negative expression in murine B cells and T cells from peripheral blood. C) Flow cytometry histograms showing confirmation of expression of KIR2DL1*003 in the peripheral blood of all mice tested, with isotype controls (top 5 grey histograms) and biological negative controls (shown in red).

8.8 Pregnancy outcome in the humanized mouse model

Finally, I mated *HLA-Cw6*^{+/+} males with *KIR2DL1*[flox/flox]*Ncr1*[cre/wt] females in order to assess pregnancy outcome in this model (experimental group). As previously discussed, I chose to breed females heterozygous for the cre-recombinase gene in order to limit potential cre-mediated toxicity, and because protein expression appeared to be sufficient with this approach. In order to control for the effect of maternal cre-recombinase expression, fetal weight in experimental fetuses was compared to *Ncr1*[cre/wt] females (no KIR2DL1*003 transgene) mated with *HLA-Cw6*^{+/+} males (control group).

At g.d. 18.5, I found no difference in any of the pregnancy outcomes measured. Primarily, there was no change in mean fetal weight, placental weight, placental efficiency or litter size (Figure 76A-D).
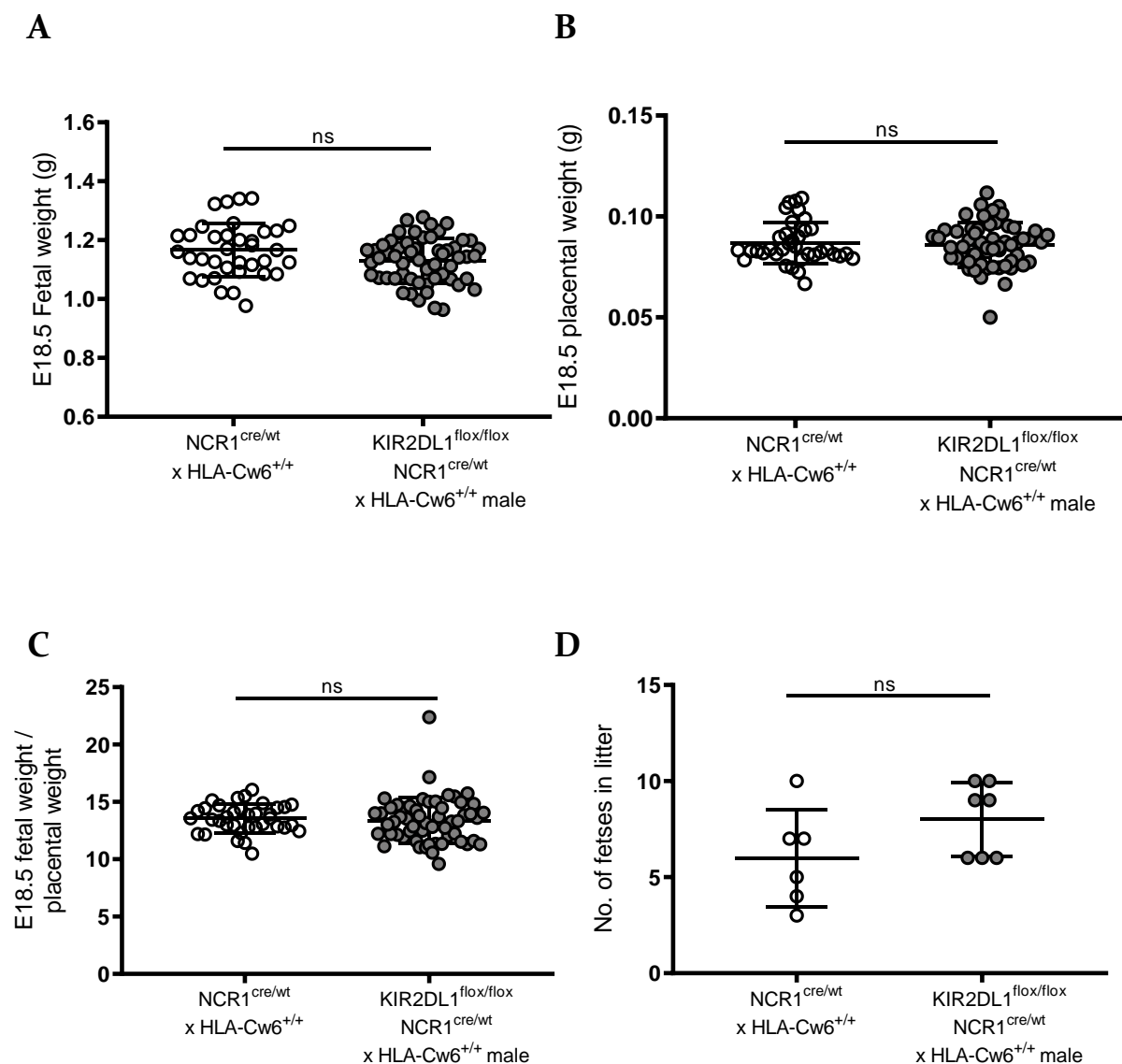
Figure 76. A comparison of A) fetal weight, B) placental weight, C) placental efficiency and D) litter size at g.d. 18.5, by group (mixed model analysis for A-C, t-test for D, p >0.05 in all). Error bars represent standard deviation.

Furthermore, an analysis was performed within the study group to measure any effect of fetal cre-recombinase and the KIR2DL1*003 on fetal weight. This hadn't been performed within our laboratory group, so would inform further work within the department, and was necessary as heterozygous dams only pass the cre-recombinase or KIR2DL1*003 transgenes on to approximately 50% of the offspring. Reassuringly, an initial analysis found no difference in terms of fetal weight in the presence of cre-recombinase or KIR2DL1*003 in the fetuses (Figure 77).
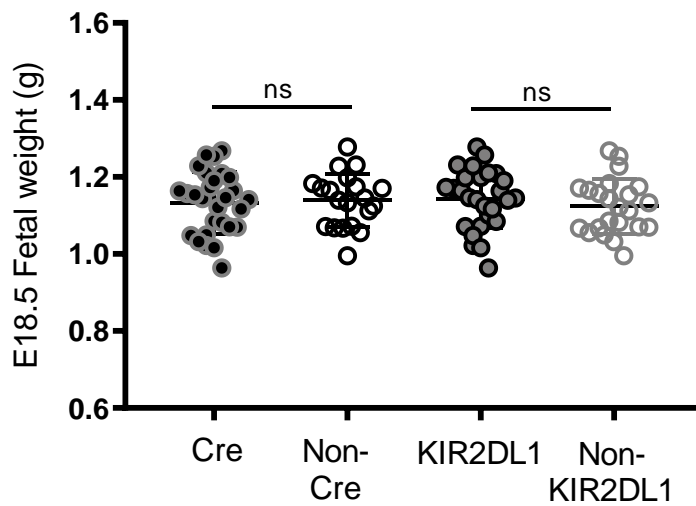
Figure 77. A comparison of fetal weight at g.d. 18.5, by fetal group, according to the presence of transgenes irrespective of maternal genotype (mixed model analyses, p >0.05 in both). Error bars represent standard deviation.

9.0 CHAPTER II – DISCUSSION

Ultimately, this project failed to meet some of its initial objectives and the hypothesis remains largely untested. This was likely to be due to a number of potential issues which could have given rise to a lack of sufficient C2+HLA-C expression, which will now be discussed. There is currently no evidence that the mice transgenic for the HLA-Cw6 gene generated in this project express the functional heterodimeric protein complex on the cell surface at sufficient levels to have a functional impact on cellular activity *in vitro*, or in pregnancy. It is therefore extremely hard to draw solid conclusions regarding the fetal weight data reported in this project. It could be that the inhibition provided by the low-level surface expression of the C2+HLA-C cannot be improved upon, and that this receptor-ligand interaction is occurring but simply cannot exert biological effect above and beyond the signaling already at large in these mice (e.g. through Ly49 receptors).

The fact that the HLA-C epitope showed such low reactivity, by two well-described and widely used antibody clones (Apps 2008), suggests several possibilities. These are as follows: a) there is a failure of the HLA-Cw6 polypeptide to separate from the GFP polypeptide, resulting in a largely non-functional product which cannot fold with murine B2M; b) the HLA-Cw6 protein does not fold sufficiently with mouse B2M, and cannot be detected as a heterodimer on the cell surface; c) the HLA-Cw6 protein is being out-competed for mouse B2M protein by the endogenous MHC class I.

When expression of more than one gene is required in cells, like in this project where GFP and HLA-Cw6 was required, bicistronic or multicistronic expression vectors are used. Various strategies employed to construct bicistronic or multicistronic vectors have been used in the past, and often an internal ribosomal entry site (IRES) is chosen as an RNA element between the two genes, which allows for translation initiation of both. However, this system has limitations, for example, translation efficiency of a gene placed after the IRES is much lower than that of a gene located before it (Kim 2011). A report by Kim et al. demonstrated that of all the self-cleaving peptides P2A peptides (thought to be more efficient than the IRES system), P2A peptide (used in this project) displayed the highest efficiency in all the context examined (Kim 2011). Therefore, scenario A (insufficient cleavage of the HLA-Cw6-GFP complex) seems unlikely, although this could be tested with Western blotting in future studies.

It seems that the need for the human HLA-Cw6 to fold with the mouse B2M is more likely to have caused issues with cell surface expression, although this is still not entirely clear. The success of cell surface expression of human MHC molecules with murine B2M may depend on

which gene has been utilized. For example, an HLA-Cw3 knock-in did not use human B2M, and found acceptable and functional levels of cell surface expression. However, in this project the researchers did knock-out endogenous mouse MHC I (Romagné 2009). The successfully expression of HLA protein in these *HLA-Cw3-tg/$K^dB^{d-/-}$* mice provides evidence that human B2M isn't necessarily required, however the lack of endogenous murine MHC I would have also reduced the competition for folding with murine B2M. In contrast, a sole HLA-Cw3 knock-in was reportedly successful (Dill 1988) in a project investigating T cell response to influenza and Sedai virus. Whilst protein expression was confirmed, they found that the HLA-Cw3 expression noted on most lymphocytes was at a lower degree than that observed in endogenous H-2K^b antigens. This was also found to be the case in another study, where HLA-B27 seemed to require human B2M to reach expression levels comparable to the endogenous class I (Krimpenfort 1987). It therefore seems that scenarios B and C are more plausible causes as to why I failed to see significant functional effects of HLA-Cw6 in either human or murine tissues, where the cognate receptors KIR2DS1 and/or KIR2DL1 were expressed.

Whilst it has been shown that the genetic knockdown of the Ly49 receptor family in mice leads to abnormal uterine crypt formation and impaired blastocyst implantation (Leon 2016), less work has been performed on MHC targets. It has been shown that inducible knockdown of MHC class I in mice (using a floxed B2M mouse model) leads to NK cell hyporesponsiveness and tolerance to missing-self, when performed on all cells. However, when the knockdown was only applied within a small fraction of hematopoietic cells, missing-self reactivity was triggered (Bern 2019). How these findings relate to pregnancy have yet to be studied, and hence remain poorly understood. This elegant mouse model provides a potential tool for directing further investigation in pregnancy, however.

Another potential technical source of error could be that the original selection cassettes inserted into the targeting vectors were not removed. These neomycin selection cassettes are inserted in order to help identify the MESCs which have successfully undergone insertion of the transgene. Positive cells are identified by their continued growth in the presence of a selective agent, where antibiotic-mediated resistance is conferred by the cassette. In this project, the cassettes used were flanked by loxP and FRT sites (an equivalent system to the LoxP-cre recombinase system) in the HLA-Cw6-tg and KIR2DL1*003-tg strains, respectively, to allow for downstream removal. It has been suggested by some that these cassettes should be removed prior to assessment of the expression of the transgene. This is often thought to be needed in order to mitigate any potential interference between the regulatory elements driving expression of the antibiotic resistance gene and the gene of interest (Davis 2008). Due to the

fact that KIR2DL1 expression seemed sufficient and at a high level, I did not remove the selection cassettes.

Future work for this project could be directed down a number of avenues. Essentially, the issue regarding C2+HLA-C expression needs to be addressed before any further functional or pregnancy outcome studies are performed. However, it is worth noting that, to our knowledge, not a single paper has been reported which demonstrates the successful protein expression of this specific gene on murine cells. One study (Taurog 1999) used rats transgenic for HLA-Cw6 as controls for in a project looking at the effect of HLA-B27 on colitis and arthritis. The rationale was that a different transgenic HLA mouse strain was needed in order to act as a control to assess any non-specific background effects of HLA transgene insertion, and HLA-Cw6 was the allotype of choice because it is one of the most frequent in Europeans. These HLA-Cw6 transgenic rats were reported as being mostly healthy, however protein expression data was not reported whatsoever. Allied to the previously discussed lack of expression of C2+HLA-C on mouse trophoblast experienced by our collaborators at the University of Oxford, one could conclude that this protein may simply not be able to be stably expressed by murine cells, for as yet unknown biological / technical reasons.

If cell surface expression of this protein is achieved – an important next step in the project will be to prove that it binds effectively to KIR2DL1. This could be achieved by cell surface staining through flow cytometry, with additional functional experiments to ensure that significant inhibition/education is achieved through the transgenic receptor/ligand interaction. Prior to this, it may be possible to test the transgenic KIR2DL1 protein function ex-vivo, by using an HLA-Cw6 expressing cell line (previously discussed) to inhibit the NK cells in vitro, where, following a suitable period of co-culture, degranulation and cytokine production could be measured using flow cytometry.

If this project is to be continued, a number of options to improve protein expression do remain. Sperm which could be used to generate a mouse strain which displays a simultaneous human B2M knock-in, and mouse *B2m* knock-out (Khare 1996) are now available to me. This mouse strain has previously been used in an HLA-B27 knock-in, where the mice showed cell surface expression of HLA-B27 similar to that of human peripheral blood mononuclear cells, and is on a C57BL/6 genetic background. If successfully crossed with the HLA-Cw6-tg mice, this could potentially eliminate two of the potential causes (B and C) of reduced cell surface expression. In addition, I also have a mouse strain available which is able to remove the neomycin selection cassette in the HLA-Cw6-tg strain. This strain, known as CMV-cre, is also

available on a C57BL/6 genetic background, and express a transgene containing cre-recombinase under the transcriptional control of a human cytomegalovirus promoter.

Whilst there were clearly many limitations to the ultimate fetal weight comparison described in this project, there were some areas of success along the way, and they are worth reflecting upon. There was no guarantee that the transgenic mESCs generated for this project would smoothly transition from the laboratory through to thriving colonies in the animal house. Germline transmission of transgenes doesn't always occur successfully, and breeding of founder animals is not always straightforward. I managed to successfully breed and genotype these strains in a short period of time, and achieve very specific conditional expression of the human KIR gene in murine NK cells. To be able to prove protein expression in a humanized mouse model, in various tissues, within 2 years of starting the project, remains a positive component to focus on when assessing the success of the project. Although the generation of future colonies may rely upon new technologies such as CrispR-Cas9 targeting, this project provides a template for future work of this type, and has also greatly added to the knowledge and experience of trouble-shooting when generating mouse models within our laboratory group.

10.0 CONCLUDING REMARKS

The data produced in the NKG2A project supports the notion this receptor is a key regulator of NK function and contributes to reproductive fitness. Novel insights into its role in human and murine pregnancy have been provided. By using clinically translatable pregnancy outcome measures, further evidence of how immune models of FGR can recapitulate the pathophysiological processes displayed in human pregnancies has also been provided. More broadly, these data represent the first evidence that NK education governs physiological processes through NKG2A.

The initial aims and objectives of the NKG2A project have largely been met, however there is scope for further experimentation to understand the role of NKG2A-specific pathways and uNK education in general, in both murine and human pregnancy. This presents an exciting opportunity for researchers in this field, as our understanding of the role of NKG2A and other inhibitory receptors in human pregnancy is only just beginning to emerge. The field of checkpoint inhibition in cancer therapy should be used as inspiration to demonstrate how the understanding of basic biological processes orchestrated by inhibitory receptors on NK cells can lead to life-changing interventions in patients.

Unfortunately, the humanised mouse project was less successful in terms of meeting its initial objectives. However, from a personal perspective, it provided me with an extremely valuable experience of problem-solving in a scientific context. I hope the resilience I learned to show in trying to solve the issue of HLA-C expression will provide me with an important grounding in adapting to biological and technical difficulties encountered in future scientific projects. As a clinician, I also feel that this experience will be of benefit to my practise going forward. I learned the value of thoroughly searching the existing literature from decades past in order to find experimental data or laboratory techniques that could inform future experiments and investigation. I also had to collaborate with, and ask the help of, many senior researchers in an attempt to solve this issue, which was an important experience.

A key challenge in the field of Reproductive Immunology is to use the elegant laboratory findings discussed throughout this thesis to inform translatable research capable of impacting on clinical practise in the context of pregnancy. Particularly in low-income countries, where maternal mortality secondary to hypertensive disorders of pregnancy is high, any basic scientific data which can be used to improve the techniques used to predict, diagnose and treat conditions such as pre-eclampsia and fetal growth restriction could potentially improve the lives of millions of people worldwide.

11.0 CONTRIBUTIONS TO OTHER PROJECTS

During the experimental period of this PhD (01/10/2016 – 01/10/2019), I also contributed substantial work to the following projects/publications relevant to the field of Reproductive Immunology and fetal growth:

1. I co-authored a review article where I contributed a section on uterine NK cell biology and its application in assisted reproduction. Reference: Lensen S, Shreeve N, Barnhart KT, Gibreel A, Ng EHY, Moffett A. In vitro fertilization add-ons for the endometrium: it doesn't add-up. Fertil Steril. 2019 Dec;112(6):987-993.

2. I co-authored a chapter entitled 'Chapter 17: The role of NK Cells in implantation after IVF and treatment strategies' to the textbook entitled 'How to Prepare the Endometrium to Maximize Implantation Rates and IVF Success', by Kovacs and Samuelson. Published 17/01/2019, Online ISBN 9781108236263.

3. I contributed experimental work in the form of antibody conjugation for mass cytometry and flow cytometry experiments, which has been included in the project entitled 'Distinctive Phenotypes and Functions of Innate Lymphoid cells in Human Decidua during early pregnancy' by O Huhn et al. This manuscript is in press in *Nature Communications* and will be published shortly.

4. I performed trial screening and data analysis for the project entitled 'Universal third trimester ultrasonic screening using fetal macrosomia in the prediction of adverse perinatal outcome.' By A Moraitis et al. This paper is currently under review at *Obstetrics & Gynaecology* (The Green Journal).

5. I contributed experimental work in the micro-CT analysis of mouse fetuses, which has been included in the project entitled 'Maternal group 2 innate lymphoid cells control fetal growth and protect from endotoxin-induced abortion in mice' by E Balmas et al. This manuscript is currently published in the open online repository ww.biorxiv.org, available at https://www.biorxiv.org/content/10.1101/348755v1.

12.0 REFERENCES

Abt MC, Lewis BB, Caballero S, Xiong H, Carter RA, Sušac B, Ling L, Leiner I, Pamer EG. Innate Immune Defenses Mediated by Two ILC Subsets Are Critical for Protection against Acute Clostridium difficile Infection. Cell Host Microbe. 2015 Jul 8;18(1):27-37

Alp N, Clarke N, Banning AP. How should patients with patent foramen ovale be managed? Heart. 2001 Mar;85(3):242-4.

Aluvihare VR, Kallikourdis M, Betz AG. Regulatory T cells mediate maternal tolerance to the fetus. Nat Immunol. 2004 Mar;5(3):266-71

Andersson KE, Williams GS, Davis DM, Höglund P. Quantifying the reduction in accessibility of the inhibitory NK cell receptor Ly49A caused by binding MHC class I proteins in cis. Eur J Immunol. 2007 Feb;37(2):516-27.

Andersson S, Fauriat C, Malmberg JA, Ljunggren HG, Malmberg KJ. KIR acquisition probabilities are independent of self-HLA class I ligands and increase with cellular KIR expression. Blood. 2009 Jul 2;114(1):95-104.

André P, Denis C, Soulas C, Bourbon-Caillet C, Lopez J, Arnoux T, Bléry M, Bonnafous C, Gauthier L, Morel A, Rossi B, Remark R, Breso V, Bonnet E, Habif G, Guia S, Lalanne AI, Hoffmann C, Lantz O, Fayette J, Boyer-Chammard A, Zerbib R, Dodion P, Ghadially H, Jure-Kunkel M, Morel Y, Herbst R, Narni-Mancinelli E, Cohen RB, Vivier E. Anti-NKG2A mAb Is a Checkpoint Inhibitor that Promotes Anti-tumor Immunity by Unleashing Both T and NK Cells. Cell. 2018 Dec 13;175(7):1731-1743.e13.

Anfossi N, André P, Guia S, Falk CS, Roetynck S, Stewart CA, Breso V, Frassati C, Reviron D, Middleton D, Romagné F, Ugolini S, Vivier E. Human NK cell education by inhibitory receptors for MHC class I. Immunity. 2006 Aug;25(2):331-42

Apps R, Gardner L, Hiby SE, Sharkey AM, Moffett A. Conformation of human leucocyte antigen-C molecules at the surface of human trophoblast cells. Immunology. 2008 Jul;124(3):322-8.

Apps R, Murphy SP, Fernando R, Gardner L, Ahad T, Moffett A. Human leucocyte antigen (HLA) expression of primary trophoblast cells and placental cell lines, determined using single

antigen beads to characterize allotype specificities of anti-HLA antibodies. Immunology. 2009 May;127(1):26-39.

Apps R, Meng Z, Del Prete GQ, Lifson JD, Zhou M, Carrington M. Relative expression levels of the HLA class-I proteins in normal and HIV-infected cells. J Immunol. 2015 Apr 15;194(8):3594-600.

Arase H, Mocarski ES, Campbell AE, Hill AB, Lanier LL. Direct recognition of cytomegalovirus by activating and inhibitory NK cell receptors. Science. 2002 May 17;296(5571):1323-6

Arase H, Saito T, Phillips JH, Lanier LL. Cutting edge: the mouse NK cell-associated antigen recognized by DX5 monoclonal antibody is CD49b (alpha 2 integrin, very late antigen-2). J Immunol. 2001 Aug 1;167(3):1141-4.

Ashkar AA, Croy BA. Interferon-gamma contributes to the normalcy of murine pregnancy. Biol Reprod. 1999 Aug;61(2):493-502.

Ashkar AA, Di Santo JP, Croy BA. Interferon gamma contributes to initiation of uterine vascular modification, decidual integrity, and uterine natural killer cell maturation during normal murine pregnancy. J Exp Med. 2000 Jul 17;192(2):259-70.

Back J, Malchiodi EL, Cho S, Scarpellino L, Schneider P, Kerzic MC, Mariuzza RA, Held W. Distinct conformations of Ly49 natural killer cell receptors mediate MHC class I recognition in trans and cis. Immunity. 2009 Oct 16;31(4):598-608

Bahado-Singh RO, Kovanci E, Jeffres A, Jeffres A, Oz U, Deren O, Copel J, Mari G. The Doppler cerebroplacental ratio and perinatal outcome in intrauterine growth restriction. Am J Obstet Gynecol 1999; 180: 750–756.

Bartemes K, Chen CC, Iijima K, Drake L, Kita H. IL-33-Responsive Group 2 Innate Lymphoid Cells Are Regulated by Female Sex Hormones in the Uterus. J Immunol. 2018 Jan 1;200(1):229-236

Beck S, Trowsdale J. The human major histocompatability complex: lessons from the DNA sequence. Annu Rev Genomics Hum Genet. 2000; 1():117-37.

Bekedam DJ, Visser GH, van der Zee AG, Snijders RJ, Poelmann-Weesjes G. Abnormal velocity waveforms of the umbilical artery in growth retarded fetuses: relationship to antepartum late heart rate decelerations and outcome. Early Hum Dev. 1990 Oct;24(1):79-89.

Bélanger S, Tu MM, Rahim MM, Mahmoud AB, Patel R, Tai LH, Troke AD, Wilhelm BT, Landry JR, Zhu Q, Tung KS, Raulet DH, Makrigiannis AP. Impaired natural killer cell self-education and "missing-self" responses in Ly49-deficient mice. Blood. 2012 Jul 19;120(3):592-602.

Bellone G, Aste-Amezaga M, Trinchieri G, Rodeck U. Regulation of NK cell functions by TGF-beta 1. J Immunol. 1995 Aug 1;155(3):1066-73.

Bern MD, Parikh BA, Yang L, Beckman DL, Poursine-Laurent J, Yokoyama WM. Inducible down-regulation of MHC class I results in natural killer cell tolerance. J Exp Med. 2019 Jan 7;216(1):99-116.

Bernabeu C, van de Rijn M, Lerch PG, Terhorst CP. Beta 2-microglobulin from serum associates with MHC class I antigens on the surface of cultured cells. Nature. 1984 Apr 12-18;308(5960):642-5.

Bernink JH, Peters CP, Munneke M, te Velde AA, Meijer SL, Weijer K, Hreggvidsdottir HS, Heinsbroek SE, Legrand N, Buskens CJ, Bemelman WA, Mjösberg JM, Spits H. Human type 1 innate lymphoid cells accumulate in inflamed mucosal tissues. Nat Immunol. 2013 Mar;14(3):221-9.

Bettiol A, Lombardi N, Crescioli G, Avagliano L, Mugelli A, Ravaldi C, Vannacci A. Pharmacological interventions for the prevention of fetal growth restriction: protocol for a systematic review and network meta-analysis. BMJ Open. 2019 Jul 26;9(7):e029467

Bieberich C, Scangos G, Tanaka K, Jay G. Regulated expression of a murine class I gene in transgenic mice. Mol Cell Biol. 1986 Apr;6(4):1339-42.

Billingham RE, Brent L, Medawar PB. "Actively acquired tolerance" of foreign cells. Nature. 1953 172: 603–606

Bilinski MJ, Thorne JG, Oh MJ, Leonard S, Murrant C, Tayade C, Croy BA. Uterine NK cells in murine pregnancy. Reprod Biomed Online. 2008 Feb;16(2):218-26

Björkström K, Riese P, Heuts F, Andersson S, Fauriat C, Ivarsson MA, Björklund AT, Flodström-Tullberg M, Michaëlsson J, Rottenberg ME, Guzmán CA, Ljunggren HG, Malmberg KJ. Expression patterns of NKG2A, KIR, and CD57 define a process of CD56dim NK-cell differentiation uncoupled from NK-cell education. Blood. 2010 Nov 11;116(19):3853-64.

Bland FA, Lemberg MK, McMichael AJ, Martoglio B, Braud VM. Requirement of the proteasome for the trimming of signal peptide-derived epitopes presented by the nonclassical major histocompatibility complex class I molecule HLA-E. J Biol Chem. 2003 Sep 5; 278(36):33747-52.

Blois SM, Kammerer U, Alba Soto C, Tometten MC, Shaikly V, Barrientos G, Jurd R, Rukavina D, Thomson AW, Klapp BF, Fernández N, Arck PC. Dendritic cells: key to fetal tolerance? Biol Reprod. 2007 Oct;77(4):590-8.

Blokhuis JH, Hilton HG, Guethlein LA, Norman PJ, Nemat-Gorgani N, Nakimuli A, Chazara O, Moffett A, Parham P. KIR2DS5 allotypes that recognize the C2 epitope of HLA-C are common among Africans and absent from Europeans. Immun Inflamm Dis. 2017 Dec;5(4):461-468.

Borrego F, Ulbrecht M, Weiss EH, Coligan JE, Brooks AG. Recognition of human histocompatibility leukocyte antigen (HLA)-E complexed with HLA class I signal sequence-derived peptides by CD94/NKG2 confers protection from natural killer cell-mediated lysis. J Exp Med. 1998 Mar 2; 187(5):813-8.

Boudreau JE, Liu XR, Zhao Z, Zhang A, Shultz LD, Greiner DL, Dupont B, Hsu KC. Cell-Extrinsic MHC Class I Molecule Engagement Augments Human NK Cell Education Programmed by Cell-Intrinsic MHC Class I. Immunity. 2016 Aug 16;45(2):280-91

Boulenouar S, Doisne JM, Sferruzzi-Perri A, Gaynor LM, Kieckbusch J, Balmas E, Yung HW, Javadzadeh S, Volmer L, Hawkes DA, Phillips K, Brady HJ, Fowden AL, Burton GJ, Moffett A, Colucci F. The Residual Innate Lymphoid Cells in NFIL3-Deficient Mice Support Suboptimal Maternal Adaptations to Pregnancy. Front Immunol. 2016 Feb 19;7:43.

Braud V, Jones EY, McMichael A. The human major histocompatibility complex class Ib molecule HLA-E binds signal sequence-derived peptides with primary anchor residues at positions 2 and 9. Eur J Immunol. 1997 May;27(5):1164-9.

(a)Braud VM, Allan DS, O'Callaghan CA, Söderström K, D'Andrea A, Ogg GS, Lazetic S, Young NT, Bell JI, Phillips JH, Lanier LL, McMichael AJ. HLA-E binds to natural killer cell receptors CD94/NKG2A, B and C. Nature. 1998 Feb 19; 391(6669):795-9.
(b)Braud VM, Allan DS, Wilson D, McMichael AJ. TAP- and tapasin-dependent HLA-E surface expression correlates with the binding of an MHC class I leader peptide. Curr Biol. 1998 Jan 1;8(1):1-10.

Brodin P, Lakshmikanth T, Johansson S, Kärre K, Höglund P. The strength of inhibitory input during education quantitatively tunes the functional responsiveness of individual natural killer cells. Blood. 2009 Mar 12;113(11):2434-41.

Bulmer JN, Hollings D, Ritson A. Immunocytochemical evidence that endometrial stromal granulocytes are granulated lymphocytes. J Pathol. 1987 Nov;153(3):281-8

Bulmer JN, Sunderland CA. Immunohistological characterization of lymphoid cell populations in the early human placental bed. Immunology. 1984 Jun;52(2):349-57.

Burnet FM and Fenner F. The Production of Antibodies (2nd Edition). Macmillan and Co., Ltd., Melbourne, Australia, 1949. Available in: J Immunol April 1, 1951, 66 (4) 485-486;

Burotto M, Gormaz JG, Samtani S, Valls N, Silva R, Rojas C, Portiño S, de la Jara C. Viable Pregnancy in a patient with metastatic melanoma treated with double checkpoint immunotherapy. Semin Oncol. 2018 Jun;45(3):164-169.

Burton GJ, Jauniaux E. What is the placenta? Am J Obstet Gynecol. 2015;213:S6–e1. S6–8.

Burton GJ, Redman CW, Roberts JM, Moffett A. Pre-eclampsia: pathophysiology and clinical implications. BMJ. 2019 Jul 15;366:l2381

Businelli C, de Wit C, Visser GHA, Pistorius LR. Ultrasound evaluation of cortical brain development in fetuses with intrauterine growth restriction. J Matern Fetal Neonatal Med. 2015 Jul;28(11):1302-1307.

Caligiuri MA. Human natural killer cells. Blood. 2008 Aug 1;112(3):461-9

Campbell KS, Purdy AK. Structure/function of human killer cell immunoglobulin-like receptors: lessons from polymorphisms, evolution, crystal structures and mutations. Immunology. 2011 Mar;132(3):315-25

Campbell S, Thoms A. Ultrasound measurement of the fetal head to abdomen circumference ratio in the assessment of growth retardation. Br J Obstet Gynaecol. 1977;84(3):165–74

Cao X, Shores EW, Hu-Li J, Anver MR, Kelsall BL, Russell SM, Drago J, Noguchi M, Grinberg A, Bloom ET, et al. Defective lymphoid development in mice lacking expression of the common cytokine receptor gamma chain. Immunity. 1995 Mar;2(3):223-38.

Carrega P, Ferlazzo G. Natural killer cell distribution and trafficking in human tissues. Front Immunol. 2012 Nov 29;3:347

Carrington M, Nelson GW, Martin MP, Kissner T, Vlahov D, Goedert JJ, Kaslow R, Buchbinder S, Hoots K, O'Brien SJ. HLA and HIV-1: heterozygote advantage and B*35-Cw*04 disadvantage. Science. 1999 Mar 12; 283(5408):1748-52.

Cartner SC, Barlow SC, Ness TJ. Loss of cortical function in mice after decapitation, cervical dislocation, potassium chloride injection, and CO2 inhalation. Comp Med. 2007 Dec;57(6):570-3.

Chalifour A, Scarpellino L, Back J, Brodin P, Devèvre E, Gros F, Lévy F, Leclercq G, Höglund P, Beermann F, Held W. A Role for cis Interaction between the Inhibitory Ly49A receptor and MHC class I for natural killer cell education. Immunity. 2009 Mar 20;30(3):337-47

Chang CH, Yu CH, Chang FM, Ko HC, Chen HY. The assessment of normal fetal brain volume by 3-D ultrasound. Ultrasound Med Biol. 2003 Sep;29(9):1267-72.

Charalambous M, Da Rocha ST, Radford EJ, Medina-Gomez G, Curran S, Pinnock SB, Ferrón SR, Vidal-Puig A, Ferguson-Smith AC. DLK1/PREF1 regulates nutrient metabolism and protects from steatosis. Proc Natl Acad Sci U S A. 2014 Nov 11;111(45):16088-93.

Choo SY. The HLA system: genetics, immunology, clinical testing, and clinical implications. Yonsei Med J. 2007 Feb 28;48(1):11-23.

Chu A, Casero D, Thamotharan S, Wadehra M, Cosi A, Devaskar SU. The Placental Transcriptome in Late Gestational Hypoxia Resulting in Murine Intrauterine Growth Restriction Parallels Increased Risk of Adult Cardiometabolic Disease. Sci Rep. 2019 Feb 4;9(1):1243

Chu A, Thamotharan S, Ganguly A, Wadehra M, Pellegrini M, Devaskar SU. Gestational food restriction decreases placental interleukin-10 expression and markers of autophagy and endoplasmic reticulum stress in murine intrauterine growth restriction. Nutr Res. 2016 Oct;36(10):1055-1067.

Clark AR, James JL, Stevenson GN, Collins SL. Understanding abnormal uterine artery Doppler waveforms: A novel computational model to explore potential causes within the utero-placental vasculature. Placenta. 2018 Jun;66:74-81

Cleaton MA, Dent CL, Howard M, Corish JA, Gutteridge I, Sovio U, Gaccioli F, Takahashi N, Bauer SR, Charnock-Jones DS, Powell TL, Smith GC, Ferguson-Smith AC, Charalambous M. Fetus-derived DLK1 is required for maternal metabolic adaptations to pregnancy and is associated with fetal growth restriction. Nat Genet. 2016 Dec;48(12):1473-1480.

Cnossen JS, Morris RK, ter Riet G, Mol BW, van der Post JA, Coomarasamy A, Zwinderman AH, Robson SC, Bindels PJ, Kleijnen J, Khan KS. Use of uterine artery Doppler ultrasonography to predict pre-eclampsia and intrauterine growth restriction: a systematic review and bivariable meta-analysis. CMAJ. 2008 Mar 11; 178(6):701-11.

Collins MK, Tay CS, Erlebacher A. Dendritic cell entrapment within the pregnant uterus inhibits immune surveillance of the maternal/fetal interface in mice. J Clin Invest. 2009 Jul;119(7):2062-73.

Colucci F. The role of KIR and HLA interactions in pregnancy complications. Immunogenetics. 2017 Aug;69(8-9):557-565

Colucci F, Soudais C, Rosmaraki E, Vanes L, Tybulewicz VL, Di Santo JP. Dissecting NK cell development using a novel alymphoid mouse model: investigating the role of the c-abl proto-oncogene in murine NK cell differentiation. J Immunol. 1999 Mar 1;162(5):2761-5.

Constância M, Hemberger M, Hughes J, Dean W, Ferguson-Smith A, Fundele R, Stewart F, Kelsey G, Fowden A, Sibley C, Reik W. Placental-specific IGF-II is a major modulator of placental and fetal growth. Nature. 2002 Jun 27;417(6892):945-8.

Creelan BC, Antonia SJ. The NKG2A immune checkpoint - a new direction in cancer immunotherapy. Nat Rev Clin Oncol. 2019 May;16(5):277-278.

Croy BA, Yamada AT, De Mayo FJ, Adamson SL (2014) The guide to investigation of mouse pregnancy. Academic Press, London

Daëron M, Jaeger S, Du Pasquier L, Vivier E. Immunoreceptor tyrosine-based inhibition motifs: a quest in the past and future. Immunol Rev. 2008 Aug;224:11-43.

Darvin P, Toor SM, Sasidharan Nair V, Elkord E. Immune checkpoint inhibitors: recent progress and potential biomarkers. Exp Mol Med. 2018 Dec 13;50(12):165.

Davis RP, Costa M, Grandela C, Holland AM, Hatzistavrou T, Micallef SJ, Li X, Goulburn AL, Azzola L, Elefanty AG, Stanley EG. A protocol for removal of antibiotic resistance cassettes from human embryonic stem cells genetically modified by homologous recombination or transgenesis. Nat Protoc. 2008;3(10):1550-8

De Clercq K, Persoons E, Napso T, Luyten C, Parac-Vogt TN, Sferruzzi-Perri AN, Kerckhofs G, Vriens J. High-resolution contrast-enhanced microCT reveals the true three-dimensional morphology of the murine placenta. Proc Natl Acad Sci U S A. 2019 Jul 9;116(28):13927-13936

de Onis M., Habicht J.P. Anthropometric reference data for international use: recommendations from a World Health Organization Expert Committee. Am J Clin Nutr. 1996;64:650–658.

Dill O, Kievits F, Koch S, Ivanyi P, Hämmerling GJ. Immunological function of HLA-C antigens in HLA-Cw3 transgenic mice. Proc Natl Acad Sci U S A. 1988 Aug;85(15):5664-8.

DiSanto JP, Müller W, Guy-Grand D, Fischer A, Rajewsky K. Lymphoid development in mice with a targeted deletion of the interleukin 2 receptor gamma chain. Proc Natl Acad Sci U S A. 1995 Jan 17;92(2):377-81.

Doisne JM, Balmas E, Boulenouar S, Gaynor LM, Kieckbusch J, Gardner L, Hawkes DA, Barbara CF, Sharkey AM, Brady HJ, Brosens JJ, Moffett A, Colucci F. Composition, Development, and Function of Uterine Innate Lymphoid Cells. J Immunol. 2015 Oct 15;195(8):3937-45

Doucey MA, Scarpellino L, Zimmer J, Guillaume P, Luescher IF, Bron C, Held W. Cis association of Ly49A with MHC class I restricts natural killer cell inhibition. Nat Immunol. 2004 Mar;5(3):328-36.

Drickamer K, Taylor ME. Biology of animal lectins. Annu Rev Cell Biol. 1993;9:237-64.

Eckelhart E, Warsch W, Zebedin E, Simma O, Stoiber D, Kolbe T, Rülicke T, Mueller M, Casanova E, Sexl V. A novel Ncr1-Cre mouse reveals the essential role of STAT5 for NK-cell survival and development Blood. 2011 Feb 3;117(5):1565-73.

Egaña-Ugrinovic G, Sanz-Cortes M, Figueras F, Bargalló N, Gratacós E. Differences in cortical development assessed by fetal MRI in late-onset intrauterine growth restriction. Am J Obstet Gynecol 2013; 209: 126.e1–8.

Eixarch E, Meler E, Iraola A, Illa M, Crispi F, Hernandez-Andrade E, Gratacos E, Figueras F. Neurodevelopmental outcome in 2-year-old infants who were small-for-gestational age term fetuses with cerebral blood flow redistribution. Ultrasound Obstet Gynecol 2008; 32: 894–899.

Enqvist M, Ask EH, Forslund E, Carlsten M, Abrahamsen G, Béziat V, Andersson S, Schaffer M, Spurkland A, Bryceson Y, Önfelt B, Malmberg KJ. Coordinated expression of DNAM-1 and LFA-1 in educated NK cells. J Immunol. 2015 May 1;194(9):4518-27.

Fauriat C, Long EO, Ljunggren HG, Bryceson YT. Regulation of human NK-cell cytokine and chemokine production by target cell recognition. Blood. 2010 Mar 18;115(11):2167-76.

FDA. http://www.accessdata.fda.gov/drugsatfda_docs/label/2015/125377s073lbl.pdf US Food and Drug Administration: Ipilimumab package insert. Revised 2015

Fernandez NC, Treiner E, Vance RE, Jamieson AM, Lemieux S, Raulet DH. A subset of natural killer cells achieves self-tolerance without expressing inhibitory receptors specific for self-MHC molecules. Blood. 2005 Jun 1;105(11):4416-23.

Ferrier P, Layet C, Caillol DH, Jordan BR, Lemonnier FA. The association between murine beta 2-microglobulin and HLA class I heavy chains results in serologically detectable conformational changes of both chains. J Immunol. 1985 Aug;135(2):1281-7

Filipovic I, Chiossone L, Vacca P, Hamilton RS, Ingegnere T, Doisne JM, Hawkes DA, Mingari MC, Sharkey AM, Moretta L, Colucci F. Molecular definition of group 1 innate lymphoid cells in the mouse uterus. Nat Commun. 2018 Oct 29;9(1):4492.

Fleiss B, Wong F, Brownfoot F, Shearer IK, Baud O, Walker DW, Gressens P, Tolcos M. Knowledge Gaps and Emerging Research Areas in Intrauterine Growth Restriction-Associated Brain Injury. Front Endocrinol (Lausanne). 2019 Mar 29;10:188.

Flores-Villanueva PO, Yunis EJ, Delgado JC, Vittinghoff E, Buchbinder S, Leung JY, Uglialoro AM, Clavijo OP, Rosenberg ES, Kalams SA, Braun JD, Boswell SL, Walker BD, Goldfeld AE. Control of HIV-1 viremia and protection from AIDS are associated with HLA-Bw4 homozygosity. Proc Natl Acad Sci U S A. 2001 Apr 24;98(9):5140-5.

Francisco LM, Sage PT, Sharpe AH. The PD-1 pathway in tolerance and autoimmunity. Immunol Rev. 2010 Jul;236:219-42.

Friedrich G, Soriano P. Promoter traps in embryonic stem cells: a genetic screen to identify and mutate developmental genes in mice. Genes Dev. 1991 Sep;5(9):1513-23.

Gaccioli F, Sovio U, Cook E, Hund M, Charnock-Jones DS, Smith GCS. Screening for fetal growth restriction using ultrasound and the sFLT1/PlGF ratio in nulliparous women: a prospective cohort study. Lancet Child Adolesc Health. 2018 Aug;2(8):569-581

Geipel A, Gembruch U. Ultrasound in Obstetrics and Gynaecology. 2009. Accessed on 14/11/19. Available at URL: https://www.sciencedirect.com/science/article/pii/B9780444518293000118?via%3Dihub

George TC, Mason LH, Ortaldo JR, Kumar V, Bennett M. Positive recognition of MHC class I molecules by the Ly49D receptor of murine NK cells. J Immunol. 1999 Feb 15;162(4):2035-43.

Ghosh G, Grewal J, Männistö T, Mendola P, Chen Z, Xie Y, Laughon SK. Racial/ethnic differences in pregnancy-related hypertensive disease in nulliparous women. Ethn Dis. 2014 Summer;24(3):283-9.

Goodridge JP, Jacobs B, Saetersmoen ML, Clement D, Hammer Q, Clancy T, Skarpen E, Brech A, Landskron J, Grimm C, Pfefferle A, Meza-Zepeda L, Lorenz S, Wiiger MT, Louch WE, Ask EH, Liu LL, Oei VYS, Kjällquist U, Linnarsson S, Patel S, Taskén K, Stenmark H, Malmberg KJ. Remodeling of secretory lysosomes during education tunes functional potential in NK cells. Nat Commun. 2019 Jan 31;10(1):514

Gramellini D, Folli MC, Raboni S, Vadora E, Merialdi A. Cerebral-umbilical Doppler ratio as a predictor of adverse perinatal outcome. Obstet Gynecol 1992; 79: 416–420.

Grawunder U, Leu TM, Schatz DG, Werner A, Rolink AG, Melchers F, Winkler TH. Down-regulation of RAG1 and RAG2 gene expression in preB cells after functional immunoglobulin heavy chain rearrangement. Immunity. 1995 Nov;3(5):601-8.

Greco A, Ragucci M, Coda AR, Rosa A, Gargiulo S, Liuzzi R, Gramanzini M, Albanese S, Pappatà S, Mancini M, Brunetti A, Salvatore M. High frequency ultrasound for in vivo pregnancy diagnosis and staging of placental and fetal development in mice. PLoS One. 2013 Oct 14;8(10):e77205.

Greenwood JD, Minhas K, di Santo JP, Makita M, Kiso Y, Croy BA.Ultrastructural studies of implantation sites from mice deficient in uterine natural killer cells. Placenta. 2000 Sep;21(7):693-702.

Guimond MJ, Wang B, Croy BA. Engraftment of bone marrow from severe combined immunodeficient (SCID) mice reverses the reproductive deficits in natural killer cell-deficient tg epsilon 26 mice. J Exp Med. 1998 Jan 19;187(2):217-23.

Gumá M, Angulo A, Vilches C, Gómez-Lozano N, Malats N, López-Botet M. Imprint of human cytomegalovirus infection on the NK cell receptor repertoire. Blood. 2004 Dec 1;104(12):3664-71.

Haanen JB, Robert C. Immune Checkpoint Inhibitors. Prog Tumor Res. 2015;42:55-66

Hadlock FP, Harrist RB, Carpenter RJ, Deter RL, Park SK. Sonographic estimation of fetal weight. The value of femur length in addition to head and abdomen measurements. Radiology 1984; 150: 535–540

Hadlock FP, Harrist RB, Sharman RS, Deter RL, Park SK. Estimation of fetal weight with the use of head, body, and femur measurements—a prospective study. Am J Obstet Gynecol 1985; 151: 333–337.

Halenius A, Gerke C, Hengel H. Classical and non-classical MHC I molecule manipulation by human cytomegalovirus: so many targets—but how many arrows in the quiver? Cell Mol Immunol. 2015 Mar;12(2):139-53.

Hanna J, Goldman-Wohl D, Hamani Y, Avraham I, Greenfield C, Natanson-Yaron S, Prus D, Cohen-Daniel L, Arnon TI, Manaster I, Gazit R, Yutkin V, Benharroch D, Porgador A, Keshet E, Yagel S, Mandelboim O. Decidual NK cells regulate key developmental processes at the human fetal-maternal interface. Nat Med. 2006 Sep;12(9):1065-74.

He Y, Tian Z. NK cell education via nonclassical MHC and non-MHC ligands. Cell Mol Immunol. 2017 Apr;14(4):321-330.

Hepworth MR, Monticelli LA, Fung TC, Ziegler CG, Grunberg S, Sinha R, Mantegazza AR, Ma HL, Crawford A, Angelosanto JM, Wherry EJ, Koni PA, Bushman FD, Elson CO, Eberl G, Artis D, Sonnenberg GF. Innate lymphoid cells regulate CD4+ T-cell responses to intestinal commensal bacteria. Nature. 2013 Jun 6;498(7452):113-7

Herberman RB, Nunn ME, Lavrin DH. Natural cytotoxic reactivity of mouse lymphoid cells against syngeneic acid allogeneic tumors. I. Distribution of reactivity and specificity. Int J Cancer. 1975 Aug 15;16(2):216-29.

Hernández-Díaz S, Toh S, Cnattingius S. Risk of pre-eclampsia in first and subsequent pregnancies: prospective cohort study. BMJ. 2009 Jun 18;338:b2255

Hiby SE, Apps R, Sharkey AM, Farrell LE, Gardner L, Mulder A, Claas FH, Walker JJ, Redman CW, Morgan L, Tower C, Regan L, Moore GE, Carrington M, Moffett A. Maternal activating KIRs protect against human reproductive failure mediated by fetal HLA-C2. J Clin Invest. 2010 Nov;120(11):4102-10. doi: 10.1172/JCI43998. Epub 2010 Oct 25. Erratum in: J Clin Invest. 2011 Jan 4;121(1):455. Redman, Christopher C [corrected to Redman, Christopher W]

Hiby SE, Walker JJ, O'shaughnessy KM, Redman CW, Carrington M, Trowsdale J, Moffett A. Combinations of maternal KIR and fetal HLA-C genes influence the risk of preeclampsia and reproductive success. J Exp Med. 2004 Oct 18;200(8):957-65.

Hilton HG, Guethlein LA, Goyos A, Nemat-Gorgani N, Bushnell DA, Norman PJ, Parham P. Polymorphic HLA-C Receptors Balance the Functional Characteristics of KIR Haplotypes. J Immunol. 2015 Oct 1;195(7):3160-70.

Hilton HG, Vago L, Older Aguilar AM, Moesta AK, Graef T, Abi-Rached L, Norman PJ, Guethlein LA, Fleischhauer K, Parham P. Mutation at positively selected positions in the binding site for HLA-C shows that KIR2DL1 is a more refined but less adaptable NK cell receptor than KIR2DL3. J Immunol. 2012 Aug 1;189(3):1418-30

Hodi FS, O'Day SJ, McDermott DF, Weber RW, Sosman JA, Haanen JB, Gonzalez R, Robert C, Schadendorf D, Hassel JC, Akerley W, van den Eertwegh AJ, Lutzky J, Lorigan P, Vaubel JM, Linette GP, Hogg D, Ottensmeier CH, Lebbé C, Peschel C, Quirt I, Clark JI, Wolchok JD, Weber JS, Tian J, Yellin MJ, Nichol GM, Hoos A, Urba WJ. Improved survival with ipilimumab in patients with metastatic melanoma. N Engl J Med. 2010 Aug 19;363(8):711-23.

Höglund P, Brodin P. Current perspectives of natural killer cell education by MHC class I molecules. Nat Rev Immunol. 2010 Oct;10(10):724-34

Hollenbach JA, Nocedal I, Ladner MB, Single RM, Trachtenberg EA. Killer cell immunoglobulin-like receptor (KIR) gene content variation in the HGDP-CEPH populations. Immunogenetics. 2012 Oct;64(10):719-37.

Hollenbach JA, Pando MJ, Caillier SJ, Gourraud PA, Oksenberg JR. The killer immunoglobulin-like receptor KIR3DL1 in combination with HLA-Bw4 is protective against multiple sclerosis in African Americans. Genes Immun. 2016 Apr;17(3):199-202

Horowitz A, Djaoud Z, Nemat-Gorgani N, Blokhuis J, Hilton HG, Béziat V, Malmberg KJ, Norman PJ, Guethlein LA, Parham P. Class I HLA haplotypes form two schools that educate NK cells in different ways. Sci Immunol. 2016 Sep;1(3). pii: eaag1672.

Hu JF, Zhang W, Zuo W, Tan HQ, Bai W. Inhibition of the PD-1/PD-L1 signaling pathway enhances innate immune response of alveolar macrophages to mycobacterium tuberculosis in mice. Pulm Pharmacol Ther. 2019 Sep 18:101842

Hughes ED, Qu YY, Genik SJ, Lyons RH, Pacheco CD, Lieberman AP, Samuelson LC, Nasonkin IO, Camper SA, Van Keuren ML, Saunders TL. Genetic variation in C57BL/6 ES cell lines and genetic instability in the Bruce4 C57BL/6 ES cell line. Mamm Genome. 2007 Aug;18(8):549-58

Huhn O, Chazara O, Ivarsson MA, Retière C, Venkatesan TC, Norman PJ, Hilton HG, Jayaraman J, Traherne JA, Trowsdale J, Ito M, Kling C, Parham P, Ghadially H, Moffett A, Sharkey AM, Colucci F. High-Resolution Genetic and Phenotypic Analysis of KIR2DL1 Alleles and Their Association with Pre-Eclampsia. J Immunol. 2018 Nov 1;201(9):2593-2601

Oisín Huhn, Martin A. Ivarsson, Lucy Gardner, Mike Hollinshead, Jane C Stinchcombe, Puran Chen, Norman Shreeve, Olympe Chazara, Lydia E. Farrell, Jakob Theorell, Hormas Ghadially, Peter Parham, Gillian Griffiths, Amir Horowitz, Ashley Moffett, Andrew M. Sharkey, Francesco Colucci. Distinctive phenotypes and functions of innate lymphoid cells in human decidua during early pregnancy. Nat Commun. 2020; 11: 381

Hung TH, Skepper JN, Charnock-Jones DS, Burton GJ. Hypoxia-reoxygenation: a potent inducer of apoptotic changes in the human placenta and possible etiological factor in preeclampsia. Circ Res. 2002 Jun 28;90(12):1274-81.

Ishida Y, Agata Y, Shibahara K, Honjo T. Induced expression of PD-1, a novel member of the immunoglobulin gene superfamily, upon programmed cell death. EMBO J. 1992 Nov;11(11):3887-95.

Ivarsson MA, Loh L, Marquardt N, Kekäläinen E, Berglin L, Björkström NK, Westgren M, Nixon DF, Michaëlsson J. Differentiation and functional regulation of human fetal NK cells. J Clin Invest. 2013 Sep;123(9):3889-901.

Janeway CA Jr, Travers P, Walport M, et al. Immunobiology: The Immune System in Health and Disease. 5th edition. New York: Garland Science; 2001.

Jiang S, Li X, Hess NJ, Guan Y, Tapping RI. TLR10 Is a Negative Regulator of Both MyD88-Dependent and -Independent TLR Signaling. J Immunol. 2016 May 1;196(9):3834-41

Johansson S, Johansson M, Rosmaraki E, Vahlne G, Mehr R, Salmon-Divon M, Lemonnier F, Kärre K, Höglund P. Natural killer cell education in mice with single or multiple major histocompatibility complex class I molecules. J Exp Med. 2005 Apr 4;201(7):1145-55.

Jokhi PP, King A, Loke YW. Production of granulocyte-macrophage colony-stimulating factor by human trophoblast cells and by decidual large granular lymphocytes. Hum Reprod. 1994 Sep;9(9):1660-9.

Joncker NT, Fernandez NC, Treiner E, Vivier E, Raulet DH. NK cell responsiveness is tuned commensurate with the number of inhibitory receptors for self-MHC class I: the rheostat model. J Immunol. 2009 Apr 15;182(8):4572-80.

Jonsson AH, Yokoyama WM. Assessing licensing of NK cells. Methods Mol Biol. 2010;612:39-49.

Kaiser BK, Pizarro JC, Kerns J, Strong RK. Structural basis for NKG2A/CD94 recognition of HLA-E. Proc Natl Acad Sci U S A. 2008 May 6;105(18):6696-701.

Kamiya T, Seow SV, Wong D, Robinson M, Campana D. Blocking expression of inhibitory receptor NKG2A overcomes tumor resistance to NK cells. J Clin Invest. 2019 Mar 12;130.

Kärre K. Natural killer cell recognition of missing self. Nat Immunol. 2008 May;9(5):477-80.

Kärre K, Ljunggren HG, Piontek G, Kiessling R. Selective rejection of H-2-deficient lymphoma variants suggests alternative immune defence strategy. Nature. 1986 Feb 20-26;319(6055):675-8

Kawamura T, Takeda K, Kaneda H, Matsumoto H, Hayakawa Y, Raulet DH, Ikarashi Y, Kronenberg M, Yagita H, Kinoshita K, Abo T, Okumura K, Smyth MJ. NKG2A inhibits invariant NKT cell activation in hepatic injury. J Immunol. 2009 Jan 1;182(1):250-8.

Kennedy PR, Chazara O, Gardner L, Ivarsson MA, Farrell LE, Xiong S, Hiby SE, Colucci F, Sharkey AM, Moffett A. Activating KIR2DS4 Is Expressed by Uterine NK Cells and Contributes to Successful Pregnancy. J Immunol. 2016 Dec 1;197(11):4292-4300

Kessous R, Aricha-Tamir B, Weintraub AY, Sheiner E, Hershkovitz R. Umbilical artery peak systolic velocity measurements for prediction of perinatal outcome among IUGR fetuses. J Clin Ultrasound. 2014 Sep;42(7):405-10

Khare SD, Hansen J, Luthra HS, David CS. HLA-B27 heavy chains contribute to spontaneous inflammatory disease in B27/human beta2-microglobulin (beta2m) double transgenic mice with disrupted mouse beta2m. J Clin Invest. 1996 Dec 15;98(12):2746-55.

Kieckbusch J, Gaynor LM, Colucci F. Assessment of Maternal Vascular Remodeling During Pregnancy in the Mouse Uterus. J Vis Exp. 2015 Dec 5;(106):e53534

Kieckbusch J, Gaynor LM, Moffett A, Colucci F. MHC-dependent inhibition of uterine NK cells impedes fetal growth and decidual vascular remodelling. Nat Commun. 2014 Feb 28;5:3359.

Kiessling R, Klein E, Wigzell H. "Natural" killer cells in the mouse. I. Cytotoxic cells with specificity for mouse Moloney leukemia cells. Specificity and distribution according to genotype. Eur J Immunol. 1975 Feb;5(2):112-7.

Kim JH, Lee SR, Li LH, Park HJ, Park JH, Lee KY, Kim MK, Shin BA, Choi SY. High cleavage efficiency of a 2A peptide derived from porcine teschovirus-1 in human cell lines, zebrafish and mice. PLoS One. 2011;6(4):e18556

Kim MJ, Lee JC, Lee JJ, Kim S, Lee SG, Park SW, Sung MW, Heo DS. Association of CD47 with natural killer cell-mediated cytotoxicity of head-and-neck squamous cell carcinoma lines. Tumour Biol. 2008;29(1):28-34.

Kim S, Iizuka K, Kang HS, Dokun A, French AR, Greco S, Yokoyama WM. In vivo developmental stages in murine natural killer cell maturation. Nat Immunol. 2002 Jun;3(6):523-8.

Kim S, Poursine-Laurent J, Truscott SM, Lybarger L, Song YJ, Yang L, French AR, Sunwoo JB, Lemieux S, Hansen TH, Yokoyama WM. Licensing of natural killer cells by host major histocompatibility complex class I molecules. Nature. 2005 Aug 4;436(7051):709-13.

(a)King A, Allan DS, Bowen M, Powis SJ, Joseph S, Verma S, Hiby SE, McMichael AJ, Loke YW, Braud VM. HLA-E is expressed on trophoblast and interacts with CD94/NKG2 receptors on decidual NK cells. Eur J Immunol. 2000 Jun;30(6):1623-31.

(b)King A. Uterine leukocytes and decidualization. Hum Reprod Update. 2000 Jan-Feb;6(1):28-36

King A, Balendran N, Wooding P, Carter NP, Loke YW. CD3- leukocytes present in the human uterus during early placentation: phenotypic and morphologic characterization of the CD56++ population. Dev Immunol. 1991;1(3):169-90

King A, Birkby C, Loke YW. Early human decidual cells exhibit NK activity against the K562 cell line but not against first trimester trophoblast. Cell Immunol. 1989 Feb;118(2):337-44.

King A, Loke YW. Human trophoblast and JEG choriocarcinoma cells are sensitive to lysis by IL-2-stimulated decidual NK cells. Cell Immunol. 1990 Sep;129(2):435-48

King A, Loke YW. On the nature and function of human uterine granular lymphocytes. Immunol Today. 1991 Dec;12(12):432-5. Review.

King A, Wellings V, Gardner L, Loke YW. Immunocytochemical characterization of the unusual large granular lymphocytes in human endometrium throughout the menstrual cycle. Hum Immunol. 1989 Mar;24(3):195-205

Klose CSN, Flach M, Möhle L, Rogell L, Hoyler T, Ebert K, Fabiunke C, Pfeifer D, Sexl V, Fonseca-Pereira D, Domingues RG, Veiga-Fernandes H, Arnold SJ, Busslinger M, Dunay IR, Tanriver Y, Diefenbach A. Differentiation of type 1 ILCs from a common progenitor to all helper-like innate lymphoid cell lineages. Cell. 2014 Apr 10;157(2):340-356.

Kohrt HE, Thielens A, Marabelle A, Sagiv-Barfi I, Sola C, Chanuc F, Fuseri N, Bonnafous C, Czerwinski D, Rajapaksa A, Waller E, Ugolini S, Vivier E, Romagné F, Levy R, Bléry M, André P. Anti-KIR antibody enhancement of anti-lymphoma activity of natural killer cells as

monotherapy and in combination with anti-CD20 antibodies. Blood. 2014 Jan 30;123(5):678-86.

Koller BH, Marrack P, Kappler JW, Smithies O. Normal development of mice deficient in beta 2M, MHC class I proteins, and CD8+ T cells. Science. 1990 Jun 8;248(4960):1227-30.

Koopman LA, Kopcow HD, Rybalov B, Boyson JE, Orange JS, Schatz F, Masch R, Lockwood CJ, Schachter AD, Park PJ, Strominger JL. Human decidual natural killer cells are a unique NK cell subset with immunomodulatory potential. J Exp Med. 2003;198:1201–1212

Krimpenfort P, Rudenko G, Hochstenbach F, Guessow D, Berns A, Ploegh H. Crosses of two independently derived transgenic mice demonstrate functional complementation of the genes encoding heavy (HLA-B27) and light (beta 2-microglobulin) chains of HLA class I antigens. EMBO J. 1987 Jun;6(6):1673-6.

Krop I, Shaffer AL, Fearon DT, Schlissel MS. The signaling activity of murine CD19 is regulated during cell development. J Immunol. 1996 Jul 1;157(1):48-56.

Landsteiner, K. & Wiener, A.S. An agglutinable factor in human blood recognized by immune sera for rhesus blood. Proc. Soc. Exp. Biol. 1940 43, 223.

Lanier LL. Up on the tightrope: natural killer cell activation and inhibition. Nat Immunol. 2008 May;9(5):495-502.

Lanier LL. Plastic fantastic innate lymphoid cells. J Exp Med. 2019 Aug 5;216(8):1726-1727.

Lanier LL, Corliss BC, Wu J, Leong C, Phillips JH. Immunoreceptor DAP12 bearing a tyrosine-based activation motif is involved in activating NK cells. Nature. 1998;391:703–707.

Leach DR, Krummel MF, Allison JP. Enhancement of antitumor immunity by CTLA-4 blockade. Science. 1996 Mar 22;271(5256):1734-6.

(a)Lee N, Llano M, Carretero M, Ishitani A, Navarro F, López-Botet M, Geraghty DE. HLA-E is a major ligand for the natural killer inhibitory receptor CD94/NKG2A. Proc Natl Acad Sci U S A. 1998 Apr 28; 95(9):5199-204.

(b)Lee N, Goodlett DR, Ishitani A, Marquardt H, Geraghty DE. HLA-E surface expression depends on binding of TAP-dependent peptides derived from certain HLA class I signal sequences. J Immunol. 1998;160:4951–4960.

(c)Lee KM, Chuang E, Griffin M, Khattri R, Hong DK, Zhang W, Straus D, Samelson LE, Thompson CB, Bluestone JA. Molecular basis of T cell inactivation by CTLA-4. Science. 1998 Dec 18;282(5397):2263-6.

Lee KM, Forman JP, McNerney ME, Stepp S, Kuppireddi S, Guzior D, Latchman YE, Sayegh MH, Yagita H, Park CK, Oh SB, Wülfing C, Schatzle J, Mathew PA, Sharpe AH, Kumar V. Requirement of homotypic NK-cell interactions through 2B4(CD244)/CD48 in the generation of NK effector functions. Blood 2006; 107: 3181–3188

Lee KM, McNerney ME, Stepp SE, Mathew PA, Schatzle JD, Bennett M, Kumar V. 2B4 acts as a non-major histocompatibility complex binding inhibitory receptor on mouse natural killer cells. J Exp Med 2004; 199: 1245–1254

Leek JT, Johnson WE, Parker HS, Jaffe AE, Storey JD. The sva package for removing batch effects and other unwanted variation in high-throughput experiments. Bioinformatics. 2012 Mar 15;28(6):882-3

Lemberg MK, Bland FA, Weihofen A, Braud VM, Martoglio B. Intramembrane proteolysis of signal peptides: an essential step in the generation of HLA-E epitopes. J Immunol. 2001;167:6441–6446

Leon L, Felker AM, Kay VR, Tu MM, Makrigiannis AP, Croy BA. Ly49 knockdown in mice results in aberrant uterine crypt formation and impaired blastocyst implantation. Placenta. 2016 Mar;39:147-50.

Levine P, Stetson RE. AN UNUSUAL CASE OF INTRA-GROUP AGGLUTINATION. JAMA. 1939;113(2):126-127.

Li C, Houser BL, Nicotra ML, Strominger JL. HLA-G homodimer-induced cytokine secretion through HLA-G receptors on human decidualmacrophages and natural killer cells. Proc Natl Acad Sci U S A. 2009 Apr 7;106(14):5767-72.

Li F, Wei H, Wei H, Gao Y, Xu L, Yin W, Sun R, Tian Z. Blocking the natural killer cell inhibitory receptor NKG2A increases activity of human natural killer cells and clears hepatitis B virus infection in mice. Gastroenterology. 2013 Feb;144(2):392-401.

Lim AI, Li Y, Lopez-Lastra S, Stadhouders R, Paul F, Casrouge A, Serafini N, Puel A, Bustamante J, Surace L, Masse-Ranson G, David E, Strick-Marchand H, Le Bourhis L, Cocchi R, Topazio D, Graziano P, Muscarella LA, Rogge L, Norel X, Sallenave JM, Allez M, Graf T, Hendriks RW, Casanova JL, Amit I, Yssel H, Di Santo JP. Systemic Human ILC Precursors Provide a Substrate for Tissue ILC Differentiation. Cell. 2017 Mar 9;168(6):1086-1100.e10.

Liu J, Fan D. Hepatitis B in China. Lancet. 2007 May 12;369(9573):1582-3

Long EO. Negative signaling by inhibitory receptors: the NK cell paradigm. Immunol Rev. 2008 Aug;224:70-84.

Loonstra A, Vooijs M, Beverloo HB, Allak BA, van Drunen E, Kanaar R, Berns A, Jonkers J. Growth inhibition and DNA damage induced by Cre recombinase in mammalian cells. Proc Natl Acad Sci U S A. 2001 Jul 31;98(16):9209-14.

Lorenz U. SHP-1 and SHP-2 in T cells: two phosphatases functioning at many levels. Immunol Rev. 2009 Mar;228(1):342-59.

Lugo-Villarino G, Maldonado-Lopez R, Possemato R, Penaranda C, Glimcher LH. T-bet is required for optimal production of IFN-gamma and antigen-specific T cell activation by dendritic cells. Proc Natl Acad Sci U S A. 2003 Jun 24;100(13):7749-54.

MacDonald TM, Hui L, Tong S, Robinson AJ, Dane KM, Middleton AL, Walker SP. Reduced growth velocity across the third trimester is associated with placental insufficiency in fetuses born at a normal birthweight: a prospective cohort study. BMC Med. 2017 Aug 31;15(1):164.

Madeja Z, Yadi H, Apps R, Boulenouar S, Roper SJ, Gardner L, Moffett A, Colucci F, Hemberger M. Paternal MHC expression on mouse trophoblast affects uterine vascularization and fetal growth. Proc Natl Acad Sci U S A. 2011 Mar 8;108(10):4012-7.

Man J, Hutchinson JC, Ashworth M, Jeffrey I, Heazell AE, Sebire NJ. Organ weights and ratios for postmortem identification of fetal growth restriction: utility and confounding factors. Ultrasound Obstet Gynecol. 2016 Nov;48(5):585-590.

Mandelboim O, Lieberman N, Lev M, Paul L, Arnon TI, Bushkin Y, Davis DM, Strominger JL, Yewdell JW, Porgador A. Recognition of haemagglutinins on virus-infected cells by NKp46 activates lysis by human NK cells. Nature. 2001 Feb 22;409(6823):1055-60.

Matthews PC, Prendergast A, Leslie A, Crawford H, Payne R, Rousseau C, Rolland M, Honeyborne I, Carlson J, Kadie C, Brander C, Bishop K, Mlotshwa N, Mullins JI, Coovadia H, Ndung'u T, Walker BD, Heckerman D, Goulder PJ. Central role of reverting mutations in HLA associations with human immunodeficiency virus set point. J Virol. 2008 Sep;82(17):8548-59

Maunu J, Ekholm E, Parkkola R, Palo P, Rikalainen H, Lapinleimu H, Haataja L, Lehtonen L; PIPARI Study Group. Antenatal Doppler measurements and early brain injury in very low birth weight infants. J Pediatr. 2007 Jan;150(1):51-56.e1.

Mayer S, Raulf MK, Lepenies B. C-type lectins: their network and roles in pathogen recognition and immunity. Histochem Cell Biol. 2017 Feb;147(2):223-237

McCutcheon JA, Gumperz J, Smith KD, Lutz CT, Parham P. Low HLA-C expression at cell surfaces correlates with increased turnover of heavy chain mRNA. J Exp Med. 1995 Jun 1;181(6):2085-95.

McWilliams EM, Mele JM, Cheney C, Timmerman EA, Fiazuddin F, Strattan EJ, Mo X, Byrd JC, Muthusamy N, Awan FT. Therapeutic CD94/NKG2A blockade improves natural killer cell dysfunction in chronic lymphocytic leukemia. Oncoimmunology. 2016 Sep 9;5(10)

Mebius RE, Rennert P, Weissman IL. Developing lymph nodes collect CD4+CD3- LTbeta+ cells that can differentiate to APC, NK cells, and follicular cells but not T or B cells. Immunity. 1997 Oct;7(4):493-504.

Medawar PB 1944. The behaviour and fate of skin autografts and skin homografts in rabbits. J Anat 78: 176–199

Medawar PB (1953) Some immunological and endocrinological problems raised by the evolution of viviparity in vertebrates. In Society for Experimental Biology, pp. 320–338. New York: Academic Press.

Mehta A, Kim KB, Minor DR. Case Report of a Pregnancy During Ipilimumab Therapy. J Glob Oncol. 2018 Sep;4:1-3.

Merino AM, Sabbaj S, Easlick J, Goepfert P, Kaslow RA, Tang J. Dimorphic HLA-B signal peptides differentially influence HLA-E- and natural killer cell-mediated cytolysis of HIV-1-infected target cells. Clin Exp Immunol. 2013 Dec;174(3):414-23

Meyer N, Schüler T, Zenclussen AC. High Frequency Ultrasound for the Analysis of Fetal and Placental Development In Vivo. J Vis Exp. 2018 Nov 8;(141)

Miller D, Motomura K, Garcia-Flores V, Romero R, Gomez-Lopez N. Innate Lymphoid Cells in the Maternal and Fetal Compartments. Front Immunol. 2018 Oct 26;9:2396

Moffett A, Chazara O, Colucci F, Johnson MH. Variation of maternal KIR and fetal HLA-C genes in reproductive failure: too early for clinical intervention. Reprod Biomed Online. 2016 Dec;33(6):763-769.

Moffett A, Colucci F. Uterine NK cells: active regulators at the maternal-fetal interface. J Clin Invest. 2014 May;124(5):1872-9.

Moffett A, Loke YW. The immunological paradox of pregnancy: a reappraisal. Placenta. 2004 Jan;25(1):1-8. Review.

Moffett A, Shreeve N. First do no harm: uterine natural killer (NK) cells in assisted reproduction. Hum Reprod. 2015 Jul;30(7):1519-25

Mol BWJ, Roberts CT, Thangaratinam S, Magee LA, de Groot CJM, Hofmeyr GJ. Pre-eclampsia. Lancet. 2016 Mar 5;387(10022):999-1011

Monticelli LA, Sonnenberg GF, Abt MC, Alenghat T, Ziegler CG, Doering TA, Angelosanto JM, Laidlaw BJ, Yang CY, Sathaliyawala T, Kubota M, Turner D, Diamond JM, Goldrath AW, Farber

DL, Collman RG, Wherry EJ, Artis D. Innate lymphoid cells promote lung-tissue homeostasis after infection with influenza virus. Nat Immunol. 2011 Nov;12(11):1045-54

Monticelli LA, Osborne LC, Noti M, Tran SV, Zaiss DM, Artis D. IL-33 promotes an innate immune pathway of intestinal tissue protection dependent on amphiregulin-EGFR interactions. Proc Natl Acad Sci U S A. 2015 Aug 25;112(34):10762-7

Morales-Roselló J, Khalil A. Fetal cerebral redistribution: a marker of compromise regardless of fetal size. Ultrasound Obstet Gynecol. 2015 Oct;46(4):385-8

Morales-Roselló J, Peralta Llorens N. Outcome of fetuses with diagnosis of isolated short femur in the second half of pregnancy. ISRN Obstet Gynecol. 2012;2012:268218

Mu J, Adamson SL. Developmental changes in hemodynamics of uterine artery, utero- and umbilicoplacental, and vitelline circulations in mouse throughout gestation. Am J Physiol Heart Circ Physiol. 2006 Sep;291(3):H1421-8.

Nakase K, Cheng J, Zhu Q,, and Marasco WA. Mechanisms of SHP-1 P2 promoter regulation in hematopoietic cells and its silencing in HTLV-1-transformed T cells. J Leukoc Biol. 2009 Jan; 85(1): 165–174.

Nakimuli A, Chazara O, Hiby SE, Farrell L, Tukwasibwe S, Jayaraman J, Traherne JA, Trowsdale J, Colucci F, Lougee E, Vaughan RW, Elliott AM, Byamugisha J, Kaleebu P, Mirembe F, Nemat-Gorgani N, Parham P, Norman PJ, Moffett A.A KIR B centromeric region present in Africans but not Europeans protects pregnant women from pre-eclampsia. Proc Natl Acad Sci U S A. 2015 Jan 20;112(3):845-50.

Narni-Mancinelli E, Chaix J, Fenis A, Kerdiles YM, Yessaad N, Reynders A, Gregoire C, Luche H, Ugolini S, Tomasello E, Walzer T, Vivier E. Fate mapping analysis of lymphoid cells expressing the NKp46 cell surface receptor. Proc Natl Acad Sci U S A. 2011 Nov 8;108(45):18324-9

Naruse M, Ono R, Irie M, Nakamura K, Furuse T, Hino T, Oda K, Kashimura M, Yamada I, Wakana S, Yokoyama M, Ishino F, Kaneko-Ishino T. Sirh7/Ldoc1 knockout mice exhibit placental P4 overproduction and delayed parturition. Development. 2014 Dec;141(24):4763-71.

Natarajan K, Dimasi N, Wang J, Margulies DH, Mariuzza RA. MHC class I recognition by Ly49 natural killer cell receptors. Mol Immunol. 2002 May; 38(14):1023-7.

Nossal GJ. Antibody production by single cells. Br J Exp Pathol. 1958 Oct;39(5):544-51.

Ohlén C, Kling G, Höglund P, Hansson M, Scangos G, Bieberich C, Jay G, Kärre K. Prevention of allogeneic bone marrow graft rejection by H-2 transgene in donor mice. Science. 1989 Nov 3;246(4930):666-8.

Ohtsuka M, Inoko H, Kulski JK, Yoshimura S. Major histocompatibility complex (Mhc) class Ib gene duplications, organization and expression patterns in mouse strain C57BL/6. BMC Genomics. 2008 Apr 17;9:178.

Oldenborg PA, Zheleznyak A, Fang YF, Lagenaur CF, Gresham HD, Lindberg FP. Role of CD47 as a marker of self on red blood cells. Science. 2000 Jun 16;288(5473):2051-4.

Olley PM, Coceani F. Prostaglandins and the ductus arteriosus. Annu Rev Med. 1981;32:375-85.

Olofsson P, Laurini RN, Marsál K. A high uterine artery pulsatility index reflects a defective development of placental bed spiral arteries in pregnancies complicated by hypertension and fetal growth retardation. Eur J Obstet Gynecol Reprod Biol. 1993 May;49(3):161-8.

Oros D, Figueras F, Cruz-Martinez R, Padilla N, Meler E, Hernandez-Andrade E, Gratacos E. Middle versus anterior cerebral artery Doppler for the prediction of perinatal outcome and neonatal neurobehavior in term small-for-gestational-age fetuses with normal umbilical artery Doppler. Ultrasound Obstet Gynecol. 2010 Apr;35(4):456-61.

Orr MT, Wu J, Fang M, Sigal LJ, Spee P, Egebjerg T, Dissen E, Fossum S, Phillips JH, Lanier LL. Development and function of CD94-deficient natural killer cells. PLoS One. 2010 Dec 3;5(12):e15184.

Ortaldo JR, Winkler-Pickett R, Wigginton J, Horner M, Bere EW, Mason AT, Bhat N, Cherry J, Sanford M, Hodge DL, Young HA. Regulation of ITAM-positive receptors: role of IL-12 and IL-18. Blood (2006) 107(4):1468–75

Ortiz MV, Roberts SS, Glade Bender J, Shukla N, Wexler LH. Immunotherapeutic Targeting of GPC3 in Pediatric Solid Embryonal Tumors. Front Oncol. 2019 Feb 26;9:108

Osińska I, Popko K, Demkow U. Perforin: an important player in immune response. Cent Eur J Immunol. 2014;39(1):109-15

Panduro M, Benoist C, Mathis D. Tissue Tregs. Annu Rev Immunol. 2016 May 20;34:609-33

Parham P. MHC class I molecules and KIRs in human history, health and survival. Nat Rev Immunol. 2005 Mar; 5(3):201-14

Parr EL, Parr MB, Zheng LM, Young JD. Mouse granulated metrial gland cells originate by local activation of uterine natural killer lymphocytes. Biol Reprod. 1991 May;44(5):834-41.

Pascal V, Schleinitz N, Brunet C, Ravet S, Bonnet E, Lafarge X, Touinssi M, Reviron D, Viallard JF, Moreau JF, Déchanet-Merville J, Blanco P, Harlé JR, Sampol J, Vivier E, Dignat-George F, Paul P. Comparative analysis of NK cell subset distribution in normal and lymphoproliferative disease of granular lymphocyte conditions. Eur J Immunol. 2004 Oct;34(10):2930-40.

Paul S, Lal G. The Molecular Mechanism of Natural Killer Cells Function and Its Importance in Cancer Immunotherapy. Front Immunol. 2017 Sep 13;8:1124.

Paust S, Gill HS, Wang BZ, Flynn MP, Moseman EA, Senman B, Szczepanik M, Telenti A, Askenase PW, Compans RW, von Andrian UH. Critical role for the chemokine receptor CXCR6 in NK cell-mediated antigen-specific memory of haptens and viruses. Nat Immunol. 2010 Dec;11(12):1127-35.

Peel S. Granulated metrial gland cells. Adv. Anat. Embryol. Cell Biol., 115 (1989), pp. 1-112

Peng H, Tian Z. Diversity of tissue-resident NK cells. Semin Immunol. 2017 Jun;31:3-10.

Platt, JS, Hunt JS. Interferon-gamma gene expression in cycling and pregnant mouse uterus: temporal aspects and cellular localization. J. Leukocyte Biol., 64 (1998), pp. 393-

Poon LC, Nicolaides KH. Early prediction of preeclampsia. Obstet Gynecol Int. 2014;2014:297397

Powe CE, Levine RJ, Karumanchi SA. Preeclampsia, a disease of the maternal endothelium: the role of antiangiogenic factors and implications for later cardiovascular disease. Circulation. 2011 Jun 21;123(24):2856-69.

PrabhuDas M, Bonney E, Caron K, Dey S, Erlebacher A, Fazleabas A, Fisher S, Golos T, Matzuk M, McCune JM, Mor G, Schulz L, Soares M, Spencer T, Strominger J, Way SS, Yoshinaga K. Immune mechanisms at the maternal-fetal interface: perspectives and challenges. Nat Immunol. 2015 Apr;16(4):328-34.

Prager I, Liesche C, van Ooijen H, Urlaub D, Verron Q, Sandström N, Fasbender F, Claus M, Eils R, Beaudouin J, Önfelt B, Watzl C. NK cells switch from granzyme B to death receptor-mediated cytotoxicity during serial killing. J Exp Med. 2019 Jul 3. pii: jem.20181454

Prior T, Mullins E, Bennett P, Kumar S. Prediction of intrapartum fetal compromise using the cerebroumbilical ratio: a prospective observational study. Am J Obstet Gynecol 2013; 208: 124.e1–6.

Ramsuran V, Naranbhai V, Horowitz A, Qi Y, Martin MP, Yuki Y, Gao X, Walker-Sperling V, Del Prete GQ, Schneider DK, Lifson JD, Fellay J, Deeks SG, Martin JN, Goedert JJ, Wolinsky SM, Michael NL, Kirk GD, Buchbinder S, Haas D, Ndung'u T, Goulder P, Parham P, Walker BD, Carlson JM, Carrington M. Elevated HLA-A expression impairs HIV control through inhibition of NKG2A-expressing cells. Science. 2018 Jan 5;359(6371):86-90

Raulet DH. Missing self recognition and self tolerance of natural killer (NK) cells. Semin Immunol. 2006 Jun;18(3):145-50.

Raz T, Avni R, Addadi Y, Cohen Y, Jaffa AJ, Hemmings B, Garbow JR, Neeman M. The hemodynamic basis for positional- and inter-fetal dependent effects in dual arterial supply of mouse pregnancies. PLoS One. 2012;7(12):e52273

Redman CW, Sargent IL. Latest advances in understanding preeclampsia. Science. 2005 Jun 10;308(5728):1592-4.

Rennie MY, Whiteley KJ, Adamson SL, Sled JG. Quantification of Gestational Changes in the Uteroplacental Vascular Tree Reveals Vessel Specific Hemodynamic Roles During Pregnancy in Mice. Biol Reprod. 2016 Aug;95(2):43.

RCOG. Green-top Guideline No. 55. Later Intrauterine Fetal Death and Stillbirth. October 2010. Available at URL https://www.rcog.org.uk/globalassets/documents/guidelines/gtg_55.pdf. Accessed 03/11/2019.

Rep A, Ganzevoort W, Van Wassenaer A, Bonsel G, Wolf H, De Vries J for the PETRA investigators. One-year infant outcome in women with early-onset hypertensive disorders of pregnancy. BJOG 2008; 115: 290–298.

Roberts RM, Green JA, Schulz LC. The evolution of the placenta. Reproduction. 2016 Nov;152(5):R179-89.

Rölle A, Pollmann J, Ewen EM, Le VT, Halenius A, Hengel H, Cerwenka A. IL-12-producing monocytes and HLA-E control HCMV-driven NKG2C+ NK cell expansion. J Clin Invest. 2014 Dec;124(12):5305-16.

Romagné F, André P, Spee P, Zahn S, Anfossi N, Gauthier L, Capanni M, Ruggeri L, Benson DM Jr, Blaser BW, Della Chiesa M, Moretta A, Vivier E, Caligiuri MA, Velardi A, Wagtmann N. Preclinical characterization of 1-7F9, a novel human anti-KIR receptor therapeutic antibody that augments natural killer-mediated killing of tumor cells. Blood. 2009 Sep 24;114(13):2667-77.

Romero R, Hernandez-Andrade E. Doppler of the middle cerebral artery for the assessment of fetal well-being. Am J Obstet Gynecol. 2015 Jul;213(1):1

Romiguier J, Ranwez V, Douzery EJ, Galtier N. Contrasting GC-content dynamics across 33 mammalian genomes: relationship with life-history traits and chromosome sizes. Genome Res. 2010 Aug;20(8):1001-9.

Rosenfeld CS. Sex-Specific Placental Responses in Fetal Development. Endocrinology. 2015 Oct;156(10):3422-34.

Sabdia S, Greer RM, Prior T, Kumar S. Predicting intrapartum fetal compromise using the fetal cerebro-umbilical ratio. Placenta 2015**; 36:**594–598.

Sağol S, Ozkinay E, Oztekin K, Ozdemir N. The comparison of uterine artery Doppler velocimetry with the histopathology of the placental bed. Aust N Z J Obstet Gynaecol. 1999 Aug;39(3):324-9.

Sala FG, Del Moral PM, Pizzato N, Legrand-Abravanel F, Le Bouteiller P, Lenfant F. The HLA-G*0105N null allele induces cell surface expression of HLA-E molecule and promotes CD94/NKG2A-mediated recognition in JAR choriocarcinoma cell line. Immunogenetics. 2004 Dec;56(9):617-24.

Sagrillo-Fagundes L, Bienvenue-Pariseault J, Vaillancourt C. Melatonin: The smart molecule that differentially modulates autophagy in tumor and normal placental cells. PLoS One. 2019 Jan 10;14(1):e0202458

Samstein RM, Josefowicz SZ, Arvey A, Treuting PM, Rudensky AY. Extrathymic generation of regulatory T cells in placental mammals mitigates maternal-fetal conflict. Cell (2012) 150:29–3810.1016

Sanz-Cortes M, Egaña-Ugrinovic G, Simoes RV, Vazquez L, Bargallo N, Gratacos E. Association of brain metabolism with sulcation and corpus callosum development assessed by MRI in late-onset small fetuses. Am J Obstet Gynecol 2015; 212: 804.e1–8.

Sasaki Y, Sakai M, Miyazaki S, Higuma S, Shiozaki A, Saito S. Decidual and peripheral blood CD4+CD25+ regulatory T cells in early pregnancy subjects and spontaneous abortion cases. Mol Hum Reprod. 2004 May;10(5):347-53.

Sato A, Mayer WE, Overath P, Klein J. Genes encoding putative natural killer cell C-type lectin receptors in teleostean fishes. Proc Natl Acad Sci U S A. 2003 Jun 24;100(13):7779-84.

Schmidt-Supprian M, Rajewsky K. Vagaries of conditional gene targeting. Nat Immunol. 2007 Jul;8(7):665-8.

Schneider CA, Rasband WS, Eliceiri KW. NIH Image to ImageJ: 25 years of image analysis. Nat Methods. 2012 Jul;9(7):671-5.

Semprini S, Troup TJ, Kotelevtseva N, King K, Davis JR, Mullins LJ, Chapman KE, Dunbar DR, Mullins JJ. Cryptic loxP sites in mammalian genomes: genome-wide distribution and relevance for the efficiency of BAC/PAC recombineering techniques. Nucleic Acids Res. 2007;35(5):1402-10.

Sesma L, Alvarez I, Marcilla M, Paradela A, López de Castro JA. Species-specific differences in proteasomal processing and tapasin-mediated loading influence peptide presentation by HLA-B27 in murine cells. J Biol Chem. 2003 Nov 21;278(47):46461-72.

Sharkey AM, Xiong S, Kennedy PR, Gardner L, Farrell LE, Chazara O, Ivarsson MA, Hiby SE, Colucci F, Moffett A. Tissue-Specific Education of Decidual NK Cells. J Immunol. 2015 Oct 1;195(7):3026-32.

Shepard MJ, Richards VA, Berkowitz RL, Warsof SL, Hobbins JC. An evaluation of two equations for predicting fetal weight by ultrasound. Am J Obstet Gynecol 1982; 142: 47–54.

Shifrin N, Raulet DH, Ardolino M. NK cell self tolerance, responsiveness and missing self recognition. Semin Immunol. 2014 Apr;26(2):138-44.

Shirai M, Arichi T, Nishioka M, Nomura T, Ikeda K, Kawanishi K, Engelhard VH, Feinstone SM, Berzofsky JA. CTL responses of HLA-A2.1-transgenic mice specific for hepatitis C viral peptides predict epitopes for CTL of humans carrying HLA-A2.1. J Immunol. 1995 Mar 15;154(6):2733-42.

Simmons, D. G., Rawn, S., Davies, A., Hughes, M. & Cross, J. C. Spatial and temporal expression of the 23 murine prolactin/placental lactogen-related genes is not associated with their position in the locus. B. M. C. Genomics. 9, 352 (2008)

Slatkin M. Linkage disequilibrium--understanding the evolutionary past and mapping the medical future. Nat Rev Genet. 2008 Jun;9(6):477-85.

Smas CM, Sul HS. Pref-1, a protein containing EGF-like repeats, inhibits adipocyte differentiation. Cell. 1993 May 21; 73(4):725-34.

Smith HR, Chuang HH, Wang LL, Salcedo M, Heusel JW, Yokoyama WM. Nonstochastic coexpression of activation receptors on murine natural killer cells. J Exp Med. 2000 Apr 17;191(8):1341-54.

Soares MJ, Iqbal K, Kozai K. Hypoxia and Placental Development. Birth Defects Res. 2017 Oct 16;109(17):1309-1329.

Soares MJ, Varberg KM, Iqbal K. Hemochorial placentation: development, function, and adaptations. Biol Reprod. 2018 Jul 1;99(1):196-211.

Sojka DK, Plougastel-Douglas B, Yang L, Pak-Wittel MA, Artyomov MN, Ivanova Y, Zhong C, Chase JM, Rothman PB, Yu J, Riley JK, Zhu J, Tian Z, Yokoyama WM. Tissue-resident natural killer (NK) cells are cell lineages distinct from thymic and conventional splenic NK cells. Elife. 2014 Jan 1; 3():e01659.

Sola C, André P, Lemmers C, Fuseri N, Bonnafous C, Bléry M, Wagtmann NR, Romagné F, Vivier E, Ugolini S. Genetic and antibody-mediated reprogramming of natural killer cell missing-self recognition in vivo. Proc Natl Acad Sci U S A. 2009 Aug 4;106(31):12879-84

Solano ME, Thiele K, Kowal MK, Arck PC. Identification of suitable reference genes in the mouse placenta. Placenta. 2016 Mar;39:7-15

Sovio U, White IR, Dacey A, Pasupathy D, Smith GCS. Screening for fetal growth restriction with universal third trimester ultrasonography in nulliparous women in the Pregnancy Outcome Prediction (POP) study: a prospective cohort study. Lancet. 2015 Nov 21;386(10008):2089-2097.

Sovio U, Goulding N, McBride N, Cook E, Gaccioli F, Charnock-Jones DS, Lawlor DA, Smith GCS. A maternal serum metabolite ratio predicts fetal growth restriction at term. Nat Med. 2020 Mar;26(3):348-353.

Spits H, Artis D, Colonna M, Diefenbach A, Di Santo JP, Eberl G, Koyasu S, Locksley RM, McKenzie AN, Mebius RE, Powrie F, Vivier E. Innate lymphoid cells--a proposal for uniform nomenclature. Nat Rev Immunol. 2013 Feb; 13(2):145-9.

Spits H, Di Santo JP. The expanding family of innate lymphoid cells: regulators and effectors of immunity and tissue remodeling. Nat Immunol. 2011 Jan;12(1):21-7.

Stewart IJ, Webster AJ. Lectin histochemical studies of mouse granulated metrial gland cells. Histochem J. 1997 Nov-Dec;29(11-12):885-92.

Taurog JD, Maika SD, Satumtira N, Dorris ML, McLean IL, Yanagisawa H, Sayad A, Stagg AJ, Fox GM, Lê O'Brien A, Rehman M, Zhou M, Weiner AL, Splawski JB, Richardson JA, Hammer RE. Inflammatory disease in HLA-B27 transgenic rats. Immunol Rev. 1999 Jun;169:209-23. Review.

Teklemariam T, Zhao L, Hantash BM. Full-length HLA-G1 and truncated HLA-G3 differentially increase HLA-E surface localization. Hum Immunol (2012) 73:898–90510.

Tesmer LA, Lundy SK, Sarkar S, Fox DA. Th17 cells in human disease. Immunol Rev. 2008 Jun;223:87-113

Thyagarajan B, Guimarães MJ, Groth AC, Calos MP. Mammalian genomes contain active recombinase recognition sites. Gene. 2000 Feb 22;244(1-2):47-54.

Tolsa CB, Zimine S, Warfield SK, Freschi M, Sancho Rossignol A, Lazeyras F, Hanquinet S, Pfizenmaier M & Huppi PS (2004). Early alteration of structural and functional brain development in premature infants born with intrauterine growth restriction. Pediatr Res 56, 132–138.

Trowbridge IS, Thomas ML. CD45: an emerging role as a protein tyrosine phosphatase required for lymphocyte activation and development. Annu Rev Immunol. 1994;12:85-116.

Ulbrecht M, Maier S, Hofmeister V, Falk CS, Brooks AG, McMaster MT, Weiss EH. Truncated HLA-G isoforms are retained in the endoplasmic reticulum and insufficiently provide HLA-E ligands. Hum Immunol. 2004 Mar;65(3):200-8.

Vacca P, Pesce S, Greppi M, Fulcheri E, Munari E, Olive D, Mingari MC, Moretta A, Moretta L, Marcenaro E. PD-1 is expressed by and regulates human group 3 innate lymphoid cells in human decidua. Mucosal Immunol. 2019 May;12(3):624-631.

Vance RE, Jamieson AM, Cado D, Raulet DH. Implications of CD94 deficiency and monoallelic NKG2A expression for natural killer cell development and repertoire formation. Proc Natl Acad Sci U S A. 2002 Jan 22;99(2):868-73.

Vance RE, Jamieson AM, Raulet DH. Recognition of the class Ib molecule Qa-1(b) by putative activating receptors CD94/NKG2C and CD94/NKG2E on mouse natural killer cells. J Exp Med. 1999 Dec 20;190(12):1801-12.

Vance RE, Kraft JR, Altman JD, Jensen PE, Raulet DH. Mouse CD94/NKG2A is a natural killer cell receptor for the nonclassical major histocompatibility complex (MHC) class I molecule Qa-1(b). J Exp Med. 1998 Nov 16;188(10):1841-8.

van Bergen J, Thompson A, van Pel M, Retière C, Salvatori D, Raulet DH, Trowsdale J, Koning F. HLA reduces killer cell Ig-like receptor expression level and frequency in a humanized mouse model. J Immunol. 2013 Mar 15;190(6):2880-5.

van Montfoort N, Borst L, Korrer MJ, Sluijter M, Marijt KA, Santegoets SJ, van Ham VJ, Ehsan I, Charoentong P, André P, Wagtmann N, Welters MJP, Kim YJ, Piersma SJ, van der Burg SH, van Hall T. NKG2A Blockade Potentiates CD8 T Cell Immunity Induced by Cancer Vaccines. Cell. 2018 Dec 13;175(7):1744-1755.e15.

Vasak B, Koenen SV, Koster MP, Hukkelhoven CW, Franx A, Hanson MA, Visser GH. Human fetal growth is constrained below optimal for perinatal survival. Ultrasound Obstet Gynecol. 2015 Feb;45(2):162-7

Vento-Tormo R, Efremova M, Botting RA, Turco MY, Vento-Tormo M, Meyer KB, Park JE, Stephenson E, Polański K, Goncalves A, Gardner L, Holmqvist S, Henriksson J, Zou A, Sharkey AM, Millar B, Innes B, Wood L, Wilbrey-Clark A, Payne RP, Ivarsson MA, Lisgo S, Filby A, Rowitch DH, Bulmer JN, Wright GJ, Stubbington MJT, Haniffa M, Moffett A, Teichmann SA. Single-cell reconstruction of the early maternal-fetal interface in humans. Nature. 2018 Nov;563(7731):347-353.

Vey N, Dumas PY, Recher C. et al. Randomized Phase 2 Trial of Lirilumab (anti-KIR monoclonal antibody, mAb) As Maintenance Treatment in Elderly Patients (pts) with Acute Myeloid Leukemia (AML): Results of the Effikir Trial. Blood 2017 130:889;

Vey N, Karlin L, Sadot-Lebouvier S, Broussais F, Berton-Rigaud D, Rey J, Charbonnier A, Marie D, André P, Paturel C, Zerbib R, Bennouna J, Salles G, Gonçalves A. A phase 1 study of lirilumab (antibody against killer immunoglobulin-like receptor antibody KIR2D; IPH2102) in patients with solid tumors and hematologic malignancies. Oncotarget. 2018 Apr 3;9(25):17675-17688

Viant C, Fenis A, Chicanne G, Payrastre B, Ugolini S, Vivier E. SHP-1-mediated inhibitory signals promote responsiveness and anti-tumour functions of natural killer cells. Nat Commun. 2014 Oct 30;5:5108.

Vilches C, Parham P. KIR: diverse, rapidly evolving receptors of innate and adaptive immunity. Annu Rev Immunol. 2002;20:217-51.

Vivier E, Artis D, Colonna M, Diefenbach A, Di Santo JP, Eberl G, Koyasu S, Locksley RM, McKenzie ANJ, Mebius RE, Powrie F, Spits H. Innate Lymphoid Cells: 10 Years On. Cell. 2018 Aug 23;174(5):1054-1066.

Vivier E, Ugolini S, Blaise D, Chabannon C, Brossay L. Targeting natural killer cells and natural killer T cells in cancer. Nat Rev Immunol. 2012 Mar 22;12(4):239-52.

Walker JA, McKenzie AN. Development and function of group 2 innate lymphoid cells. Curr Opin Immunol. 2013 Apr;25(2):148-55.

Walsh NC, Kenney LL, Jangalwe S, Aryee KE, Greiner DL, Brehm MA, Shultz LD. Humanized Mouse Models of Clinical Disease. Annu Rev Pathol. 2017 Jan 24;12:187-215.

Walzer T, Bléry M, Chaix J, Fuseri N, Chasson L, Robbins SH, Jaeger S, André P, Gauthier L, Daniel L, Chemin K, Morel Y, Dalod M, Imbert J, Pierres M, Moretta A, Romagné F, Vivier E. Identification, activation, and selective in vivo ablation of mouse NK cells via NKp46. Proc Natl Acad Sci U S A. 2007 Feb 27;104(9):3384-9.

Weizman OE, Adams NM, Schuster IS, Krishna C, Pritykin Y, Lau C, Degli-Esposti MA, Leslie CS, Sun JC, O'Sullivan TE. ILC1 Confer Early Host Protection at Initial Sites of Viral Infection. Cell. 2017 Nov 2;171(4):795-808.e12.

Wheelock MD, Hect JL, Hernandez-Andrade E, Hassan SS, Romero R, Eggebrecht AT, Thomason ME. Sex differences in functional connectivity during fetal brain development. Dev Cogn Neurosci. 2019 Apr;36:100632

Whitley GS, Cartwright JE. Cellular and molecular regulation of spiral artery remodelling: lessons from the cardiovascular field. Placenta. 2010 Jun;31(6):465-74.

Wilson A, Held W, MacDonald HR. Two waves of recombinase gene expression in developing thymocytes. J Exp Med. 1994 Apr 1;179(4):1355-60.

Woo JS, Wan CW, Cho KM. Computer-assisted evaluation of ultrasonic fetal weight prediction using multiple regression equations with and without the fetal femur length. J Ultrasound Med 1985; 4: 65–67.

Yalniz FF, Daver N, Rezvani K, Kornblau S, Ohanian M, Borthakur G, DiNardo CD, Konopleva M, Burger J, Gasior Y, Pierce S, Kantarjian H, Garcia-Manero G. A Pilot Trial of Lirilumab With or Without Azacitidine for Patients With Myelodysplastic Syndrome. Clin Lymphoma Myeloma Leuk. 2018 Oct;18(10):658-663.e2.

Yamaleyeva LM, Pulgar VM, Lindsey SH, Yamane L, Varagic J, McGee C, daSilva M, Lopes Bonfa P, Gurley SB, Brosnihan KB. Uterine artery dysfunction in pregnant ACE2 knockout mice is associated with placental hypoxia and reduced umbilical blood flow velocity. Am J Physiol Endocrinol Metab. 2015 Jul 1;309(1):E84-94

Yawata M, Yawata N, Draghi M, Partheniou F, Little AM, Parham P. MHC class I-specific inhibitory receptors and their ligands structure diverse human NK-cell repertoires toward a balance of missing self-response. Blood. 2008 Sep 15;112(6):2369-80.

Yeager, M., Kumar, S. & Hughes, A. L. Sequence convergence in the peptide-binding region of primate and rodent MHC class Ib molecules. Mol. Biol. Evol. 14, 1035–1041 (1997).

Yokoyama, W. M. Inhibitory receptors signal activation. Immunity 29, 515–517 (2008).

Yokoyama WM, Seaman WE. The Ly-49 and NKR-P1 gene families encoding lectin-like receptors on natural killer cells: the NK gene complex. Annu Rev Immunol. 1993;11:613-35.

Yu J, Wei M, Mao H, Zhang J, Hughes T, Mitsui T, Park IK, Hwang C, Liu S, Marcucci G, Trotta R, Benson DM Jr, Caligiuri MA. CD94 defines phenotypically and functionally distinct mouse NK cell subsets. J Immunol. 2009 Oct 15;183(8):4968-74

Yung HW, Calabrese S, Hynx D, Hemmings BA, Cetin I, Charnock-Jones DS, Burton GJ. Evidence of placental translation inhibition and endoplasmic reticulum stress in the etiology of human intrauterine growth restriction. Am J Pathol. 2008 Aug;173(2):451-62

Yunis EJ, Romero V, Diaz-Giffero F, Zuñiga J, Koka P. Natural Killer Cell Receptor NKG2A/HLA-E Interaction Dependent Differential Thymopoiesis of Hematopoietic Progenitor Cells Influences the Outcome of HIV Infection. J Stem Cells. 2007;2(4):237-248

Xu HC, Huang J, Pandyra AA, Lang E, Zhuang Y, Thöns C, Timm J, Häussinger D, Colonna M, Cantor H, Lang KS, Lang PA. Lymphocytes Negatively Regulate NK Cell Activity via Qa-1b following Viral Infection. Cell Rep. 2017 Nov 28;21(9):2528-2540

Xu W, Moor RJ, Walpole ET, Atkinson VG. Pregnancy with successful foetal and maternal outcome in a melanoma patient treated with nivolumab in the first trimester: case report and review of the literature. Melanoma Res. 2019 Jun;29(3):333-337

Zenclussen AC. Regulatory T cells in pregnancy. Springer Semin Immunopathol. 2006 Aug;28(1):31-9.

Zhang J, Croy BA. Using ultrasonography to define fetal-maternal relationships: moving from humans to mice. Comp Med. 2009 Dec;59(6):527-33.

Zhang JH, Yamada AT, Croy BA. DBA-lectin reactivity defines natural killer cells that have homed to mouse decidua. Placenta. 2009 Nov;30(11):968-73

Zhang X, Feng J, Chen S, Yang H, Dong Z. Synergized regulation of NK cell education by NKG2A and specific Ly49 family members. Nat Commun. 2019 Nov 1;10(1):5010.

Zhou Y, Zhou B, Pache L, Chang M, Khodabakhshi AH, Tanaseichuk O, Benner C, Chanda SK. Metascape provides a biologist-oriented resource for the analysis of systems-level datasets. Nat Commun. 2019 Apr 3;10(1):1523.

Zumla A, Marguerie C, So A, Yokoyama WM, Saito T, Batchelor JR, Lechler RI. Co-expression of human T cell receptor chains with mouse CD3 on the cell surface of a mouse T cell hybridoma. J Immunol Methods. 1992 Apr 27;149(1):69-76.

13.0 LIST OF ABBREVIATIONS

AC   abdominal circumference
ACE2   angiotensin-converting enzyme 2
ADCC   antibody-dependent cellular cytotoxicity
AEDF   absent end diastolic flow
AGA   average-for-gestational age
AIDS   acquired immunodeficiency syndrome
ANXA1   anti-inflammatory lipocortin I protein
APCs   antigen presenting cells

BPD   bi-parietal diameter

CAF   Combined Animal Facility
CBAL   Core Biochemical Assay Laboratory
CBS   Central Biomedical Service
CFSE   carboxyfluorescein diacetate succinimidyl ester
CPR   cerebroplacental ratio
CTLA-4   cytotoxic T-lymphocyte antigen-4

DC   dendritic cells
DNAM-1   DNAX accessory molecule-1

EDF   End diastolic flow
EDTA   ethylenediaminetetraacetic acid
EDV   end diastolic velocity
EFW   estimated fetal weight
ELISA   enzyme-linked immunosorbent assay
EVT   extravillous trophoblast

FACS   fluorescence-activated cell sorting
FDA   Food and Drug Administration
FDR   false discovery rate
FGR   fetal growth restriction
FL   femur length

GFP   green fluorescent protein
GM-CSF   granulocyte macrophage colony-stimulating factor

H&E   hematoxylin and eosin
HBV   hepatitis B virus
HBSS   Hank's balanced saline solution
HC   head circumference
HDFN   haemolytic disease of the fetus and newborn
HIV   human immunodeficiency virus
HLA   human leucocyte antigen

IFN   interferon
IHC   immunohistochemistry
IL   interleukin
ILCs   innate lymphoid cells
IP   interferon-inducible protein
ITAM   immunoreceptor tyrosine-based activation motif

ITIM	immunoreceptor tyrosine-based inhibition motif
IUGR	intra-uterine growth-restriction
KIR	killer-cell immunoglobulin-like receptor
KLR	killer cell C-type lectin receptors
KO	knock-out
LD	linkage disequilibrium
LFA-1	lymphocyte function-associated antigen 1
LGL	large granular lymphocyte
LTi	lymphoid tissue-inducer cells
MCA	middle cerebral artery
MCMV	Mouse cytomegalovirus
mESC	Mouse embryonic stem cell
MHC	major histocompatibility
Micro-CT	micro-commuted tomography
Micro-US	micro-ultrasound
MLAP	mesometrial lymphoid aggregate of pregnancy
MRI	magnetic resonance imaging
NICU	neonatal intensive care unit
NK	natural killer
NKC	NK gene complex
ON	overnight
PAPP-A	pregnancy associated plasma protein A
PBMCs	peripheral blood mononuclear cells
pbNK	peripheral blood NK cells
PBS	phosphate buffered saline
PCR	polymerase chain reaction
PD-1	programmed death-1
PD-L1	programmed death-ligand 1
PI	pulsatility index
PLGF	placental growth factor
PPH	post-partum haemorrhage
PSV	peak systolic velocity
PTI	protein transport inhibitor
PW	pulsed wave
RBC	red blood cell
REDF	reversed end diastolic flow
RT	room temperature
RT-qPCR	Real time-quantitative polymerase chain reaction
SD	standard deviation
SGA	small-for-gestational age
SHP-1	Src-homology region 2 domain-containing phosphatase-1
SIRPα	signal regulatory protein alpha
sNK	splenic NK cells
SNP	single nucleotide polymorphism
SPINK2	serine protease inhibitor Kazal-type 2
SPP	signal peptide peptidase

TAP	transporter associated with antigen presentation
TAV	time-averaged velocity
TCR	T cell receptor
Th	T-helper
TLR	Toll-like receptor
TNF	tumour necrosis factor
Tregs	regulatory T cells
UA	umbilical artery
UAPI	umbilical artery pulsatility index
uNK	uterine natural killer
UTR	untranslated region
VEGF	vascular endothelial growth factor